

Alma Mater Studiorum – Università di Bologna

**DOTTORATO DI RICERCA IN
CHIMICA**

Ciclo XXVII°

Settore Concorsuale di afferenza: 03 / A1

Settore Scientifico disciplinare: CHIM / 01

**OPTIMIZATION OF PURIFICATION PROCEDURES IN ORGANIC
SEMICONDUCTOR SYNTHESIS FOR IMPROVING THE PERFORMANCES
OF ORGANIC FIELD-EFFECT TRANSISTORS**

Presentata da: EDOARDO BONARETTI

Coordinatore Dottorato

Chiar.mo Prof. ALDO RODA

Relatore

Prof. MARCO TADDIA

Correlatore

Dr. STEFANO TOFFANIN

Esame finale anno 2015

CONTENTS

ABSTRACT.....	7
---------------	---

PART I – INTRODUCTION

CHAPTER 1

CHARGE TRANSPORT IN ORGANIC SEMICONDUCTORS.....

1.1 Organic semiconductors physics.....	11
1.2 Alternative charge conduction dynamics.....	15
1.2.1 Tunneling Model.....	17
1.2.2 Hopping Model.....	20
1.2.3 Polaron Model.....	23
REFERENCES.....	27

CHAPTER 2

ORGANIC SEMICONDUCTORS DESCRIPTION.....

2.1 Classification by charge transport.....	30
2.2 Classification by molecular structure.....	36
2.2.1 <i>n</i> -type semiconductors.....	36
2.2.2 <i>p</i> -type semiconductors.....	42
REFERENCES.....	49

<u>CHAPTER 3</u>	
OFET DEVICE	
PHYSICS.....	53

REFERENCES.....	62
-----------------	----

PART II – EXPERIMENTALS AND DATA DISCUSSION

<u>CHAPTER 1</u>	
ORGANIC SEMICONDUCTORS PURIFICATION AND	
PERFORMANCES	
IMPROVEMENT.....	65

1.1 Thermal treatments for organic molecules.....	65
---	----

1.2 Sublimation dynamics.....	67
-------------------------------	----

1.3 Sublimation technique and experimental parameters.....	69
--	----

1.4 Comparison between crude and sublimed semiconductor performances.....	71
---	----

1.4.1 Study on DH4T performances before and after sublimation.....	72
--	----

1.4.2 Study on DHF4T performances before and after sublimation.....	80
---	----

1.5 Conclusions and remarks.....	88
----------------------------------	----

REFERENCES.....	89
-----------------	----

<u>CHAPTER 2</u>	
SYNTHETIC STRATEGY TO IMPROVE THE PURITY OF AN ORGANIC SEMICONDUCTOR.....	91
2.1 DH4T.....	91
2.2 DH4T commercial synthesis.....	92
2.3 New metal-free synthesis of DH4T.....	96
2.4 OFETs fabrication and compared characterization.....	99
2.5 Investigation on the effects of organometallic impurities on DH4T performances.....	110
2.6 Synthesis of the organic impurity and study of its effects on DH4T performances.....	126
2.7 Conclusions and remarks.....	137
REFERENCES.....	139

PART III – TECHNICAL DETAILS

<u>CHAPTER 1</u>	
HIGH VACUUM CHAMBER FOR OFET FABRICATION.....	143

<u>CHAPTER 2</u>	
OFET DEVICE CHARACTERIZATION.....	153

ABSTRACT

The aim of the research activity focused on the investigation of the correlation between the degree of purity in terms of chemical dopants in organic small molecule semiconductors and their electrical and optoelectronic performances once introduced as active material in devices.

The first step of the work was addressed to the study of the electrical performances variation of two commercial organic semiconductors after being processed by means of thermal sublimation process.

In particular, the *p*-type 2,2'''-Dihexyl-2,2':5',2'':5'',2'''-quaterthiophene (**DH4T**) semiconductor and the *n*-type 2,2'''- Perfluoro-Dihexyl-2,2':5',2'':5'',2'''-quaterthiophene (**DHF4T**) semiconductor underwent several sublimation cycles, with consequent improvement of the electrical performances in terms of charge mobility and threshold voltage, highlighting the benefits brought by this treatment to the electric properties of the discussed semiconductors in OFET devices by the removal of residual impurities.

The second step consisted in the provision of a metal-free synthesis of **DH4T**, which was successfully prepared without organometallic reagents or catalysts in collaboration with Dr. Manuela Melucci from ISOF-CNR Institute in Bologna.

The new synthesis was carried on by selective bromination followed by Grignard reactive preparation, which was finally added to a living stable radical. The comparison between the electric performances of the metal-free **DH4T** and commercial **DH4T** semiconductors pointed out the benefits of the new synthesis method were mainly due to the avoidance of organometallic pollutants typically present in standard synthesis methods (such as cross-coupling reactions) for organic molecules.

Indeed the experimental work demonstrated that those compounds are responsible for the electrical degradation by intentionally doping the semiconductor obtained by metal-free method by Tetrakis(triphenylphosphine)palladium(0) (Pd(PPh₃)₄) and

Tributyltin chloride (Bu_3SnCl), as well as with an organic impurity, like 5-hexyl-2,2':5',2''-terthiophene (HexT_3) at, in different concentrations (1, 5 and 10% w/w). After completing the entire evaluation process loop, from fabricating OFET devices by vacuum sublimation with implemented intentionally-doped batches to the final electrical characterization in inherent-atmosphere conditions, commercial **DH4T**, metal-free **DH4T** and the intentionally-doped **DH4T** were systematically compared. Indeed, the fabrication of OFET based on doped **DH4T** clearly pointed out that the vacuum sublimation is still an inherent and efficient purification method for crude semiconductors, but also a reliable way to fabricate high performing devices: this technique embodies the sublimation benefits with the smartness of the solvent-free deposition methods, guaranteeing the removal of great part of impurities and the minimization of interferences from the environment.

PART I

-

INTRODUCTION

CHAPTER 1

CHARGE TRANSPORT IN ORGANIC SEMICONDUCTORS

1.1 Organic semiconductors physics

It is universally known that elements, substances and materials can be divided in three classes depending on their electric conductivity: conductors, insulators and semiconductors.

According with the Electronic Band Structure theory (EBS) [1] it is always possible to define a Valence Band (VB), generated by the linear combination of all the atomic or molecular bonding orbitals, and a Conduction Band (CB) which is the result of the linear combination of all the unoccupied orbitals. The energy difference between those bands leads to the classification expressed before.

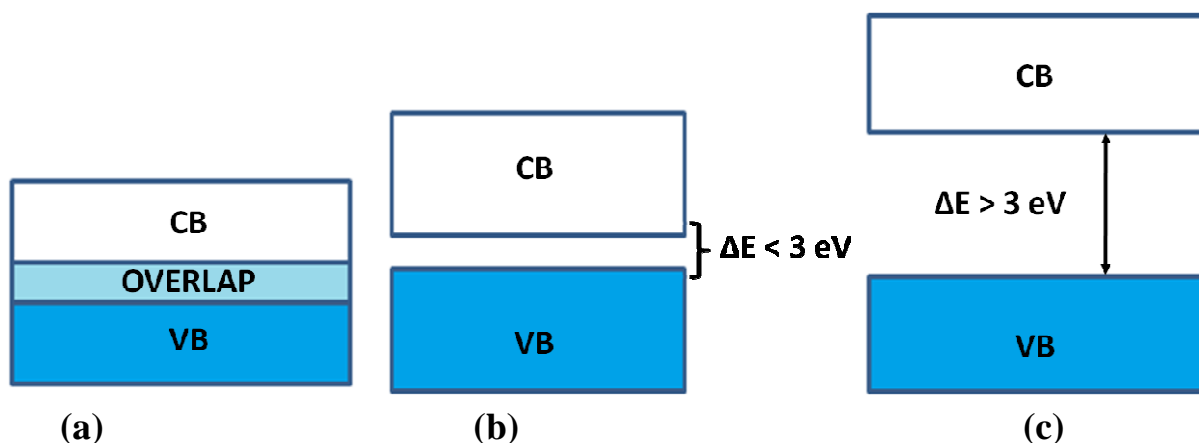


Figure 1.1: electronic bands representation for (a) conductor, (b) semiconductor and (c) insulator.

Due to its little energy band gap, a semiconductor can transport charge carriers under an applied electric field (conduction) as well as under a charge concentration gradient (diffusion);

furthermore, its conductivity increases with temperature and it usually has a great thermoelectric power factor [2].

While metal, covalent compounds and ionic crystals properties can be easily predicted using classic EBS model, organic semiconductors must be investigated with in a special way due to the fact they are small molecules-type or polymeric molecular crystals.

The quantum mechanical approach is the one called Tight Binding (TB) method [3]: it is based on the approximation that the total energy Hamiltonian of a lattice system can be represented as a single orbital Hamiltonian.

First it is necessary to introduce molecular orbitals, each of them represented by a space dependent wavefunction $\varphi_{\text{molecular}}(\mathbf{r})$ which must be eigenfunctions of the Hamiltonian of a single isolated atom (H_{atom}).

When the considered atom is placed in crystal lattice, its orbitals will overlap with those of other atoms: the tighter will be the electrons bond, the lesser will be the overlap effect.

So the Hamiltonian of the system energy can be written as the summation of all the single H_{atom} calculated for every possible position in the lattice.

$$H_{\text{system}}(\mathbf{r}) = \sum_{\mathbf{R}_{\text{atomic site}}} H_{\text{atom}}(\mathbf{r} - \mathbf{R}_{\text{atomic site}}) + \Delta E_{\text{overlap}}$$

Equation 1.1: calculation of the total energy Hamiltonian for an atoms in a crystal lattice interacting with each other.

where $\mathbf{R}_{\text{atomic site}}$ is the position vector of the atom in the lattice and $\Delta E_{\text{overlap}}$ is the atomic potential correction generated by the interaction between the orbitals.

Then a possible solution $\psi(\mathbf{r})$ of single electron Schrödinger equation is approximated as a linear combination of molecular orbitals wavefunctions, such $\varphi_{\text{molecular}}(\mathbf{r} - \mathbf{R}_{\text{atomic site}})$ which have the translational periodicity of the crystal lattice.

$$\psi_{\mathbf{n}}(\mathbf{r}) = \sum_{\mathbf{R}_{\text{atomic site}}} C(\mathbf{R}_{\text{atomic site}}) \varphi_{\text{molecular}}(\mathbf{r} - \mathbf{R}_{\text{atomic site}})$$

Equation 1.2: calculation of a single energy level wavefunction in a crystal lattice; $C(\mathbf{R}_{\text{atomic site}})$ is the orbitals linear combination coefficient for a single lattice position.

Equation 1.2 is good for a single \mathbf{n} -th energetic level: to predict all the contributions given by all the lattice energetic levels, another summation is needed:

$$\Psi_{\text{total}}(\mathbf{r}) = \sum_{\mathbf{n}} \psi_{\mathbf{n}}(\mathbf{r})$$

Equation 1.3: calculation of the lattice orbital total wavefunction considering all the possible energy levels.

Once defined the wavefunction for the lattice molecular orbitals having constant periodicity, then a single electron wavefunction is needed to be written.

Using Bloch approximation [4] it is possible to describe a function dependent on the energy assumed by a free electron: it has exponential form since it is assumed that the field in which electron moves is constant [5].

$$\Psi_{\mathbf{K}} = \Psi_{\text{total}}(\mathbf{r}) \cdot e^{i \mathbf{K} \mathbf{R}_{\text{atomic site}}}$$

Equation 1.4: calculation of the total wavefunction for a single electron put in the lattice molecular orbital; all the possible energy levels are considered.

In Equation 1.4 \mathbf{K} is the wave number vector, defined as $|\mathbf{K}| = 2\pi / \lambda$; consequently the energy $E(\mathbf{K})$ of an electron with a given \mathbf{K} is

$$E(\mathbf{K}) = \mathbf{K}^2 \cdot (\hbar^2 / 2m)$$

Equation 1.5: correlation between the energy associated to an electron and the wave number vector; m is the particle mass.

The values of \mathbf{K} are closely spaced so $E(\mathbf{K})$ is almost a continuous function until $\Psi_{\text{total}}(\mathbf{r})$ remains constant: when this latter function varies greatly within a unit cell and falls to zero between adjacent cells, then the considered electron is free no more and this is what is called Tight Binding condition [6].

If $\Psi_{\text{total}}(\mathbf{r})$ becomes a space-dependent variable, like in a real molecular crystal lattice, then separation between \mathbf{K} values appears and so $E(\mathbf{K})$ ceases to be continuous, allowing the generation of electronic bands.

1.2 Alternative charge conduction dynamics

Tight Binding is not the only model which can properly describe the charge transport in organic semiconductor. Several other theories have been developed during years to justify charge transfer mechanisms in a wide range of compounds: the most important are Tunneling Model (TM), Hopping Model (HM) and Polaron Model (PM).

All the mentioned mechanisms fit with molecules having short-range interactions, explaining organic semiconductors behavior by complementary approaches.

As shown in Figure 1.2, TM assumption is that an electron can pass through a potential energy barrier (the boundary between adjacent cells or molecules) even if it has not acquired enough energy pass over it; HM states that an electron can pass the considered barrier moving over it via a molecular activated state.

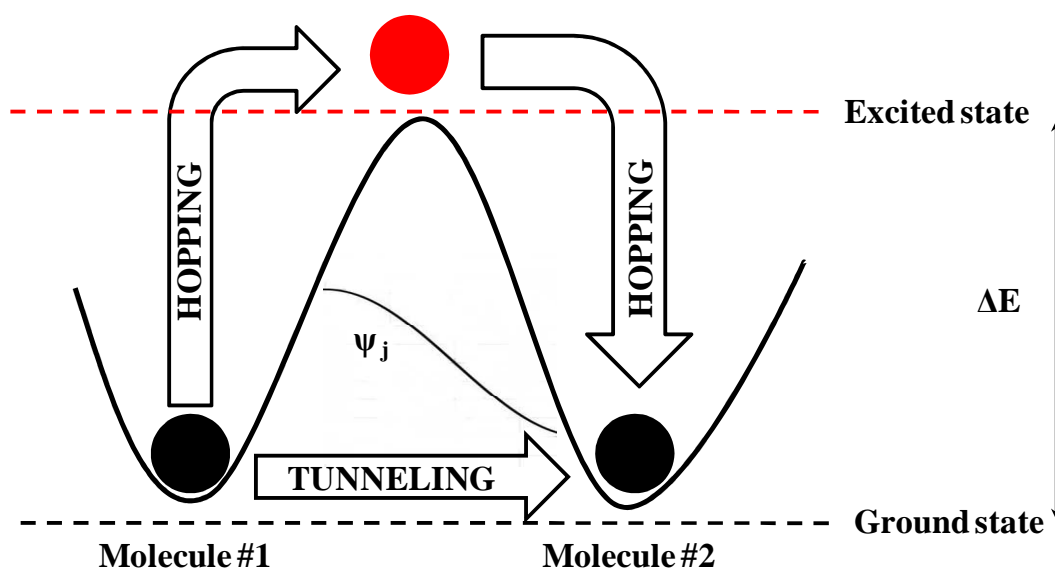


Figure 1.2: Qualitative explanation of Tunneling and Hopping charge transport dynamics.

PM is mainly based on the electrostatic induction approach, which involves the polarization of a molecule due to the delocalized charge of a neighboring one. The conduction is made by the carrier that moves under an electric field along with the polarization cloud itself: this quasi-particle entity is what is called *polaron*. The starting delocalized charge can be generated by dipole induction phenomena (between molecules or chemical bonds of the same molecule) or by introducing odd

charges in the lattice system. PM is very useful to explain polarization behavior in organic materials and to understand electrostatic phenomena involving lattice dominions.

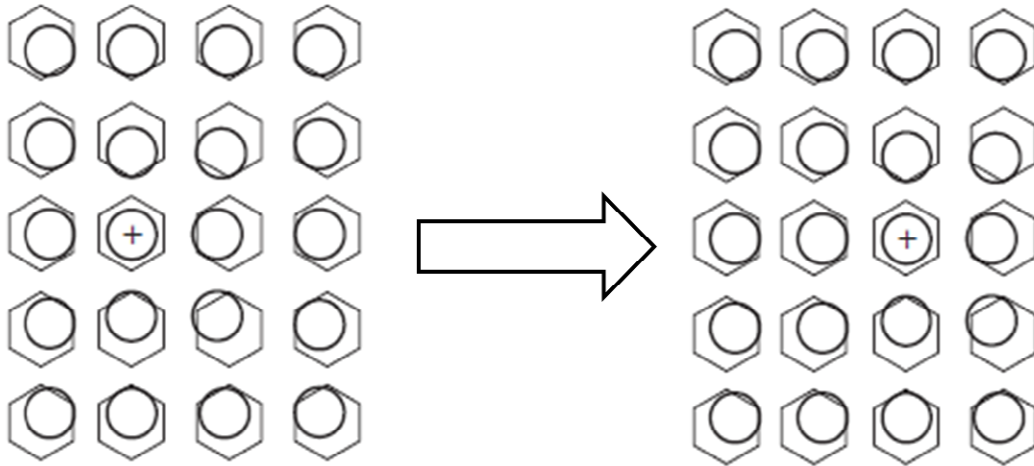


Figure 1.3: Qualitative explanation of Polaron charge transport dynamics [7].

1.2.1 Tunneling Model

In a molecular crystal two molecules, or at least two crystalline domains, can be seen as identical potential wells, being the distance between them nothing but a finite energy barrier as shown in Figure 1.4 .

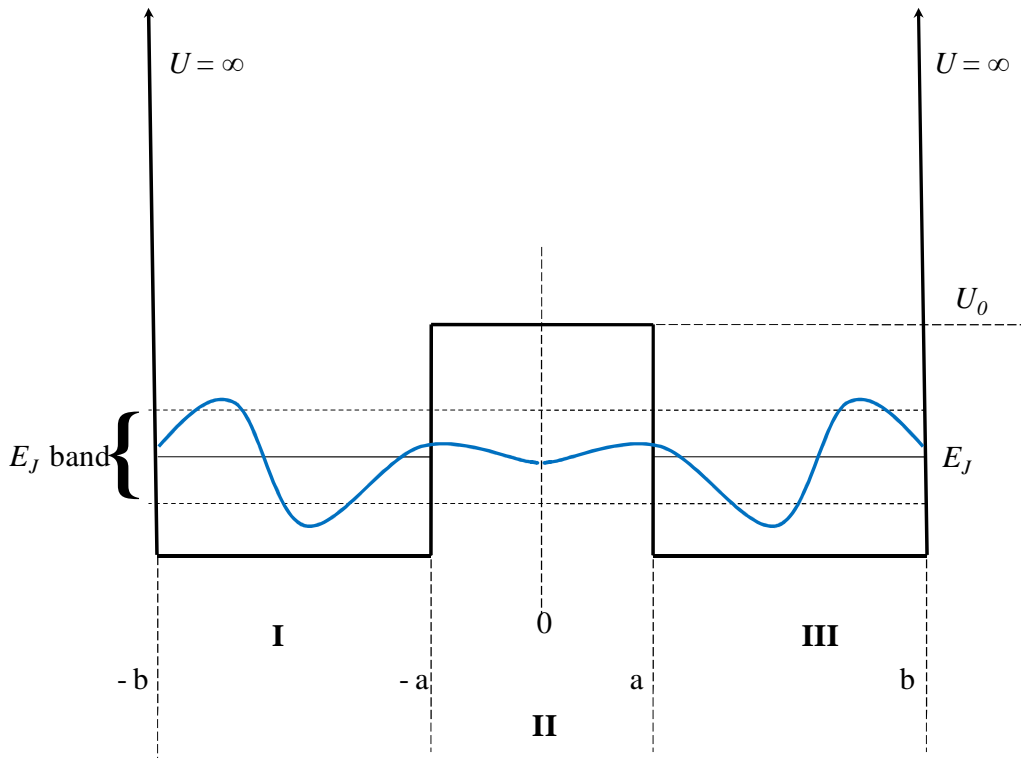


Figure 1.4: representation of the Tunneling Effect between two potential wells separated by an energy barrier.

Quantum mechanics demonstrates that a particle can trespass a potential while having an energy below the barrier top value; the total energy associated to the electron is E_J , where J is a quantum number which defines the energy level. It is interesting to point out that energy levels become more widely spaced as J increases.

When J is an odd number, in Regions I and III ($-b < x \leq -a$ and $a \leq x < b$) the electron wavefunction is $\psi_j = 2A \cos(\alpha x)$ falling to zero at infinite energy boundaries ($x = \pm b$).

In Region II it is possible to define two zones:

- in the first, where $-a < x \leq 0$, $\psi_j = [2A \cos(\alpha x)] e^{\beta(x+a)}$
- in the second, where $0 \leq x < a$, $\psi_j = [2A \cos(\alpha x)] e^{-\beta(x-a)}$

where $\alpha = (8 \pi^2 m E_J) / h^2$ and $\beta = [(8 \pi^2 m) / h^2] (U_0 - E_J)$ [8] .

The probability that the particle will actually tunnel depends on the thickness and on the height of the energy barrier as well as on the energy level involved; furthermore, if J was even the cosine function would have to be replaced by the corresponding sine function multiplied for the imaginary unit.

To explain photoconduction in organic molecular crystals a mechanism based on tunneling model was proposed by Eley [9]: it involves two steps to explain the energy acquisition for light emission and the charge carriers transport.

The first stage is the excitation of the molecule by heat or light to produce an exciton [10]: the electron goes then in the first unoccupied orbital at higher energy while the hole remains in the normally occupied ground state orbital; in the second stage, due to tunneling effect, both the electron and the hole can pass through the potential barrier to occupy the corresponding orbital in the adjacent molecule, moving in opposite directions.

The Eley's mechanism is widely used to explain charge conduction in organic free radicals [11], proteins [12] and solid charge transfer complexes [13].

Since a single crystal energy levels are replaced by energy bands in a bulk material, the electrons can be considered delocalized.

The energy spread between the levels increases with the overlap efficiency between the electrons wavefunctions in adjacent single cells: the greater is this spread and so the band width, the greater is the charge mobility; in reverse narrow bands lead to a lower mobility [14].

The Tight Binding Band theory does not mention potential wells or barriers, but it allows to define wavefunctions for every considered lattice assuming that the

structure has a noticeable periodicity just like the potential associated to the bands. Only when this condition is satisfied Tunneling Model can be considered strictly related to the Tight Binding modeling, otherwise the spacing between cells and consequently the energy walls must be calculated including all the irregularities and all the defects.

1.2.2 Hopping Model

Initially used for ionic crystals [15], HM was then successfully applied to explain the charge motion in organic solids [16].

The first assumption is that the charge carriers move from one molecule to another in random way except for the anisotropy caused by the applied electric field; the second assumption states that, since the mean free path (L) is proportional to charge mobility (μ), HM can be invocated only when $\mu < 1 \text{ cm}^2 / (\text{V s})$, thus when L is as small or smaller than lattice spacing [17].

$$\mu = \frac{f e N_S (a k_B T)^2}{h^3 v_{\text{relax}}^2} e^{-E_S / (k_B T)}$$

Equation 1.6: classic Hopping mobility calculation for charges moving in ionic crystals; f is the average hopping angle with regard to the direction of the electric field, a is the lattice characteristic constant, N_S is the number of neighboring sites, E_S is the energy barrier between molecules.

It is worthy to be remarked that charge carriers mobility is inverse proportional to the square relaxation frequency of the particle in the two direction in the energy barrier point normal with the electric field direction: the shorter is the electron relaxation period ($\tau_{\text{relax}} = 1 / \nu_{\text{relax}}$), the smaller is the mobility because the electron has more probabilities to decay to the ground state than to remain in the activated state and pass over the energy wall. Electron hopping from one molecule to a neighboring one is due to the interaction between charged particle relaxation frequency and lattice vibration frequency: when τ_{relax} is long compared with the shortest lattice vibration period ($\tau_{\text{vib}} = 1 / \nu_{\text{vib}}$), then HM is expected to apply [18].

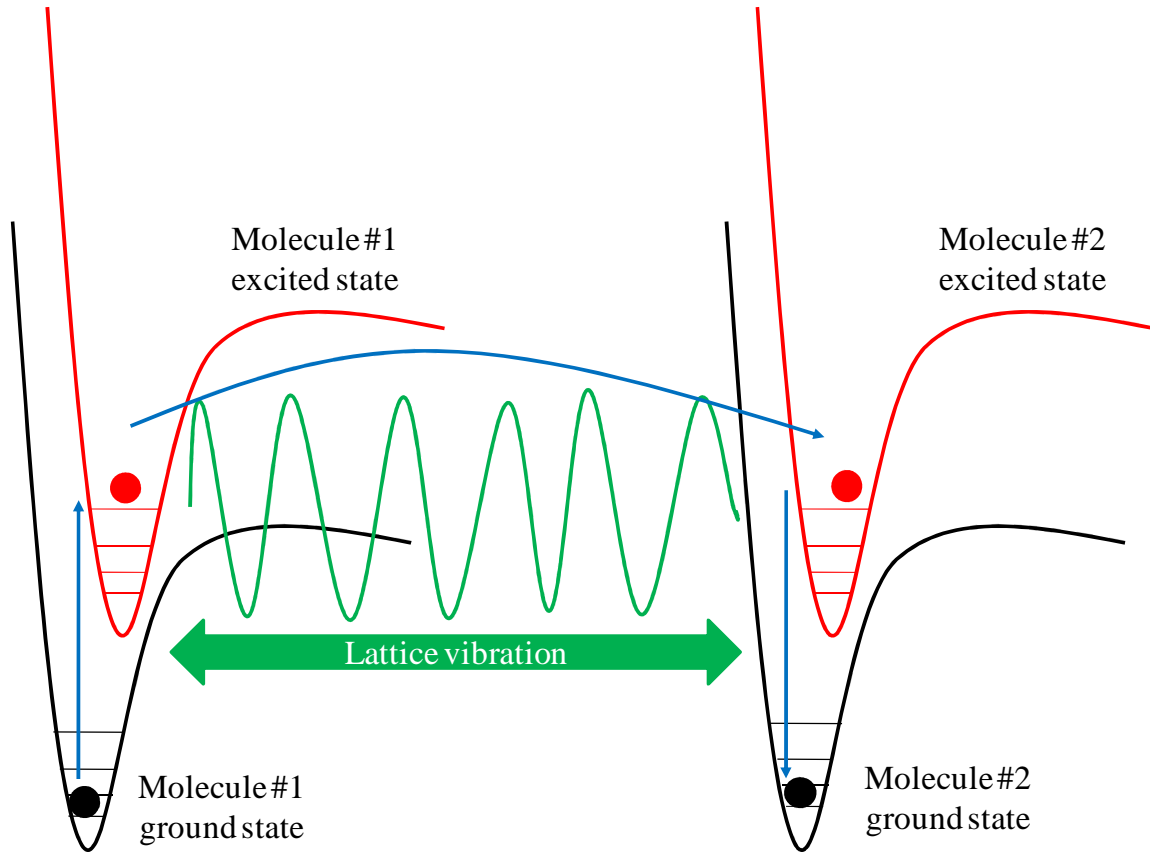


Figure 1.5: representation of molecular crystal Hopping mechanism.

To quantify the interaction between the electron and the lattice in molecular crystals it is useful to define first the charge mobility, explained in a more apt form like the following:

$$\mu = \frac{e a^2}{k_B T} v_{\text{relax}}$$

Equation 1.7: expression for Hopping charge mobility calculation; e is the elementary electric charge and a is the characteristic lattice constant.

In this case v_{relax} is calculated after replacing lattice vibrational oscillators with harmonic ones (ω_0) having the same frequency [19], as shown in Equation 1.8 .

$$v_{\text{relax}} = \frac{2 \pi \beta_u^2}{\hbar^2 \omega_0} e^{-\gamma (2S + 1)} I \{2\gamma \sqrt{S(S + 1)}\}$$

Equation 1.8: expression for electron relaxation frequency; β_u is a matrix which connects molecular functions on sites separated by a distance u , I is a Bessel function and $S = 1 / [\exp(\hbar\omega_0 / k_B T) - 1]$.

Equation 1.8 explains how the charge mobility is temperature-dependent:

γ is a dimensionless electron-lattice interaction parameter and if its value is below 10 then the charge mobility either does not change or decreases with temperature; otherwise normal behavior is expected [20].

To explain HM working $\tau_{\text{relax}} > \tau_{\text{vib}}$ condition is not enough: for the hopping model to be valid $\hbar\omega_0 \gg \beta_u$ and $\tau_{\text{relax}} \gg 2\pi / \omega_0$. That means the carrier must remain in a lattice site much longer than the vibration period [21].

Despite its approach seems to be more qualitative than the other ones, preventing computational in depth-analysis, HM gives good theoretical instrument to rationalize conduction in polymers and oligomers.

1.2.3 Polaron Model

Every time it is need to use the PM approach it is necessary to define two parameters which help to understand if there is a real possibility for a polaron to be generated and move towards the lattice system: the residence time (τ_{res}), which corresponds to the average time a charge will reside on a

Molecule, and the electronic polarization time (τ_{elec}) is the time it takes for the polarization cloud to form around the charge [22].

Both periods can be easily calculated from Heisenberg formula, once defined the characteristic energy barriers: usually for organic materials the magnitude is 10^{-14} s for residence time and 10^{-15} s for polarization time [23].

To explain charge transport in polarizable media Marcus model [24] can be very useful: it was developed to describe the charge transport from a donor molecule to an acceptor one and it can be also applied to organic semiconductor matters.

Introducing the classic Arrhenius exponential form, the electron transfer kinetic constant (k_{ET}) can be calculated as:

$$k_{\text{ET}} = A e^{-\Delta G^* / k_B T}$$

Equation 1.9: electron transfer rate constant calculation by Arrhenius classic kinetic approach.

The **A** factor is the product of the weighted average nuclear frequency (ν_N), usually equal to 10^{13} Hz, and the transmission coefficient (κ_t), which is related to the electronic interactions between two molecules.

In case of non-adiabatic charge transfer, **A** factor can be approximated starting from a Landau-Zener probabilistic treatment [25].

$$A = \frac{2\pi |H_{AB}|^2}{\hbar \sqrt{4\pi\lambda k_B T}}$$

Equation 1.10: exploitation of Arrhenius pre-exponential factor.

$|H_{AB}|$ is the charge transfer integral which represent the electronic coupling energy between the system initial state and the system final state; λ is the system reorganization energy, which is defined as the energy that would be required to reorganize the system structure from initial to final reaction coordinates without making the charge transfer.

The activation free energy (ΔG^*) is strictly related to the process free energy (ΔG^0) and to the system reorganization energy according with Equation 1.11 :

$$\Delta G^* = \frac{(\Delta G^0 + \lambda)^2}{4\lambda}$$

Equation 1.11: basic relationship involving the three energies on which Marcus theory focuses on.

Figure 1.6 shows the physical meaning of the parameters discussed above, explaining the generalization of Marcus theory which is often associated with Hopping Model in order to have a mathematic instrument apt to a wider problems range.

In the following Figure the abscissa is the transferred amount of charge or sometimes the total induced polarization \mathbf{P} : they have the same meaning as reaction coordinate; the ordinate is the Gibbs free energy.

In a bimolecular system it is always possible to recognize a donor and an acceptor species: when a charge transfer occurs the reaction coordinates, thus the total polarization, change. In the general case of two different molecules (whose energetic coordinates are the black slope), an activation free energy and a process free energy can be defined and the system reorganization energy is calculated as the charge

transfer would take place between two identical molecule (broken red slope) having the same energetic coordinates of the final products (green slope).

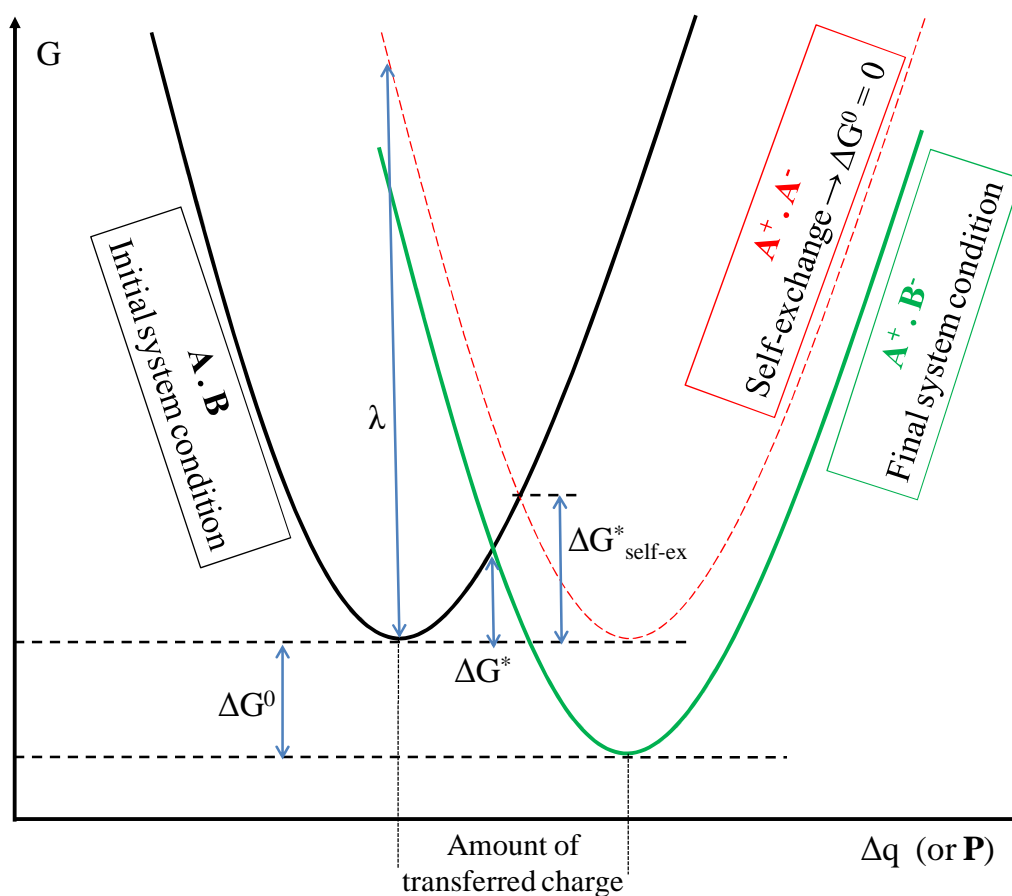


Figure 1.6: representation of the Marcus model energetic discussion.

Since the organic semiconductor crystals have molecules of the same kind ($A \cdot A \rightarrow A^+ \cdot A^-$), the charge transport can be actually considered a self-exchange, so the activation free energy is equal to $\lambda / 4$.

Charge mobility is therefore calculated as

$$\mu = \frac{q a^2}{k_B T} k_{ET}$$

Equation 1.11: charge mobility calculation for Polaron conduction model; q is the transferred charge and a is the characteristic lattice constant.

A generalization of the Marcus theory establishes an important criterion for activation-less or localized transport: since the reorganization energy and the charge transfer integral are linked to the molecular polarization time and to the residence time respectively, the first kind of transport occurs when $2|H_{AA}| > \lambda$ while the second one can be represented by

$$2|H_{AA}| < \lambda \text{ [26].}$$

REFERENCES

- [1] C. Kittel, *Introduction to Solid State Physics* (7th Edition), **1996**, New York, Wiley;
- [2] S. M. Sze, *Physics of Semiconductor Devices* (2nd Edition), **1981**, John Wiley and Sons;
- [3] J. C. Slater, G. F. Koster, *Physical Review*, **1954**, 94 (6): 1498–1524;
- [4] F. Bloch, *Z. Physik*, **1928**, 52, 555;
- [5] F. Gutmann, L. E. Lyons, *Organic Semiconductors*, John Wiley & Sons;
- [6] F. Gutmann, L. E. Lyons, *Organic Semiconductors*, John Wiley & Sons;
- [7] Inspired by Z. Bao, J. Locklin, *Organic Field-Effect Transistors*, **2007**, CRC Press, p. 81;
- [8] T. E. Hartmann, *J. App. Phys.* , 33, 3427 (**1962**);
- [9] D. D. Eley, G. D. Parfitt, *Trans. Faraday Soc.* , 51, 1529 (**1955**);
- [10] D. D. Eley, G. D. Parfitt, M. J. Perry, D. H. Taysum, *Trans. Faraday Soc.*, 49, 79 (**1953**);
- [11] D. D. Eley, M. R. Willis, *Symposium on Electrical Conductivity in Organic Solids*, Interscience, New York, **1961**, p.257;
- [12] M. H. Cardew, D. D. Eley, *Discussions Faraday Soc.*, 27, 115 (**1957**);
- [13] D. D. Eley, H. Inokuchi, *Discussions Faraday Soc.*, 28, 54 (**1959**);
- [14] F. Gutmann, L. E. Lyons, *Organic Semiconductors*, John Wiley & Sons;
- [15] F. Seitz, *Phys. Rev.*, 76, 1376, November **1949**;
- [16] H. A. Pohl, David A. Opp, *J. Phys. Chem.*, **1962**, 66 (11), pp 2121–2126;
- [17] S. H. Glarum, *J. of Phys. and Chem. of Solids*, Vol 24, Issue 12, Dec **1963**, pp 1577–1583;
- [18] F. Gutmann, L. E. Lyons, *Organic Semiconductors*, John Wiley & Sons;
- [19] J. Yamashita, T. Kurosawa, *J. of Phys. and Chem. of Solids*, Vo 5, Issues 1–2, **1958**, p 34–43;
- [20] F. Gutmann, L. E. Lyons, *Organic Semiconductors*, John Wiley & Sons;

- [21] S. H. Glarum, *J. of Phys. and Chem. of Solids*, Vol 24, Issue 12, Dec **1963**, p 1577–1583;
- [22] Z. Bao, J. Locklin, *Organic Field-Effect Transistors*, **2007**, CRC Press;
- [23] E.A. Silinsh, V. Čápek, *Organic molecular crystals: Interaction, localization, and transport phenomena*, AIP Press, New York, **1994**;
- [24] R. A. Marcus, *J. Chem. Phys.*, **1965**, 43 (2): 679;
- [25] R. A. Marcus, *Electron transfer in chemistry. Theory and experiment*, Rev. Mod. Phys., 65, 599, **1993**;
- [26] Z. Bao, J. Locklin, *Organic Field-Effect Transistors*, **2007**, CRC Press;

CHAPTER 2

ORGANIC SEMICONDUCTORS DESCRIPTION

Organic semiconductors classification is basically made considering which kind of charge carriers they can transport and the distinguishing molecular structure.

These two basic features are related to each other mainly by the fact that the charge transport depends both on the chemical bonds configuration and the molecular orbitals structure; electric device performances are then the macroscopic effects generated by the sum of the indivisible quantum-mechanical and chemical contributions.

After having analyzed the difference between holes and electrons transport, the second part of this Chapter is focused on a quick review on the mainstream semiconductors, whose most important families are discussed basically categorizing them on molecular structure and on chemical nature.

This is not intended to be an exhaustive essay on organic semiconductors: it is only a mere summary on the principal materials used to fabricate OFET devices.

2.1 Classification by charge transport

In semiconductor field of study the charge transport is made by two kind of carriers: electrons and holes.

Electrons are negative-charged particles, while holes are defined as the vacant positions left by moving electrons: since they are generated by negative charge absence holes are considered positive charges and, due the fact they are related to *fermions* particles, they are considered as *quasiparticles* in order to simplify the mathematic treatment [1].

An hole and an electron have thus the same mass and opposite electric charges. Both electron and holes undergo the Fermi-Dirac distribution [2], which describes a distribution of particles over energy states in systems consisting of many identical particles that obey the Pauli exclusion principle, having half-integer spin number and negligible mutual interactions. Assuming the thermodynamic equilibrium conditions, the ratio between an excited state population (N_i) and the ground state total population (N_0) is defined in Equation 2.1:

$$N(E) = \frac{N_i}{N_0} = \frac{1}{1 + e^{[(E - \mu) / (k_B T)]}}$$

Equation 2.1: Fermi-Dirac distribution function [3]; E is the system energy being the same for every particle, and μ is the total chemical potential.

For electron and holes in a semiconductor, the total chemical potential is identical with the so-called *Fermi level* (E_F) [4]; E_F represents the energy at which the probability that a given energy level is occupied is exactly equal to 50 % [5].

Fermi-Dirac distribution is exclusively temperature dependent and it contains the quantum restrictions apt for charge carriers mathematic treatment.

The normalized ($N_0 = 1$) Fermi-Dirac function is shown in Figure 2.1 , plotted for different temperatures. At absolute zero temperature the distribution reduces to a

completely degenerate function, thus to a square distribution, and consequently the energy states below the *Fermi level* have an occupation number equal to 1, while those above it have essentially zero probabilities to be occupied [6].

Fermi level is the inflection point of all the slopes associated to non-zero temperatures; when $(E - E_F) \gg k_B T$ then $N_i \rightarrow 0$ and by reverse $N_i \rightarrow 1$ when $(E_F - E) \gg k_B T$.

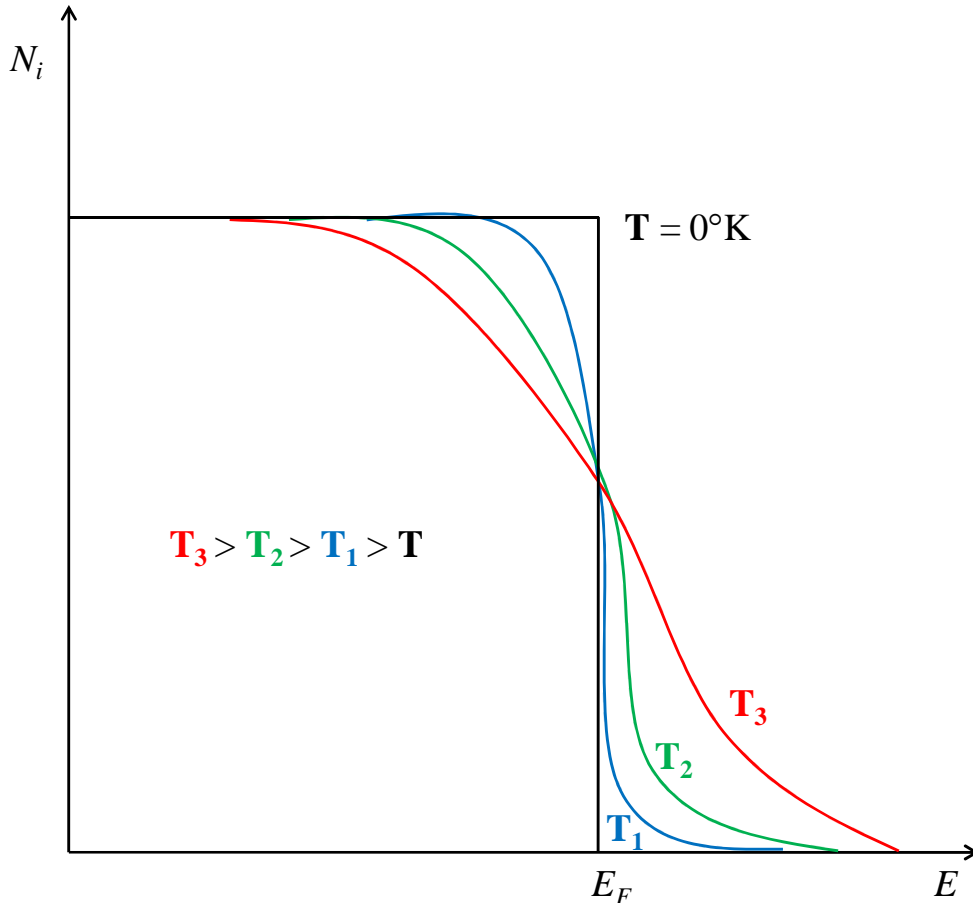


Figure 2.1: qualitative representation of the Fermi-Dirac function at different temperatures.

Fermi-Dirac distribution goes over the classical Boltzmann-Maxwell thermodynamic distribution every time $E \gg E_F$ or $k_B T \gg E_F$: at those conditions the exponential term in the Fermi-Dirac function overwhelms the unit [7].

Since the charge transport in organic semiconductors has been discussed in Chapter 1 with the Tight Binding theory, it necessary to explain how the Fermi-Dirac distribution matches with the electronic bands in order to show the difference between the *p*-type and *n*-type conduction.

After having discussed the population distribution function ($N(E)$, see Equation 2.1), an energy states density function $\rho(E)$ is needed to be defined [8], in order to calculate the particles concentration function, which is

$$n(E) = N(E) \cdot \rho(E) .$$

$$\rho(E) = \frac{4\pi (2me \cdot 10^7)^{3/2}}{h^3} \sqrt{E}$$

Equation 2.2: energy states density function; m is the electron mass, e is the electron charge and E is the system energy.

The product between Equations 2.1 and 2.2 gives the particles concentration function, defined as:

$$n(E) = \frac{(4\pi / h^3) (2me \cdot 10^7)^{3/2} \sqrt{E}}{1 + e^{[(E - E_F) / (k_B T)]}}$$

Equation 2.3: particles concentration function for any semiconductor; the factor $(4\pi / h^3) (2me \cdot 10^7)^{3/2}$ is equal to $6.82 \cdot 10^{21}$ particles / $(\text{cm}^3 \text{ eV}^{3/2})$.

Organic semiconductors are intrinsic ones since no doping or impurities are inoculated into them; thus the concentrations of negative (electrons, $n_n(E)$) and positive (holes, $n_p(E)$) charge carriers are equal.

In the following discussion E_C represents the Conduction Band bottom energy and E_V is the Valence Band top energy.

$$n_n(E) = \frac{(4\pi / h^3) (2me \cdot 10^7)^{3/2} \sqrt{E}}{1 + e^{[(E_C - E_F) / (k_B T)]}} \quad \text{(a)}$$

$$n_p(E) = \frac{(4\pi / h^3) (2me \cdot 10^7)^{3/2} \sqrt{E}}{1 + e^{[(E_F - E_V) / (k_B T)]}} \quad \text{(b)}$$

Equation 2.4: particles concentration functions for electrons (a) and holes (b), calculated according with Equation 2.3 .

Since $n_n(E) = n_p(E)$, we have to impose $(E_C - E_F) = (E_F - E_V)$ from which $E_F = (E_C + E_V) / 2$; intrinsic semiconductor *Fermi level* is halfway in the forbidden zone, equidistant from the top of the Valence Band and the bottom of the Conduction Band [9].

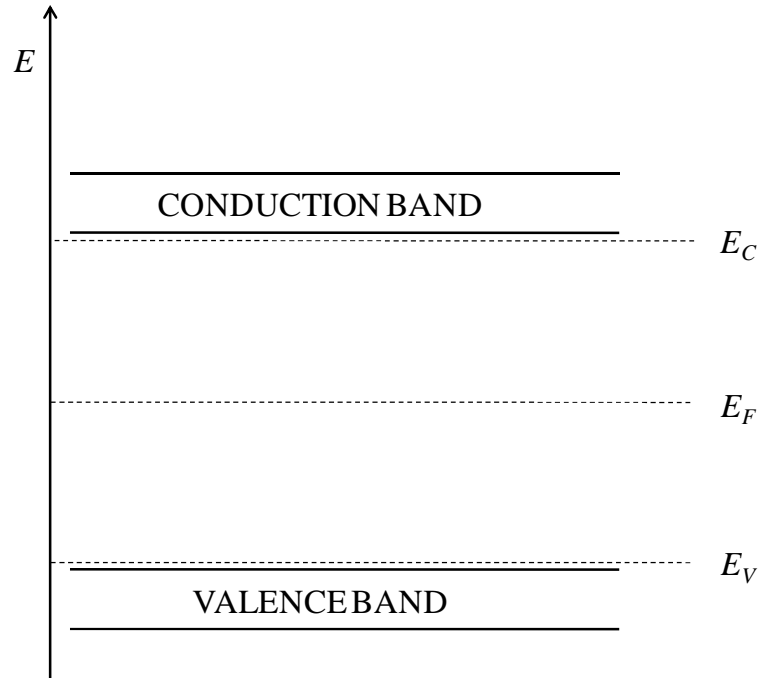


Figure 2.2: electronic bands and energy levels in a ideal organic semiconductor
 Now let's consider an OFET architecture (see Figure 2.3) which will be discussed in Chapter 3: if there is no voltage applied to the Gate electrode, the organic intrinsic semiconductor is undoped so it will not show any charge carriers: direct injection from the Source and Drain electrodes is the only way to create flowing current, which will be relatively small due to high resistance of the organic semiconductor and large distance between the electrodes [10].

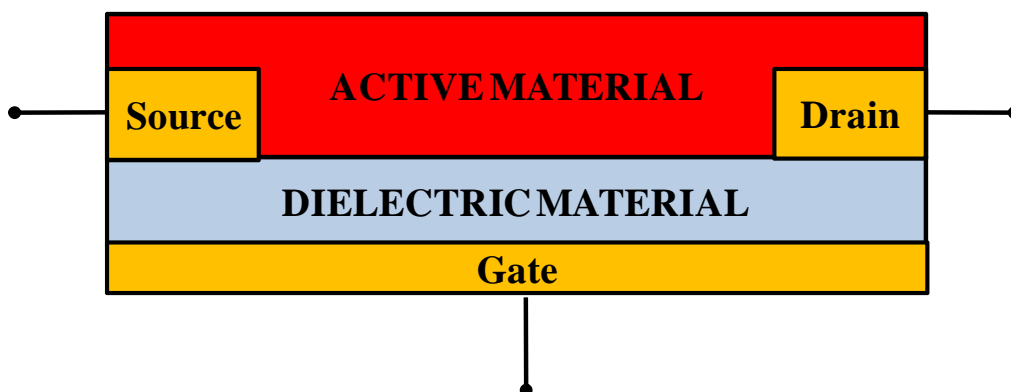


Figure 2.3: OFET architecture simplified scheme.

If a positive voltage was applied to the Gate electrode an ideal organic semiconductor would transport electrons, as well as it would make holes flow if the Gate voltage was switched to negative values.

Real organic semiconductors molecules have structures which allow the orbitals to interact and to combine with each others: since every energy level contains numbers of vibrational and rotational levels, the interaction between charges is far from being strictly like the one described by quantum theory. Furthermore, molecules packing during crystals growth and the chemical bonds rotations contribute to shift the discussed energy levels and to bend or even to warp the Electronic Bands.

These are the reasons why a real organic semiconductors often shows different mobilities for the two types of charge carriers: they are thus divided between n -type

and p -type semiconductive materials. In some organic semiconductors, both electrons and holes can be transported, an effect known as *ambipolarity*.

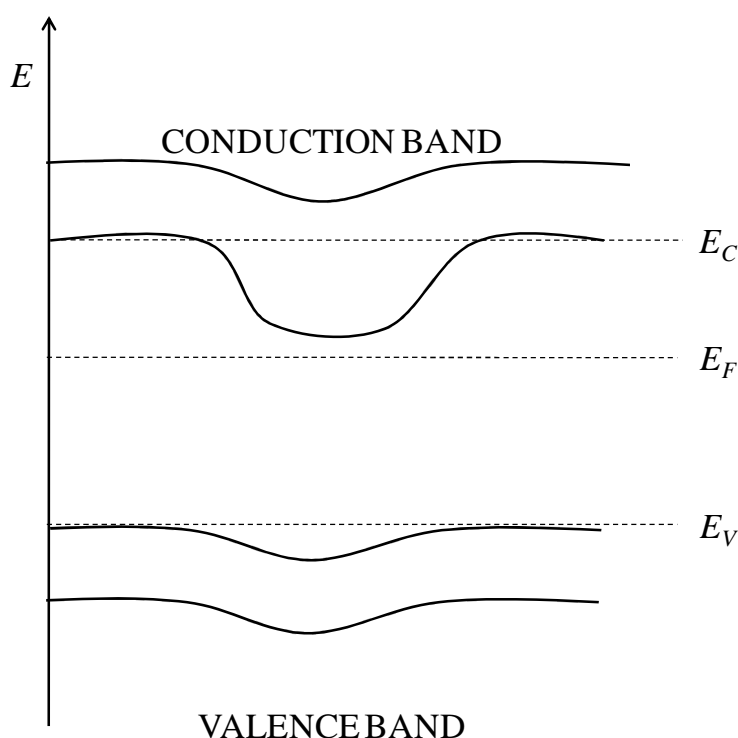


Figure 2.4: real n -type semiconductor warped electronic bands and energy levels positions; qualitative representation.

Charge transport in a n -type semiconductor is made by electrons; the semiconductor shows the Conduction and the Valence Bands warped downwards allowing the existence of electronic levels in the energy gap forbidden zone; the *Fermi level* is shifted near the Conduction Band projection in the forbidden zone and, since $k_B T \gg E_F$ in normal working conditions, it can be even located inside the band.

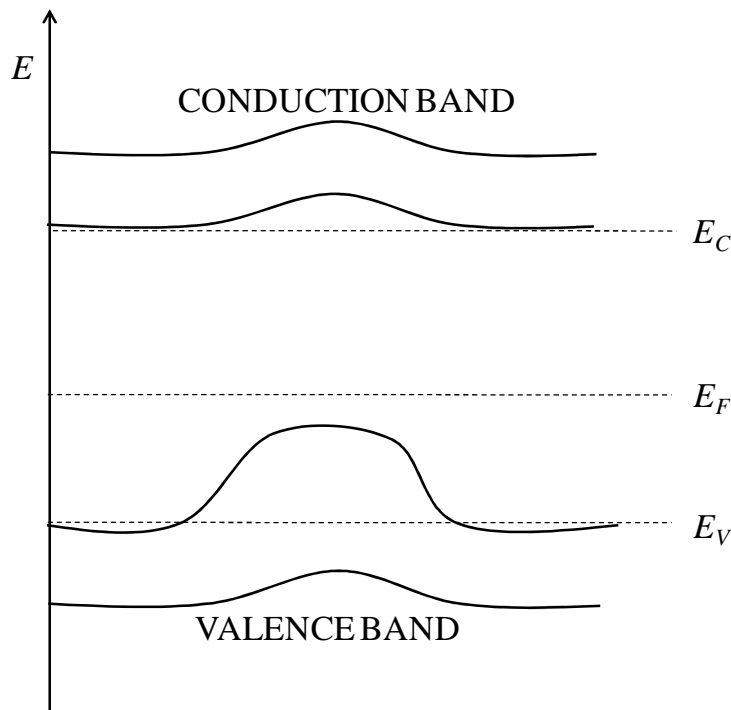


Figure 2.5: real p -type semiconductor warped electronic bands and energy levels positions; qualitative representation.

Charge transport in a p -type semiconductor is made by holes; the semiconductor shows the Conduction and the Valence Bands warped upwards allowing the existence of electronic levels in the energy gap forbidden zone; the *Fermi level* is shifted near the Valence Band projection in the forbidden zone and, since $k_B T \gg E_F$ in normal working conditions, it can be even located inside the band.

2.2 Classification by molecular structure

2.2.1 *n*-type semiconductors

In this class of materials it is possible to find molecules whose ionization potentials match quite well with the work functions of typical metals used as source and drain electrodes, like Gold or Silver; *n*-type semiconductors can also have the electrons injection facilitated by low-workfunction metals like Calcium and Aluminum [11]. In order to shrink the gap between the *Fermi level* and the LUMO band (Conduction Band), strong electron-withdrawing groups are often added to the molecular structure through synthetic design: those groups stabilize the molecule anionic form, increasing the electron affinity and thus making efficient the charge injection and transport [12]. Due to their anionic working behavior, *n*-type semiconductors show great reactivity especially with oxygen and atmospheric moisture [13].

- Fullerenes

Due to their isotropic charge transport, Fullerenes have been studied since the beginning of organic semiconductor electronics. A C₆₀ and C₉₀ 9:1 blend was tested as Field-Effect Transistor active layer [14], showing a charge mobility of $5 \cdot 10^{-4} \text{ cm}^2 / (\text{V s})$; polycrystalline C₆₀ films brought then to a mobility of $0.08 \text{ cm}^2 / (\text{V s})$ [15] and giving the chance to be restored by annealing treatment after the degradation due to ambient exposure [16]. Soluble methano-fullerenes have also been synthesized in order to use Fullerene (see Figure 2.6a) derivatives in solution-deposition techniques: the most widely used is PCBM [17] ([6,6]-Phenyl C61-butyric acid methyl ester, see Figure 2.6b), that is commercially available. Functional groups were then added to Fullerene structure in order to obtain a Dendron architecture, with field-effect mobility reaching $1.7 \cdot 10^{-3} \text{ cm}^2 / (\text{V s})$ [18].

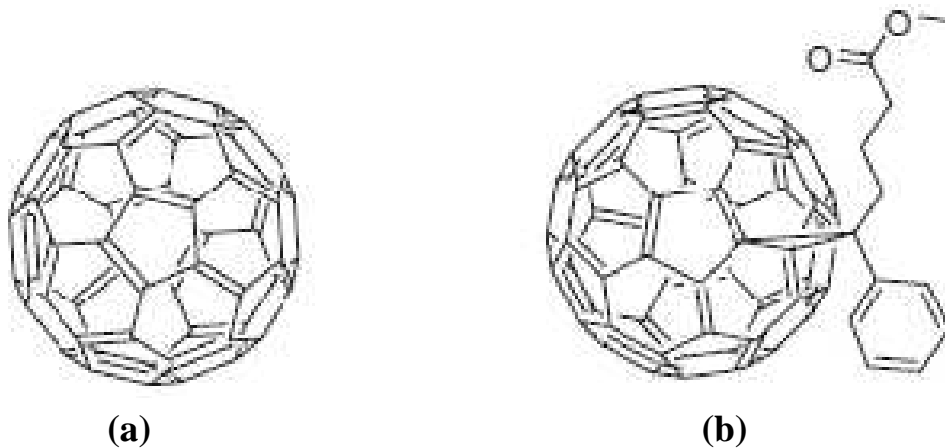


Figure 2.6: Fullerene (a) and PCBM (b) structures [19].

- Phthalocyanines

Unsubstituted Phthalocyanines, which usually present a *p*-channel mobilities, can change their charge carriers type by adding electron withdrawing groups at their periphery; for example hexadecafluoro-substituted Copper Phthalocyanine (see Figure 2.7a) shows mobility increased as high as $0.03 \text{ cm}^2 / (\text{V s})$, with good stability even under ambient conditions [20]. Changing the functional groups added to Phthalocyanine core brings to different crystal morphology and different grain size of the films, thus to different mobility values [21].

Water soluble Copper Phthalocyanines, carrying with sulfonic acid (see Figure 2.7b) or methyl-pyridinium groups, present ambipolar mobility while Drain-Source currents increase non-linearly with increasing V_{DS} at a given Gate potential; furthermore, the entire set of I-V curves shifts up with repeated scans while the ON/OFF decreases [22].

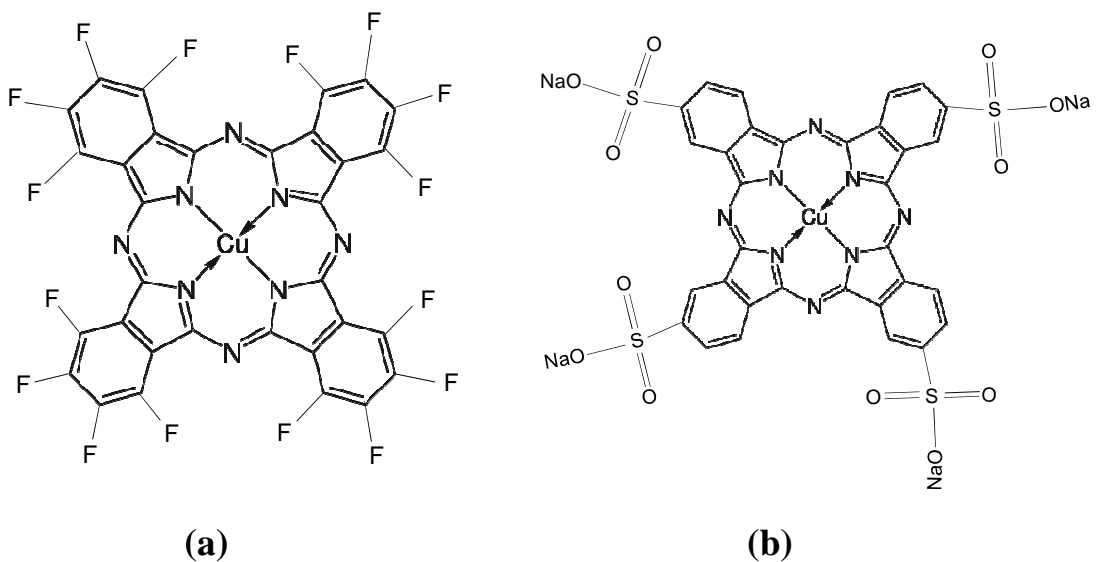


Figure 2.7: hexadecafluoro-substituted Copper Phthalocyanine (a) and water soluble Copper Phthalocyanine with sulfonic groups (b) structures.

- Naphthalene derivatives

Naphthalene tetracarboxylic dianhydride (NTCDA, see Figure 2.8a) and other imide derivatives are synthesized from commercial materials. Measured under vacuum conditions the NTCDA deposited at a substrate temperature of 25°C shows a mobility of about $1 \cdot 10^{-4} \text{ cm}^2 / (\text{V s})$; when the same material is deposited at a substrate temperature of 55°C, mobility increases to $3 \cdot 10^{-3} \text{ cm}^2 / (\text{V s})$ but it is very sensible to air exposure [23]. Adding alkyl groups to Naphthalene tetracarboxylic diimide (NTCDI, see Figure 2.8b) brings to mobilities which become lower as the alkyl chains length increases. Stability under ambient condition can be given to NTCDI by fluoro-alkyl groups on the side chains, obtaining mobilities as high as $0.03\text{-}0.06 \text{ cm}^2 / (\text{V s})$ [24]. Solid state packing effects play a major role in explaining the stability of Naphthalene derivatives: close-packing nature of fluorinated side chains provide a kinetic barrier to oxidation [25].

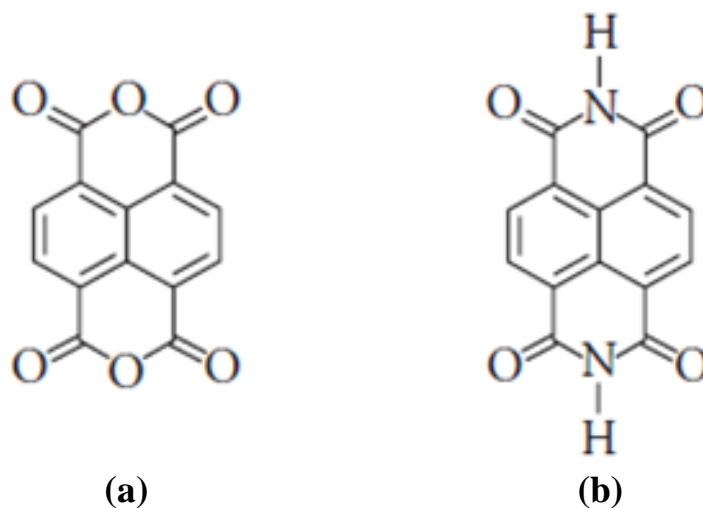


Figure 2.8: NTCDA (a) and NTCDI (b) structures.

- Perylene derivatives

Perylene (see Figure 2.9a) has been employed as the active-layer in OFETs, exhibiting low *p*-channel mobilities and no *n*-channel mobility [26]. Dianhydride and diimide derivatives of Perylene have also been studied, showing a *n*-channel mobility of about $1 \cdot 10^{-4} \text{ cm}^2 / (\text{V s})$ like Perylene tetracarboxylic dianhydride (PTCDA, see Figure 2.9b) [27].

The Perylene tetracarboxylic diimides (PTCDI, see Figure 2.9c) are easily synthesized in order to obtain energy levels of alkyl substituted diimides similar to unsubstituted versions (3.4 eV and 5.4 eV for electrons and holes referenced to vacuum level) [28]. PTCDI substituted with octyl sidechains shows the highest mobility for a Perylene derivative, reaching a value of $1.3 \text{ cm}^2 / (\text{V s})$ under vacuum; pentyl and dodecyl sidechains substituents bring instead to mobilities of 0.06 and $0.5 \text{ cm}^2 / (\text{V s})$ respectively [29]. Thin films of these derivatives adopt a molecular packing comparable to the single-crystal structure. Furthermore, the molecules can pack with a face-to-face, slipped π -stacked structure with a minimum interplanar spacing of 3.4 Å [30].

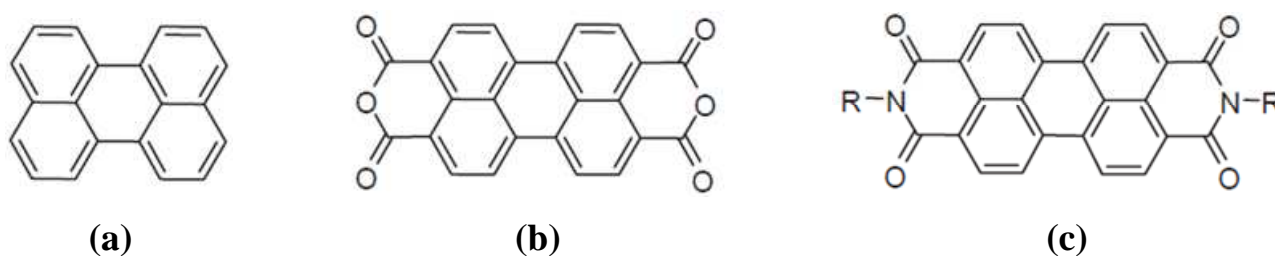


Figure 2.9: Perylene (a), PTCDA (b) and PTCDI (c) structures.

- Thiophene based oligomers

Perfluoroalkyl substitution has been widely performed on oligothiophenes [31], switching the charge transport from holes to electrons and then presenting a mobility of about $0.028 \text{ cm}^2 / (\text{V s})$ [32].

The influence of the halogenated substitutions on thiophene system exhibits a strong σ -inductive electron-withdrawing effect [33], as well as the carbonyl group that allows the possibility of further chemical functionalization and that makes mobility increase to $0.6 \text{ cm}^2 / (\text{V s})$ [34].

Perfluorophenyl group can be also attached to the sides of a quarterthiophene core showing poor ring conjugation within molecular structure and thus giving a mobility of $0.08 \text{ cm}^2 / (\text{V s})$ [35].

Thiophene oligomers can also incorporate Phenacyl groups in order to fabricate OFETs with electron mobilities as high as $0.45 \text{ cm}^2 / (\text{V s})$; these materials can be also cast from solution to fabricate devices with mobilities of $0.21 \text{ cm}^2 / (\text{V s})$ [36].

An *n*-channel perfluorinated version of pentacene has recently been synthesized: this compound adopts a herringbone geometry and shows a mobility of $0.11 \text{ cm}^2 / (\text{V s})$, allowing also the possibility to fabricate inverter circuits featuring pentacene as the *p*-channel semiconductor [37].

2.2.2 *p*-type semiconductors

- Aromatic hydrocarbons

Among the most widely studied organic *p*-type semiconductors particular attention has been paid to linear polycyclic aromatic hydrocarbons, which are π -functional materials composed of laterally fused benzene rings, called linear acenes or oligoacenes.

The HOMO energy level significantly increases with the number of rings, which facilitates the injection of holes at the interface between the Source and semiconductor layer under an applied Gate voltage; in addition the planar shape facilitates crystal packing and enhances the intermolecular overlap of π -systems [38].

Tetracene and Pentacene (see Figure 2.10a and 2.10b) are the most promising molecular semiconductors for OFETs.

Tetracene has a slightly high degree of conjugation: OFET devices fabricated from single crystals [39] of this molecule show a mobility of up to $1.3 \text{ cm}^2 / (\text{V s})$, whereas thin-films [40] yield a mobility of $0.1 \text{ cm}^2 / (\text{V s})$. Substitution of bromo or chloro groups on Tetracene lowers HOMO and LUMO levels: the halogen groups also promote cofacial π -stacking [41]. The halogenated derivatives differ in position of substitution providing a useful system to investigate the effect of molecular packing on charge transport: X-ray crystallography on single crystals showed that the number of halogen substitutions is a key parameter and can be used to control molecular packing [42]. The mono-substituted Tetracene derivatives are shown to pack in a herringbone fashion whereas the di-substituted analogues π -stack in a slipped face-to-face manner; mobilities range from $1.4 \cdot 10^{-4}$ to $1.6 \text{ cm}^2 / (\text{V s})$.

Pentacene is one of the most widely studied organic semiconductors. The highest thin-film mobilities have been recorded $0.3\text{--}0.7\text{ cm}^2 / (\text{V s})$ on SiO_2 / Si substrates, $1.5\text{ cm}^2 / (\text{V s})$ on chemically modified SiO_2 / Si substrates and $3\text{--}6\text{ cm}^2 / (\text{V s})$ on polymer Gate dielectrics [43].

An obvious advantage of substituted Pentacene is the improved solubility, which simplifies purification and transistor processing.

The mobility of can be further enhanced if the material is forced to pack in a face-to-face manner rather than the usually observed herringbone structure: thus methyl groups were introduced at the four terminal carbon atoms of Pentacene. Thin films of $\text{Me}_4\text{-Pentacene}$ (see Figure 2.10c) exhibit a mobility of $0.3\text{ cm}^2 / (\text{V s})$ [44] which can be improved by longer alkyl chains [45].

Bulky solubilizing trialkylsilyl groups have been substituted at the 6,13-positions of the Pentacene molecule in order to impart solubility and disrupt herringbone packing of Pentacene core; the functionalized derivatives are very soluble and can be crystallized from common organic solvents [46].

Triisopropylsilyl (TIPS) Pentacene (see Figure 2.10d) shows that the in a 2D columnar molecular array with significantly larger overlap of the aromatic rings compared to unsubstituted, herringbone-packed Pentacene; TIPS-Pentacene presents a mobility of $0.4\text{ cm}^2 / (\text{V s})$ [47].

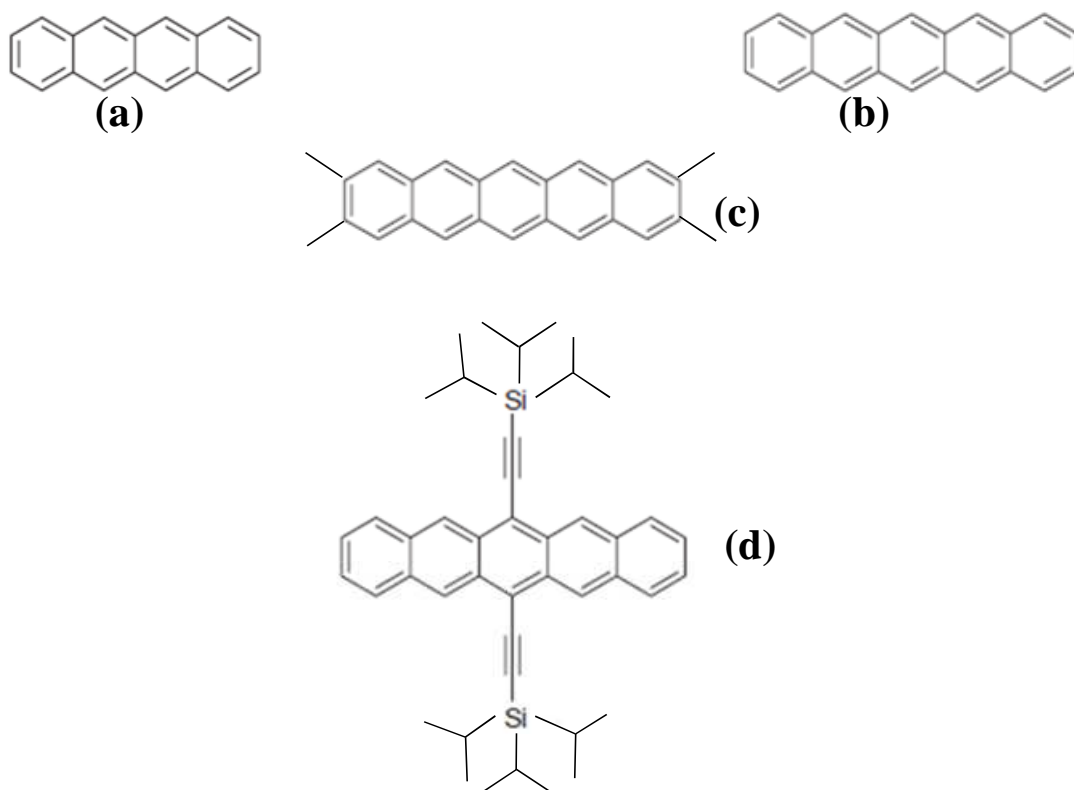


Figure 2.10: Tetracene (a), Pentacene (b), Me₄-Pentacene (c) and TIPS-Pentacene (d) structures.

- Heteroarenes

Heteroarenes are an interesting class of π -functional materials. Substitution of one of several carbon atoms in oligoacenes with a heteroatom such as nitrogen or sulphur in different valence state may induce unique properties in these π -electron systems, by the decrease of HOMO-LUMO gap [48].

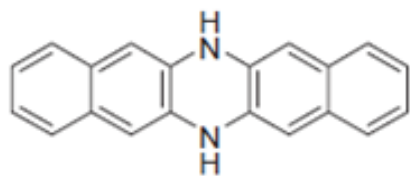
Dihydrodiazapentacene (see Figure 2.11a) derivatives have been synthesized with nitrogens replacing carbons in the phenyl rings of Pentacene in order to avoid oxidation, obtaining mobilities values from $5 \cdot 10^{-5}$ to $6 \cdot 10^{-3} \text{ cm}^2 / (\text{V s})$ [49].

Imidazolylquinoline (see Figure 2.11b) derivatives have also been tested in OFETs, showing mobilities of $0.093 \text{ cm}^2 / (\text{V s})$ [50].

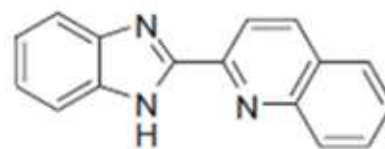
Bis(benzodithiophene) (see Figure 2.11c) was synthesized with an embedded benzenes fused-ring system in order to limit the conformational freedom and thereby reducing interrupted conjugation

that is possible in oligothiophenes [51]; this aromatic system was further extended to a fully fused-ring compound with dibenzo[b,b']thieno[2,3-f:5,4-f']benzothiophene (DBTBT, see Figure 2.11d), which has an extended π -conjugation and completely constrains conformational freedom, giving an hole mobility of $0.15 \text{ cm}^2 / (\text{V s})$ [52].

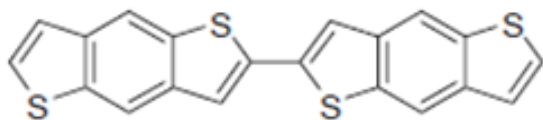
New semiconductors based on derivatives of a tertiary diamine structure (5,11-disubstituted indolo[3,2-b]carbazole, see Figure 2.11e) have been also studied: they are soluble in organic solvents such as toluene, chloroform, and chlorobenzene; these carbazole derivatives exhibit *p*-channel behavior with mobilities of up to $0.12 \text{ cm}^2 / (\text{V s})$ [53].



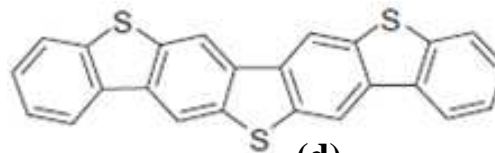
(a)



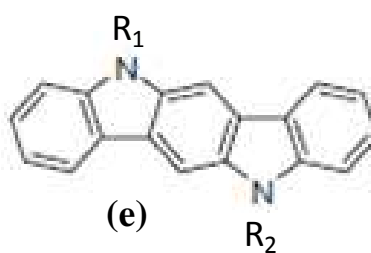
(b)



(c)



(d)



(e)

Figure 2.11: Dihydrodiazapentacene (a), Imidazolylquinoline (b), Bis(benzodithiophene) (c), DBTBT (d) and 5,11-disubstituted indolo[3,2-b]carbazole (e) structures.

- Thiophene based oligomers

Due to the synthetic versatility of the Thiophene heterocycle, oligothiophenes and their alkyl-substituents have been among the most intensely investigated organic semiconductors [54]. Because of their ease in functionalization, oligothiophenes provide the opportunity to study systematic variations in molecular structure by controlling the number of repeat units in the conjugated backbone or varying the length and

functionality of alkyl substituents.

One of the most widely studied oligothiophenes is α -sexithiophene (α -6T, see Figure 2.12a): through years its hole mobility has improved from $1 \cdot 10^{-4}$ to greater than $0.07 \text{ cm}^2 / (\text{V s})$ [55]. It has also been shown that the orientation and morphology of thermally evaporated thin films of α -6T depend strongly on the substrate temperature: increasing substrate temperature from -204°C to 280°C improves the thin-film morphology, making mobility increase from 0.006 to $0.025 \text{ cm}^2 / (\text{V s})$ [56]. Furthermore α -octithiophene (α -8T, see Figure 2.12b) charge mobilities are near $0.2 \text{ cm}^2 / (\text{V s})$ for OFETs with films deposited at a substrate temperatures of 150°C and higher [57].

Oligothiophenes are less soluble as conjugation length increase; this characteristic makes purification and deposition more difficult using traditional wet techniques, such as column chromatography and spin-coating [58].

One way to increase the solubility of oligothiophenes in organic solvents is to introduce alkyl substituents at the β -position of the thiophene ring: alkyl substitution results also in a remarkable improvement of the structural organization of molecules thus creating highly ordered thin films, resulting in enhanced mobilities [59].

The self-organization induced by the alkyl groups results in a preferred orientation of the substituted oligomers, with their long molecular axes roughly perpendicular to the substrate plane, leading to an order of magnitude increase in mobility from about 0.01 to $0.13 \text{ cm}^2 / (\text{V s})$ [60].

Since very low mobilities are observed for thin films that exhibited poor structural order, the positions of the alkyl chains on the conjugated backbone are also important; it was also found that OFET performance depends critically on the length of the side chains, but is relatively insensitive to the length of the conjugated backbone [61].

In addition to linear alkyl chains, cyclohexyl groups have also been attached as side substituents: although slightly bulkier, the thin films of dicyclohexyl-quarterthiophene (see Figure 2.12c) show mobility of $0.038 \text{ cm}^2 / (\text{V s})$ [62], higher than that of the dihexyl-substituted compound. Other polar species, such as phosphonate groups, have also been incorporated as end-substituents and used in OFETs with spin-cast films, presenting a mobility of $4.9 \cdot 10^{-3} \text{ cm}^2 / (\text{V s})$ [63].

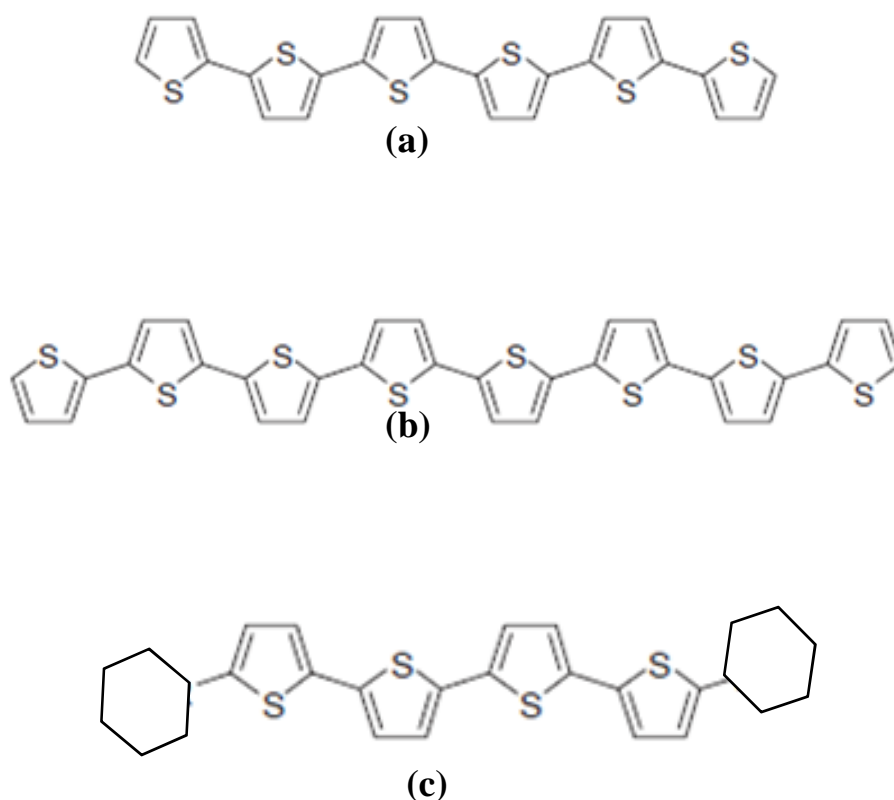


Figure 2.12: α -sexithiophene (a), α -octithiophene (b) and dicyclohexyl-quarterthiophene (c) structures.

REFERENCES

- [1] A. A. Abrikosov, L. P. Gor'kov, and I. E. Dzyaloshinski, *Methods of Quantum Field Theory in Statistical Physics* (**1963, 1975**). Prentice-Hall, New Jersey; Dover Publications, New York;
- [2] C. Kittel, *Introduction to Solid State Physics* (4th ed.) (**1971**), New York, John Wiley & Sons;
- [3] F. Gutmann, L. E. Lyons; *Organic Semiconductors*, John Wiley & Sons;
- [4] J. S. Blakemore, *Semiconductor Statistics*, (**2002**), Dover;
- [5] F. Gutmann, L. E. Lyons; *Organic Semiconductors*, John Wiley & Sons;
- [6] C. Kittel, *Introduction to Solid State Physics* (4th ed.) (**1971**), New York, John Wiley & Sons;
- [7] F. Gutmann, L. E. Lyons; *Organic Semiconductors*, John Wiley & Sons;
- [8] F. Gutmann, L. E. Lyons; *Organic Semiconductors*, John Wiley & Sons;
- [9] A. F. Ioffe, *Physics of Semiconductor*, Academic Press, New York, **1960**;
- [10] Th. B. Singh , N. S.Sariciftci, M, Jaiswal, R. Menon, *Organic Field-Effect Transistors: From Materials to Device Physics*, Chapter of *Handbook of Organic Electronics and Photonics*, Edited by Hari Singh Nalwa Volume 3: Page 153;
- [11] C. R. Newman et al., *Chem. Mater.*, 16 (23), 4436-4451, **2004** ;
- [12] L. L. Chua et al., *Nature*, 434 (7030), 194-199, **2005**;
- [13] Z. Bao, J. Locklin, *Organic Field-Effect Transistors*, 2007, CRC Press;
- [14] J. Kastner, J.P., H. Kuzmany, *Fullerene field-effect transistors*, in *Electronic Properties of High-Tc superconductors*, H. Kuzmany, M. M., J. Fink Springer-Verlag, Berlin, **1993**, pp. 512-515;
- [15] R. C. Haddon et al., *Appl. Phys. Lett.* 67 (1), 121-123, **1995** ;
- [16] S. Kobayashi et al., *Appl. Phys. Lett.* 82 (25), 4581-4583, **2003**;
- [17] E. J. Meijer et al., *Nat. Mater.*, 2 (10), 678-682, **2003**;
- [18] H. Kusai et al., *Appl. Phys. Lett.*, 88 (17), **2006**;
- [19] Z. Bao, J. Locklin, *Organic Field-Effect Transistors*, **2007**, CRC Press;

- [20] Z. A. Bao, A.J. Lovinger, J. Brown, *J. Am. Chem. Soc.*, 120 (1), 207-208, **1998**;
- [21] Z. Bao, J. Locklin, *Organic Field-Effect Transistors*, **2007**, CRC Press;
- [22] J. Locklin et al., *Chem. Mater.*, 15 (7), 1404-1412, **2003**;
- [23] J.G. Laquindanum et al., *J. Am. Chem. Soc.*, 118 (45), 11331-11332, **1996**;
- [24] H. E. Katz et al., *Nature*, 404 (6777), 478-481, **2000**;
- [25] H. E. Katz et al., *Chem. Lett.*, 32 (6), 508-509, **2003**;
- [26] J. L. Bredas et al., *Proc. Natl. Acad. Sci.*, 99 (9), 5804-5809, **2002**;
- [27] J. R. Ostrick et al., *J. Appl. Phys.* 81(10), 6804-6808, **1997** ;
- [28] M. Hiramoto et al., *J. Appl. Phys.*, 78 (12), 7153-7157, **1995**;
- [29] R. J. Chesterfield et al., *J. Phys.Chem.*, B 108 (50), 19281-19292, **2004**;
- [30] Z. Bao, J. Locklin, *Organic Field-Effect Transistors*, **2007**, CRC Press;
- [31] A. Facchetti et al., *Angew. Chem. Int. Ed.*, 39 (24), 4547, **2000**;
- [32] A. Facchetti et al., *Chem. Mater.*, 16 (23), 4715-4727, **2004**;
- [33] Z. Bao, J. Locklin, *Organic Field-Effect Transistors*, **2007**, CRC Press;
- [34] M. H. Yoon et al., *J. Am. Chem. Soc.*, 127 (5), 1348-1349, **2005**;
- [35] A. Facchetti et al., *Angew. Chem.-Int. Edit.* 42 (33), 3900-3903, **2003**;
- [36] Letizia, J.A. et al., *J. Am. Chem. Soc.* 127 (39), 13476-13477, **2005**;
- [37] Y. Sakamoto et al., *J. Am. Chem. Soc.*, 126 (26), 8138-8140, **2004**;
- [38] Z. Bao, J. Locklin, *Organic Field-Effect Transistors*, **2007**, CRC Press;
- [39] C. Goldmann et al., *J. Appl. Phys.*, 96 (4), 2080-2086, **2004**;
- [40] D. J. Gundlach et al., *Appl. Phys. Lett.*, 80 (16), 2925-2927, **2002**;
- [41] J. A. R. P. Sarma and G. R. Desiraju, *Acc. Chem. Res.*, 19 (7), 222-228, **1986**;
- [42] H. Moon et al., *J. Am. Chem. Soc.*, 126 (47), 15322-15323, **2004**;
- [43] Y. Y. Lin et al., *IEEE Trans. Elect. Dev.*, 44 (8), 1325-1331, **1997**;
- [44] H. Meng et al., *Adv. Mater.*, 15 (13), 1090, **2003**;
- [45] T. P. Smith, D. E. Vogel, K. M. Vogel, *Preparation of dialkylpentacenes as semiconductor materials*, **2003**;
- [46] J. E. Anthony et al., *J. Am. Chem. Soc.*, 123 (38), 9482-9483, **2001**;
- [47] C. D. Sheraw et al, *Adv. Mater.*, 15 (23), 2009-2011, **2003**;

- [48] Z. Bao, J. Locklin, *Organic Field-Effect Transistors*, **2007**, CRC Press;
- [49] Q. Miao et al., *J. Am. Chem. Soc.* 125 (34), 10284-10287, **2003**;
- [50] T. R. Chen, A. Yeh, J. D. Chen, *Tet. Lett.*, 46, 1569-1571, **2005**;
- [51] J. G. Laquindanum et al., *Adv. Mater.*, 9 (1), 36-39, **1997**;
- [52] H. Sirringhaus et al., *J. Mater. Chem.*, 9, 2095-2101, **1999**;
- [53] Wakim, S. et al., *Chem. Mater.* 16 (23), 4386-4388, **2004**;
- [54] Y. Sakamoto et al., *J. Am. Chem. Soc.* 126 (26), 8138-8140, **2004**;
- [55] M. Halik et al., *Adv. Mater.*, 15 (11), 917, **2003**;
- [56] F. Garnier et al., *J. Am. Chem. Soc.*, 115 (19), 8716-8721, **1993**;
- [57] M. Halik et al., *Adv. Mater.*, 15 (11), 917, **2003**;
- [58] Z. Bao, J. Locklin, *Organic Field-Effect Transistors*, **2007**, CRC Press;
- [59] Z. Bao, J. Locklin, *Organic Field-Effect Transistors*, **2007**, CRC Press;
- [60] C. D. Dimitrakopoulos et al., *Synth. Met.*, 92 (1), 47-52, **1998**;
- [61] R. Hajlaoui et al., *Adv. Mater.*, 9 (7), 557, **1997**;
- [62] J. Locklin et al., *Chem. Mater.*, 17 (13), 3366-3374, **2005**;
- [63] A. Afzali, T. L. Breen, C. R. Kagan, *Chem. Mater.*, 14 (4), 1742-1746, **2002**;

CHAPTER 3

OFET DEVICE PHYSISCS

Organic Field-Effect Transistors (OFETs), developed for the first time by Tsumura and coworkers in 1986 [1], have received greater focus attention through years due to their potential applications in integrated circuits for large-area, flexible, and ultralow-cost electronics. The performances of OFETs have been improved immensely over the past decades, meaning high charge carrier mobilities, large ON/OFF ratios, and low threshold voltages.

A simplified structure of a *common Source* biased OFET is reported in Figure 3.1 : the device architecture shown is very useful to easily understand the device physics and it will be discussed later in this Chapter.

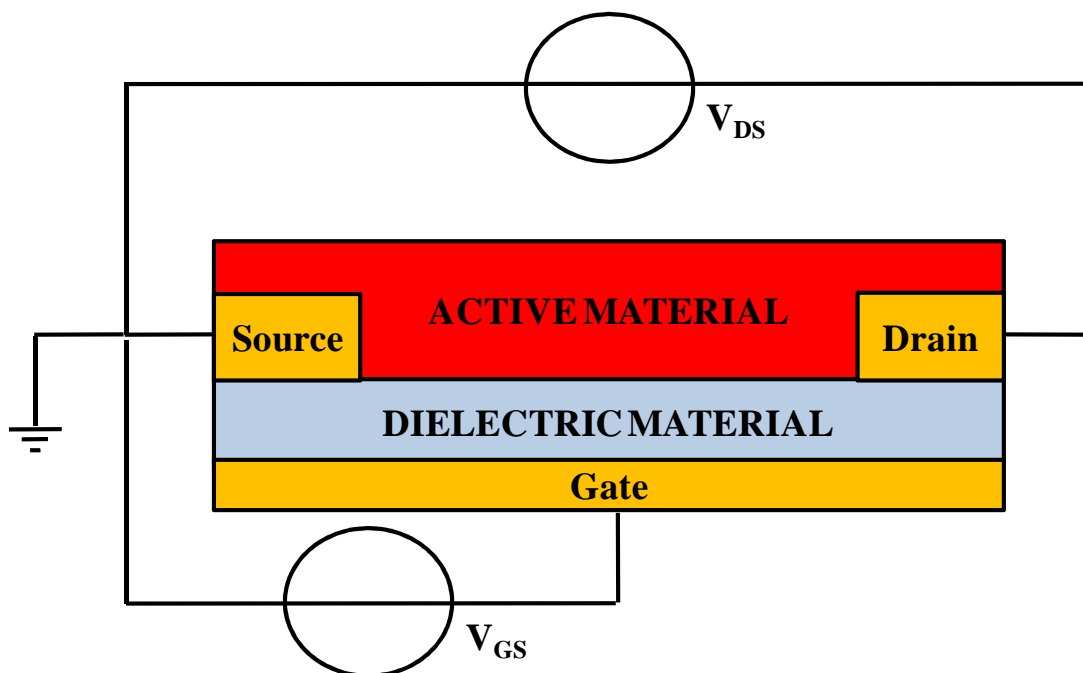


Figure 3.1: OFET architecture with *common Source* biasing.

When a potential difference (V_{DS}) is applied between Source and Drain electrodes, charges are injected from Source metal contact into the active material. The injection goes on until the electric field generated by charge accumulation matches the

transversal one applied between Source and Drain; this happens within nanometers from the electrodes.

Due to the fact it is applied on the full device length, only the Gate voltage (calculated as the potential difference V_{GS} between Gate and Source) can allow the charge carriers to move from Source to Drain, thus opening the *conduction channel*. The dielectric material is thereby an insulator which is polarized by the Gate potential, allowing the polarization of the active material and avoiding short-circuit effects between Gate and the other two electrodes. The minimum V_{GS} that is needed to create a conducting path between the Source and Drain terminals is called *threshold voltage* (V_{TH}).

Charge transport is tunable by sweeping V_{GS} values, defining the OFET working regime.

When $|V_{GS}| \ll |V_{TH}|$ (see Figure 3.2a) the device works as a capacitor: charges gather near the Gate side and no current is measured (*cut-off regime*).

V_{GS} increase brings to the *depletion regime* (see Figure 3.2b): while V_{GS} becomes comparable with V_{TH} , the capacitor gets discharged until its plates swap their polarities after having passed through neutrality. Despite the current between Drain and Source should ideally be zero when the transistor is being used as a turned-off switch, there is a weak-inversion current sometimes called *subthreshold leakage*.

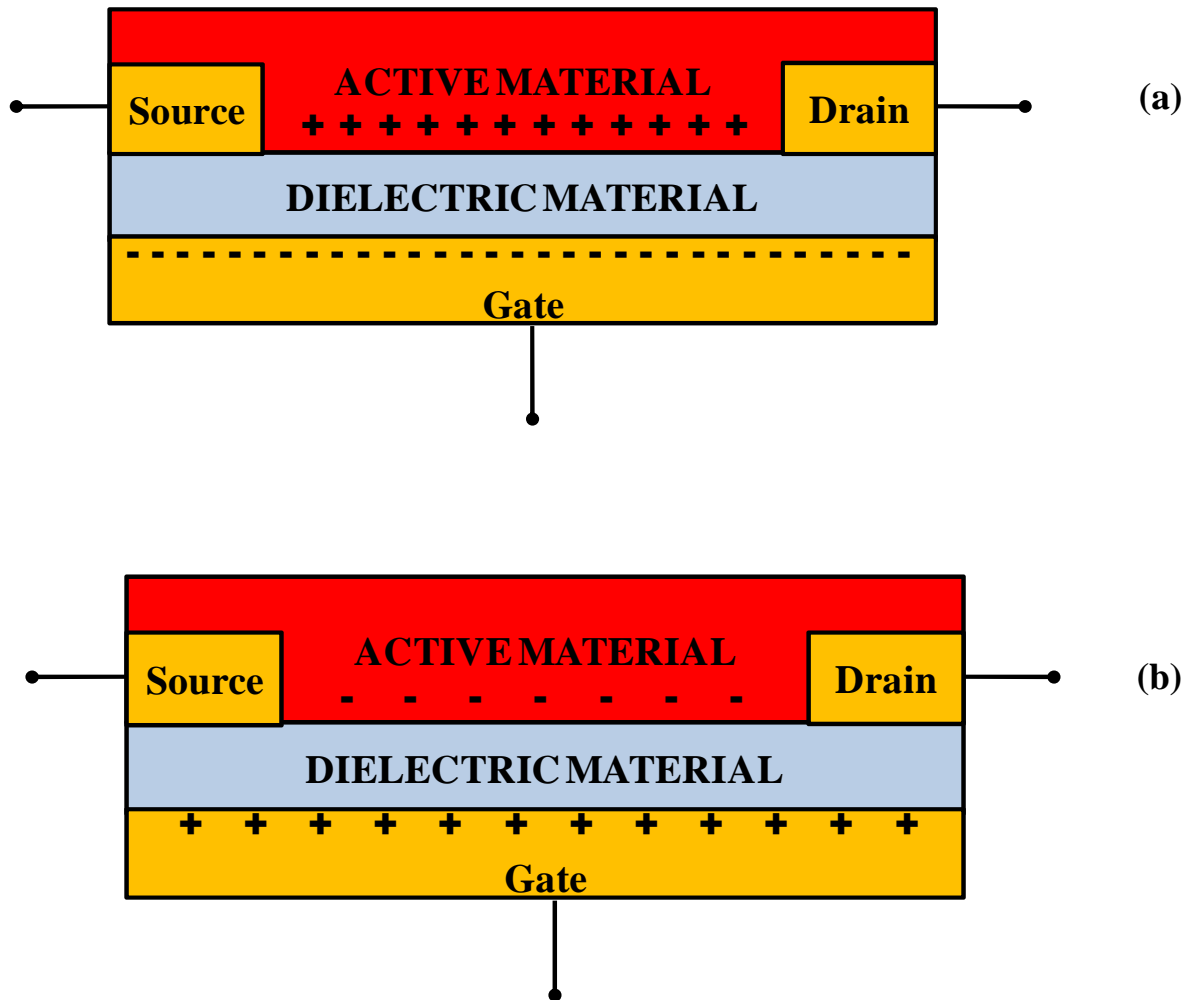


Figure 3.2: electric charges in OFET device biased in cut-off mode (a) and in depletion mode (b); these examples refer to a *n*-type active material.

OFET starts working as a transistor when the conduction channel is opened by the reaching of the *inversion regime*, thus when $|V_{GS}| \geq |V_{TH}|$.

Charge density increases in the active material layer bulk and the carriers begin to flow from Source to Drain (the measured electric current is I_{DS}).

When $|V_{GS}| \geq |V_{TH}|$ and $|V_{DS}| < |V_{GS} - V_{TH}|$, the device is considered to be in *ohmic inversion regime* (see Figure 3.3), since the resistance is proportional to the charge density generated next to the Gate side.

The OFET operates like a resistor controlled by the Gate voltage.

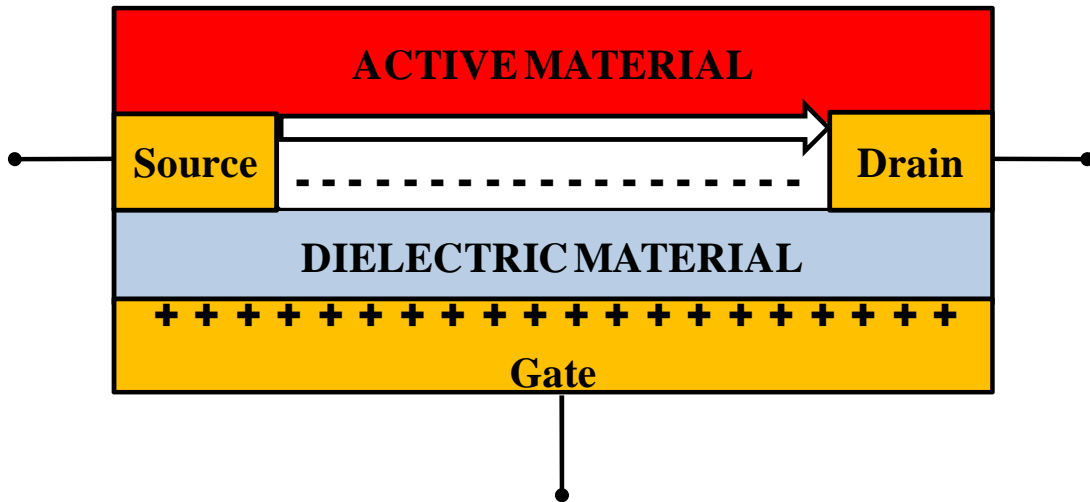


Figure 3.3: OFET ohmic inversion regime for a n -type semiconductor.

When $|V_{GS}| \geq |V_{TH}|$ and $|V_{DS}| \geq |V_{GS} - V_{TH}|$, the device is considered to be in *saturation inversion regime* (see Figure 3.4), since the Gate voltage is no more able to generate the electric field necessary to avoid the channel warping near the Drain terminal, where V_{DS} counter-effect is dramatic. The charges spread out and conduction is not through a narrow channel but through a broader, two- or three-dimensional current distribution extending away from the interface and deeper in the substrate: the lack of channel region near the Drain is also known as *pinch-off*. Now I_{DS} is weakly dependent upon V_{DS} and it is primarily controlled by V_{GS} .

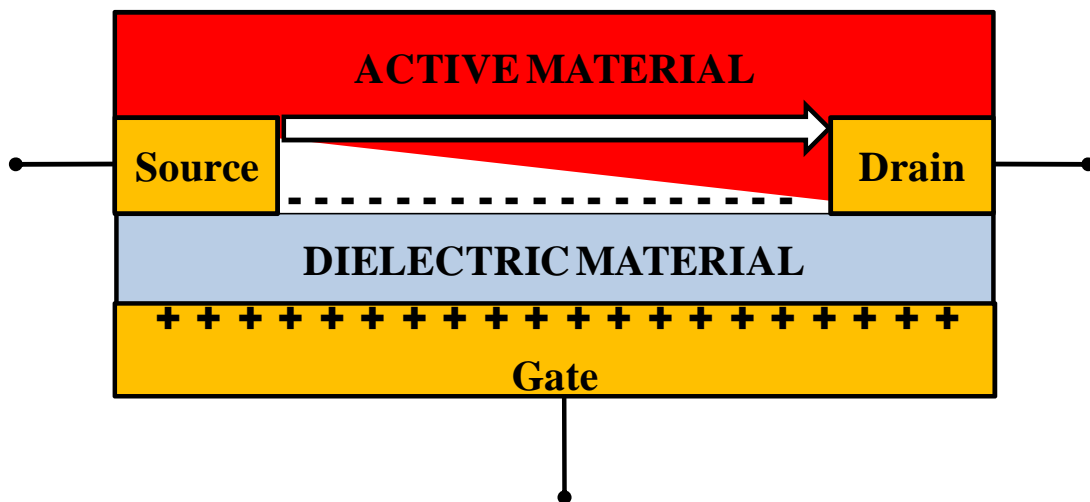


Figure 3.4: OFET saturation inversion regime for a n -type semiconductor.

In Organic Field-Effect Transistors the current-voltage relationship at Source-Drain pair of terminals depends on voltage (or sometimes on current) applied on the Gate terminal; this is usually displayed on a more complex current–voltage graph with multiple curves (see Figure 3.5), each one representing the $I_{DS} - V_{DS}$ relationship at a different value of V_{GS} .

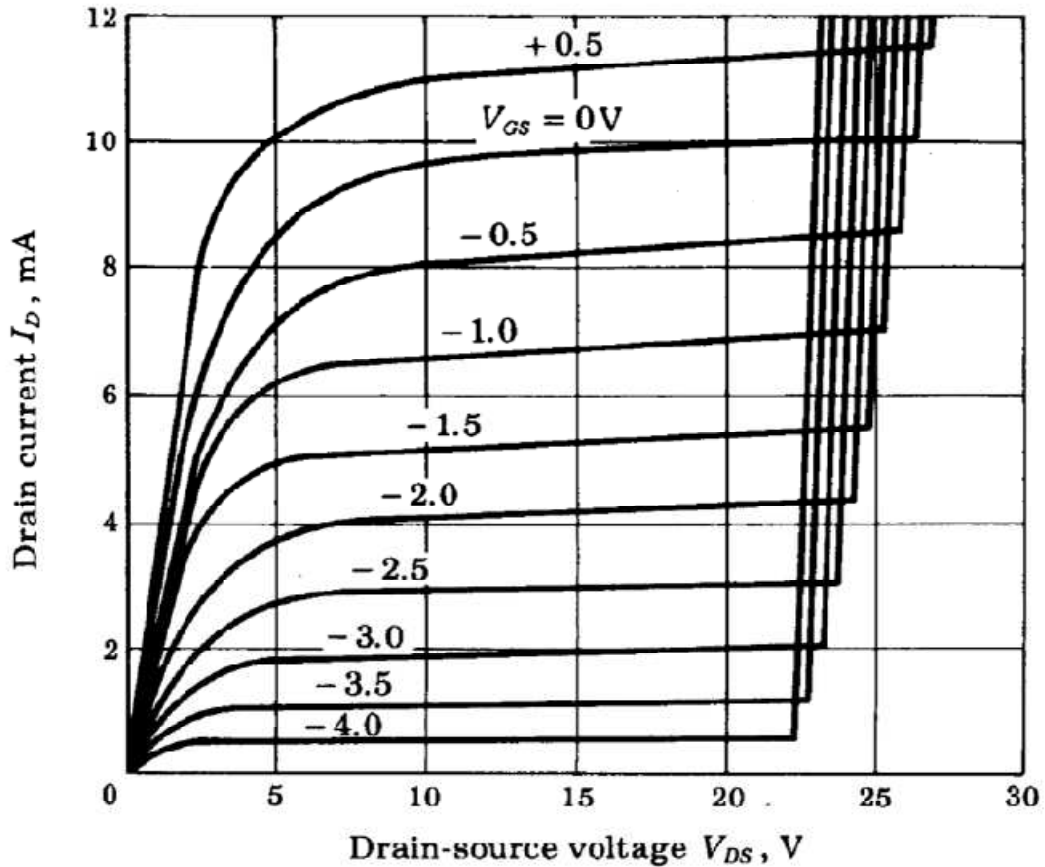


Figure 3.5: current-voltage characteristic output curves for a n -type semiconductor [2].

I_{DS} in ohmic regime is found to be equal to

$$I_{DS} = \frac{W \mu C_i}{L} [V_{DS} (V_{GS} - V_{TH})] - \frac{V_{DS}^2}{2}$$

Equation 3.1: mathematic relationship between Drain current and the voltages applied to OFET.

Saturation regime is featured by a different I_{DS} behavior, which can be expressed as:

$$I_{DS} = \frac{W \mu C_i}{L} \frac{(V_{GS} - V_{TH})^2}{2}$$

Equation 3.2: mathematic relationship between Drain current and the voltages applied to OFET.

In Equations 3.1 and 3.2 , W is the width of the transistor channel, L is its length, C_i is the specific dielectric capacitance (the capacitance per unit area of insulating layer) and μ is the charge electrical mobility.

Electrical mobility is s the ability of charged carriers (such as electrons or holes) to move through a medium in response to an electric field that is pulling them. In other words, mobility is the proportionally constant between the electric field (E) and the charges drift velocity (v): thus it is commonly measured in $\text{cm}^2 / (\text{V s})$.

$$v = \mu E$$

Equation 3.3: physical definition of charge carriers mobility.

Electrical mobility is the most important parameter that points out the global efficiency of an OFET device: it depends on the semiconductor performances, on its morphology and thus on the interaction between the active and the dielectric layers. Insulating material roughness affects the deposition of the organic semiconductor on it: the molecular order and the grains dispositions is a key factor for an optimal charge transport.

The device architecture plays also a major role in improving the mobility and then the OFET working performances: the same semiconductor can behave in very different ways depending on the device structure.

There are two main architectures to choose from in OFET fabrication: the *top contacts* and the *bottom contacts* configurations (see Figure 3.6a and 3.6b), both with *bottom-Gate* feature.

The physical difference between the two is the Source / Drain contacts are either deposited before or after the semiconductor layer is deposited to create a bottom contact or top contact device, respectively [3].

Top contacts OFETs generally exhibit the lowest contact resistances: this is because of the increased metal–semiconductor contact area in this configuration [4].

A major contribution to contact resistance in the *top contacts* configuration is access resistance, which results from the requirement that charge carriers must travel from the Source contact on top of the film down to the channel at the semiconductor–insulator interface and then back up to the drain contact to be extracted [5].

With the *bottom contacts* architecture access resistance is not an issue because the contacts are in the same plane as the OFET channel. In addition, very small channel dimensions can be pre-patterned on the insulator using conventional photolithography. Limitations to the bottom contact configuration are due to the film morphology in the vicinity of the contacts is often non ideal [6].

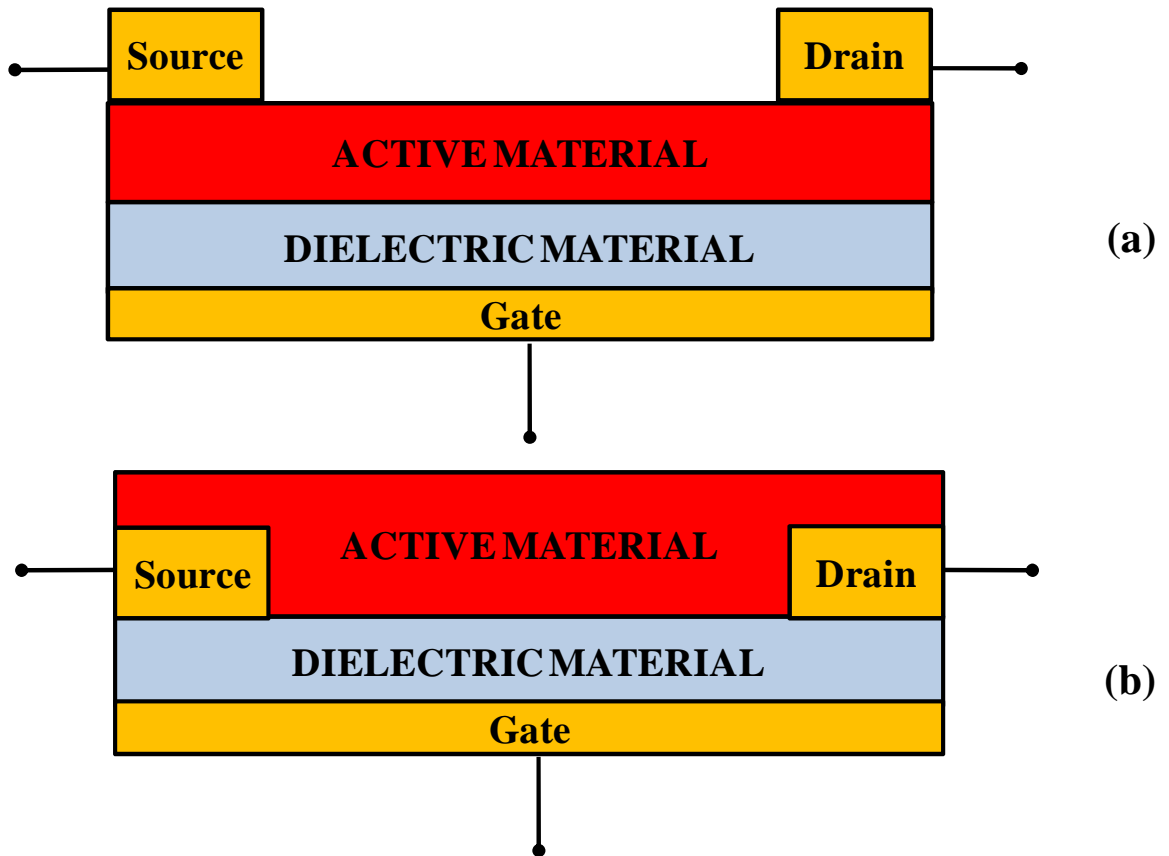


Figure 3.6: *top contacts / bottom-Gate (a) and bottom contacts / bottom-Gate (b) architectures.*

Of the two *top-Gate* OFET architectures (see Figure 3.7a and 3.7b), the *top contacts* configuration is the more favorable of the two because *bottom contacts* devices suffer from access resistance [7].

Top-Gate architectures face the additional problem of semiconductor top surface roughness (where the channel will form) and forming a stable interface between the insulator and the top of the semiconductor film [8].

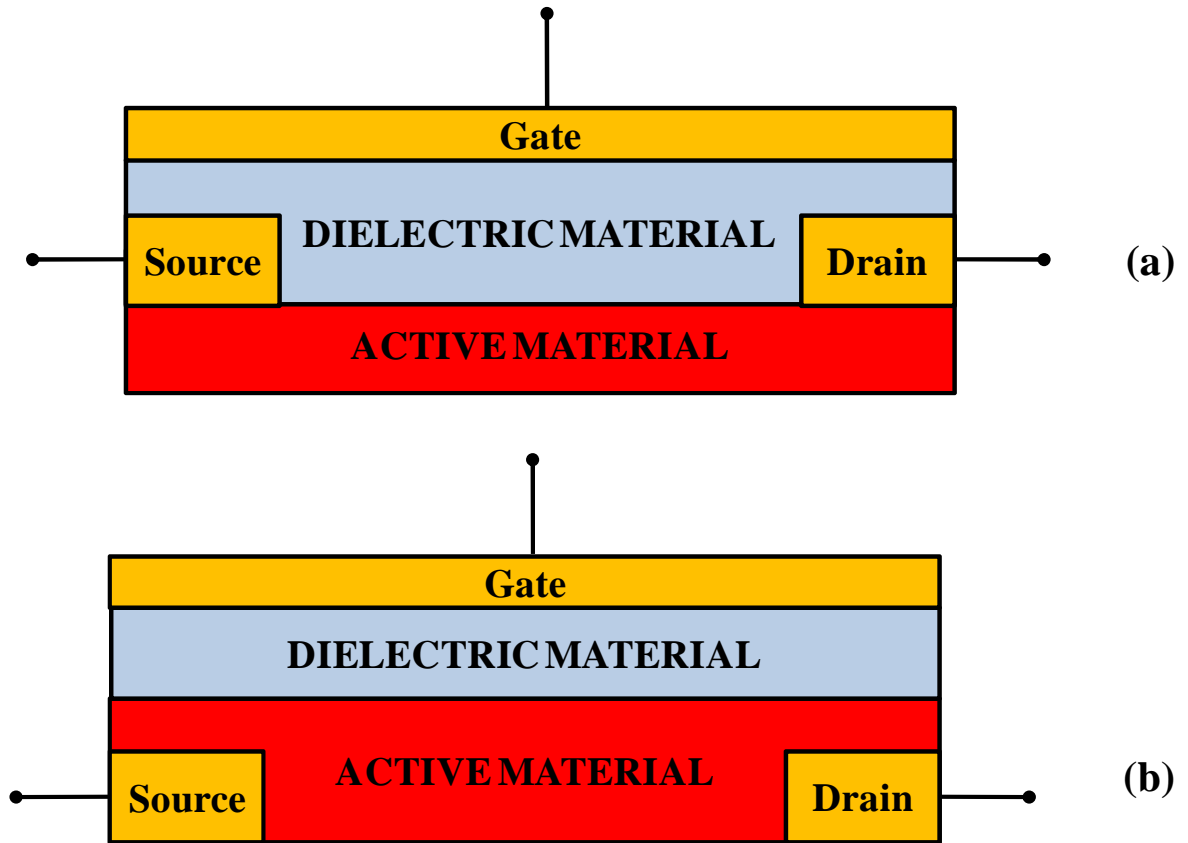


Figure 3.6: *top contacts / top-Gate (a) and bottom contacts / top-Gate (b) architectures.*

Regarding the alignment of the Gate contact to the OFET channel in *top-Gate* devices, care must also be taken to ensure that the gate reaches completely across the entire length of the device, or additional contact resistance will be introduced [9]. The immediate opportunity of the use of organic dielectric is in the *top-Gate* structure of OFET, since it does not destroy the underlying organic semiconductors. *Top-Gate / bottom-contacts* structure devices allow patterning of the bottom Source-Drain electrodes on top of any flexible or rigid substrate first before building the rest of the device; *top-Gate / top-contacts* structure devices allow growing organic semiconductor films on top of any flexible or rigid substrate [10]. Finally, another important parameter to evaluate the OFET performances is the ON / OFF ratio: it is the ratio of the current intensity while the device saturates for a given applied V_{GS} to that when no V_{GS} is applied. It represents the difference between two logic device states and the higher it will be, the easier the signal processing will be.

REFERENCES

- [1] A. Tsumura, H. Koezuka, T. Ando, *Appl. Phys. Lett.*, **1986**, 49, 1210;
- [2] J. Millman, C. C. Halkias, *Integrated Electronics*, **1972**, Tata McGraw-Hill Publishing Company;
- [3] Matthew J. Panzer and C. Daniel Frisbie, *Contact Effects in Organic Field-Effect Transistors*, Section 2.4 of *Organic field-Effect Transistors*, CRC Press;
- [4] Matthew J. Panzer and C. Daniel Frisbie, *Contact Effects in Organic Field-Effect Transistors*, Section 2.4 of *Organic field-Effect Transistors*, CRC Press;
- [5] Matthew J. Panzer and C. Daniel Frisbie, *Contact Effects in Organic Field-Effect Transistors*, Section 2.4 of *Organic field-Effect Transistors*, CRC Press;
- [6] Matthew J. Panzer and C. Daniel Frisbie, *Contact Effects in Organic Field-Effect Transistors*, Section 2.4 of *Organic field-Effect Transistors*, CRC Press;
- [7] Matthew J. Panzer and C. Daniel Frisbie, *Contact Effects in Organic Field-Effect Transistors*, Section 2.4 of *Organic field-Effect Transistors*, CRC Press;
- [8] Matthew J. Panzer and C. Daniel Frisbie, *Contact Effects in Organic Field-Effect Transistors*, Section 2.4 of *Organic field-Effect Transistors*, CRC Press;
- [9] Matthew J. Panzer and C. Daniel Frisbie, *Contact Effects in Organic Field-Effect Transistors*, Section 2.4 of *Organic field-Effect Transistors*, CRC Press;
- [10] Th. B. Singh, N. S. Sariciftci, M. Jaiswal, R. Menon, *Handbook of Organic Electronics and Photonics*, edited by Hari Singh Nalwa, Volume 3, page 154;

PART II

-

EXPERIMENTALS AND DATA DISCUSSION

CHAPTER 1

ORGANIC SEMICONDUCTORS PURIFICATION AND PERFORMANCES IMPROVEMENT

1.1 Thermal treatments for organic molecules

Due to their chemical-physical properties, organic semiconductors show interesting characteristics which allow them to be thermally processed in order to reach a higher purity grade; this is an important perspective especially for small molecules and oligomers, because they have quite high decomposition temperatures (about 300°C or more) and they can crystallize easily under a thermal gradient.

Tris(8-hydroxyquinoline)aluminum(III), a widely used emitting material commonly known as Alq₃, was refined in order to obtain a new crystal structure [1], which shows a blue luminescence radiation when irradiated by UV source; appreciated for their dye properties in optoelectronics applications and for being gain mediums in organic lasers, Stilbene isomers can undergo zone refinement purification process [2] in order to improve emitting performances; furthermore, the same treatment can be applied to Naphthalene and Phenanthrene [3], which are the bases for new generation *p-type* semiconductors. One of the oldest and most studied purification methods for organic compounds is the sublimation: Phthalocyanines and related molecules are often processed [4] by this technique, as well as *p-type* semiconductor Pentacene [5], laser dye Rhodamine B [6] and Perylene derivatives [7]. Sublimation was the way we chose to investigate the effects of the purification on 2,2'''-Dihexyl-2,2':5',2'':5'',2'''-quaterthiophene (**DH4T**) and 2,2'''-Perfluoro-Dihexyl-2,2':5',2'':5'',2'''-quaterthiophene (**DHF4T**), respectively the *p-type* and *n-type* semiconductor used by Capelli *et al.* to fabricate a trilayer light emitting Organic Field-Effect Transistor [8].

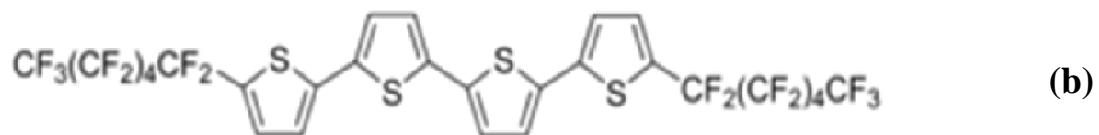
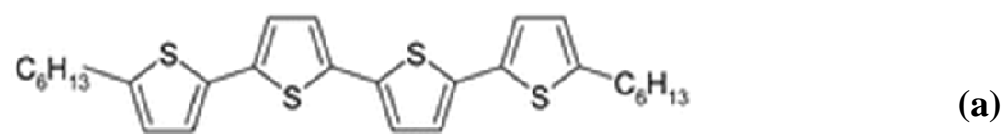


Figure 1.1: DH4T (a) and DHF4T (b) molecular structures.

1.2 Sublimation dynamics [9]

Every phase transition is a process between two different thermodynamic systems, each of them having uniform characteristics and properties, involving a certain amount of energy which is the driving force of the macroscopic changes.

Regardless of the substance or the element, throughout a sublimation (a transition from solid to vapor phase) four important thermodynamic parameters are always involved: the pressure (p), the specific latent heat (λ), the specific volume difference between the two considered phases

($\Delta v = v_{\text{vapor}} - v_{\text{solid}}$) and the temperature (T); this latter remains constant for *first order* transitions.

Clausius-Clapeyron equation (see Equation 1.1) gives a satisfactory explanation of the pressure-temperature relationship and fits with the all possible equilibrium states between the solid phase and the vapor one.

$$\frac{dp}{dT} = \frac{\lambda}{(v_{\text{vapor}} - v_{\text{solid}}) T}$$

Equation 1.1: differential form of Clausius-Clapeyron equation.

The sublimation occurs when the substance vapor pressure (the pressure generated by the vapor phase at thermodynamic equilibrium with the solid phase) is equal to the environmental pressure.

Since the vapor specific volume exceeds that of the solid phase, it is possible to approximate $\Delta v \approx v_{\text{vapor}}$; then, assuming that the vapor phase complies with the ideal gases law, v_{vapor} can be written as:

$$v_{\text{vapor}} = \frac{V}{m} = \frac{n R T}{m p} = \frac{R T}{M W p} = \frac{\hat{R} T}{p}$$

where m is the mass, V is the volume, n is the mole number, MW is the molecular weight, R is the universal gas constant and \hat{R} is the specific gas constant.

Now it is easy to integrate Equation 1.1, which takes the form expressed as following:

$$\ln(p) = - \frac{\lambda}{\hat{R} T}$$

Equation 1.2: integral form of Clausius-Clapeyron equation.

To purify organic semiconductors two sublimation ways are usually followed: the first involves low static vacuum system, which works with slow sublimation rates but leads to a very good crystal growth; the second, called *entrainer sublimation*, requires low pressure inert gas flow, which quicken the process while producing condensates or crystal powders. Furthermore several experiments demonstrated how slow sublimation rates at low temperatures yield well-developed crystals, while fast processes at higher temperatures promote amorphous condensates [10].

1.3 Sublimation technique and experimental parameters

In order to accomplish the purification of both **DH4T** and **DHF4T** we used an horizontal solid tube furnace (Thermcraft Incorporated) with three heating zones with electronic controls.

To better understand the following explanation see Figure 1.2 .

The tube envelops a glass pipe which can host about thirteen hollow glass cylinders; the organic material has to be put in a metal boat, which is inserted in the glass cylinder whose position in the pipe matches with the first heating zone.

After having filled it with all the other little cylinders, the glass pipe mouths are closed with the sleeves connected to the Argon-pump system; the pressure in the pipe is set with a needle valve.

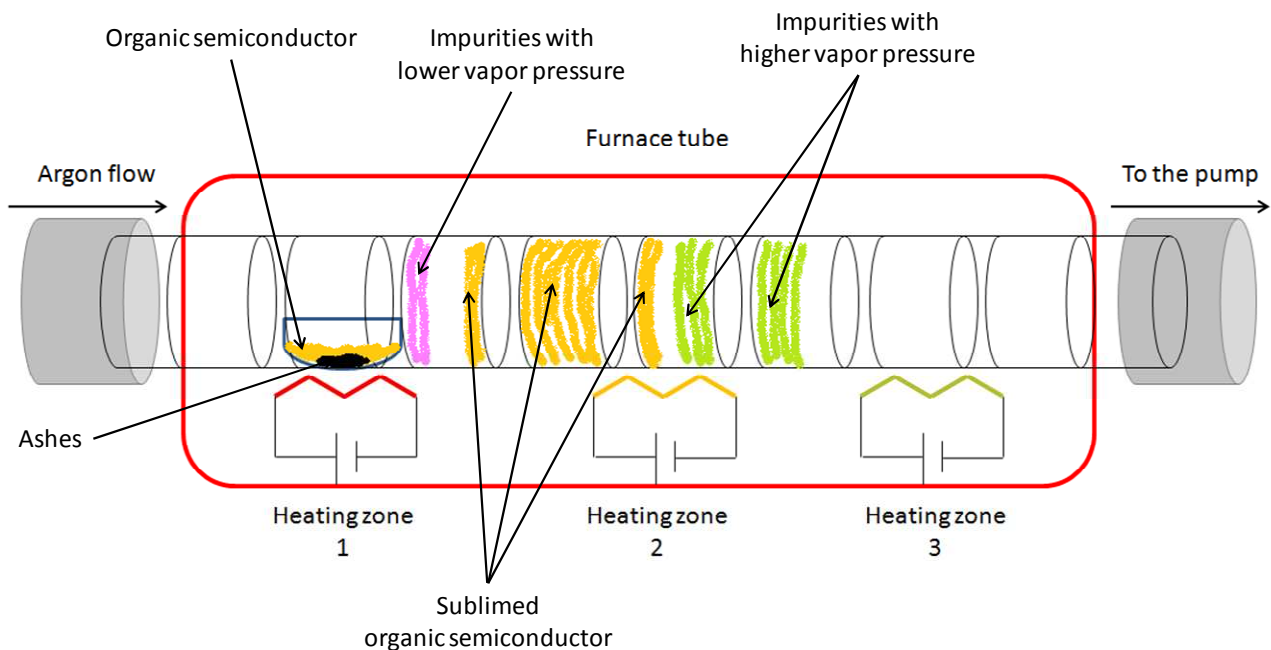


Figure 1.2: working *entrainer sublimator* scheme.

The organic material recovering must be done carefully after dismantling the system. The cylinders with the sublimed semiconductor must be separated from the others; perceiving the semiconductor from the impurities is not always an easy job, thus sometimes it is possible to irradiate the cylinders with an UV source in order to immediately recognize the semiconductor, which often has a luminescent behavior. The sublimation data for **DH4T** and **DHF4T** are collected in Table 1.1 : they are referred to the best conditions tested for each material.

Semiconductor	Heating zone temperature (°C)			Argon pressure (mbar)	Sublimation yield (w/w %)	Sublimed material characteristics
	First	Second	Third			
DH4T	230	180	0	0.23	92.8	Yellow flakes easy to recover; next to the metal boat the material condenses in a compact solid phase
DHF4T	290	210	0	0.23	61.5	Yellow subtle disperse powder, hard to recover due to electrostatic charges

Table 1.1: *entrainer sublimator* parameters for the two studied semiconductors.

1.4 Comparison between crude and sublimed semiconductor performances

Fabricating Field-Effect Transistor devices is very useful in order to investigate the benefits given to the semiconductor electric properties by the purification process. Several works published in the last decades repeatedly demonstrated that measuring the substance conductivity (σ) is one of the best methods to achieve a purity criterion [11].

Since the conductivity is proportional to charge carriers mobility (μ), as shown in Equation 1.3, it is possible to estimate the purity grade of an organic semiconductor from mobility values obtained by OFET measurements. If further purifications cause no further change in the measured value of charge mobility, it is reasonable to assume that mobility itself is the semiconductor one and it is unaffected by residual impurities [12].

$$\sigma = z \rho e \mu$$

Equation 1.3: relationship between conductivity and mobility, where z is the charge value, ρ is the charge density and e is the elementary electric charge.

OFET devices fabrication will be widely explained in Paragraph 2.4 of Chapter 2, Part II, where all the processes and the operations related to the core topic are discussed; high vacuum growth steps and parameters are the same for both **DH4T** and **DHF4T**, except for the growth temperature: 190°C for the first one, 230°C for the second one.

1.4.1 Study on DH4T performances before and after sublimation

After completing the high vacuum evaporation process, the **DH4T**-made Field-Effect Transistors were fully characterized: the collected plots are shown from Figure 1.3 to Figure 1.14, while the elaborated statistical data are reported in Table 1.2.

Number of sublimation cycles	Charge mobility \pm standard deviation ($\text{cm}^2/\text{V s}$)	Threshold voltage \pm standard deviation (V)	ON / OFF ratio (only magnitude)
0 (crude material)	$(1.19 \pm 0.04) \cdot 10^{-1}$	-37.6 ± 2.0	10^4
1 (one purification)	$(1.72 \pm 0.06) \cdot 10^{-1}$	-25.8 ± 1.8	10^4
2 (two purifications)	$(2.50 \pm 0.09) \cdot 10^{-1}$	-22.3 ± 1.1	10^4

Table 1.2: charge mobility and threshold voltage data for **DH4T** before sublimation, for *mono*-sublimed **DH4T** and *bis*-sublimed **DH4T**.

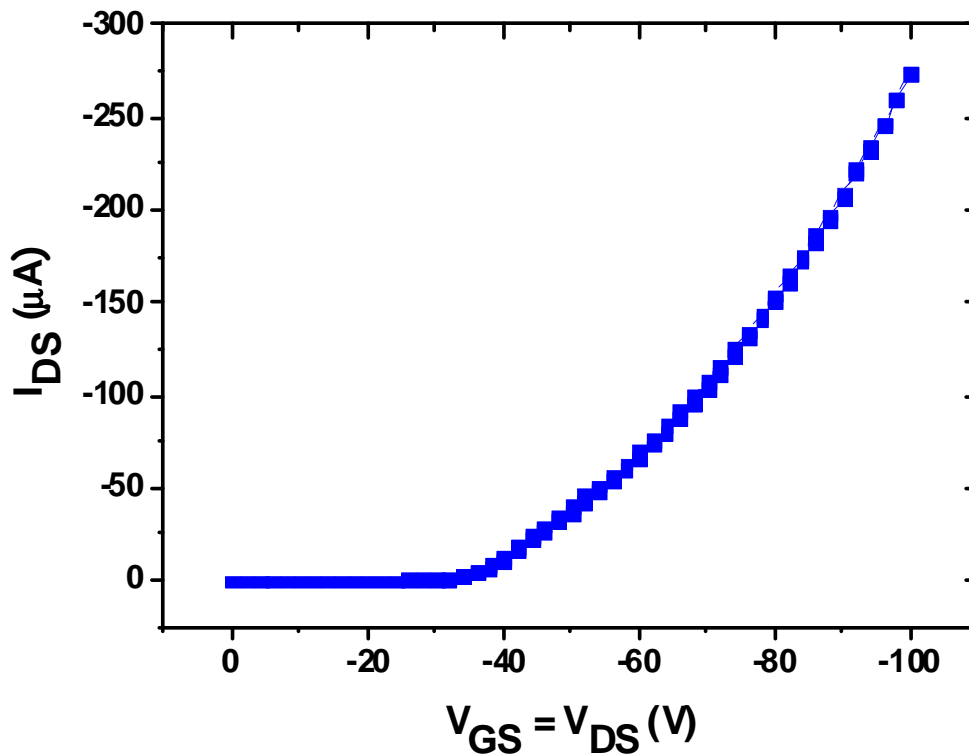


Figure 1.3: LOCUS curve for crude **DH4T**.

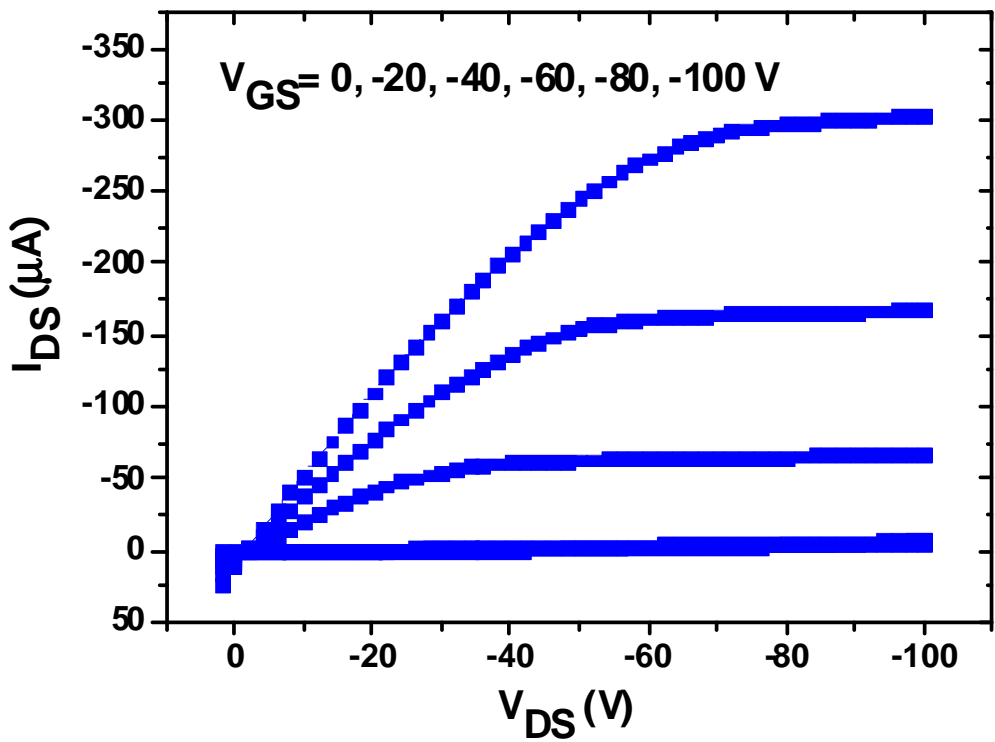


Figure 1.4: MULTIPLE OUTPUT curves for crude **DH4T**.

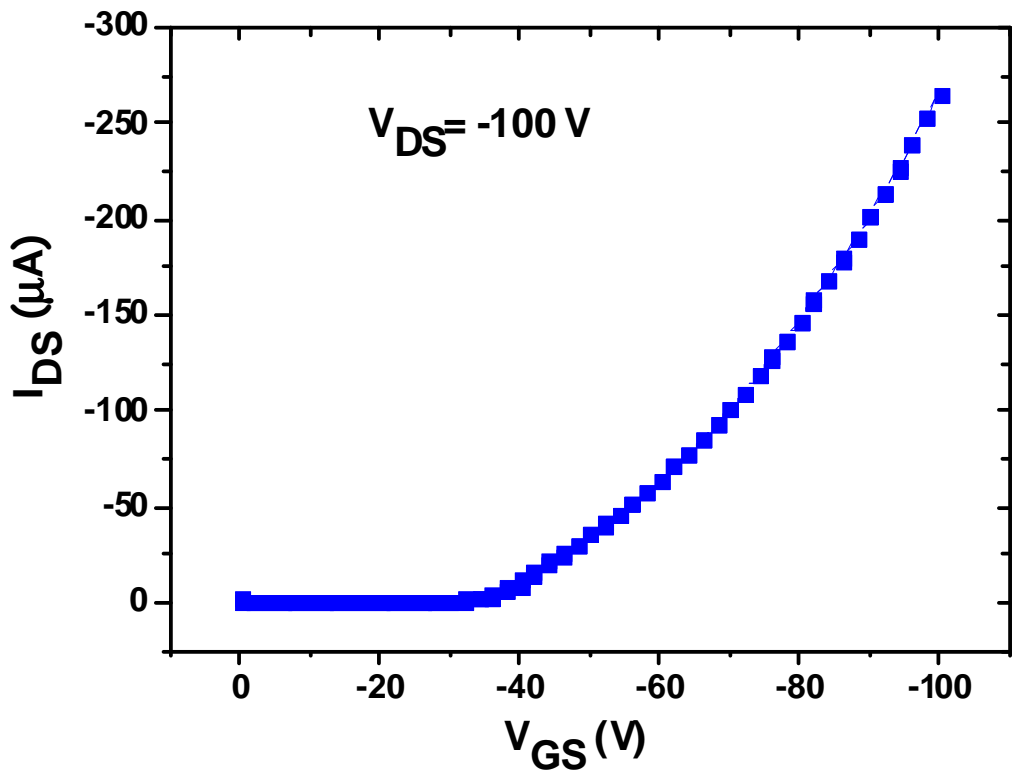


Figure 1.5: SATURATION TRANSFER curve for crude **DH4T**.

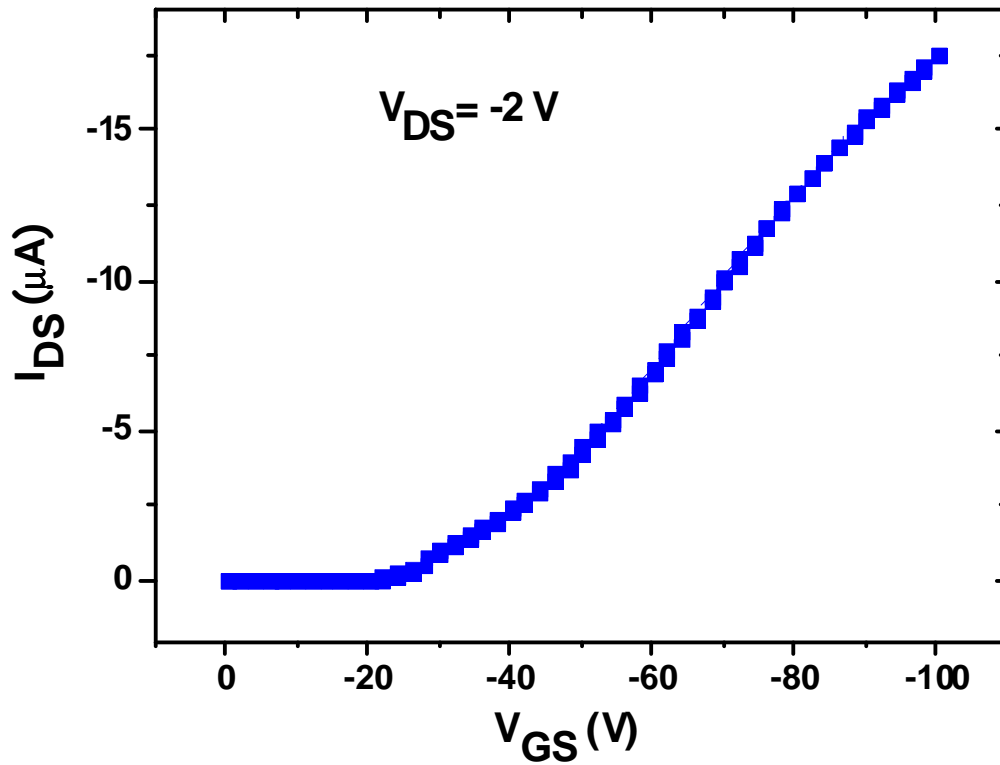


Figure 1.6: LINEAR TRANSFER curve for crude **DH4T**.

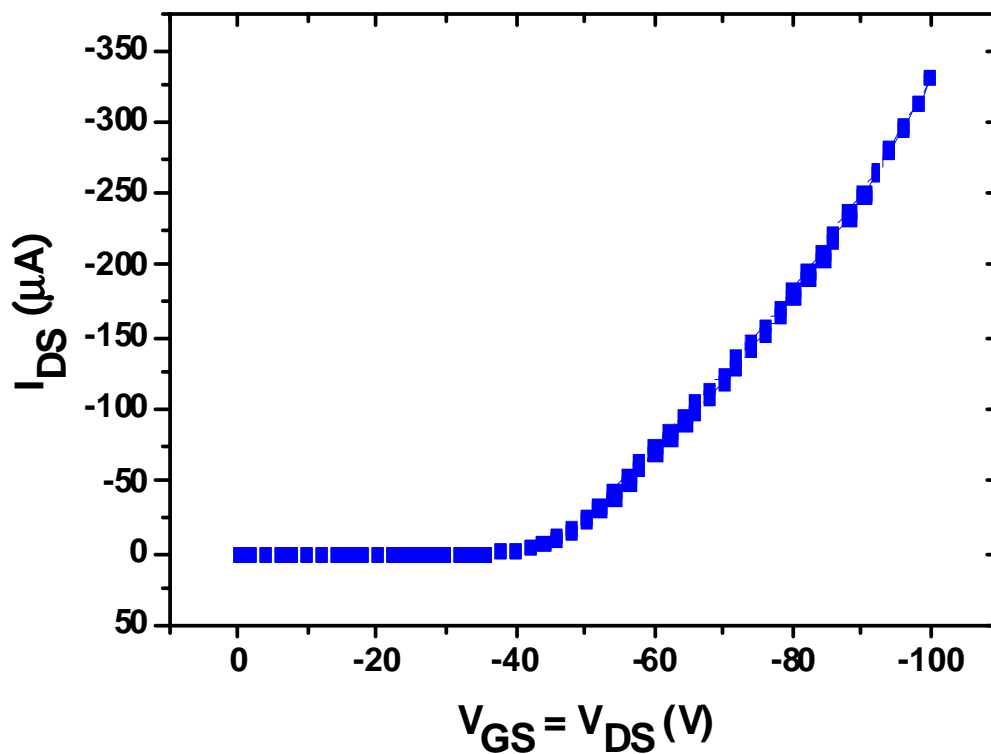


Figure 1.7: LOCUS curve for *mono*-sublimed **DH4T**.

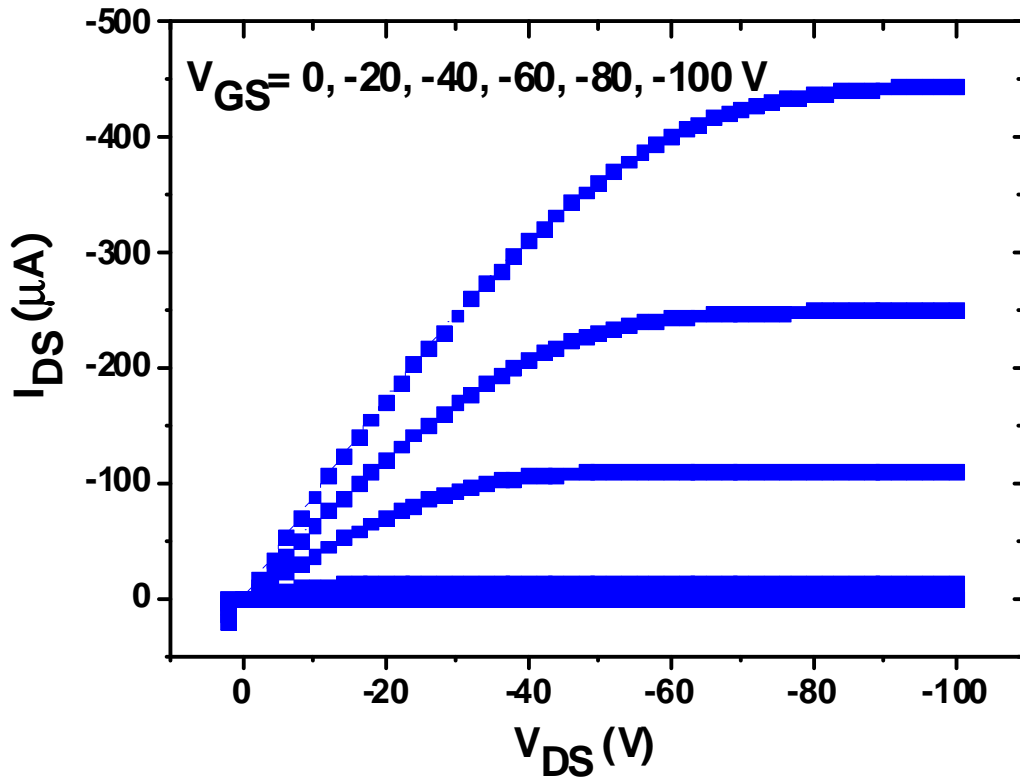


Figure 1.8: MULTIPLE OUTPUT curves for *mono*-sublimed **DH4T**.

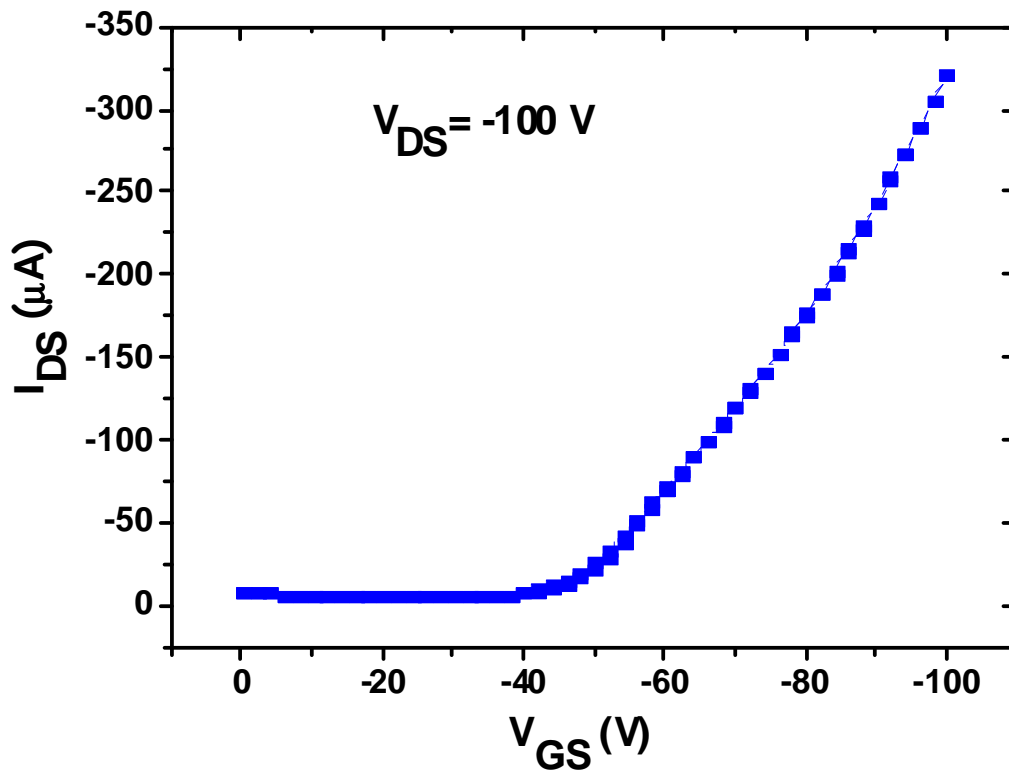


Figure 1.19: SATURATION TRANSFER curve for *mono*-sublimed **DH4T**.

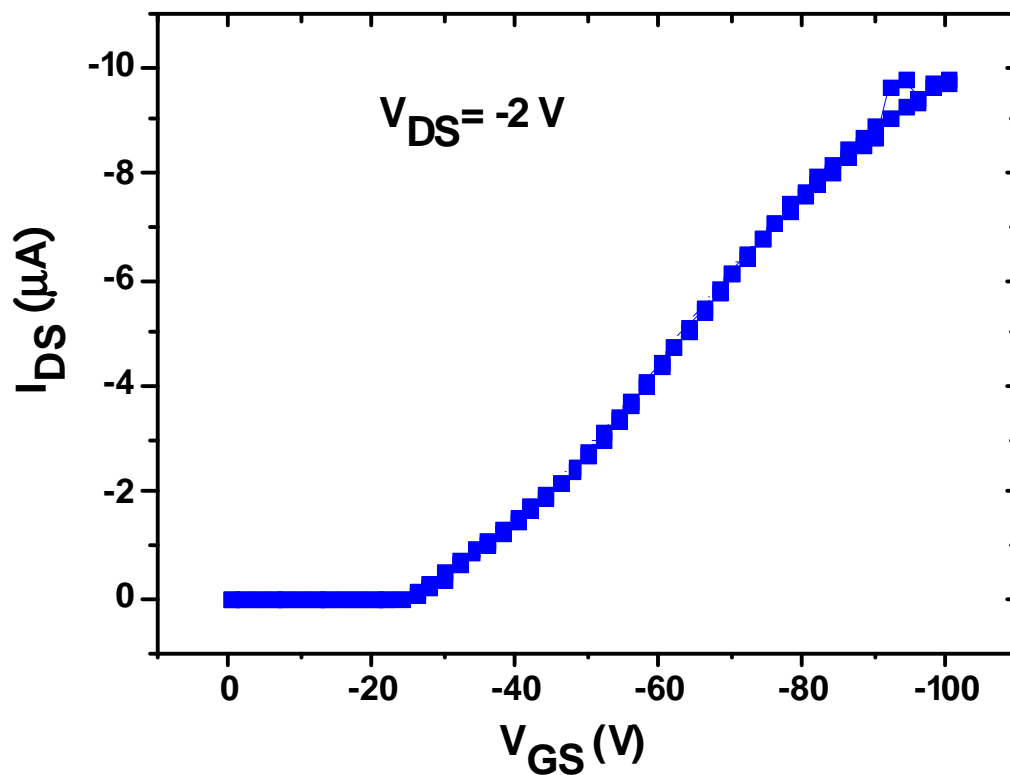


Figure 1.10: LINEAR TRANSFER curve for *mono*-sublimed DH4T.

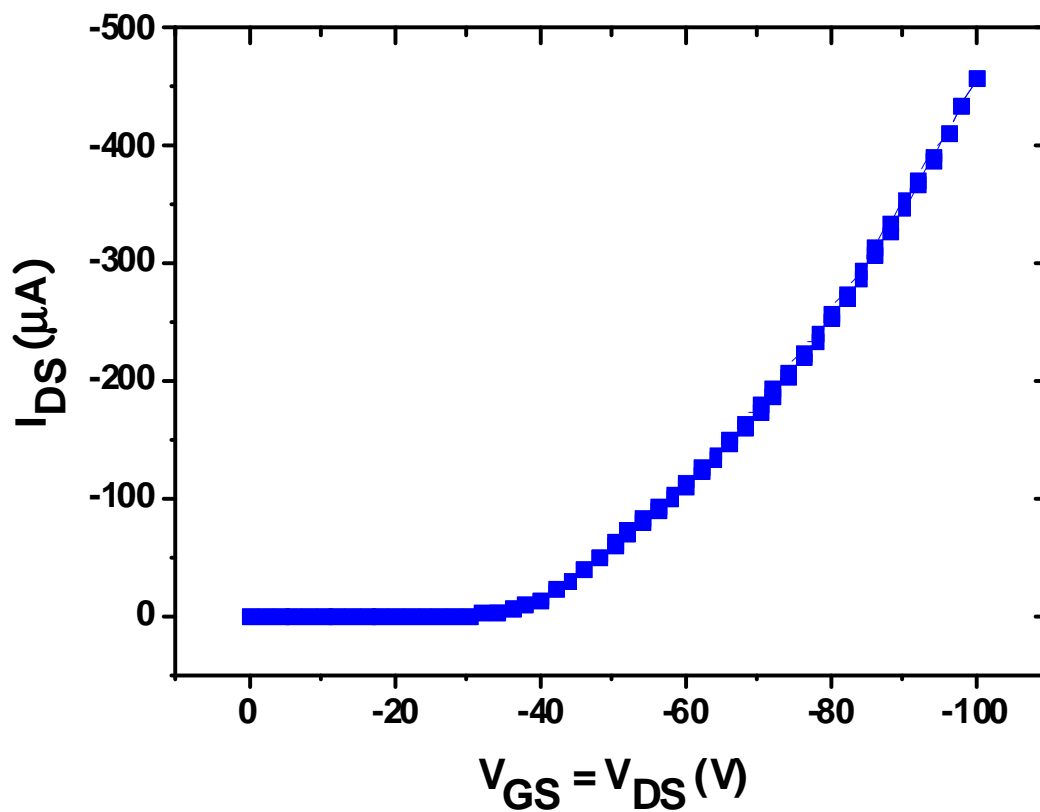


Figure 1.11: LOCUS curve for *bis*-sublimed DH4T.

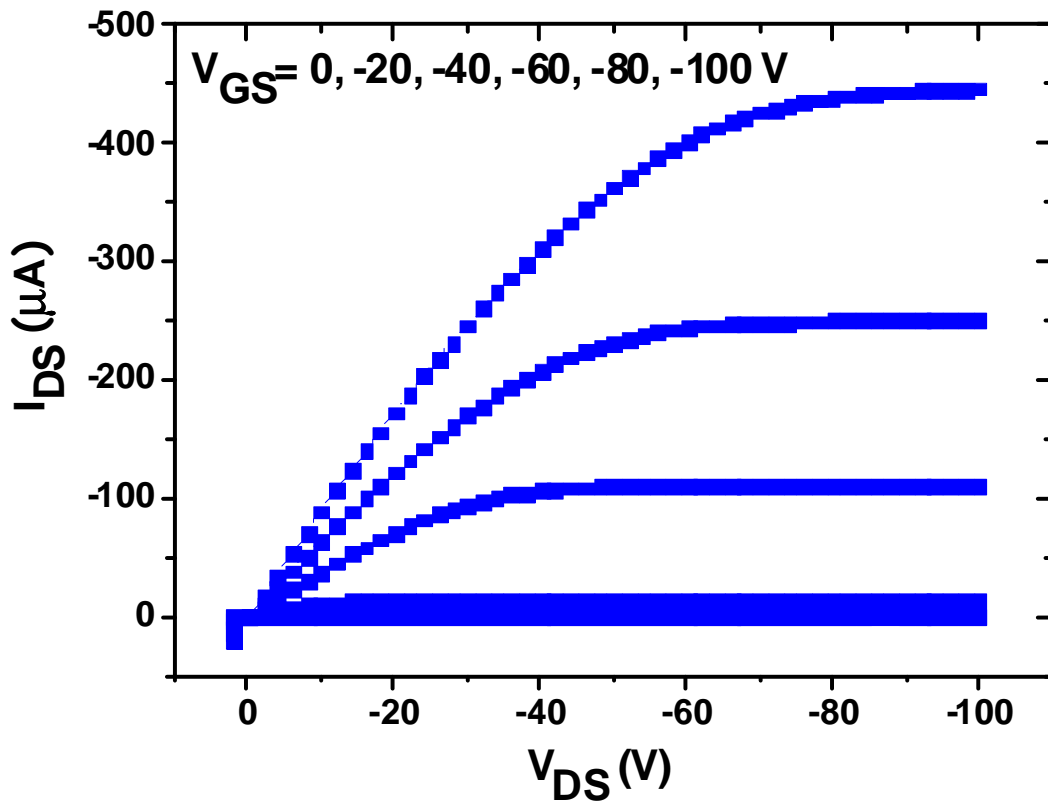


Figure 1.12: MULTIPLE OUTPUT curves for *bis*-sublimed DH4T.

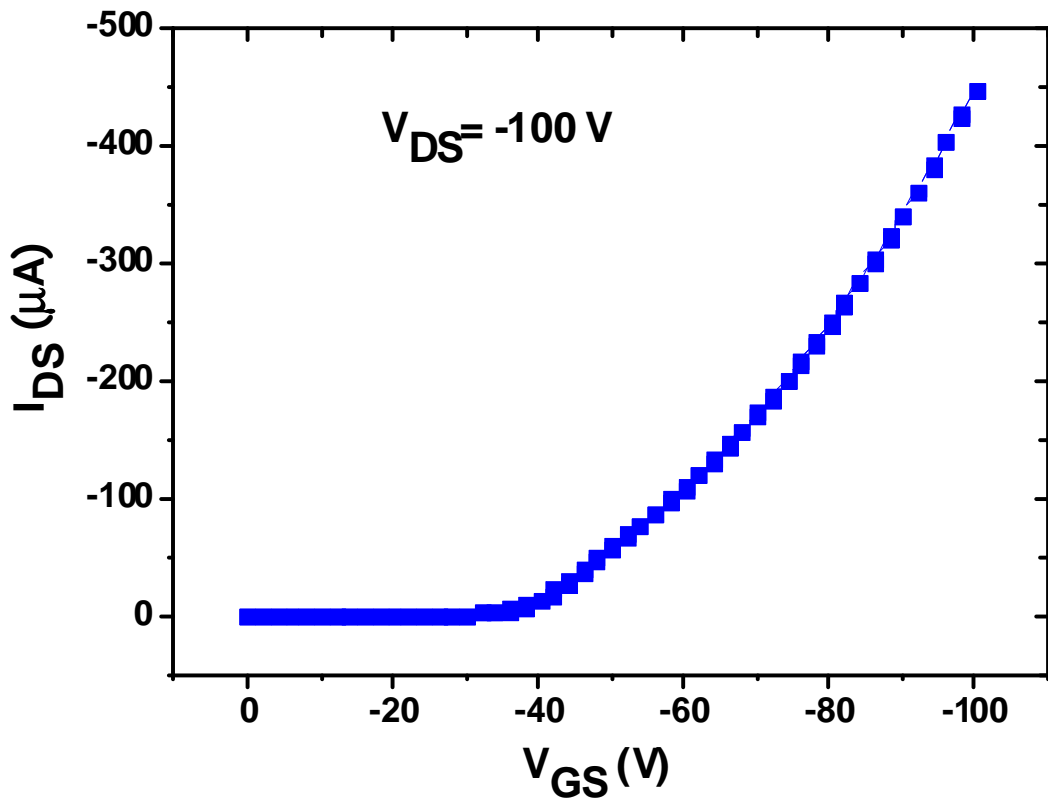


Figure 1.13: SATURATION TRANSFER curve for *bis*-sublimed DH4T.

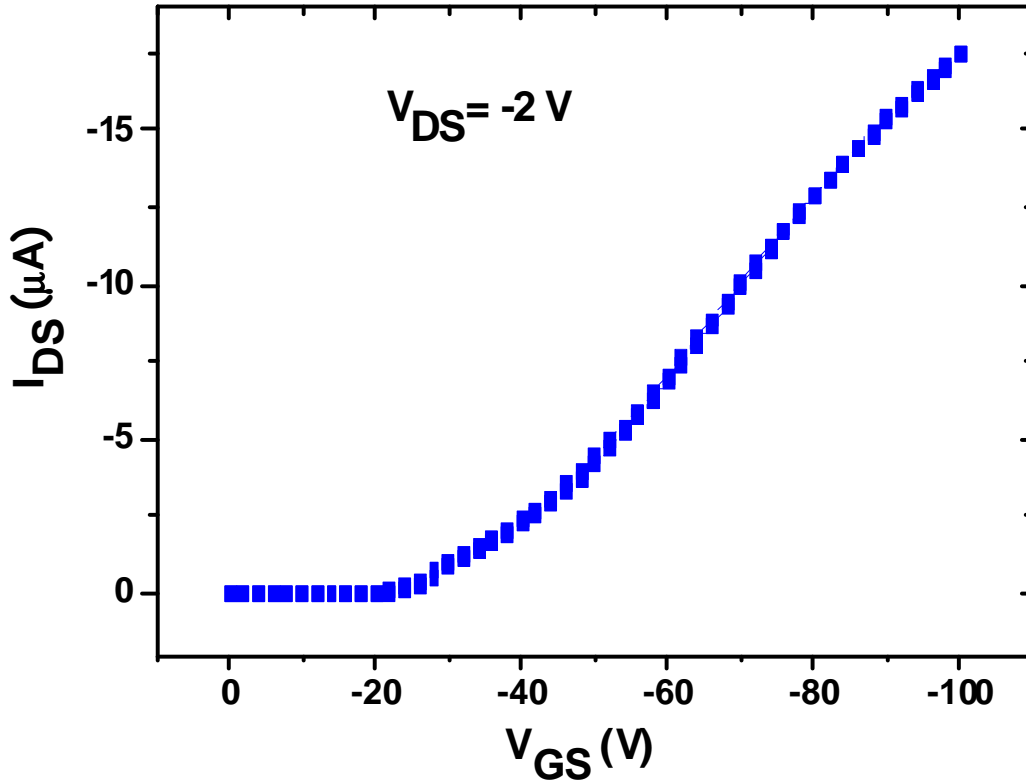


Figure 1.14: LINEAR TRANSFER curve for *bis*-sublimed **DH4T**.

Entrainer sublimation is a very good purification technique to improve **DH4T** electric performances.

Charge mobility increases as the semiconductor repeatedly undergoes sublimation: this is a clear evidence of the benefits brought by impurities removal; threshold voltage reaches lower values after two complete processes, although it is still too high for being interesting.

None of the LOCUS curves shows hysteresis loop, thus the OFETs active layers were not damaged during the fabrication; the ohmic linear part of the plots is shrunk by the increase of purification cycles number.

All the MULTIPLE OUTPUT plots show their linear parts crossing in one origin, revealing neither dielectric current leakage nor free charges in dielectric/active layers interface; the saturation zones are flat, thus the devices have no free charges localized in the boundary between the dielectric and the active layers.

Every SATURATION TRANSFER plot is similar to the corresponding LOCUS: this is a very good feature that follows the true ideal behavior, because both kinds of measurement are collected in OFET saturation regime; LINEAR SATURATION curves don't show hysteresis loop and each of them has a pretty constant slope, highlighting the perfect charge injection from the metal electrodes.

The confrontation between the **DH4T** performances experimentally obtained before and after the sublimation cycles demonstrates how the organic semiconductor behavior can be improved with just two sublimation steps; the impurities which affect the semiconductor can be easily separated with the discussed sublimation system.

1.4.2 Study on DHF4T performances before and after train sublimation

After completing the high vacuum evaporation process, the **DHF4T**-made Field-Effect Transistors were fully characterized: the collected plots are shown from Figure 1.15 to Figure 1.26, while the elaborated statistical data are reported in Table 1.3.

Number of sublimation cycles	Charge mobility \pm standard deviation ($\text{cm}^2/\text{V s}$)	Threshold voltage \pm standard deviation (V)	ON / OFF ratio (only magnitude)
0 (crude material)	$(2.71 \pm 0.02) \cdot 10^{-1}$	$+32.9 \pm 1.3$	10^4
1 (one purification)	$(5.35 \pm 0.08) \cdot 10^{-1}$	$+46.1 \pm 2.2$	10^4
2 (two purifications)	$(8.43 \pm 0.05) \cdot 10^{-1}$	$+56.4 \pm 1.9$	10^4

Table 1.3: charge mobility and threshold voltage data for **DHF4T** before sublimation, for *mono*-sublimed **DHF4T** and *bis*-sublimed **DHF4T**.

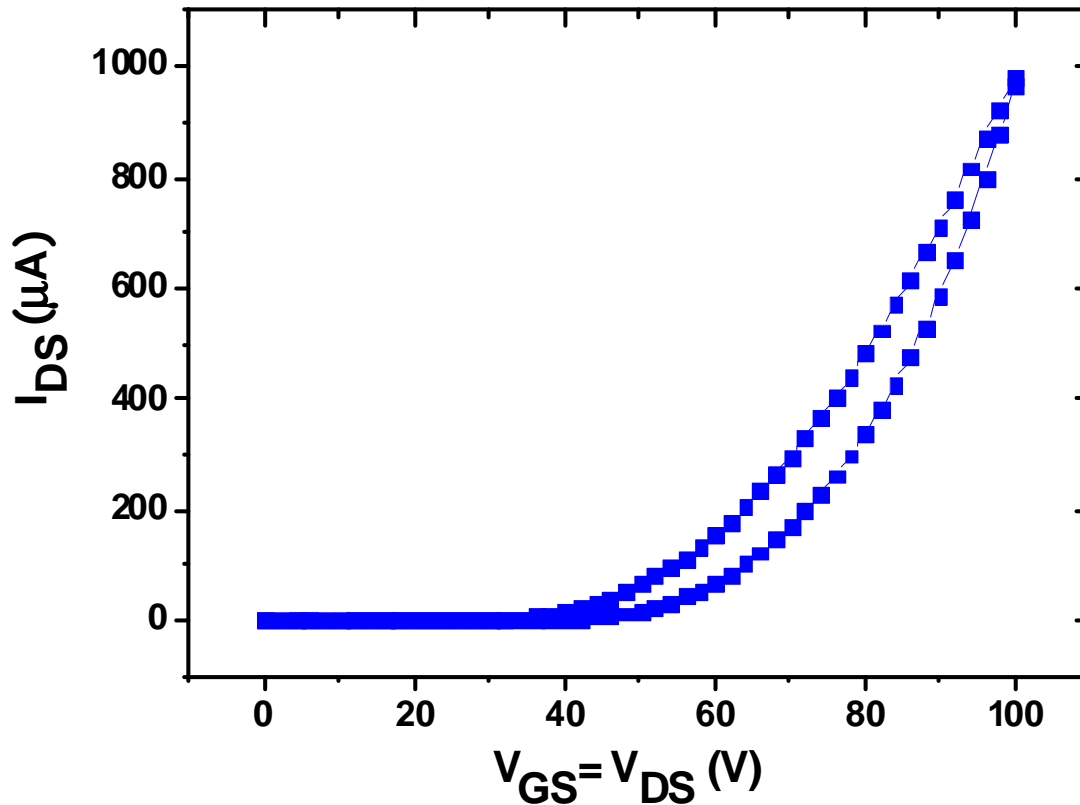


Figure 1.15: LOCUS curve for crude **DHF4T**.

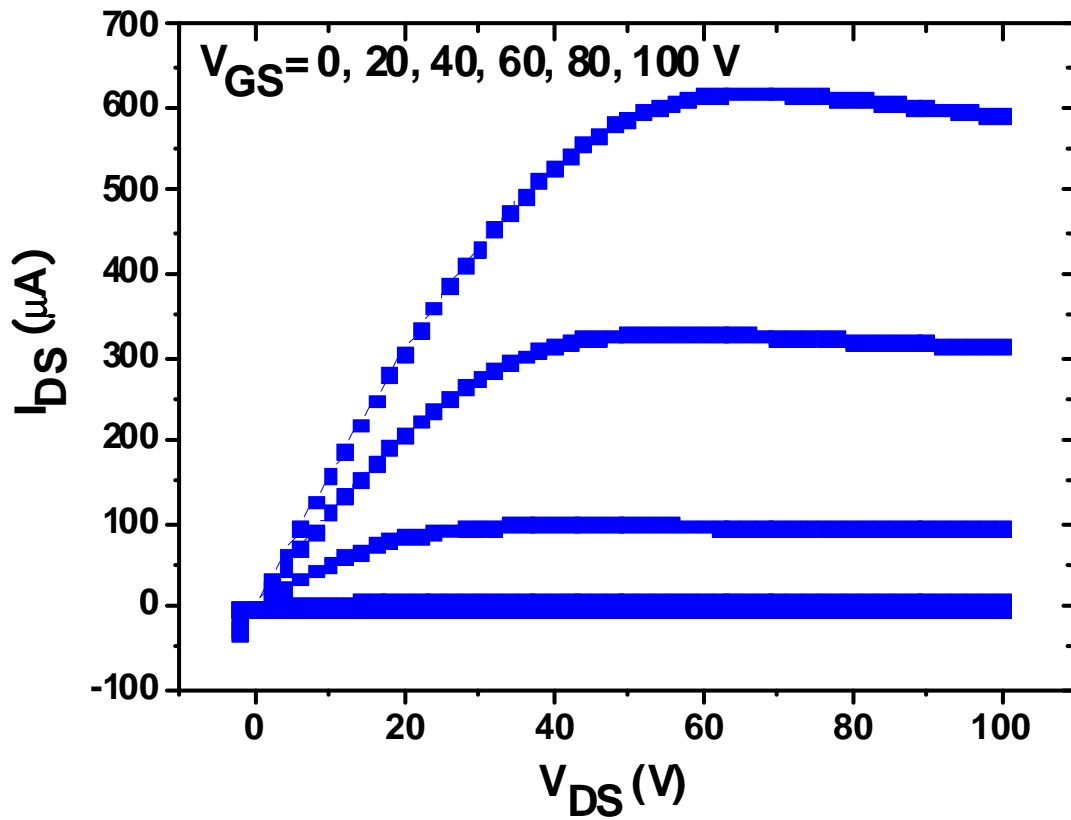


Figure 1.16: MULTIPLE OUTPUT curves for crude **DHF4T**.

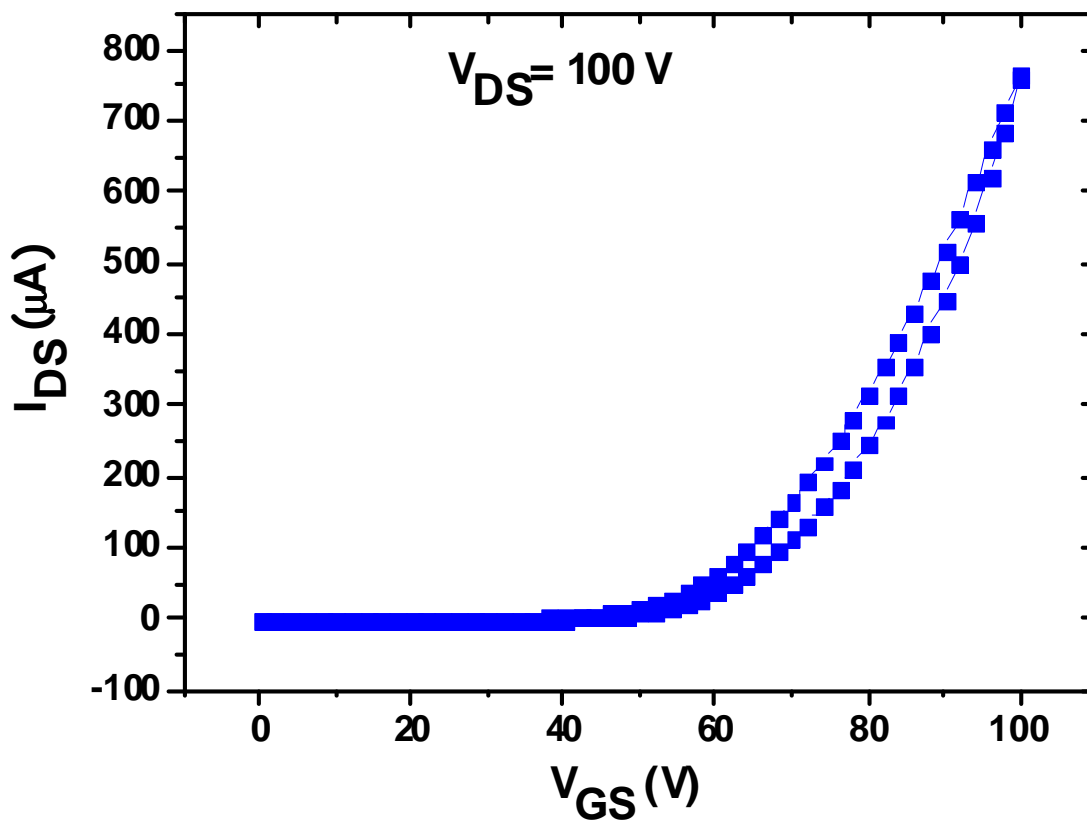


Figure 1.17: SATURATION TRANSFER curve for crude **DHF4T**.

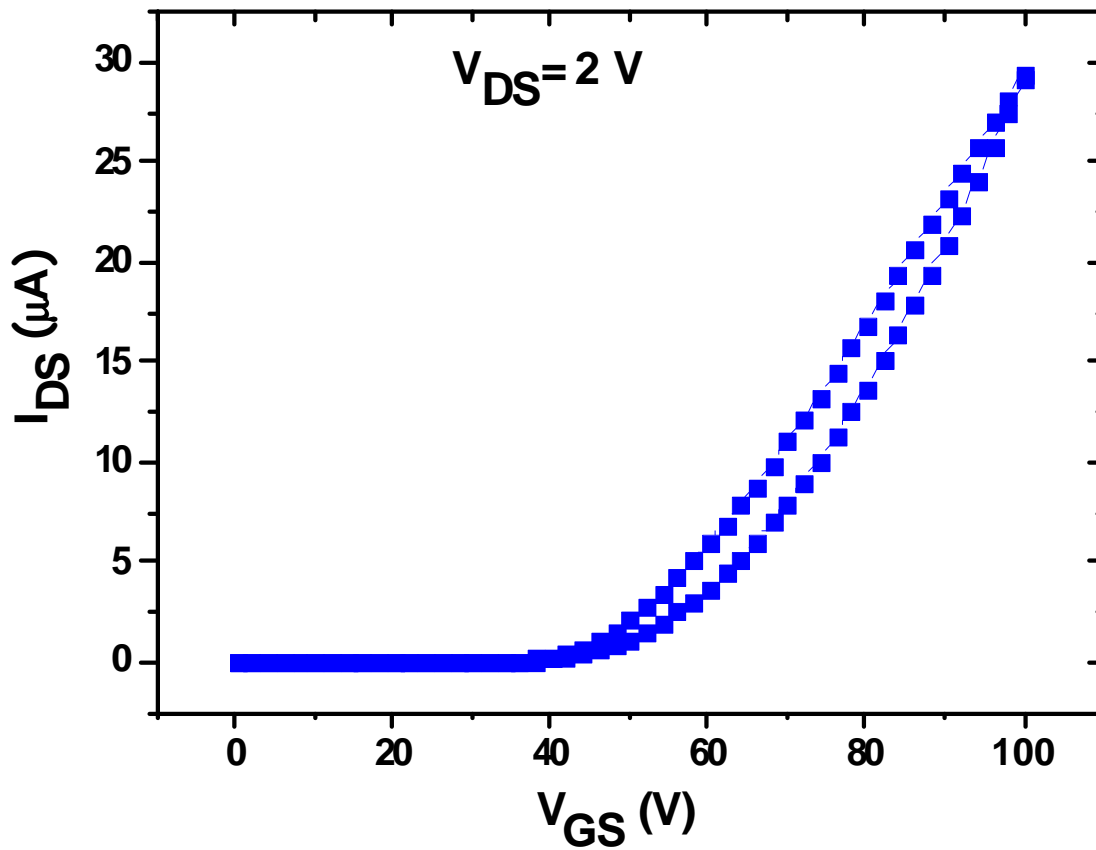


Figure 1.18: LINEAR TRANSFER curve for crude **DHF4T**.

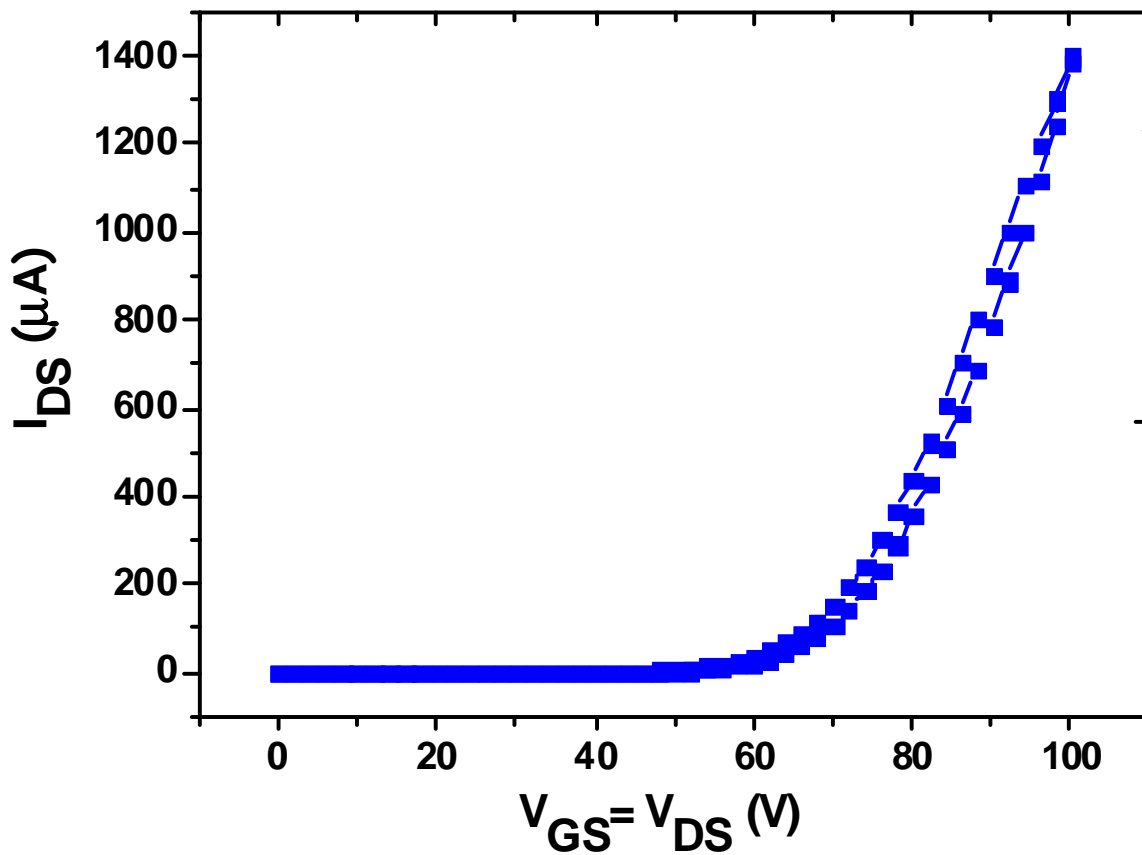


Figure 1.19: LOCUS curve for *mono*-sublimed **DHF4T**.

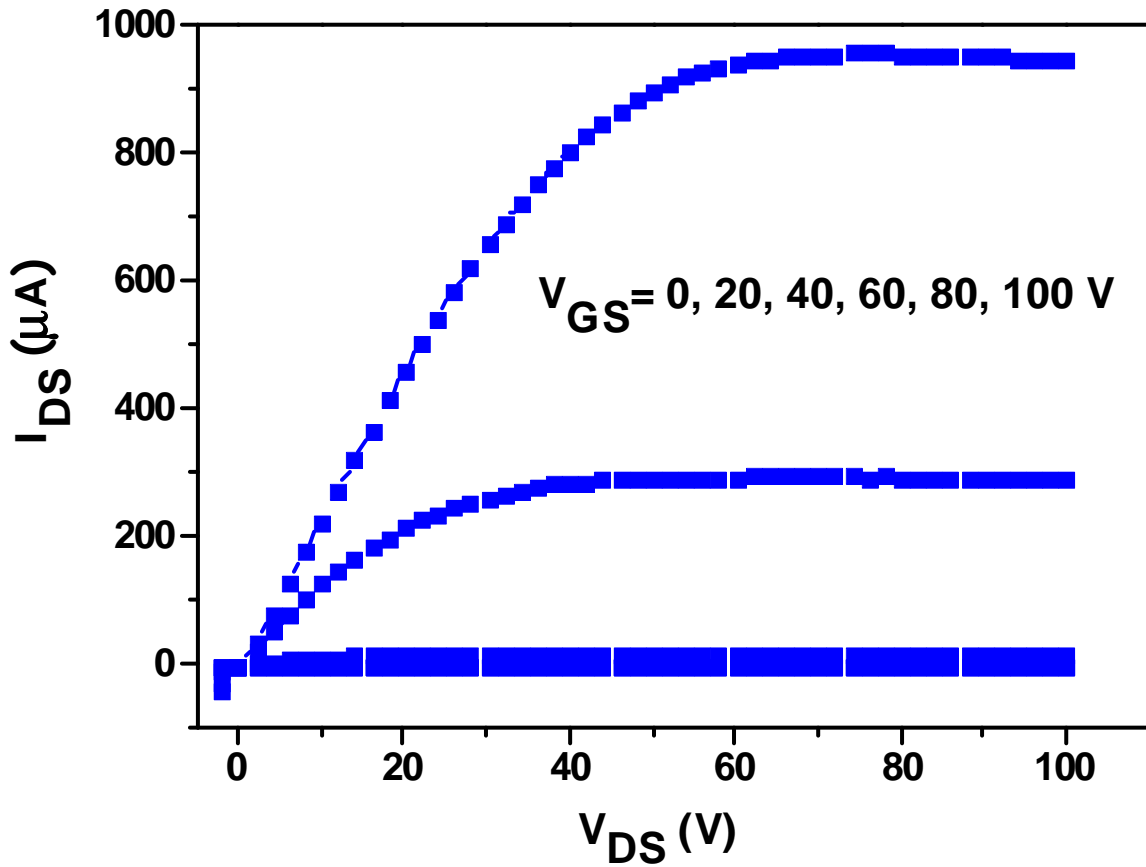


Figure 1.20: MULTIPLE OUTPUT curves for *mono*-sublimed DHF4T.

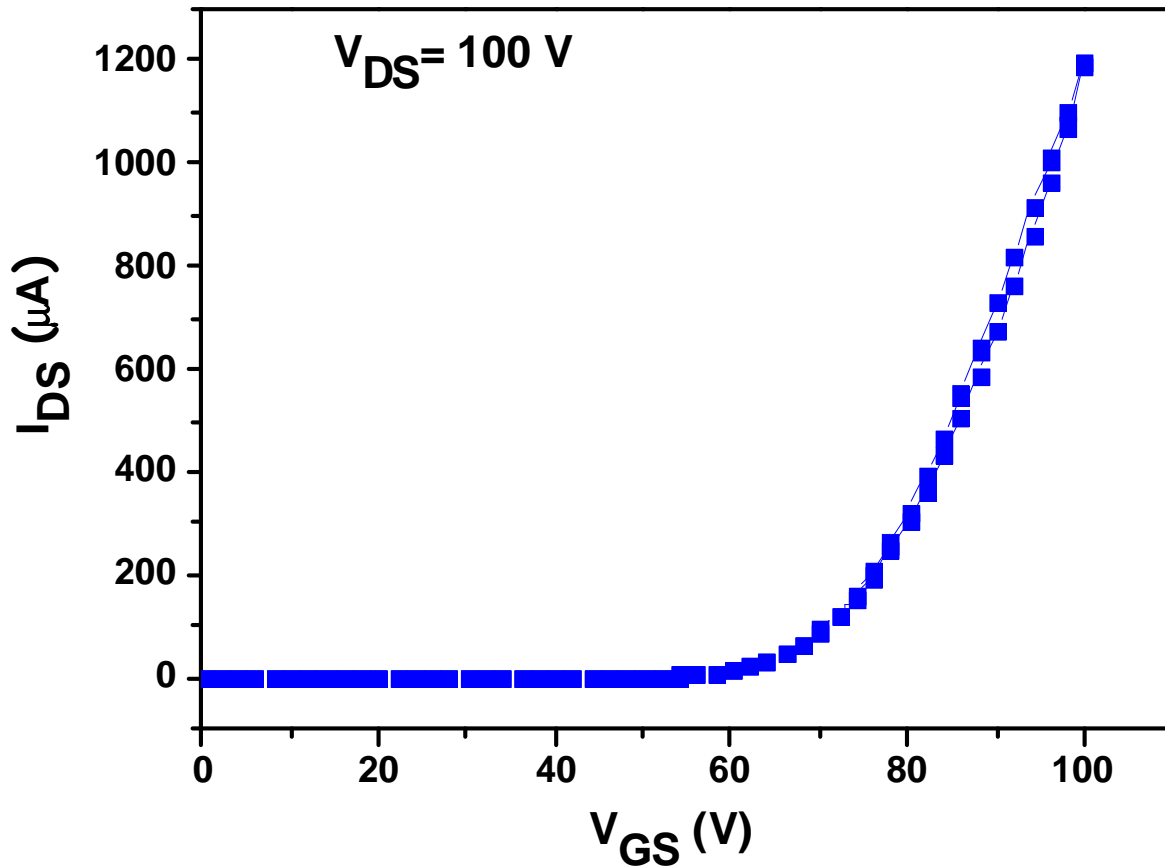


Figure 1.21: SATURATION TRANSFER curve for *mono*-sublimed DHF4T.

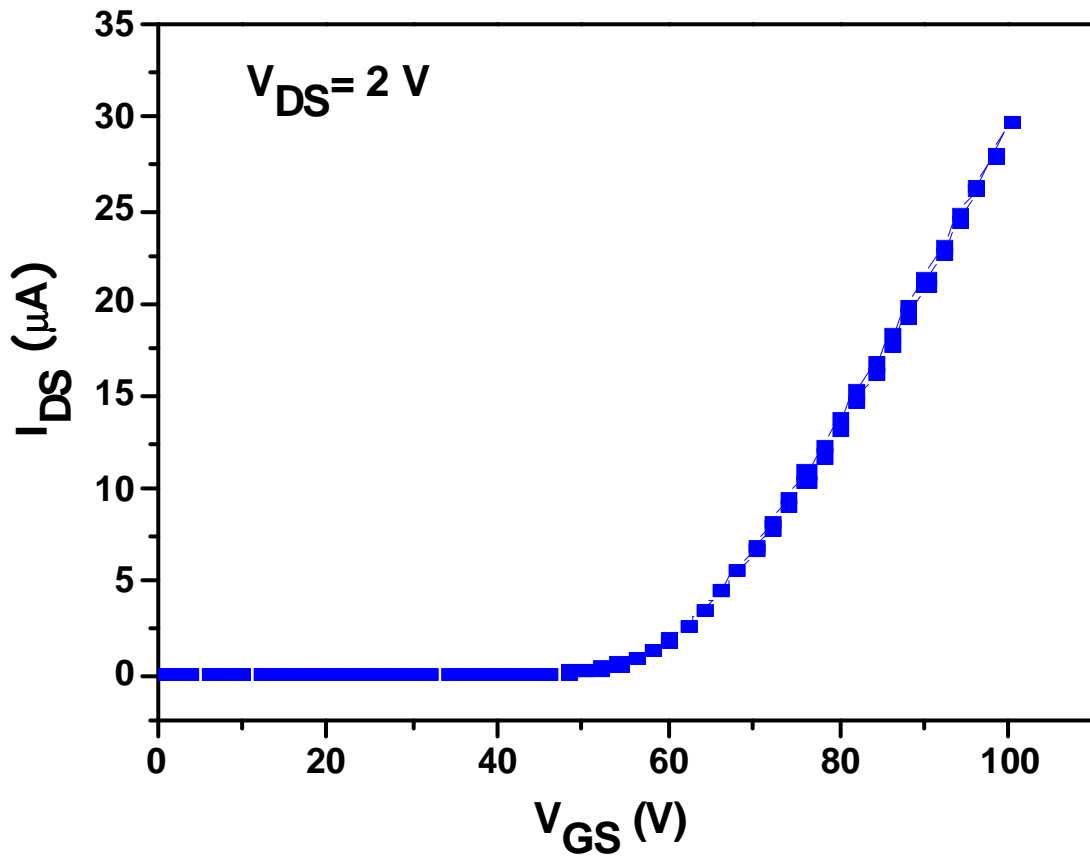


Figure 1.22: LINEAR TRANSFER curve for *mono*-sublimed DHF4T.

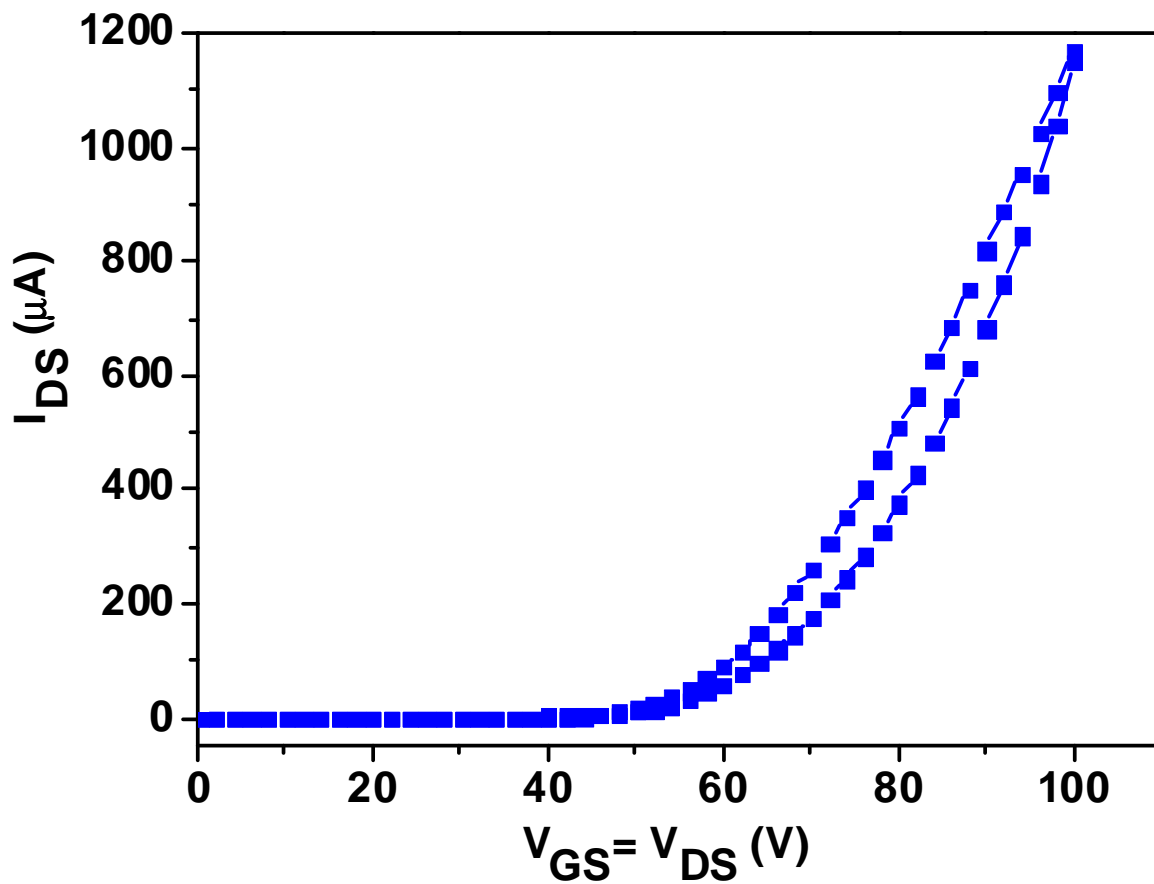


Figure 1.23: LOCUS curve for *bis*-sublimed DHF4T.

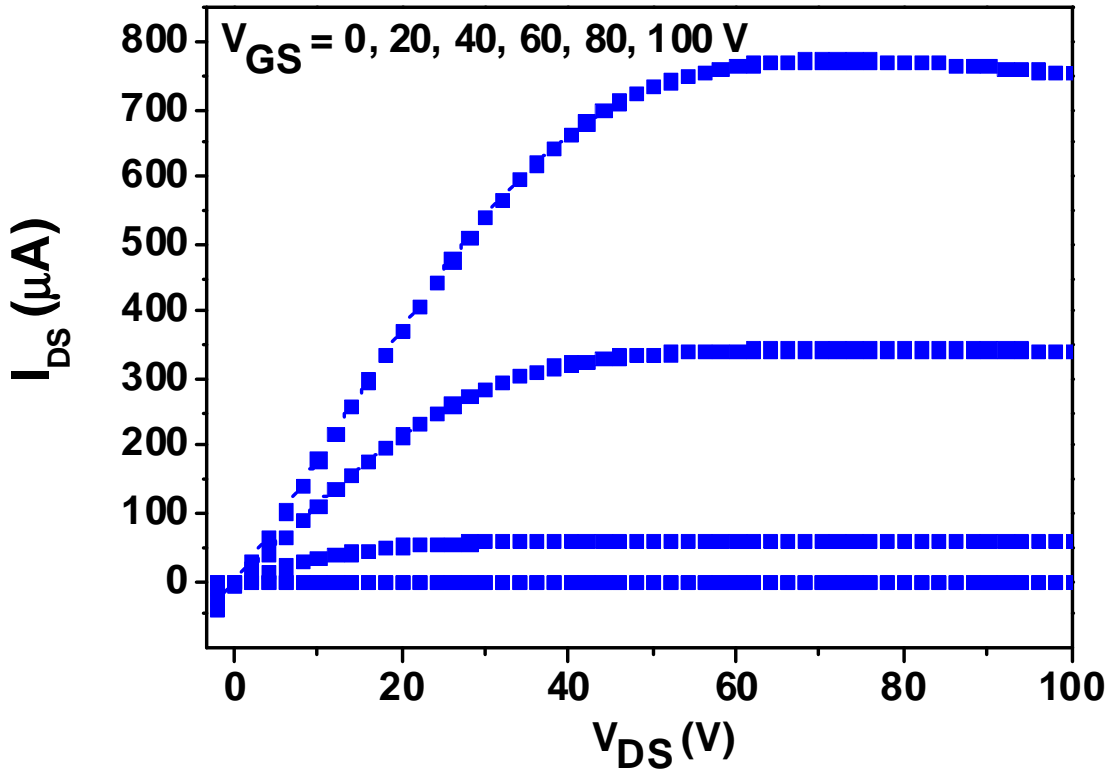


Figure 1.24: MULTIPLE OUTPUT curves for *bis*-sublimed DHF4T.

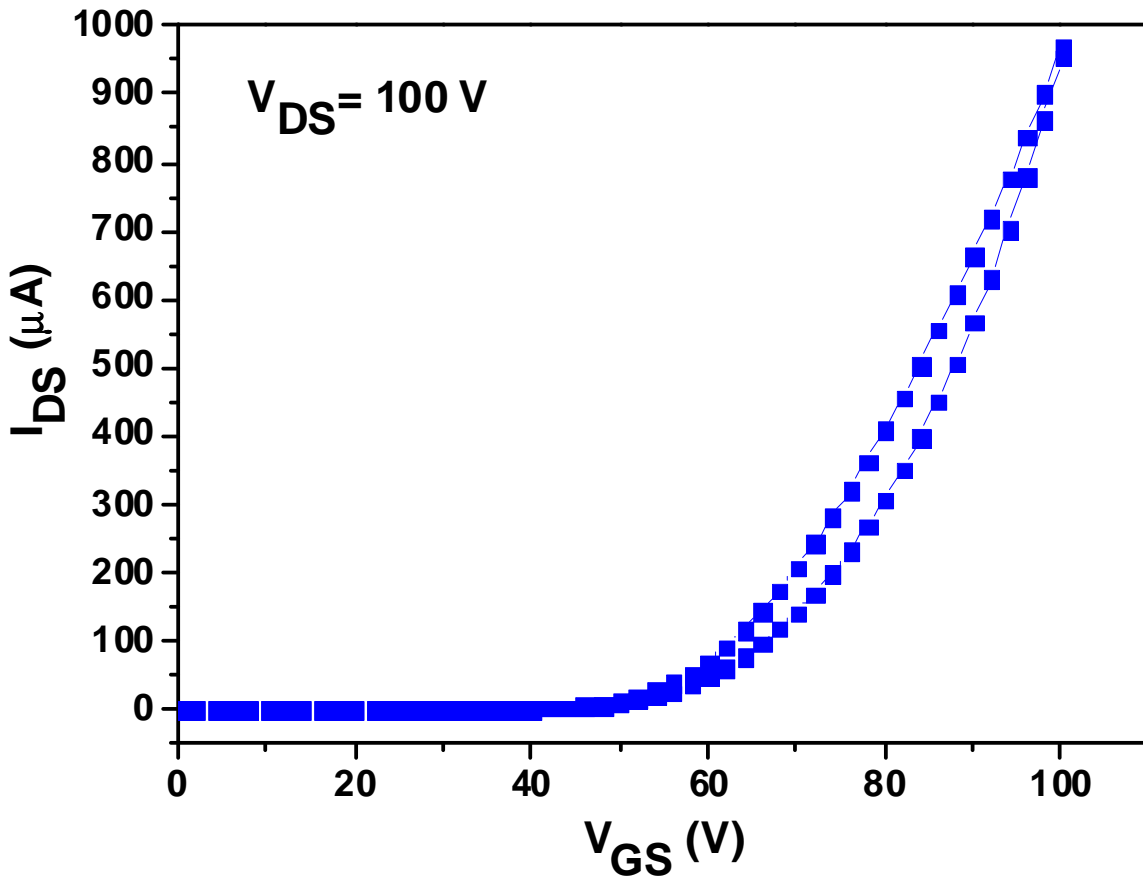


Figure 1.25: SATURATION TRANSFER curve for *bis*-sublimed DHF4T.

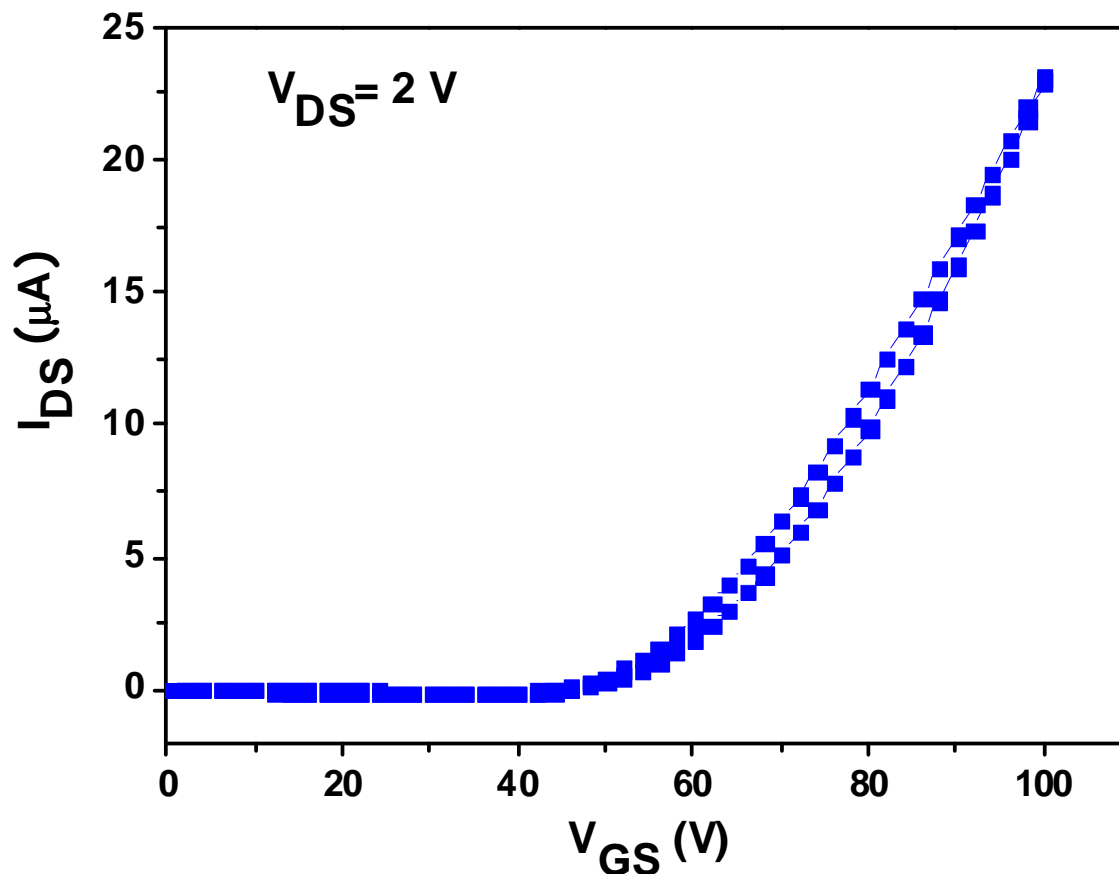


Figure 1.26: LINEAR TRANSFER curve for *bis*-sublimed **DHF4T**.

DHF4T is harder to be purified than **DH4T**, despite it differs from the latter only by the perfluorohexyl chains in α and ω positions.

Charge mobility increases as the semiconductor repeatedly undergoes sublimation, while threshold voltage becomes higher after every complete process. Crude semiconductor LOCUS curve shows notable hysteresis loop, thus the OFETs active layers have trapped charges inside; the *mono*-sublimed plot seems to be less affected by electric hysteresis, which returns greater in the *bis*-sublimed LOCUS. This is an evidence of the sublimation limits: a substance, which is hard to be recovered or is not very suitable for the purification process, becomes newly affected by impurities after further sublimation cycles. In all the discussed curves ohmic linear part is negligible. MULTIPLE OUTPUT plots show their linear parts crossing in one origin, revealing neither dielectric current leakage nor abnormal Gate geometry; the

saturation zones are not perfectly flat, thus the devices have free charges localized in the bulk active layers.

Every SATURATION TRANSFER curves is similar to the corresponding LOCUS, confirming the active layer charge trapping highlighted by the hysteresis behavior; this feature is found also in the LINEAR SATURATION plots whose functions have a pretty constant slope however, pointing out the perfect charge injection from the metal electrodes.

The confrontation between the **DHF4T** performances experimentally obtained before and after the sublimation cycles demonstrates how the organic semiconductor behavior during the sublimation influences the OFET performances.

1.5 Conclusions and remarks

2,2'''-Dihexyl-2,2':5',2'':5'',2'''-quaterthiophene (**DH4T**) and 2,2'''- Perfluoro-Dihexyl-2,2':5',2'':5'',2'''-quaterthiophene (**DHF4T**) were chosen to investigate the benefits of entrainer sublimation on organic semiconductors.

Despite the fact the two molecules are very similar to each other, except for the perfluoro-alkyl side chains, they behave in very different ways: **DH4T** shows a very good crystal look after sublimation, it is easy to recover and its electric performances gain with the number of sublimation cycles; **DHF4T** instead aggregates in subtle powder after sublimation, it is hard to recover and its electric performances but the charge mobility generally get worse increasing the number of sublimation cycles.

The crystal properties and the behavior during the purification process are critical to obtain good results but the kind and the concentration of impurities play a decisive role, despite they are unknown, and make the difference between a sublimation suitable semiconductor and one not.

The physical-chemical properties of the pollutants are the key factor to understand if they are easy to remove from the organic material or not: each molecule has its own impurities because they are the residual byproduct and sideproducts of the syntheses used to produce the semiconductor itself.

Organic and organometallic pollutants represent the most important limit for a sublimation treatment, due to the impossibility to totally separate them during the recovery step and due to their physical properties which are sometimes very similar to those of the semiconductor.

REFERENCES

- [1] M. Rajeswaran, T. N. Blanton, *Z. Kristallogr. NCS* 218 (2003) 439–440;
- [2] E. F. G. Herrington, *Endeavour*, 19, 191 (1960);
- [3] N. Karl, *Molecular Crystals and Liquid Crystals Incorporating Nonlinear Optics*, Vol. 171, Issue 1, 1989;
- [4] P. E. Fielding, F. Gutmann, *J. Chem. Phys.*, 26, 411 (1957); PhD Thesis, University of NSW, 1956;
- [5] D. K. Kearns, M. Calvin, *J. Chem. Phys.*, 34, 2026 (1961);
- [6] J. W. Weigl, *J. Chem. Phys.*, 32, 324 (1960);
- [7] H. Akamatu, H. Inokuchi, Y. Matsunaga, *Bull. Chem. Soc. Japan*, 29, 213 (1956);
- [8] R. Capelli, S. Toffanin, G. Generali, A. Facchetti, M. Muccini, *Nature Mat.*, Vol 9, June 2010;
- [9] P. W. Atkins, J. de Paula, *Physical Chemistry* (9th ed., 2010), Oxford University Press;
- [10] F. Gutmann, L. E. Lyons, *Organic Semiconductors*, John Wiley & Sons;
- [11] N. Parkins, A.R. Ubbelohde, *J. Chem. Soc.*, 4188, (1960);
- [12] F. Gutmann, L. E. Lyons, *Organic Semiconductors*, John Wiley & Sons;

CHAPTER 2

SYNTHETIC STRATEGY TO IMPROVE THE PURITY OF AN ORGANIC SEMICONDUCTOR

2.1 DH4T

2,2'''-Dihexyl-2,2':5',2'':5'',2'''-quaterthiophene (**DH4T**) is one of the most studied and tested materials for organic electronics and its *p*-type characteristics are widely known as well as its chemical-physical properties.

In thin films it exhibits large two-dimensional crystalline domains, which guarantee high conductivity and thickness-dependent mobility [1]; furthermore it can match easily with other semiconductors due to its optimal morphological and energetic coupling features [2]. It is also successfully used as hole carrier in the fabrication of an organic trilayer OLET, whose efficiency outperforms the conventional OLED one [3], and to improve several low-power devices in analog circuits [4]. Like many organic semiconductors [5] **DH4T** itself sometimes shows a poor reproducibility for what concerns the results and the performances of the OTFTs, supposedly caused by residual impurities or molecules hardly removable from the crude product.

DH4T common synthesis process involves metal-aided couplings, like oxidative homocoupling reactions, or metal-catalyzed carbon-carbon coupling, involving Stille and Suzuki reactions steps which require organometallic reagents such organotin or boronic esters compounds and palladium phosphine complexes.

While having a quantitative yield and being easy to control, transition metals catalyzed reactions give both homo and heterocoupling side-products along with metallorganic waste, which are not so simply to separate from the target oligothiophene. It is impossible to predict the type and the concentration of residual impurities given by classic synthetic way, so **DH4T** performances are not explainable only with physical or electronic experiments.

2.2 DH4T commercial synthesis

The first way to obtain **DH4T** with high global yield is the oxidative homocoupling process [6].

It involves the lithiation steps with n-butyllithium and tetramethylenediamine and the additions of Zinc and Copper (II) chlorides, which are spaced out by cooling, room temperature warming and intermediate purifications.

Two problems must be faced after a synthesis of this kind: the metals which take part in the reactions are easily ionizable and have work functions very similar to the **DH4T** HOMO (-5.80 eV) and LUMO (-2.89 eV) levels, as shown in Table 2.1 [7] .

METAL	WORK FUNCTION (eV)	IONIZATION ENERGY (eV)
Copper	4.53	(1 st) 7.73 (2 nd) 20.29
Lithium	2.90	(1 st) 5.39
Tin	4.42	(1 st) 7.34 (2 nd) 14.63
Zinc	3.63	(1 st) 9.39 (2 nd) 17.96

Table 2.1: work functions of common metals involved in **DH4T** oxidative homocoupling synthesis.

Low ionization energies and work functions values near the HOMO and LUMO energy levels turn the atoms of these common elements into traps generators and charge carriers competitors; furthermore they introduce dislocations and defects in the semiconductor lattice, reducing the conductivity.

The second synthetic approach to fabricate **DH4T** is the Palladium-catalyzed coupling [8]: several steps are often necessary to complete the whole process, usually carried in mild temperature conditions and without the necessity of anhydrous solvents or inert atmospheres. All the catalytic couplings derive from the Heck reaction [9] (see Figure 2.1a), which allows the formation of a C-C between an aromatic halide and an alkene in presence of a base.

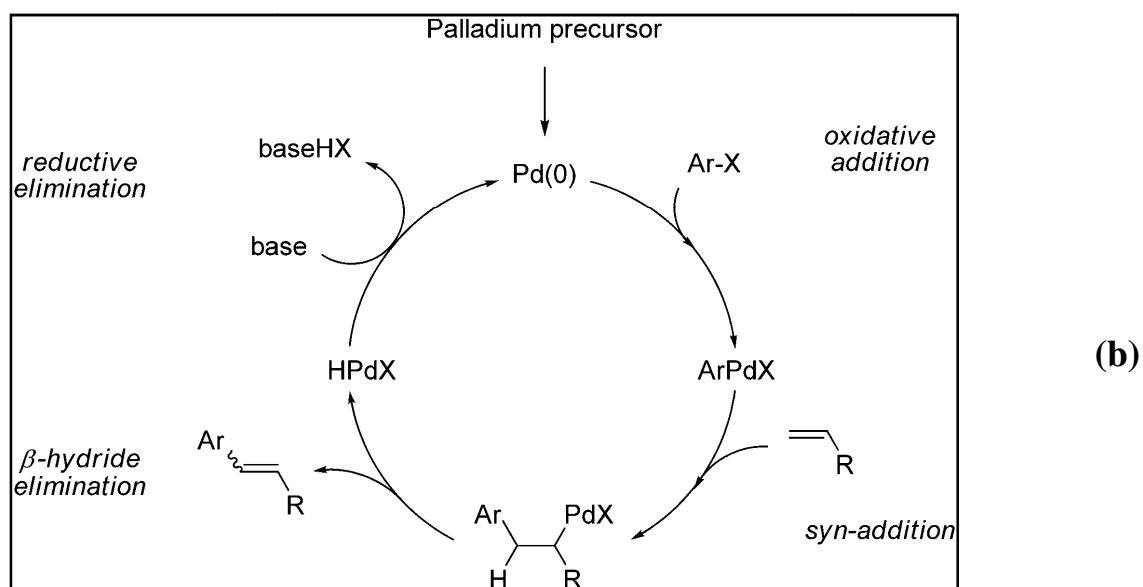
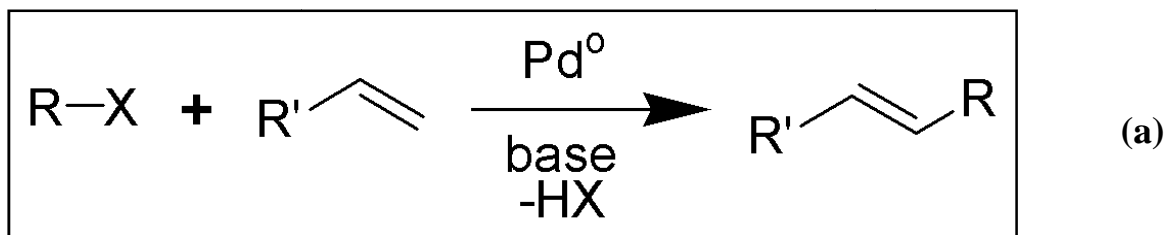


Figure 2.1: (a) basic scheme of Heck reaction; (b) catalytic mechanism of Heck reaction [10].

This reaction was studied through years and a lot of variations were produced to extend the efficiency of the Palladium catalytic cycle (see Figure 2.1b) to the highest possible number of reagents, often involving transmetalation mechanism.

Table 2.2 shows all the Heck-born reactions, comparing the reagents.

REACTION	FIRST REAGENT	SECOND REAGENT
Heck	Aryl halide	Alkene
Suzuki	Aryl halide	Boronic acid or ester
Stille	Organohalide (sp^2 carbon)	Organotin compound
Hiyama	Organohalide (sp^2 carbon)	Organosilicon compound
Sonogashira (Copper (I) iodide as co-catalyst)	Aryl halide	Alkyne
Negishi	Organohalide (sp^2 carbon)	Halogenated organozinc compound

Table 2.2: list of the reactions which share the Heck catalytic cycle completed with the respective reagents.

All the cross-coupling processes are affected by a lot of consecutive and parallel reactions, which lead to a large number of byproducts and sideproducts whose nature is both inorganic and organometallic.

In addition to the problems discussed with the oxidative homocoupling process, now the influence of oligomers or small organic molecules on the main product properties is worthy to be considered.

For example, Palladium complexes decompose during the reaction and generate Palladium (0) nanoparticles, which can affect the semiconductor performances [11], as well as tin, copper and nickel impurities [12]; Figure 2.2 shows how the effects of transition metals impurities dramatically increase in photovoltaic application.

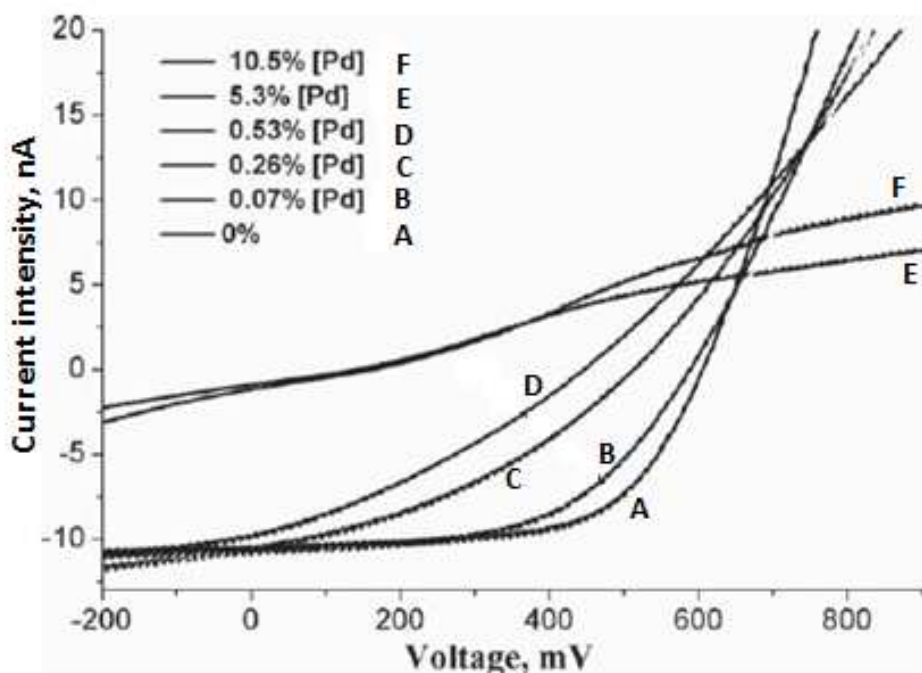


Figure 2.2: effects of the concentration of Palladium impurities on the I–V characteristics of P3HT/PCBM organic solar cells [13].

In OFET applications the semiconductor purity plays a leading role: decreasing of charge mobility and power efficiency are all evidences of the impurities presence [14], while unfortunately purification methods like solvent extraction, train sublimation, chromatography or crystallization don't guarantee the complete removal of byproducts and of exhausted organometallic waste.

Due to the impossibility to control the **DH4T** purity to “electron grade” level, as it is usually for inorganic semiconductors, it was our aim to achieve a cleaner synthetic path in order to bypass common metallic and metalorganic reagents as well as intermediate purification processing.

2.3 New metal-free synthesis of DH4T

The starting point of our process was the synthesis of half **DH4T** molecule, which had to be coupled with itself later: 5-Bromo-5'-hexyl-2,2'-bithiophene (**HexT₂Br**) is made from the 5-Hexyl-2,2'-bithiophene (**HexT₂**, Sigma Aldrich) by selective bromination at low temperature, as Figure 2.3 shows.

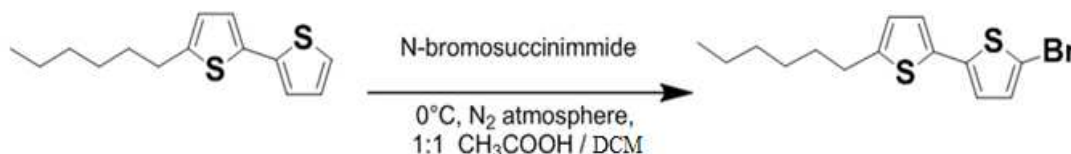


Figure 2.3: scheme of **HexT₂Br** synthesis.

HexT₂ was dissolved in a balloon under nitrogen atmosphere using a 1:1 blend of DCM and Acetic Acid; after covering the balloon with aluminum foil and cooling the solution to 0°C with water and ice, 1 equivalent of *N*-Bromosuccinimide (Sigma Aldrich) was added little by little (a spatula tip every 20 minutes).

Until the brominating reagent is over, the temperature and the ice quantity were constantly and carefully controlled.

Twelve hours after the last addition, the reaction was quenched with water and then the product is extracted with DCM/H₂O (x 3).

The organic fraction was then dried with Na₂SO₄ and, after removing the solvent, the product purification was carried on with a chromatographic column (silica flash as solid phase and Petroleum Ether 30-40 as eluent).

Reaction yield is very high (94%).

CHARACTERIZATION DATA OF HexT₂Br

EI-MS (*m/z*): 328.

¹H-NMR: (400 MHz, CDCl₃, 25°C TMS) δ 0.89 (t, 3H), 1.28-1.39 (m, 6H), 1.68 (quint., 2H), 2.77 (t, 2H), 6.66 (d, 1H), 6.82 (d, 1H), 6.91 (d, 1H), 6.93 (d, 1H).

¹³C-NMR: (100.6 MHz, CDCl₃, 25°C TMS) δ 14.0 (CH₃), 22.6 (CH₂), 28.9 (CH₂), 30.2 (CH₂), 31.6 (CH₂), 32.4 (CH₂), 110.6 (C_q), 123.6 (CH), 124.2 (CH), 124.6 (CH), 127.4 (CH), 137.6 (C_q), 137.8 (C_q), 146.1 (C_q).

To obtain the **DH4T** molecule it is necessary to activate the **HexT₂Br** turning it into a Grignard reagent, which then is able to make homocoupling in the presence of a stable radical.

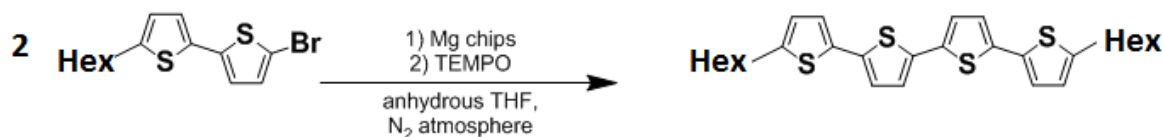


Figure 2.4: scheme of **DH4T** synthesis from **HexT₂Br**.

After the bromination **HexT₂Br** was dissolved in anhydrous THF and then the solution was added slowly to 1.2 equivalents of Magnesium chips (Sigma Aldrich) in a balloon under nitrogen atmosphere; the mixture was heated under stirring condition until the beginning of the Grignard reaction, revealed by bubbles appearance.

After 2h from the total expend of the Magnesium, 1.7 equivalents of 2,2,6,6-Tetramethylpiperidin-1-yl)oxyl stable radical (TEMPO, Sigma Aldrich) were dissolved in anhydrous THF and then drop-added to the Grignard reactive. After other 2h the reaction was quenched with water and the crude **DH4T** was extracted with DCM/H₂O (x 3).

The organic fraction was dried with Na₂SO₄ and, after removing the solvent, the product purification was carried on with a chromatographic column (silica flash as solid phase and Petroleum Ether 30-40 as eluent).

Reaction yield is about 30%.

CHARACTERIZATION DATA OF DH4T

EI-MS (*m/z*): 498.

UV absorption: One peak at 400 nm.

PL emission: Two peaks at 460 and 500 nm.

¹H-NMR: (400 MHz, CDCl₃, 25°C TMS) δ 0.90 (t, 3H $J = 6.499$ Hz), 1.28-1.44 (m, 6H), 1.69 (quint, 2H, $J = 6.499$ Hz), 2.80 (t, 2H, $J = 7.433$ Hz), 6.67 (d, 1H, $J = 8.846$), 6.69 (d, 1H, $J = 8.846$), 6.98 (d, 1H, $J = 8.775$), 7.30 (d, 1H, $J = 8.775$).

¹³C-NMR: (100.6 MHz, CDCl₃, 25°C TMS) δ 14.07 (CH₃), 22.56 (CH₂), 28.75 (CH₂), 30.19 (CH₂), 31.56 (CH₂), 43.10 (CH₂), 123.39 (CH), 123.55 (CH), 124.00 (2CH), 134.1 (C_q), 136.6 (2C_q), 142.9 (C_q).

2.4 OFETs fabrication and compared characterization

After achieving **DH4T** laboratory synthesis, the semiconductor has to be compared with the commercial one by the fabrication and the characterization of Organic Field – Effect Transistors (*bottom Gate / top contacts* configuration), by which it is possible to know if the accomplished synthetic process is good as the classic catalytic approach or even better.

The OFET electric performances are a unique instrument to check the purity and the efficiency of a semiconductor: easy to measure and to understand, they offer an instant overview of the synergic working of the device architecture and of the semiconductor properties.

We used two commercially available **DH4Ts** with different purity grades to make the comparison with our product.

In order to have a platform on which test OFETs could be fabricated, glass-made substrates (2.5 x 2.5 cm, Visiontek Systems) were chosen with a shaped Indium-Tin Oxide (ITO) film of 120 nm sputtered on them to play the role of the Gate electrode contact (see Figure 2.5).

After washing the substrates two times in Acetone and one last in 2-Propanol, a *Poly*-(methyl methacrylate) (PMMA, ALLRESIST AR-P 669-06) dielectric layer was spin-coated on them (6000 rpm, 60 s, 6000 rpm/s), annealed in a vacuum oven (18h at 90°C) and finally etched on the substrate borders to expose the ITO contacts (see Figure 2.6).

The ideal dielectric layer thickness is 450 nm, with a specific capacitance of about 7.58 nF/cm².

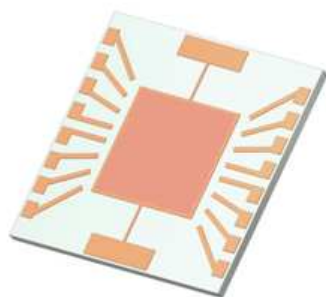


Figure 2.5:

basic glass/ITO substrate.

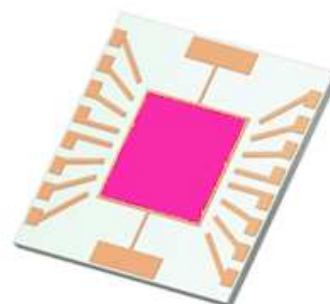


Figure 2.6:

glass/ITO substrate with etched PMMA layer.

The high vacuum sublimation provides a good technique to fabricate organic electronic devices without polluting the semiconductors with solvents or other materials: thus both commercial and synthesized **DH4Ts** were grown in thin films using a high vacuum sublimation machine (see Figure 2.7). Description of the real high vacuum sublimation machine can be found in Part 3 – Chapter 1.

The organic material was put in a high temperature quartz crucible inside an heating cell, while two glass/ITO/PMMA substrates are fixed on a sample holder with a special grid mask on their front face oriented downwards to the cell. The **DH4T** active layers are 15 nm thick, grown with a rate of 0.6 nm/min (0.1 Å/s) setting heating temperature at 190°C under $1 \cdot 10^{-6}$ mbar of vacuum condition.

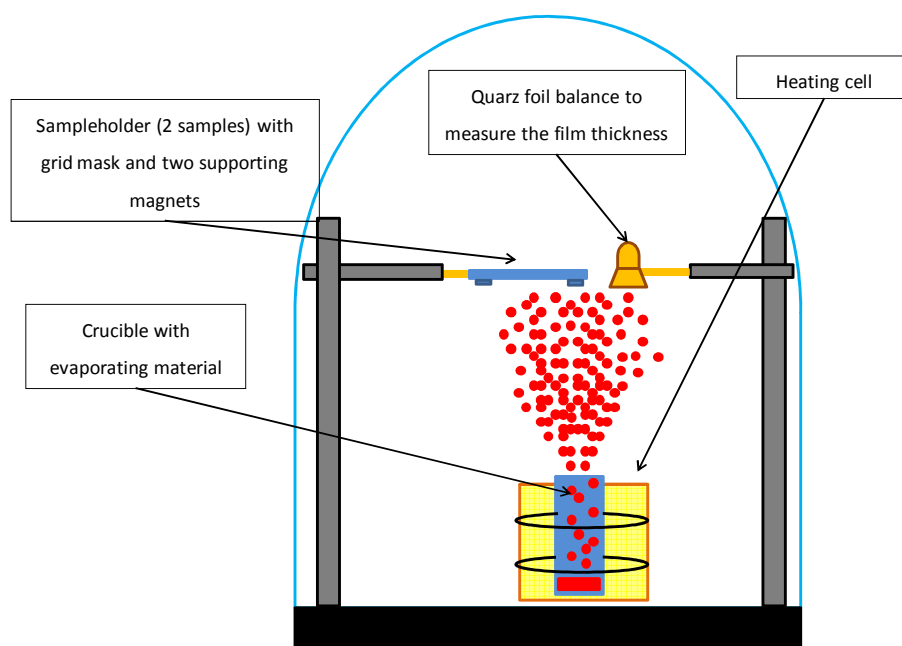


Figure 2.7: simplified scheme of an high vacuum sublimation system.

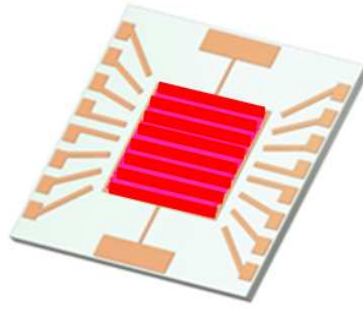


Figure 2.8: DH4T active layers evaporated on the glass/ITO/PMMA substrate.

Source and Drain electrodes are fabricated by Gold evaporation (see Figure 2.9): metal chips were put in a high temperature Al_2O_3 crucible inside an heating cell, while two glass/ITO/PMMA/DH4T substrates are fixed on a sample holder with a special grid mask on their front face oriented downwards to the cell.

The Gold electrodes are 70 nm thick, grown with a rate of 1.8 nm/min (0.3 \AA/s) setting the heating intensity current at 60 A under $1 \cdot 10^{-6}$ mbar of vacuum condition.

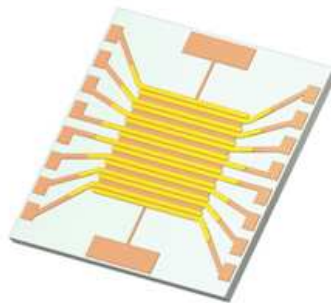


Figure 2.9: Gold Source and Drain electrodes evaporated on the glass/ITO/PMMA/DH4T substrate.

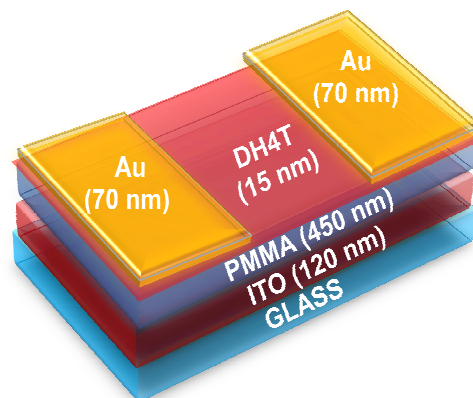


Figure 2.10: tridimensional scheme of a standard device structure.

Once the OFET fabrication process is over, every substrate carries eight complete devices whose channel dimensions are 12 mm of width and 70 μm of length.

After having collected the electric plots for metal-free **DH4T** transistors as well as for the commercial **DH4T** ones (see from Figure 2.11 to Figure 2.22), charge carriers mobility, threshold voltage and ON/OFF ratio are calculated from every device and then a statistic value is extracted (see Table 2.3).

Semiconductor	Charge mobility \pm standard deviation ($\text{cm}^2/\text{V}\cdot\text{s}$)	Threshold voltage \pm standard deviation (V)	ON / OFF ratio (only magnitude)
Metal-free DH4T	$(1.08 \pm 0.02) \cdot 10^{-1}$	-18.6 ± 1.3	10^4
Commercial DH4T #1	$(1.92 \pm 0.05) \cdot 10^{-1}$	-21.3 ± 1.6	10^4
Commercial DH4T #2	$(2.93 \pm 0.04) \cdot 10^{-2}$	-20.6 ± 2.7	10^3

Table 2.3: OFETs electric performances obtained for the synthesized **DH4T** and for the commercial ones.

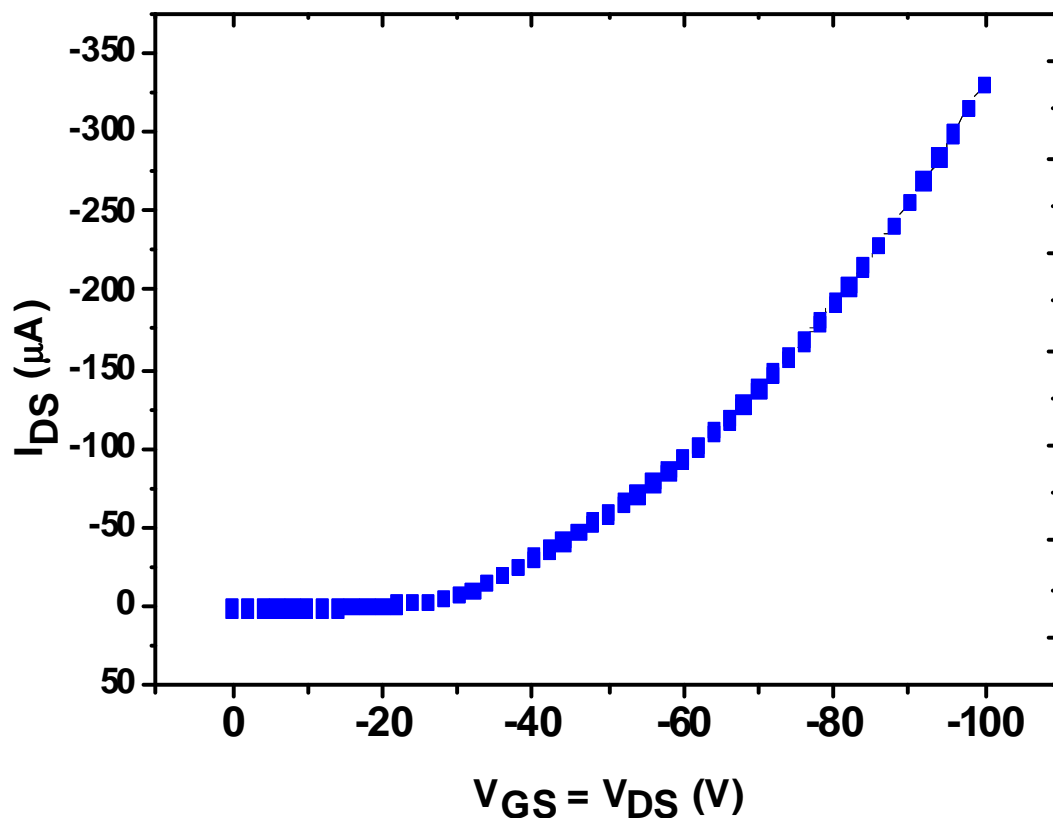


Figure 2.11: LOCUS curve of metal-free **DH4T**.

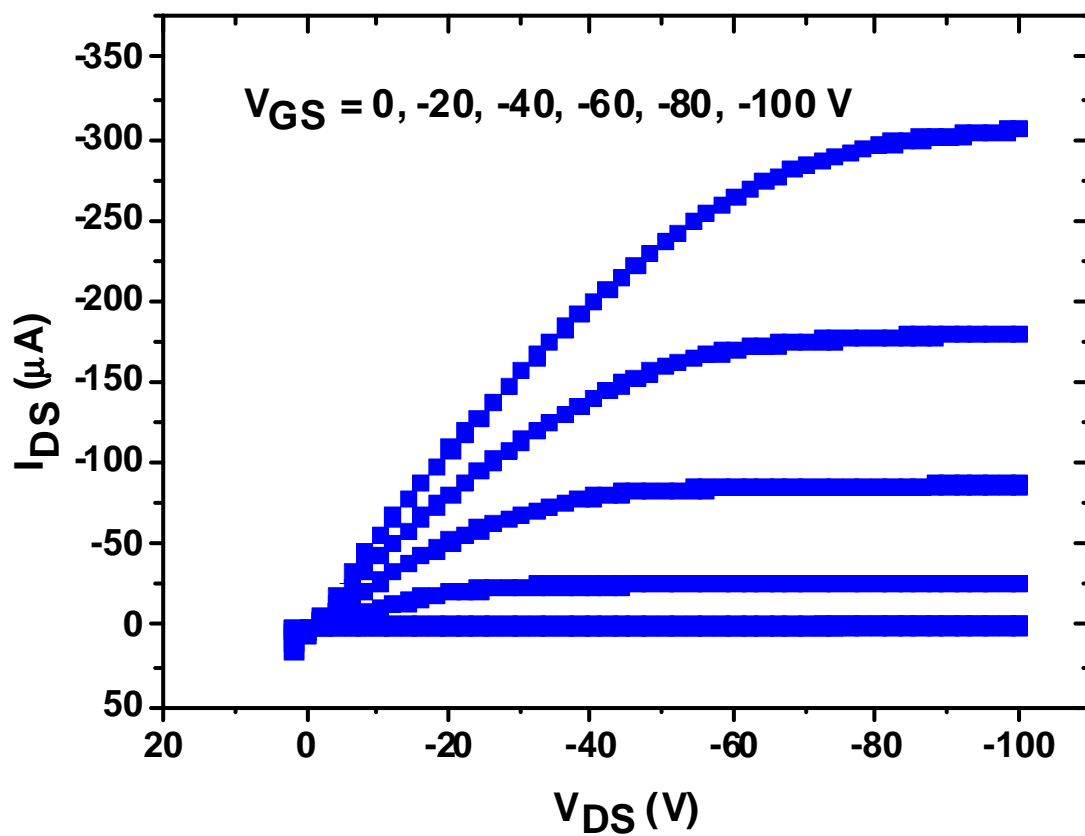


Figure 2.12: MULTIPLE OUTPUT curves of metal-free **DH4T**.

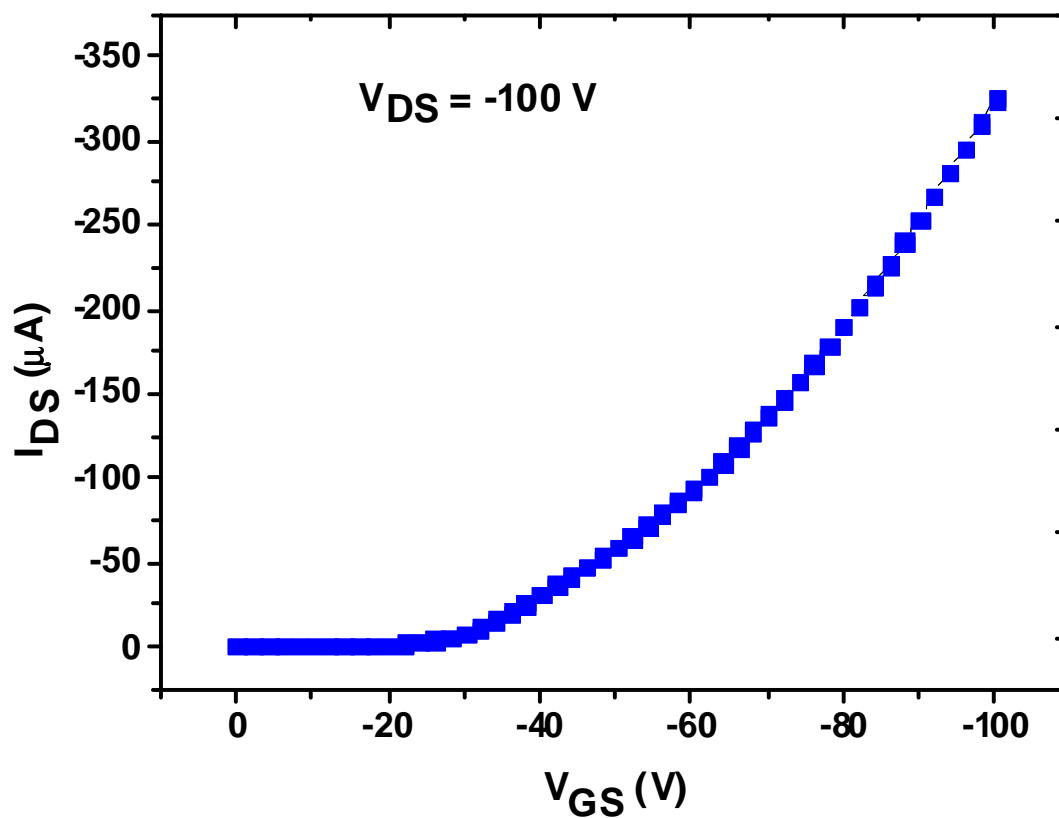


Figure 2.13: SATURATION TRANSFER curve of metal-free **DH4T**.

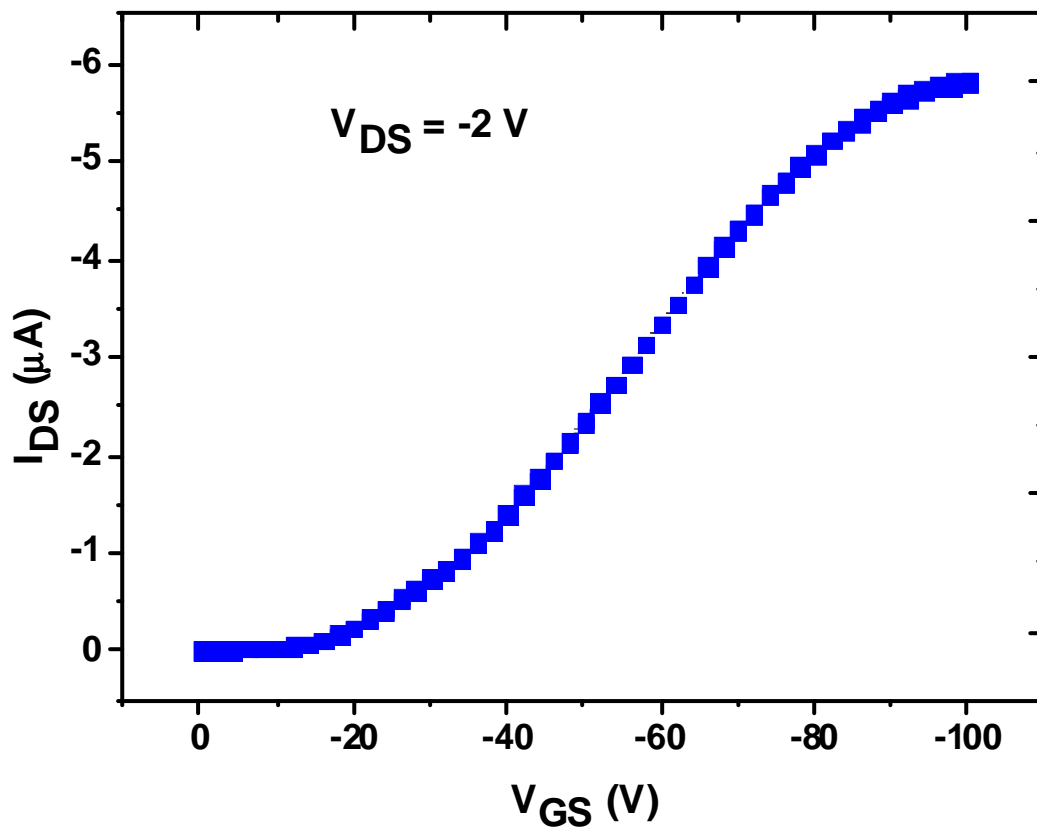


Figure 2.14: LINEAR TRANSFER curve of metal-free **DH4T**.

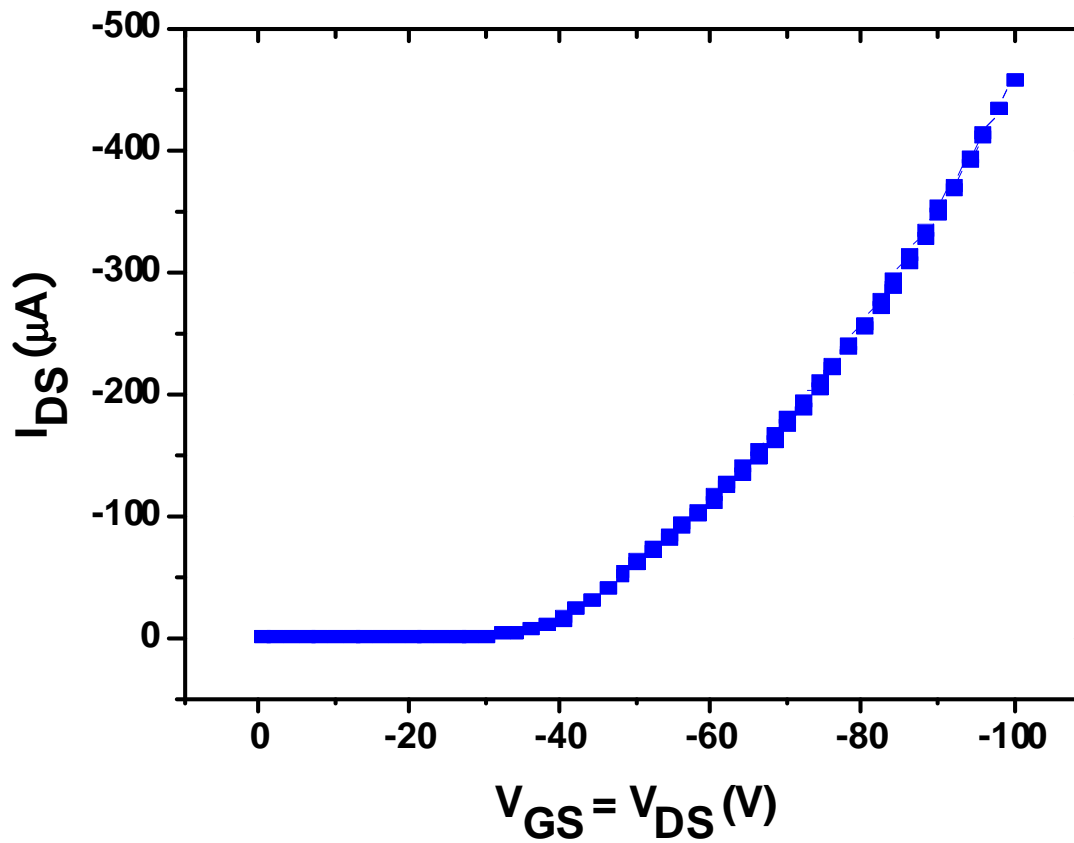


Figure 2.15: LOCUS curve of commercial **DH4T** #1.

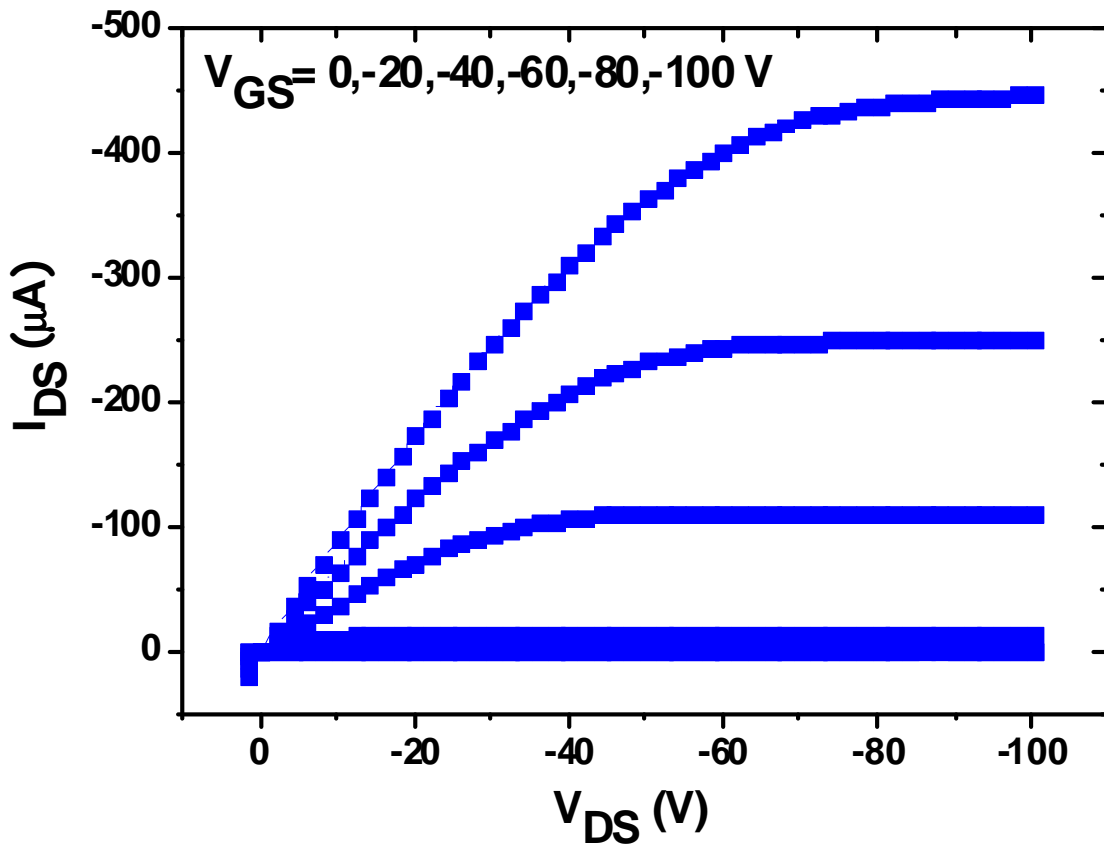


Figure 2.16: MULTIPLE OUTPUT curves of commercial **DH4T** #1.

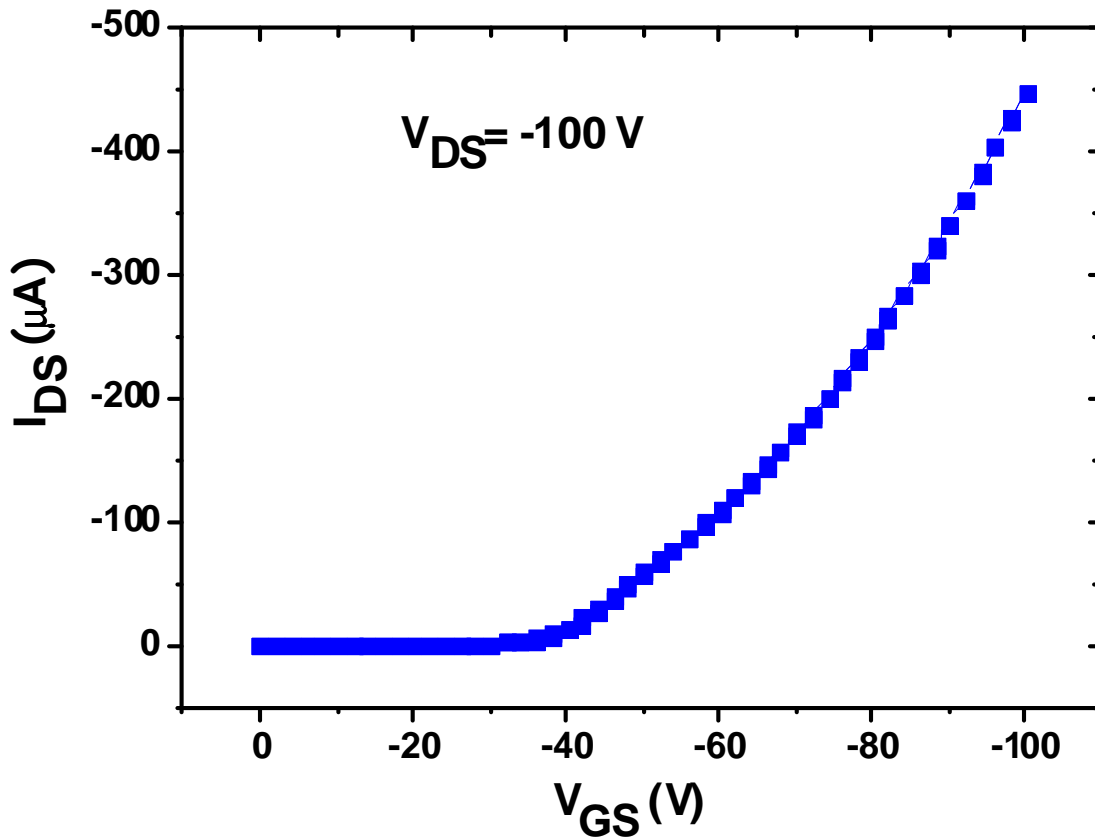


Figure 2.17: SATURATION TRANSFER curve of commercial **DH4T**#1.

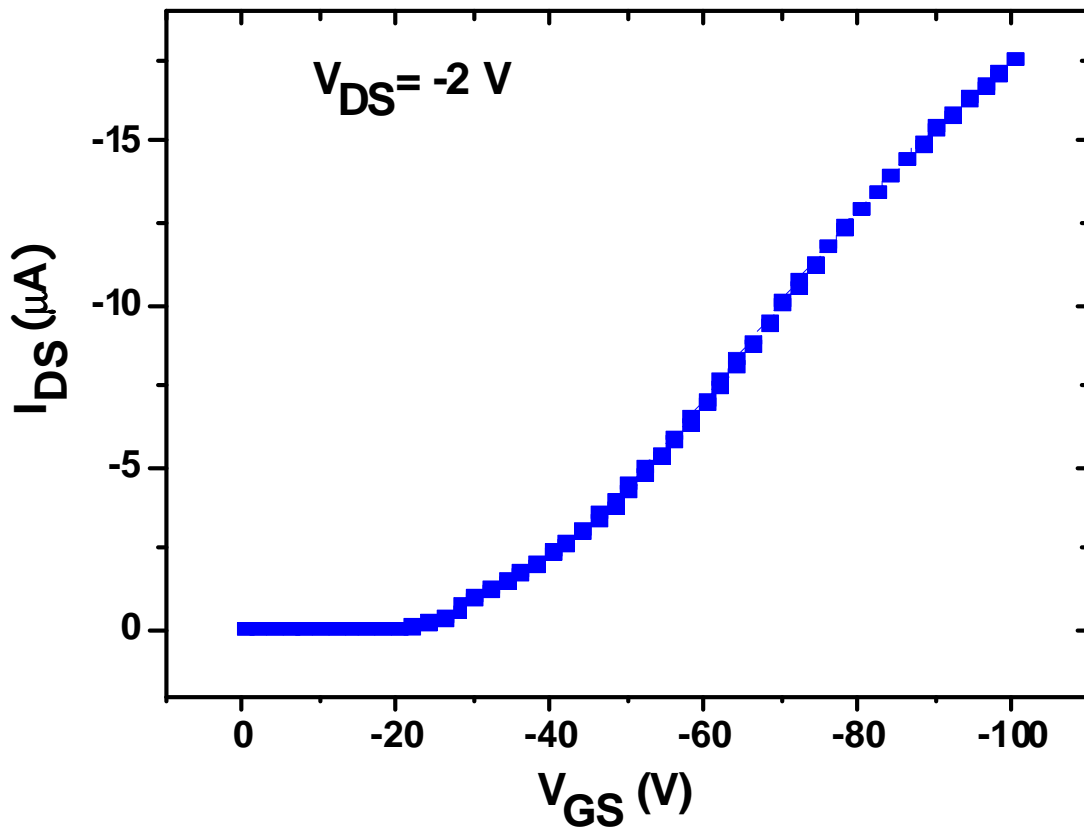


Figure 2.18: LINEAR TRANSFER curve of commercial **DH4T #1**.

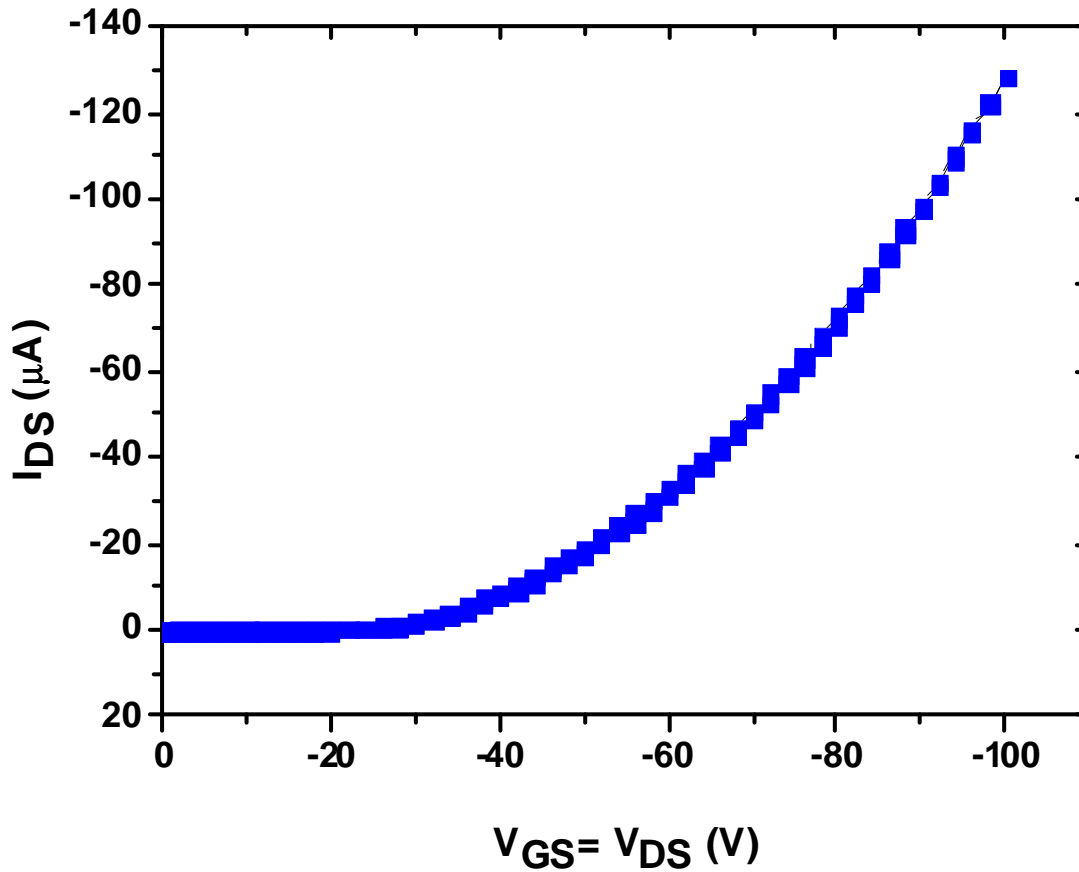


Figure 2.19: LOCUS curve of commercial **DH4T #2**.

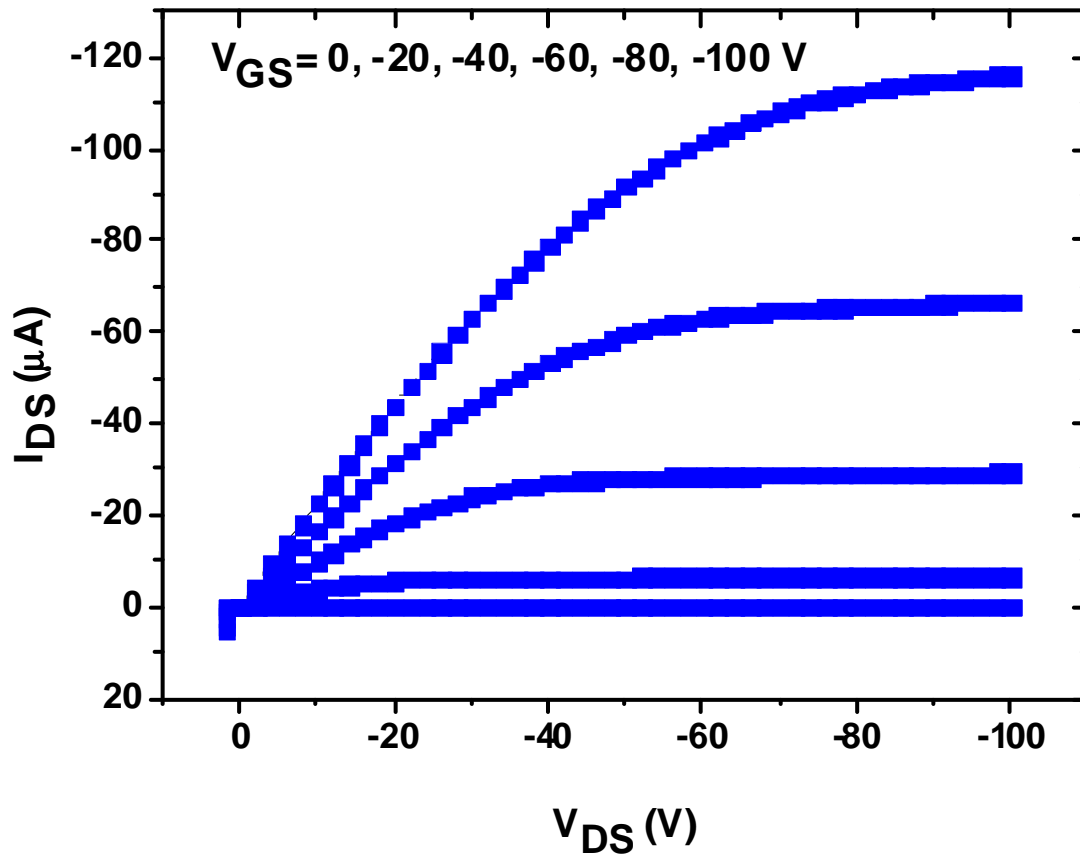


Figure 2.20: MULTIPLE OUTPUT curves of commercial **DH4T #2**.

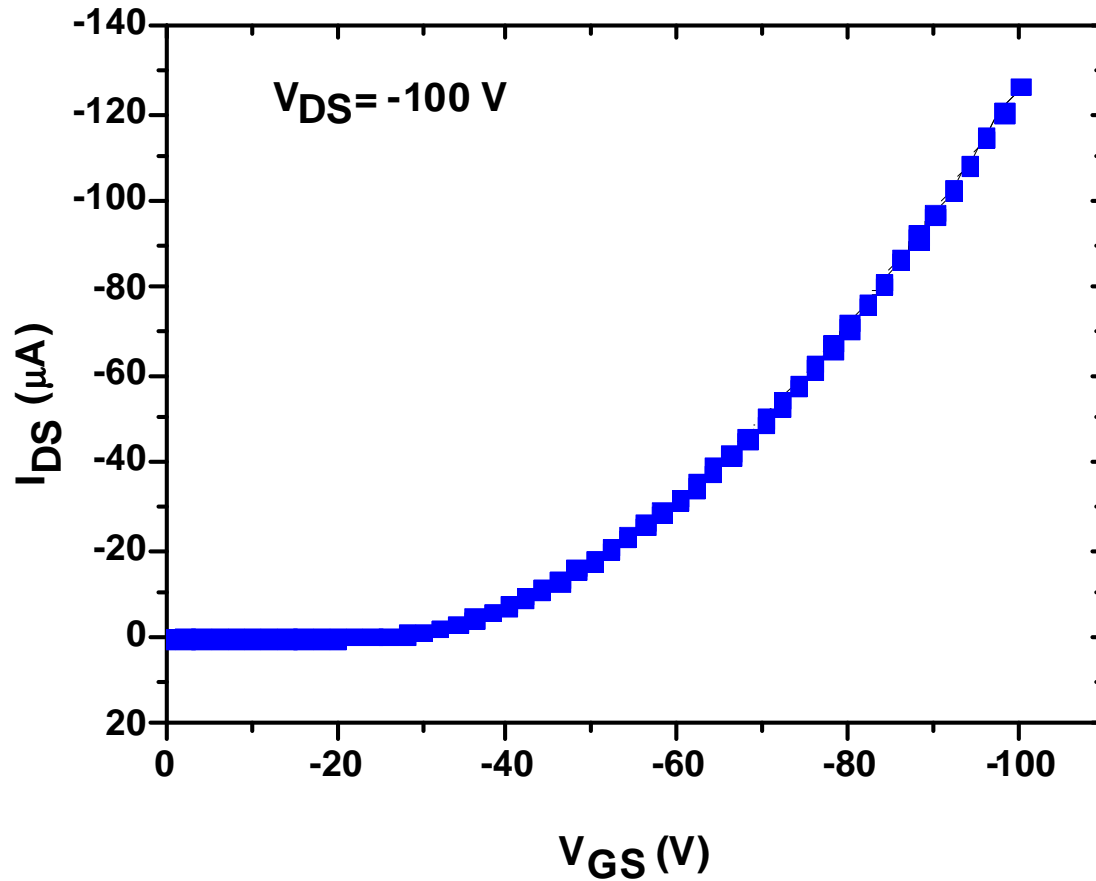


Figure 2.21: SATURATION TRANSFER curve of commercial **DH4T#2**.

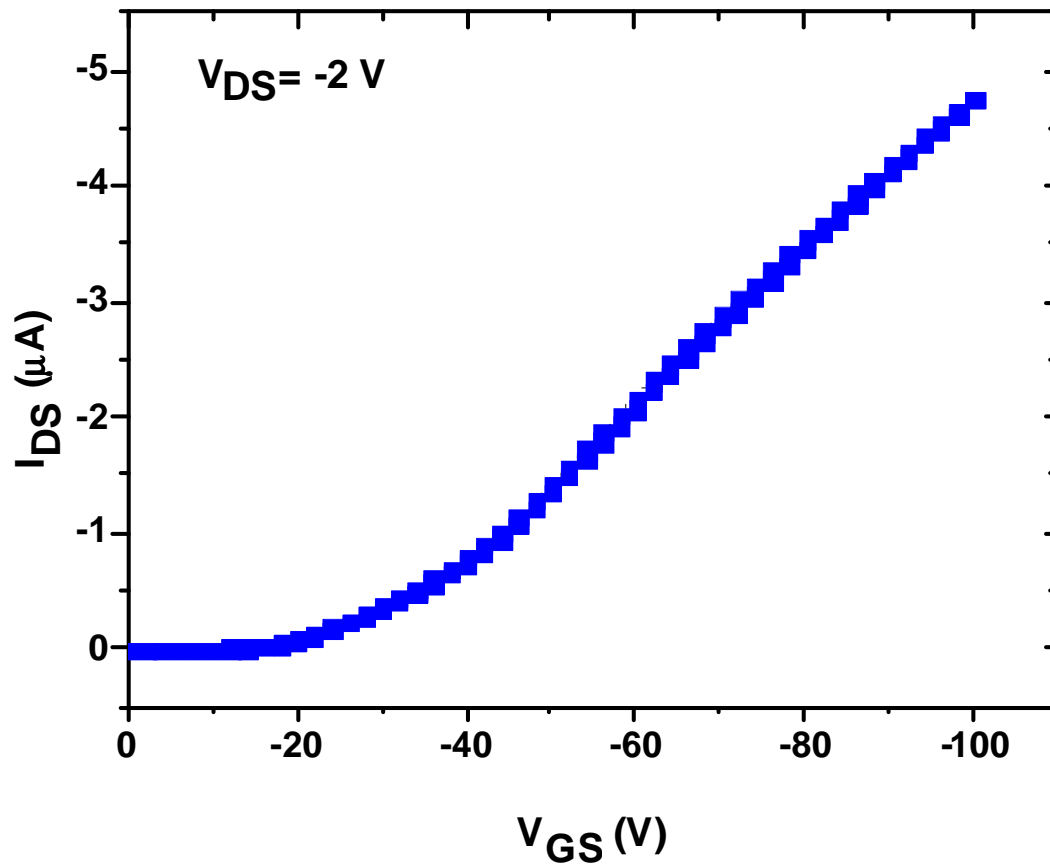


Figure 2.22: LINEAR TRANSFER curve of commercial **DH4T** #2.

Since the commercial products have been synthesized in different ways, thus having different purity grades, it is interesting to highlight the different behaviors.

All the MULTIPLE OUTPUT plots have flat saturation regime parts and show their linear parts crossing in one origin, revealing neither dielectric current leakage nor free charges in dielectric/active layers interface; LOCUS curves have no hysteresis loop, thus the OFETs active layers were not damaged during the fabrication.

Every SATURATION TRANSFER plot is similar to the corresponding LOCUS: this is a very good feature that follows the true ideal behavior, because both kinds of measurement are collected in OFET saturation regime.

LINEAR SATURATION curves don't show hysteresis loop and almost all of them have a pretty constant slope, highlighting the perfect charge injection from the metal electrodes; the final part of metal-free **DH4T** one show to be affected by charge injection inefficiency between Gold contacts and active layer.

Commercial **DH4T** #2 shows the worst performances, probably due to an ineffective purification procedure. Our metal-free **DH4T** has the lowest threshold voltage and its ON/OFF ratio reaches the same magnitude of the Commercial **DH4T** #1, which has the best charge mobility.

The confrontation between the **DH4T** obtained with the new synthetic method and the commercial products is pretty promising and demonstrates how the new metal-free synthesis is a good way to achieve the production of the semiconductor.

2.5 Investigation on the effects of organometallic impurities on DH4T performances

As already discussed in Paragraph 2.2, the reagents and catalysts of both metallic and organometallic nature, widely used in organic semiconductor synthesis, lead to a great variety of sideproducts and byproducts; the limits of laboratory purification practices make the impurities amount hard to determine and also varying each time. These are the reasons by which it is very troubling to define a correlation between pollutants concentration in an organic material and the performances of the finished device: since there is an unknown quantity of a certain impurity in the semiconductor batch, it has to be analytically determined and this often requires destructive technique expending precious material. A complete pollutants screening would waste a lot of product.

Obtaining **DH4T** with a new metal-free synthesis give us the chance to have a pure semiconductor with no transition metals traces and no coupling-born byproducts, thus it is possible to study the most common **DH4T** impurities on a virgin material.

Two organometallic molecules are chosen to make a controlled contamination: Tetrakis(triphenylphosphine)Palladium(0) (**Pd(PPh₃)₄**, Sigma Aldrich), the most common cross-coupling reactions catalyst, and TributylTin chloride (**Bu₃SnCl**, Sigma Aldrich), one of the Stille reaction sideproducts.

Pollutant molecule	Molecular weight (g/mol)	Density (g/cm ³)
Pd(PPh₃)₄	1155.56	/
Bu₃SnCl	325.51	1.20

Table 2.4: properties of tested organometallic impurities.

The doping agents were tested apart in different concentration using for each one a 10 mg batch of virgin **DH4T**; in Table 2.5 the doping data are reported.

Pd(PPh₃)₄ dissolved in DCM* (mg/10 ml)	Volume of Bu₃SnCl added to 10 mg batch of DH4T (μ l)	Impurity concentration in a 10 mg DH4T batch (w/w %)
1	0.8	1
5	4.2	5
10	8.3	10
* = 1 ml of solution is added to a 10 mg DH4T batch and the solvent is then removed.		

Table 2.5: controlled doping data for the organometallic impurities.

With every doped **DH4T** batch OFET devices were fabricated as explained in Paragraph 2.4 plus reference OFET devices made with virgin **DH4T**.

After completing the high vacuum sublimation process, the Field-Effect Transistors are fully characterized: the collected plots are shown from Figure 2.23 to Figure 2.46 while the elaborated statistical data are reported in Table 2.6.

Impurity kind and concentration (w/w %)	Charge mobility \pm standard deviation ($\text{cm}^2/\text{V}\cdot\text{s}$)	Threshold voltage \pm standard deviation (V)	ON / OFF ratio (only magnitude)
Reference virgin DH4T (0 %)	$(1.05 \pm 0.06) \cdot 10^{-1}$	-19.1 ± 1.3	10^4
Pd(PPh₃)₄ (1 %)	$(9.02 \pm 0.05) \cdot 10^{-2}$	-22.4 ± 2.4	10^3
Pd(PPh₃)₄ (5 %)	$(8.40 \pm 0.09) \cdot 10^{-2}$	-26.7 ± 1.8	10^3
Pd(PPh₃)₄ (10 %)	$(7.53 \pm 0.13) \cdot 10^{-2}$	-29.5 ± 1.5	10^3
Bu₃SnCl (1 %)	$(9.36 \pm 0.10) \cdot 10^{-2}$	-19.4 ± 2.6	10^3
Bu₃SnCl (5 %)	$(8.42 \pm 0.07) \cdot 10^{-2}$	-19.5 ± 1.9	10^3
Bu₃SnCl (10 %)	$(8.12 \pm 0.08) \cdot 10^{-2}$	-21.1 ± 1.9	10^3

Table 2.6: electric parameters measured for each pollutant concentration.

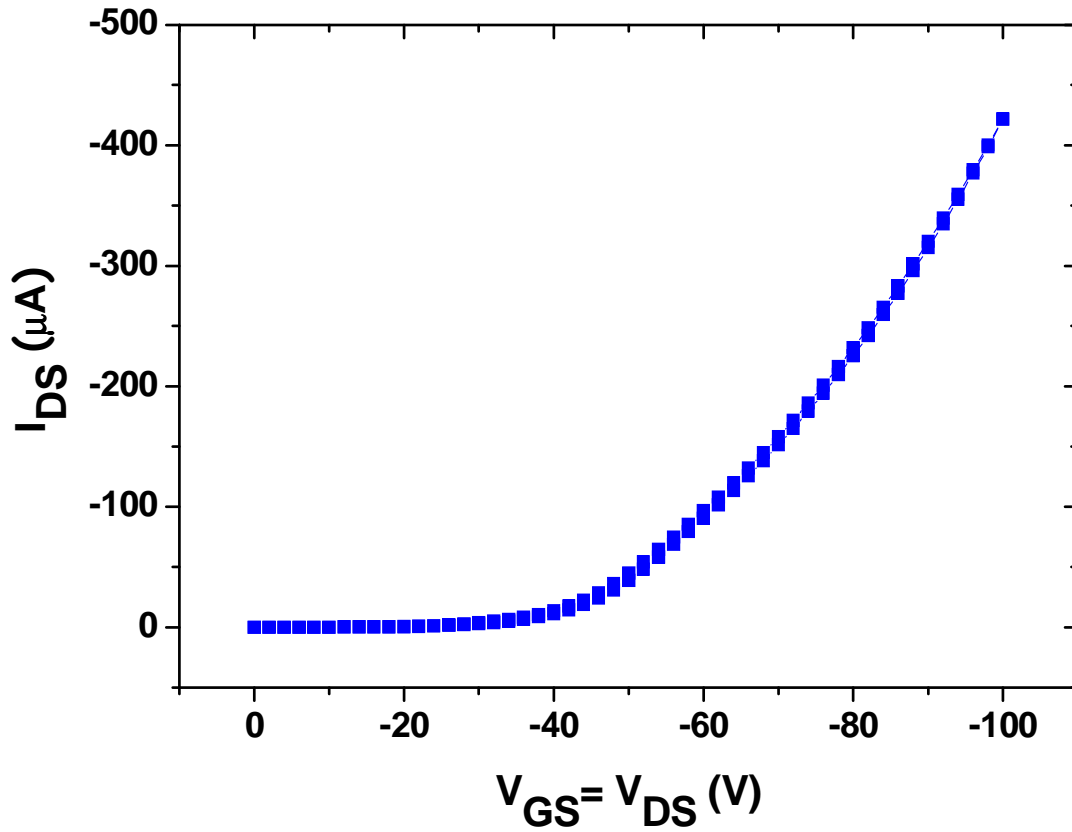


Figure 2.23: LOCUS curve of DH4T doped with 1 % w/w of Pd(PPh₃)₄ .

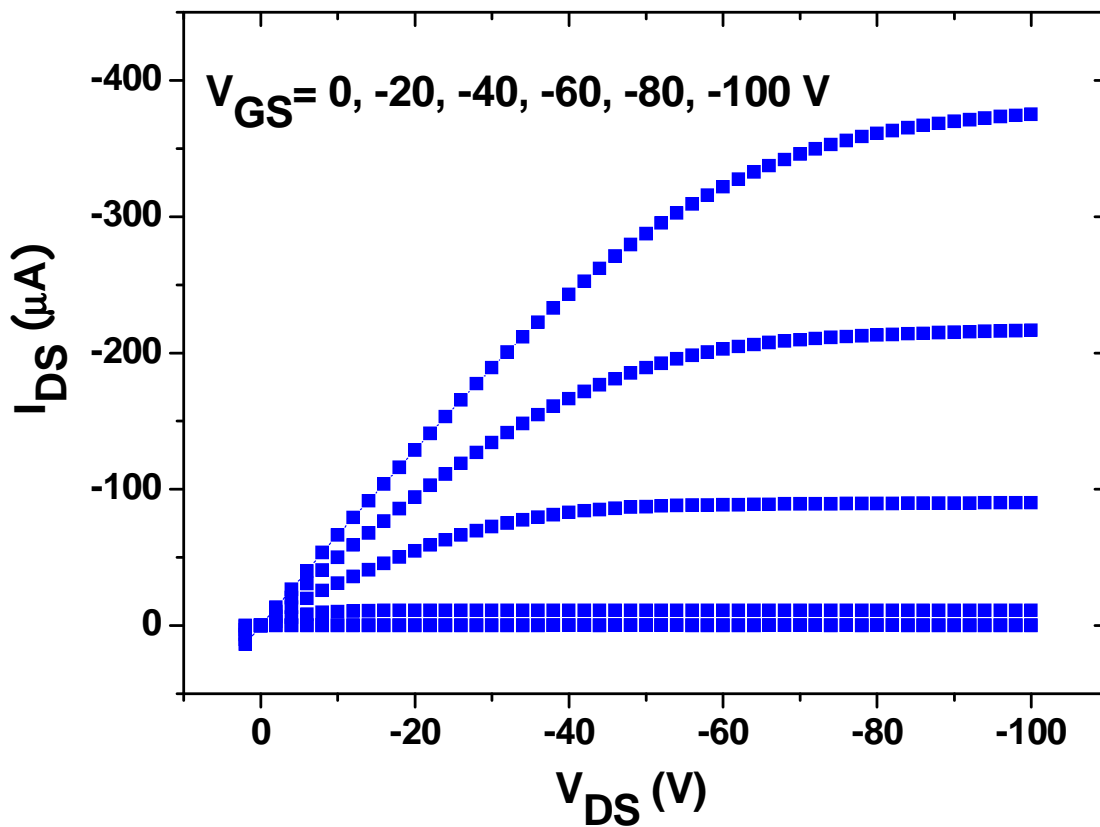


Figure 2.24: MULTIPLE OUTPUT curves of DH4T doped with 1 % w/w of Pd(PPh₃)₄ .

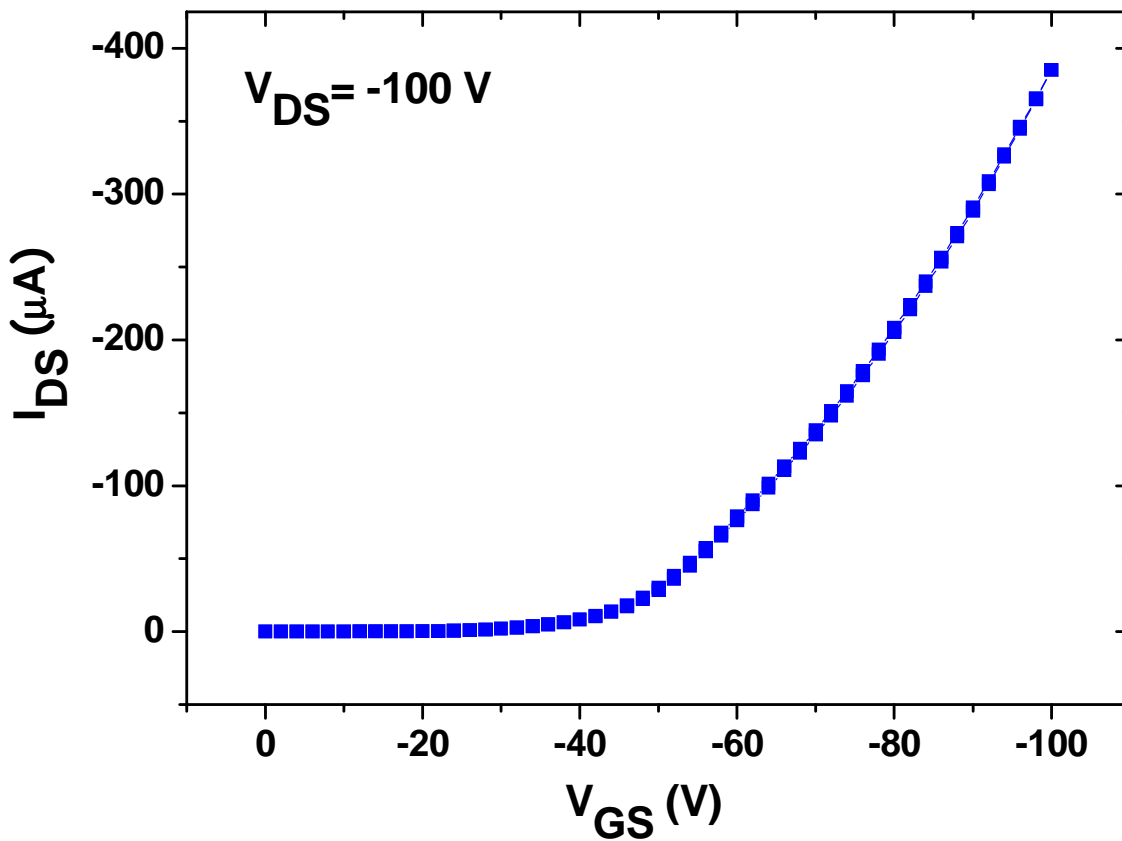


Figure 2.25: SATURATION TRANSFER of **DH4T** doped with 1 % w/w of **Pd(PPh₃)₄** .

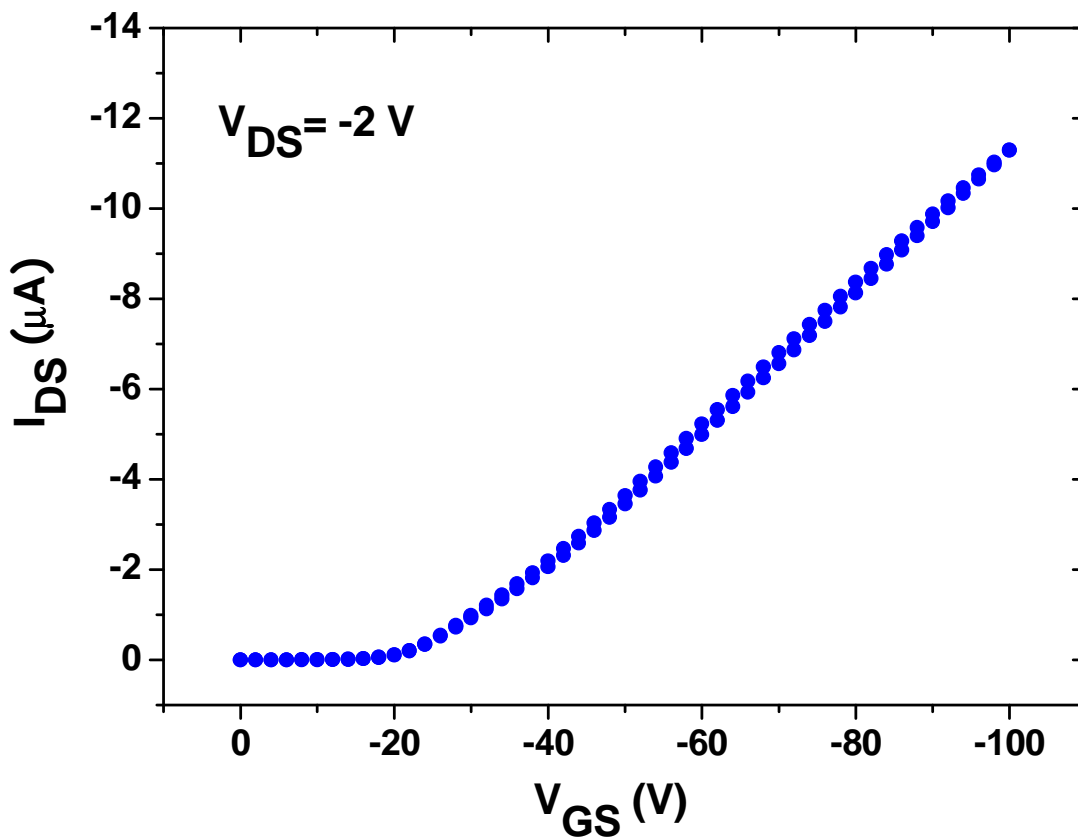


Figure 2.26: LINEAR TRANSFER of **DH4T** doped with 1 % w/w of **Pd(PPh₃)₄** .

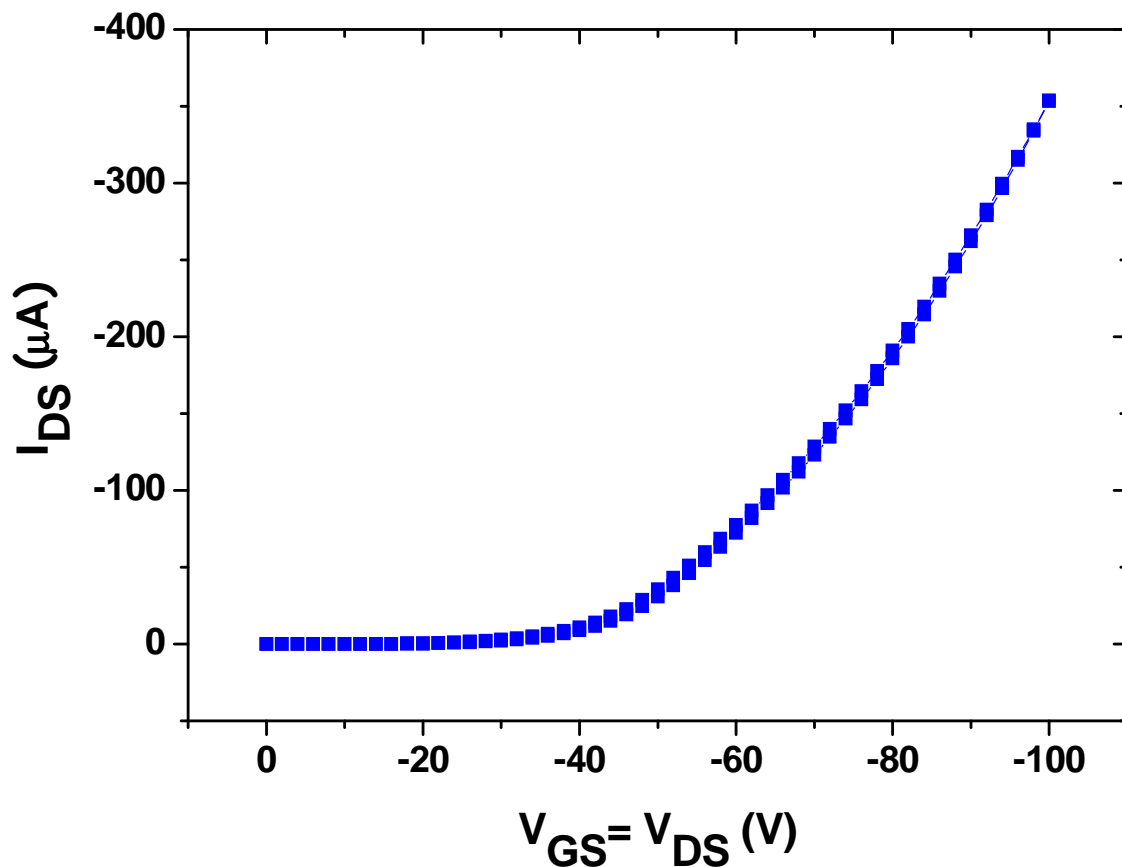


Figure 2.27: LOCUS curve of **DH4T** doped with 5 % w/w of $\text{Pd}(\text{PPh}_3)_4$.

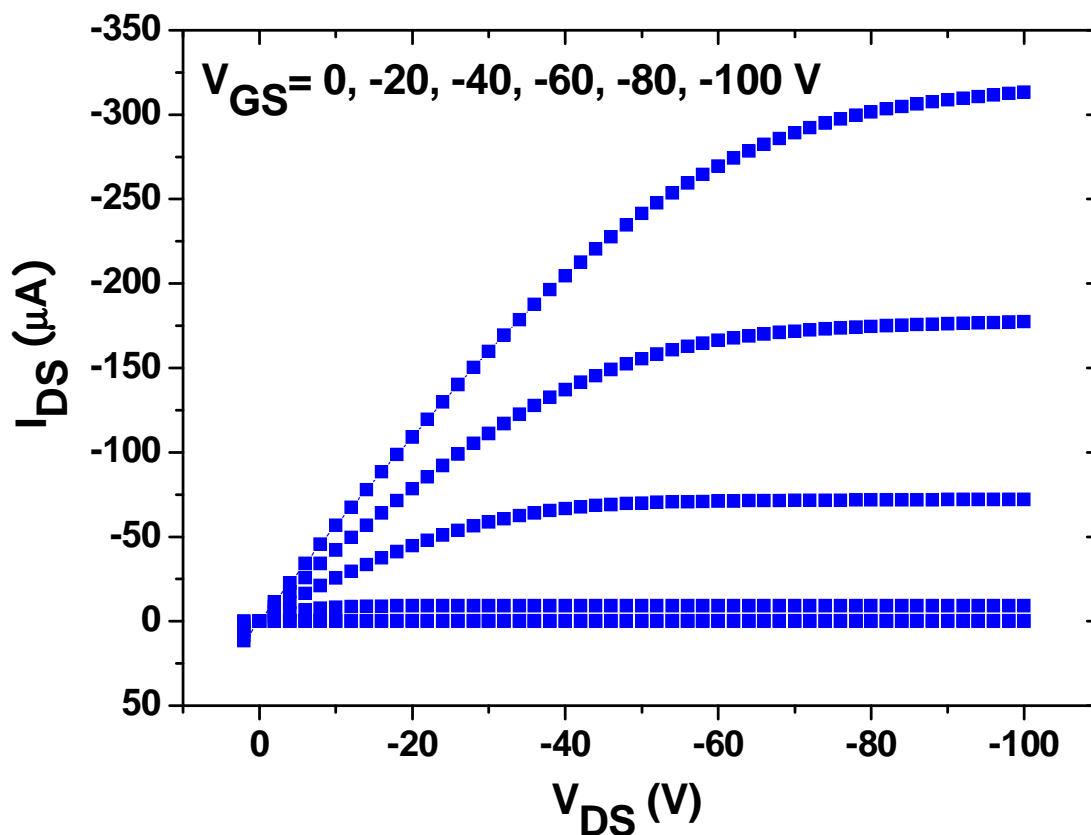


Figure 2.28: MULTIPLE OUTPUT curves of **DH4T** doped with 5 % w/w of $\text{Pd}(\text{PPh}_3)_4$.

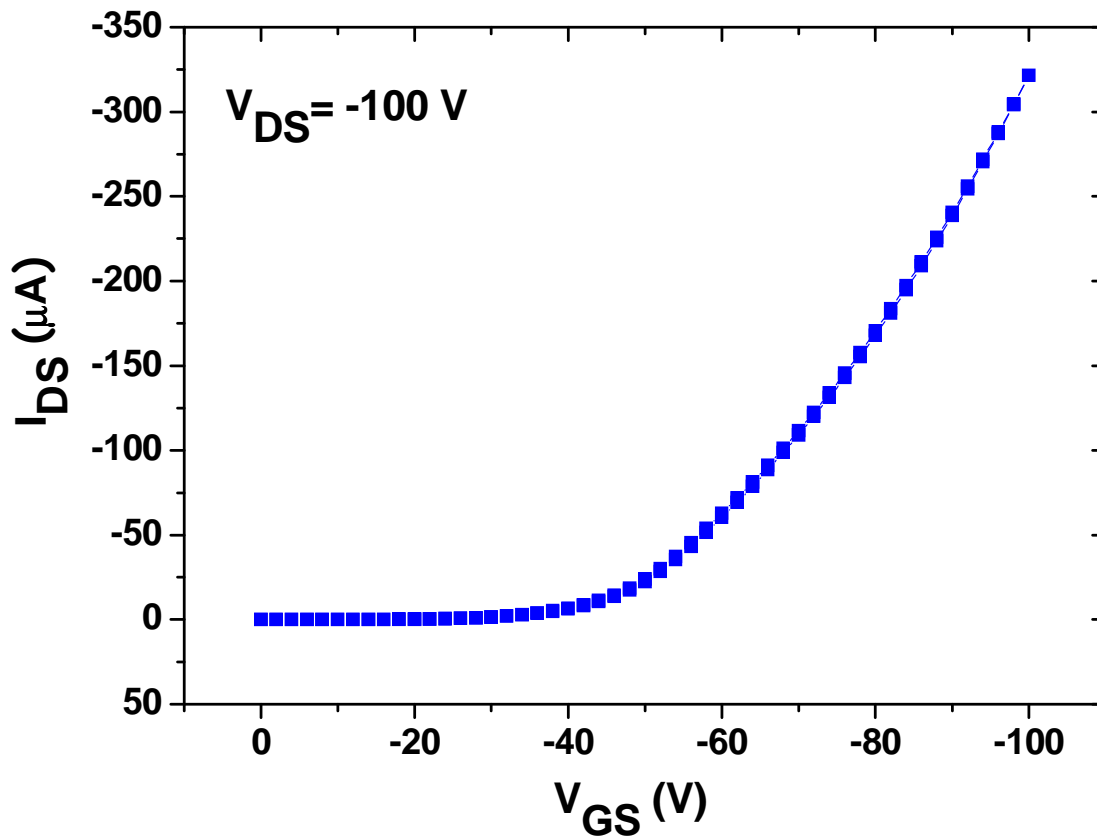


Figure 2.29: SATURATION TRANSFER of **DH4T** doped with 5 % w/w of **Pd(PPh₃)₄** .

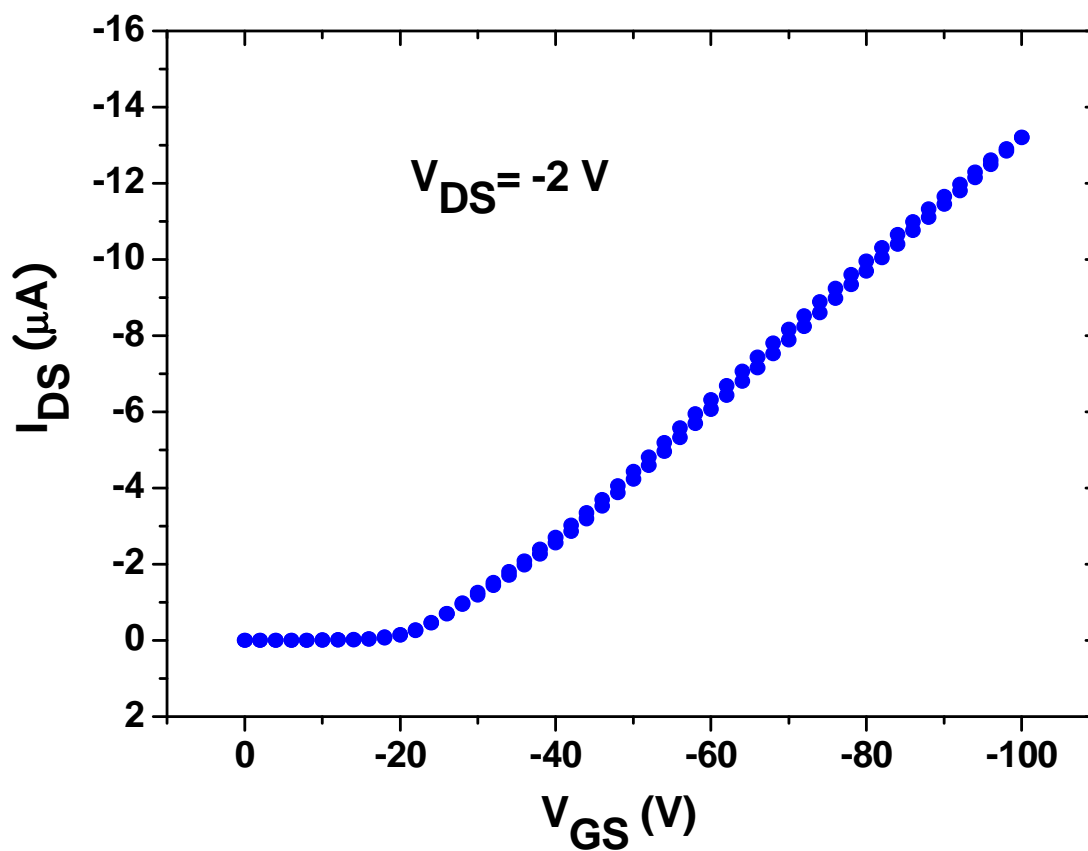


Figure 2.30: LINEAR TRANSFER of **DH4T** doped with 5 % w/w of **Pd(PPh₃)₄** .

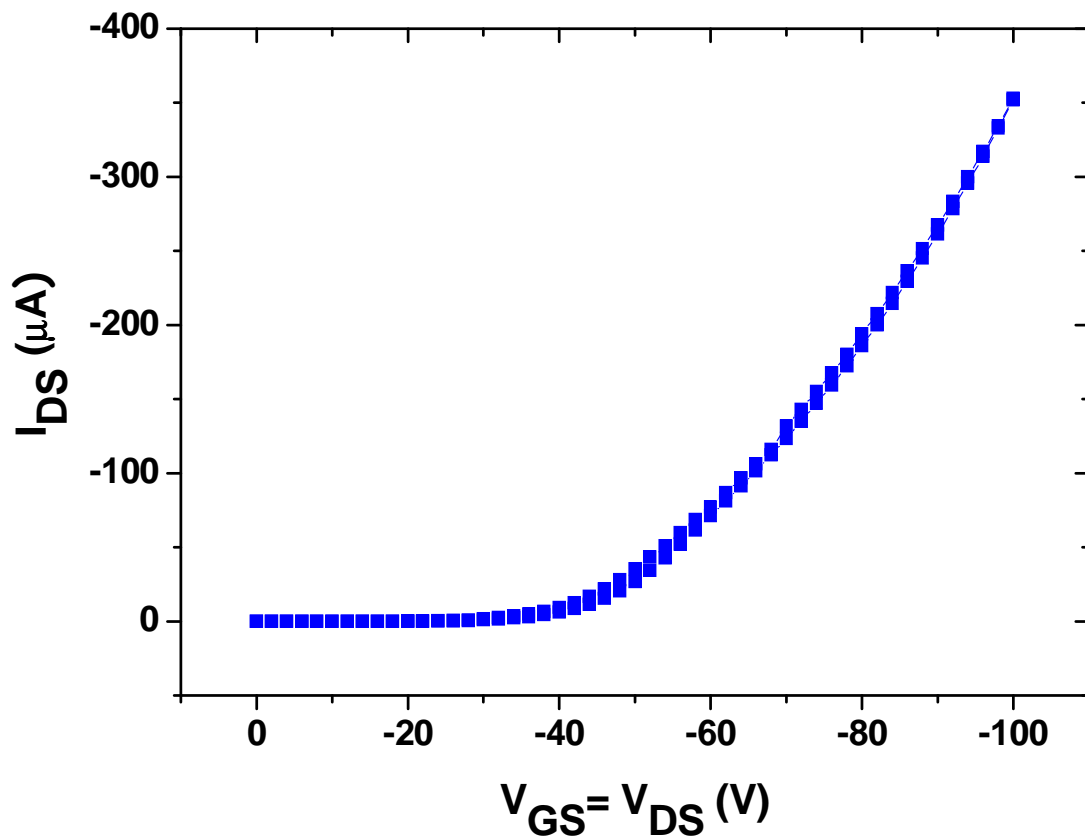


Figure 2.31: LOCUS curve of DH4T doped with 10 % w/w of $\text{Pd}(\text{PPh}_3)_4$.

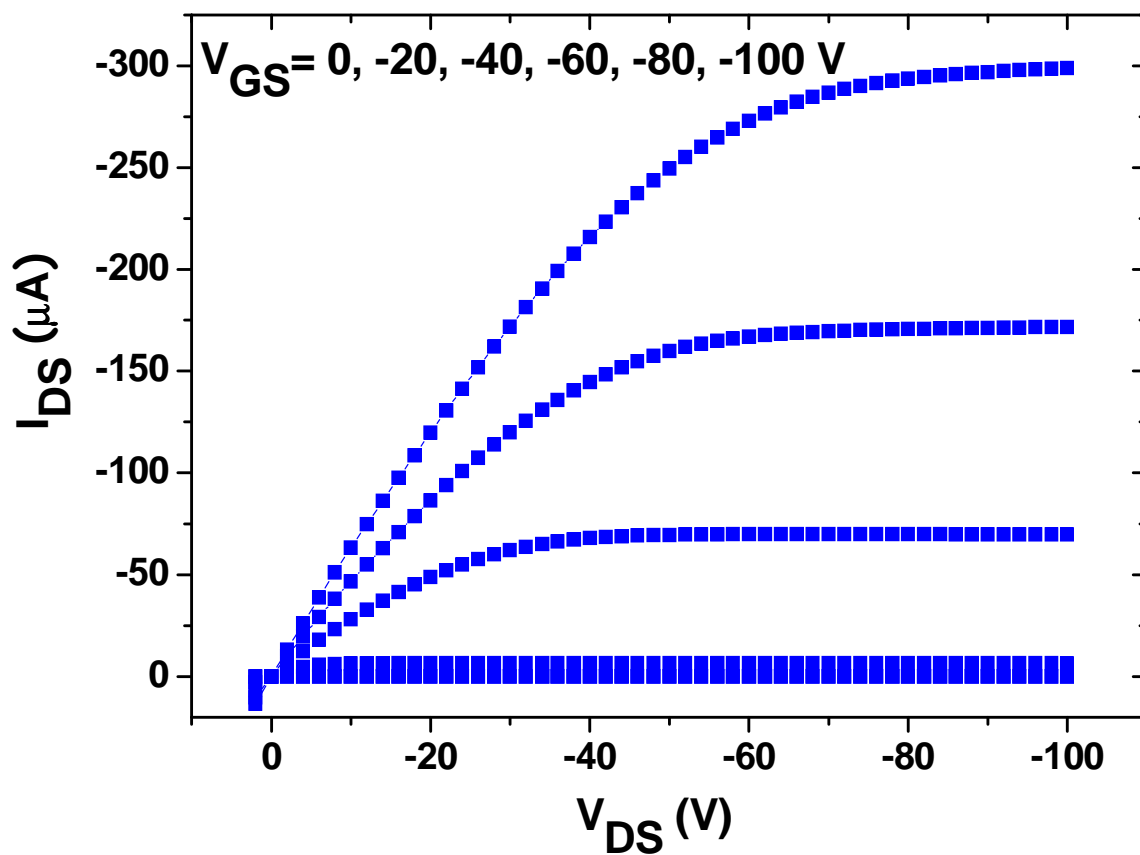


Figure 2.32: Multiple Output Curves of DH4T doped with 10 % w/w of $\text{Pd}(\text{PPh}_3)_4$.

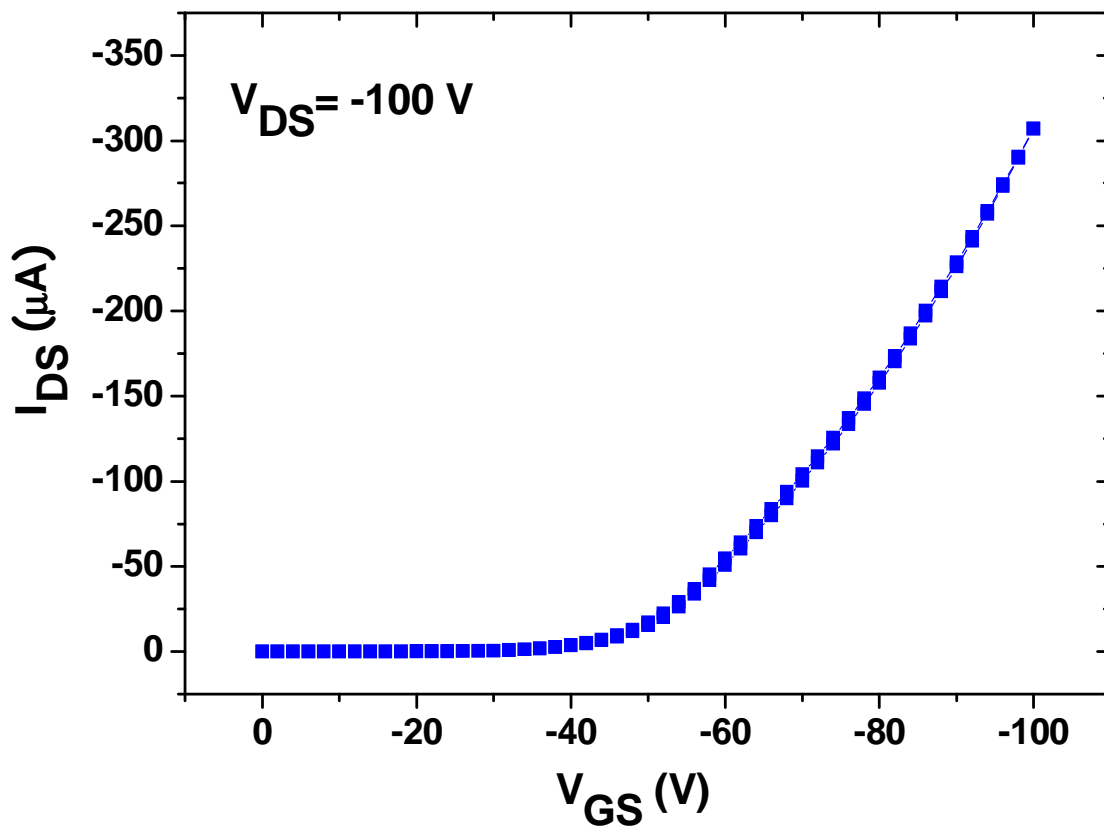


Figure 2.33: SATURATION TRANSFER of DH4T doped with 10 % w/w of $\text{Pd}(\text{PPh}_3)_4$.

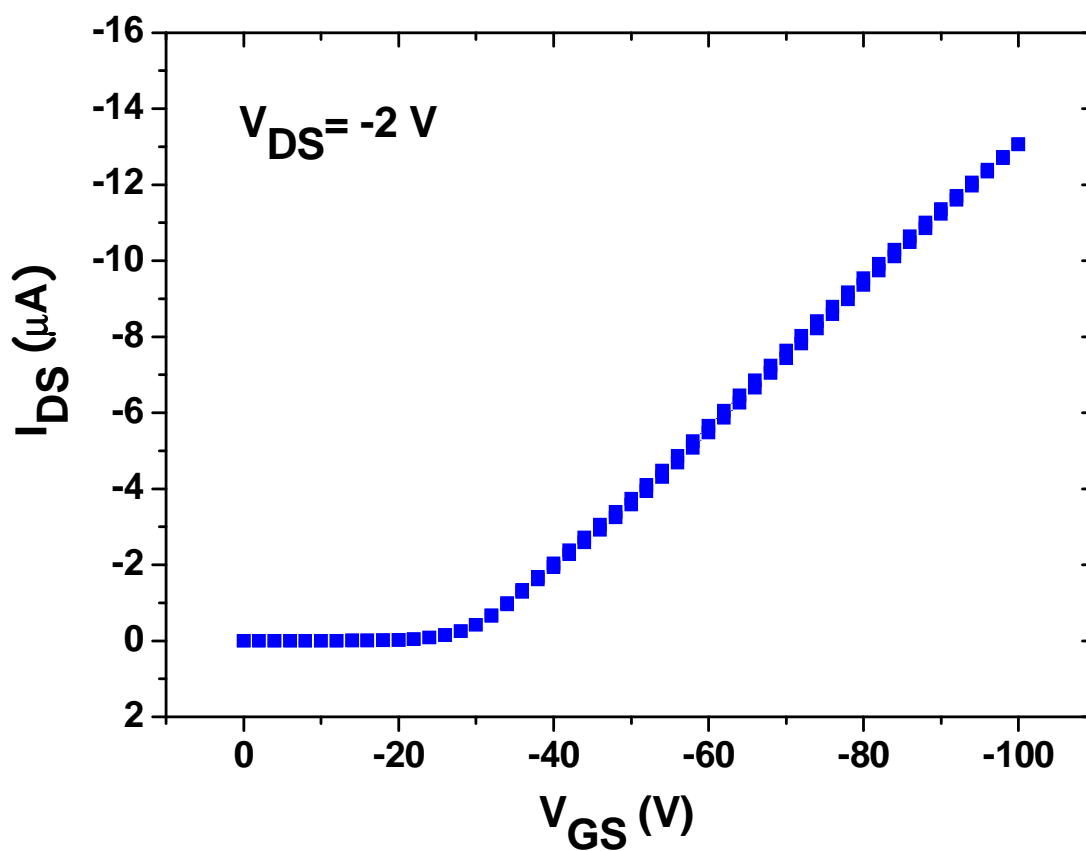


Figure 2.34: LINEAR TRANSFER of DH4T doped with 10 % w/w of $\text{Pd}(\text{PPh}_3)_4$.

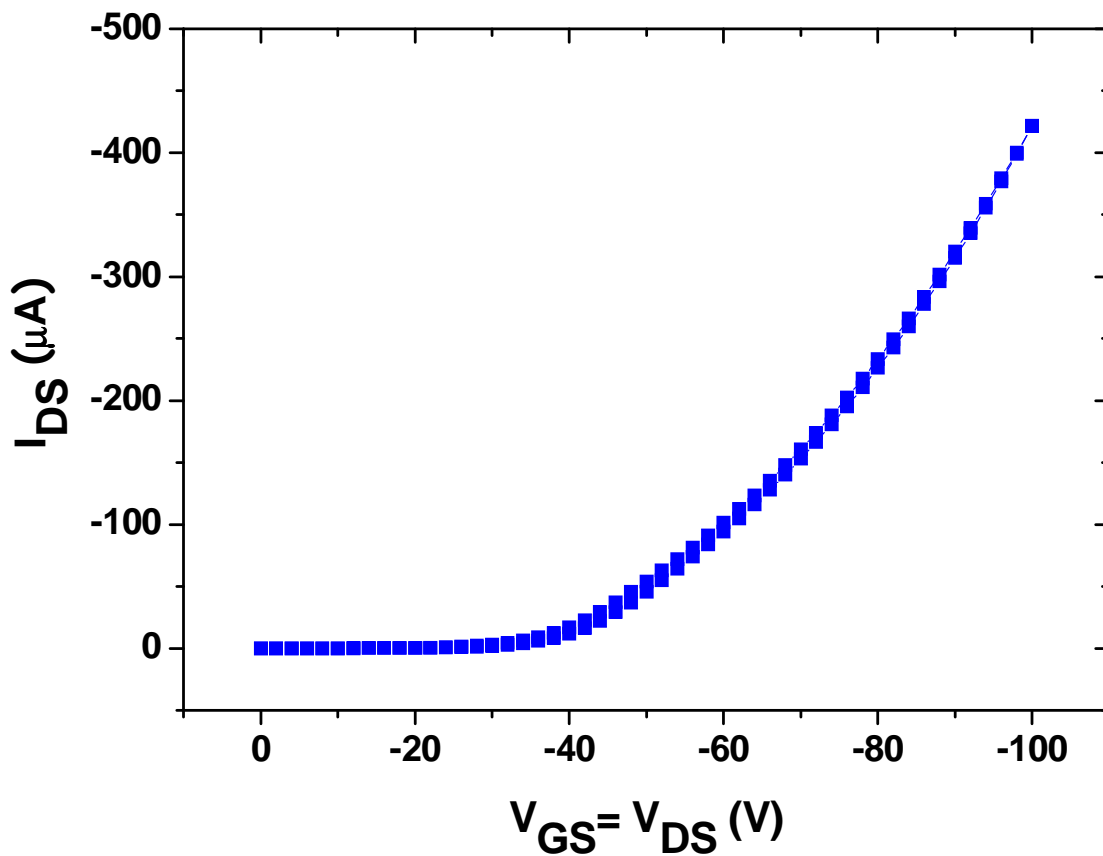


Figure 2.35: LOCUS curve of DH4T doped with 1 % w/w of Bu_3SnCl .

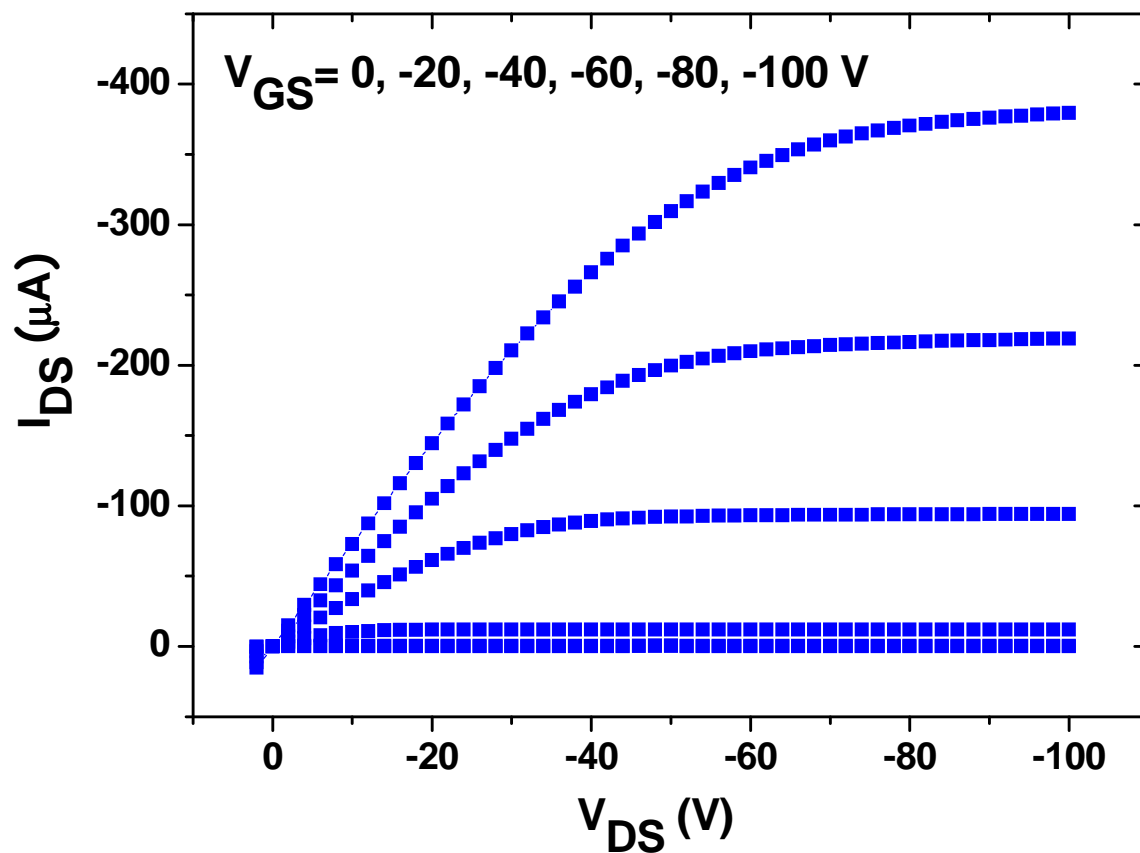


Figure 2.36: MULTIPLE OUTPUT curves of DH4T doped with 1 % w/w of Bu_3SnCl .

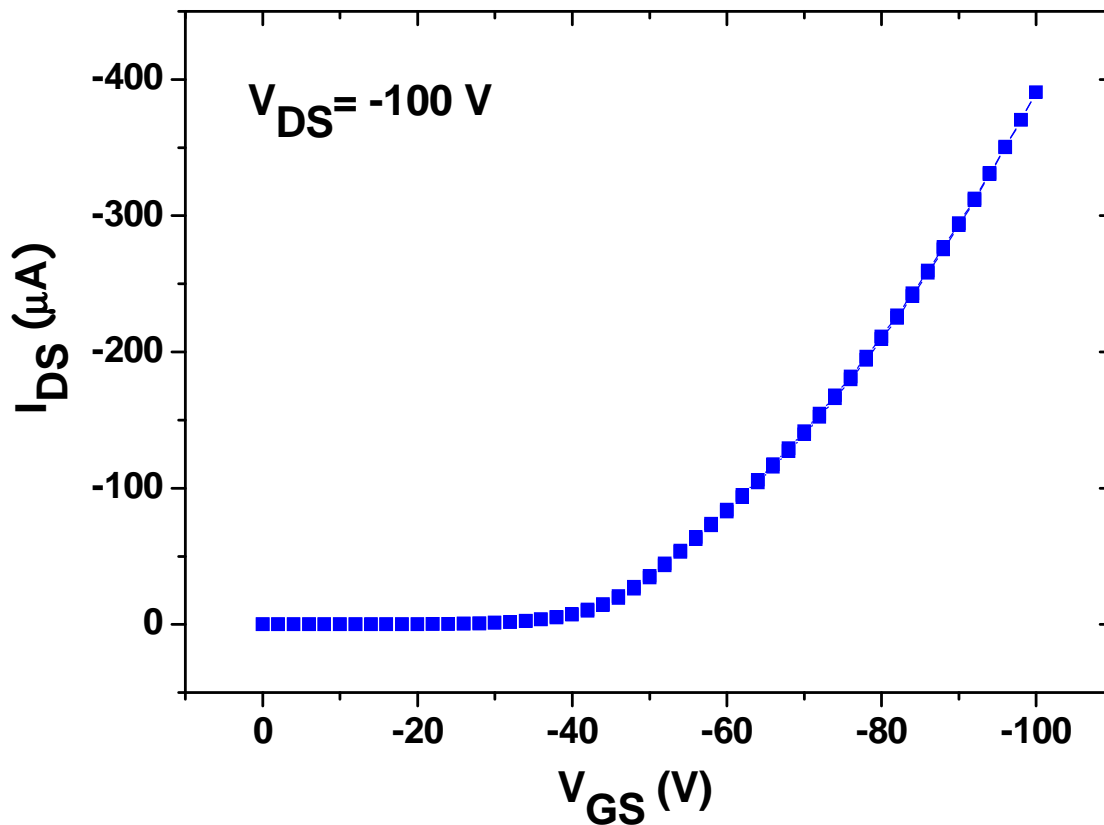


Figure 2.37: SATURATION TRANSFER of DH4T doped with 1 % w/w of Bu_3SnCl .

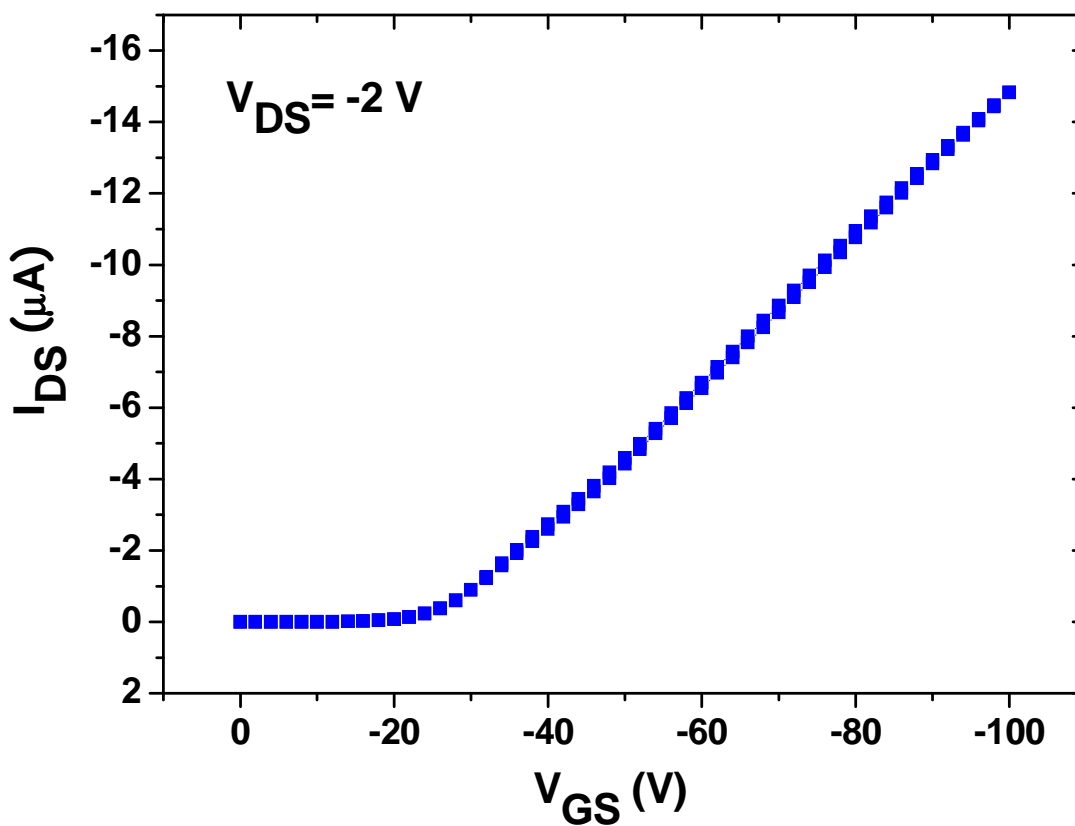


Figure 2.38: LINEAR TRANSFER of DH4T doped with 1 % w/w of Bu_3SnCl .

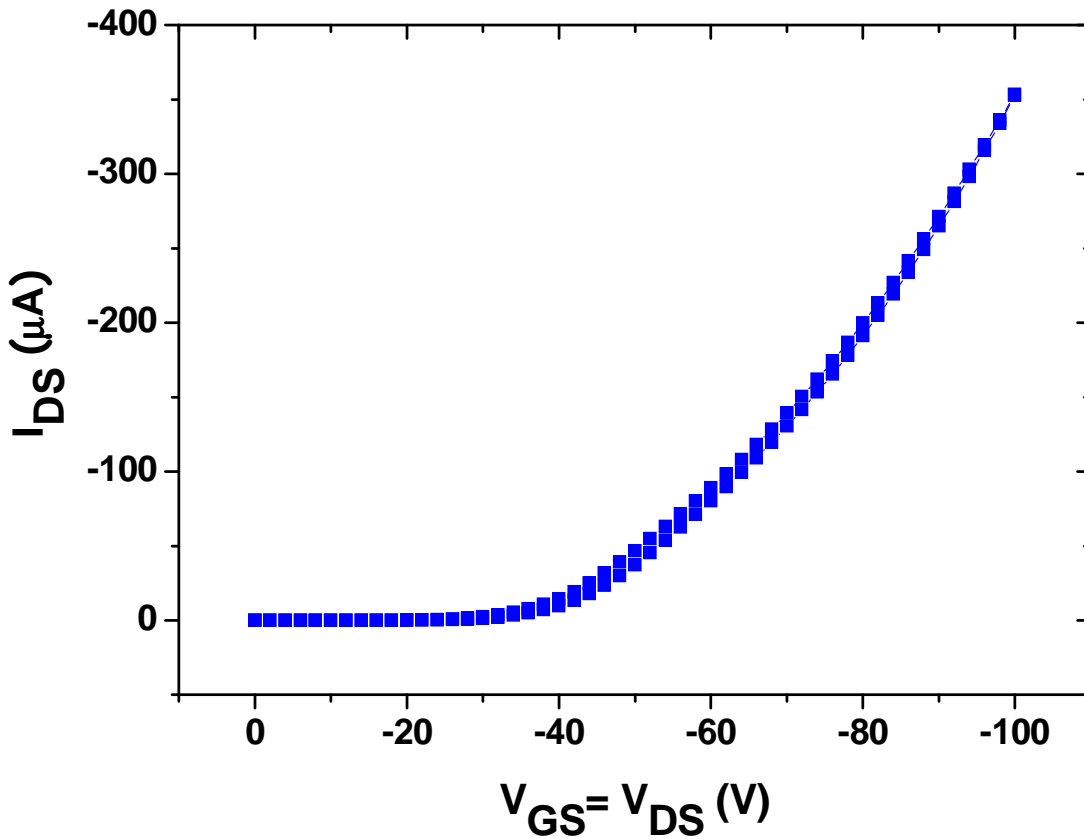


Figure 2.39: LOCUS curve of DH4T doped with 5 % w/w of Bu_3SnCl .

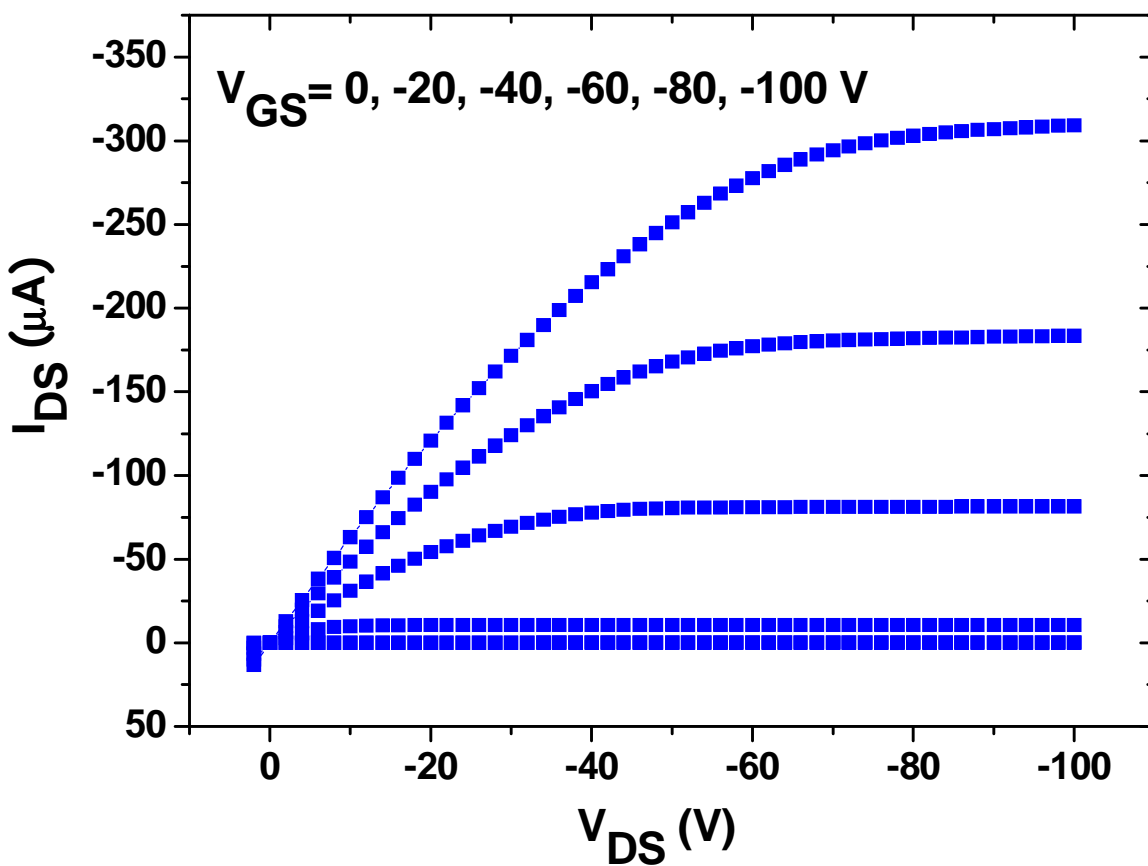


Figure 2.40: MULTIPLE OUTPUT curves of DH4T doped with 5 % w/w of Bu_3SnCl .

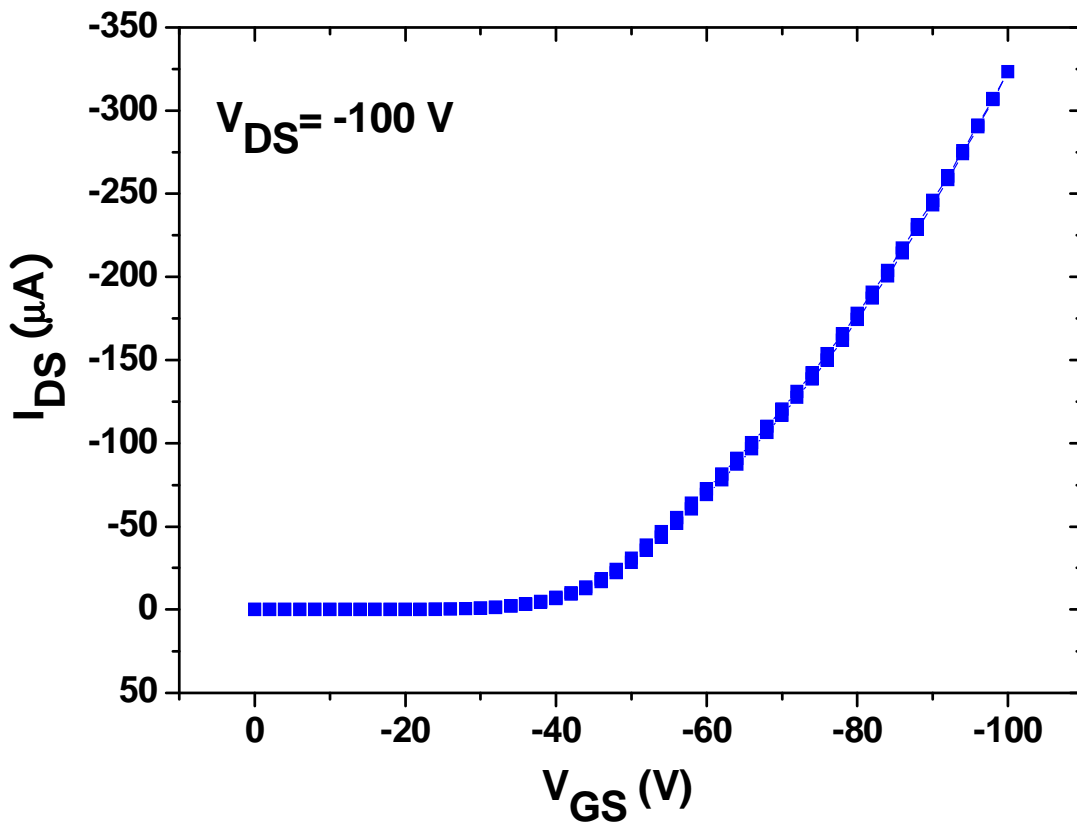


Figure 2.41: SATURATION TRANSFER of **DH4T** doped with 5 % w/w of **Bu₃SnCl** .

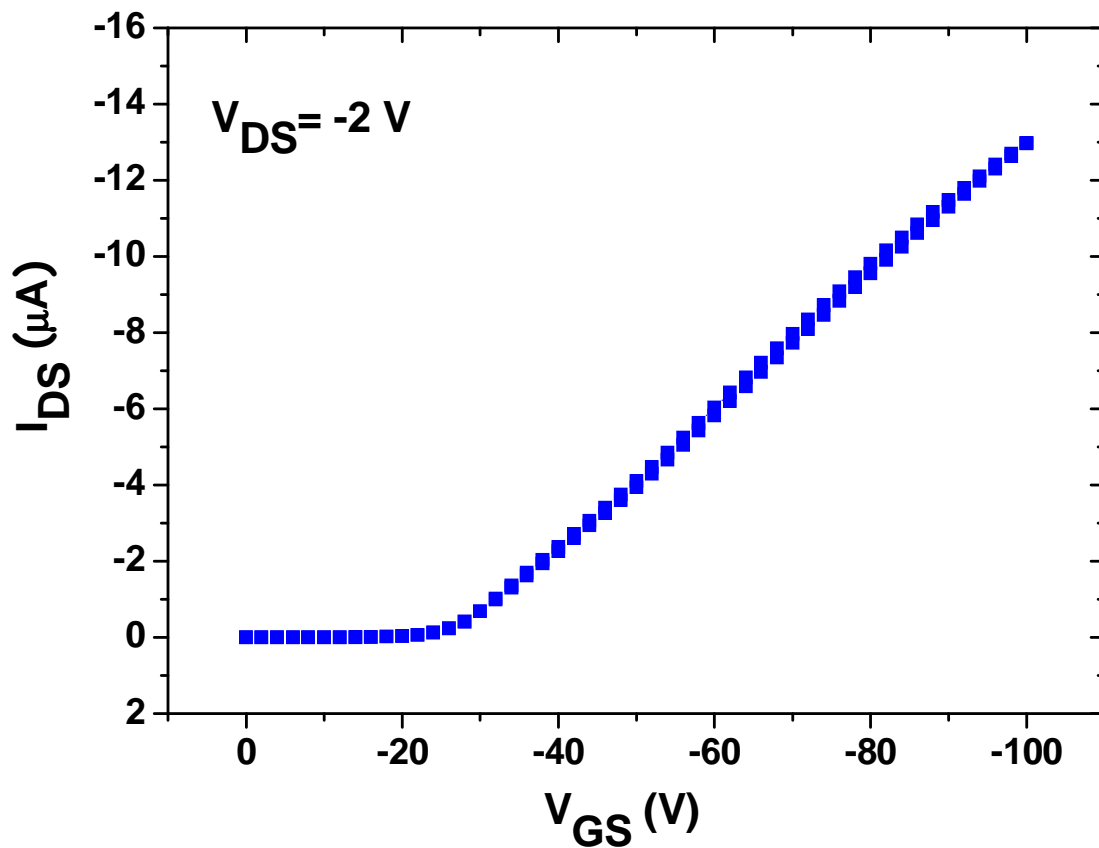


Figure 2.42: LINEAR TRANSFER of **DH4T** doped with 5 % w/w of **Bu₃SnCl** .

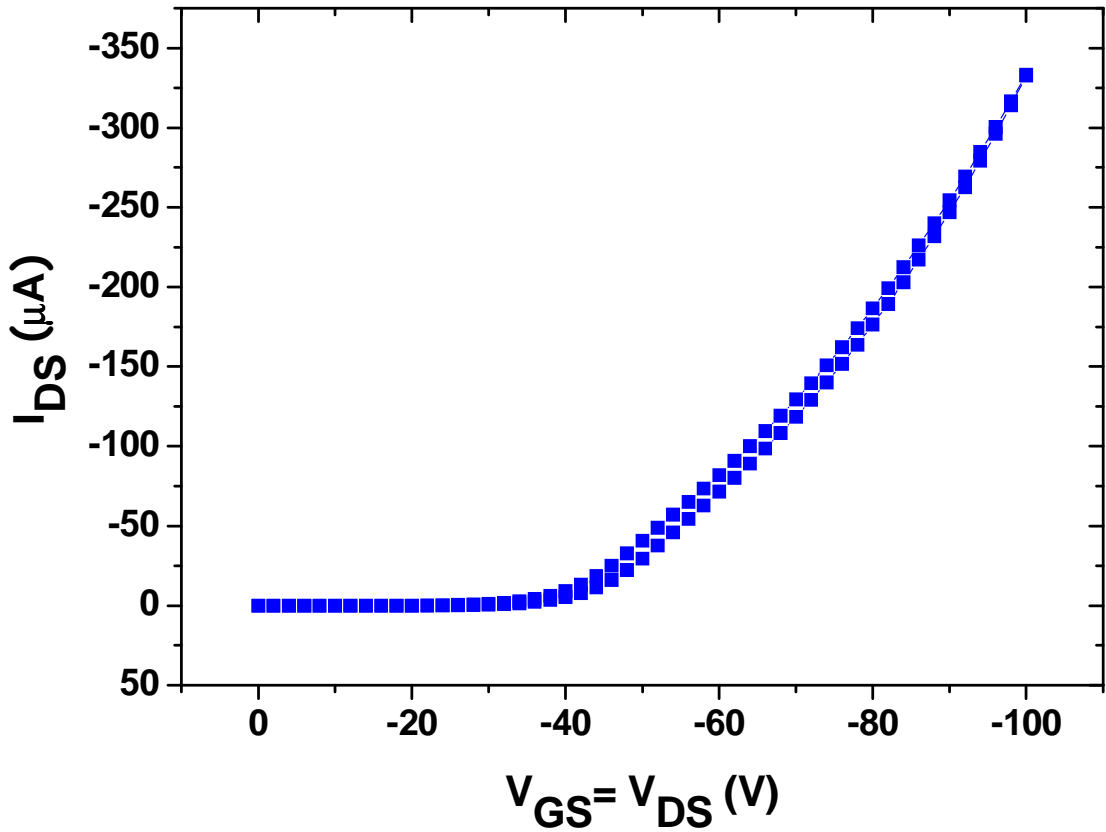


Figure 2.43: LOCUS curve of **DH4T** doped with 10 % w/w of **Bu₃SnCl** .

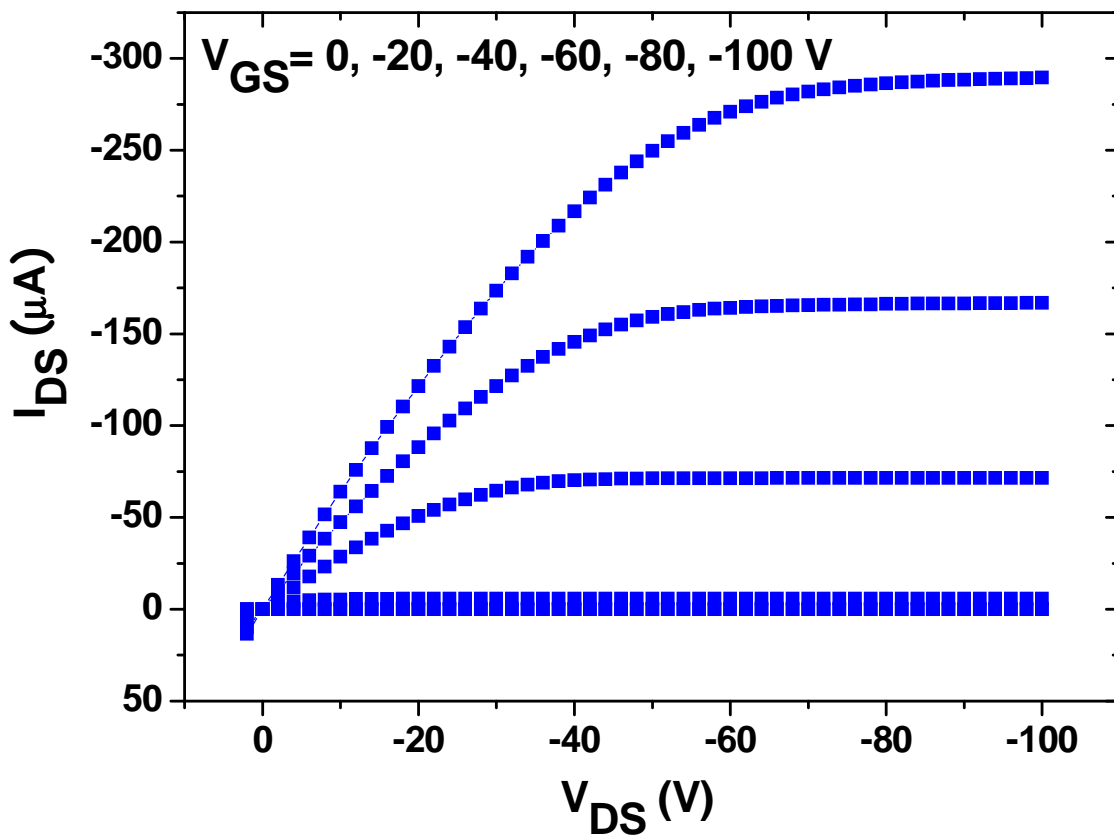


Figure 2.44: MULTIPLE OUTPUT curve of **DH4T** doped with 10 % w/w of **Bu₃SnCl** .

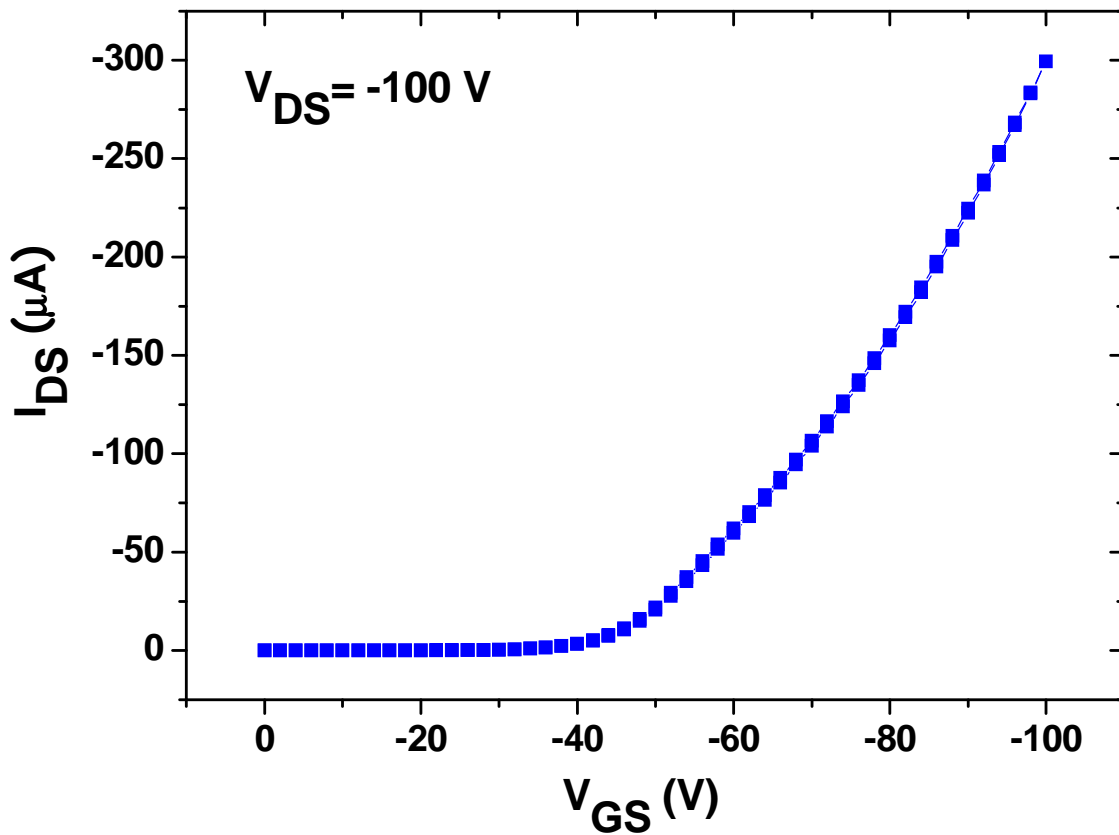


Figure 2.45: SATURATION TRANSFER of DH4T doped with 10 % w/w of Bu_3SnCl .

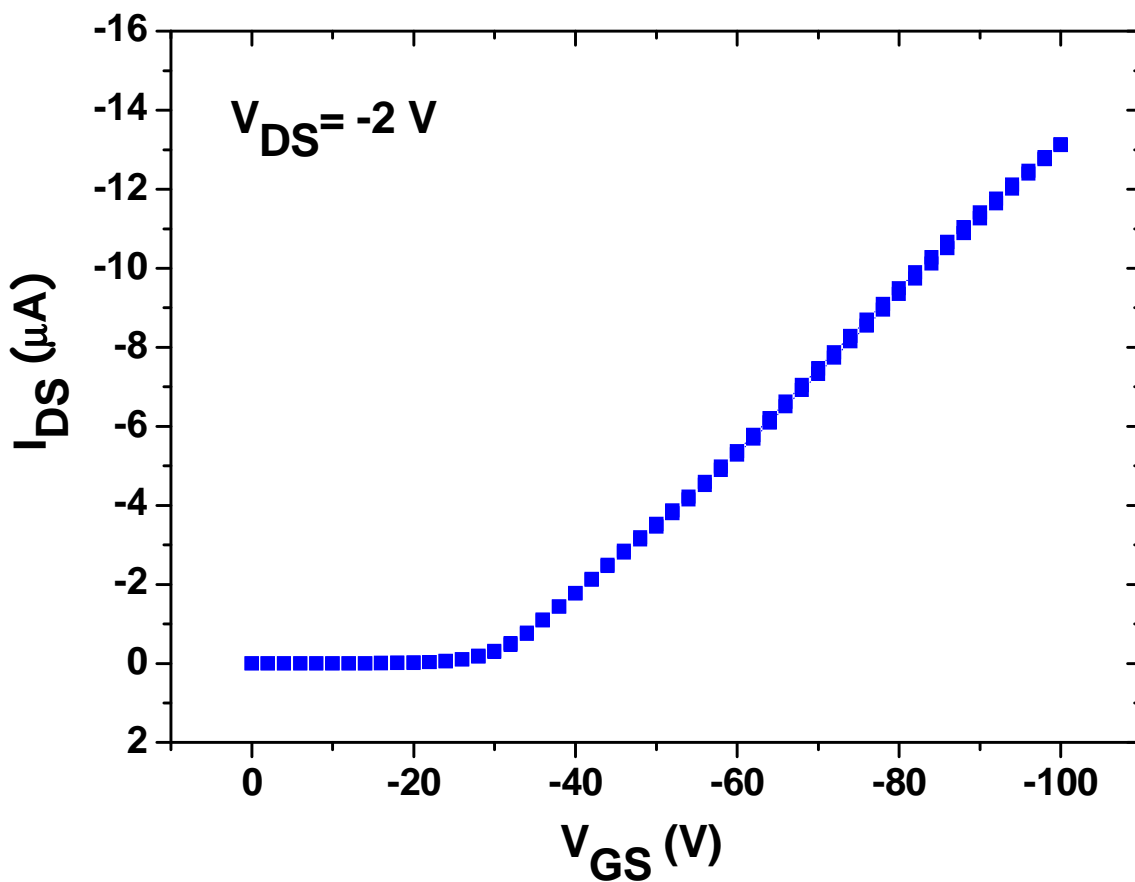


Figure 2.46: LINEAR TRANSFER of DH4T doped with 5 % w/w of Bu_3SnCl .

The increase of the pollutant concentration brings to a more prominent hysteresis behavior, pretty noticeable in the LOCUS plots of the devices made with **DH4T** doped with **Bu₃SnCl**. OFET electric hysteresis usually reveals trapped charges in foreign energetic levels, probably belonging to impurities molecules; furthermore the Drain current intensity returns to the beginning values, pointing out that the active organic layer is not damaged in any case.

LOCUS curves also show that the ohmic linear part extends its dominion as the impurity concentration increases: OFETs drift to resistors because the conduction is influenced by metals and ligands orbitals, which affect the charge transport holding the saturation regime back.

MULTIPLE OUTPUT curves show their linear parts crossing in one origin, revealing neither dielectric current leakage nor free charges in dielectric/active layers interface; the saturation zones are flat, thus the devices have no free charges localized in the boundary between the dielectric and the active layers.

Every SATURATION TRANSFER plot is quite similar to the corresponding LOCUS: this is a very good feature that follows the true ideal behavior, because both kinds of measurement are collected in OFET saturation regime.

LINEAR SATURATION curves don't show hysteresis loop and almost all of them have a pretty constant slope, highlighting the perfect charge injection from the metal electrodes; the final part of metal-free **DH4T** one show to be affected by charge injection inefficiency between Gold contacts and active layer.

Despite the organometallic pollutants were tested in very high concentrations, they produce a charge mobility decrease of only about

25 % at most: they both affect the semiconductor with the same trend and the Palladium complex leads to the lowest mobility values.

Palladium phosphine compound also dramatically worsens the threshold voltage, unlike the organotin impurity which affects it very little; finally ON/OFF ratio is reduced by one order of magnitude for every doping agent and for every concentration.

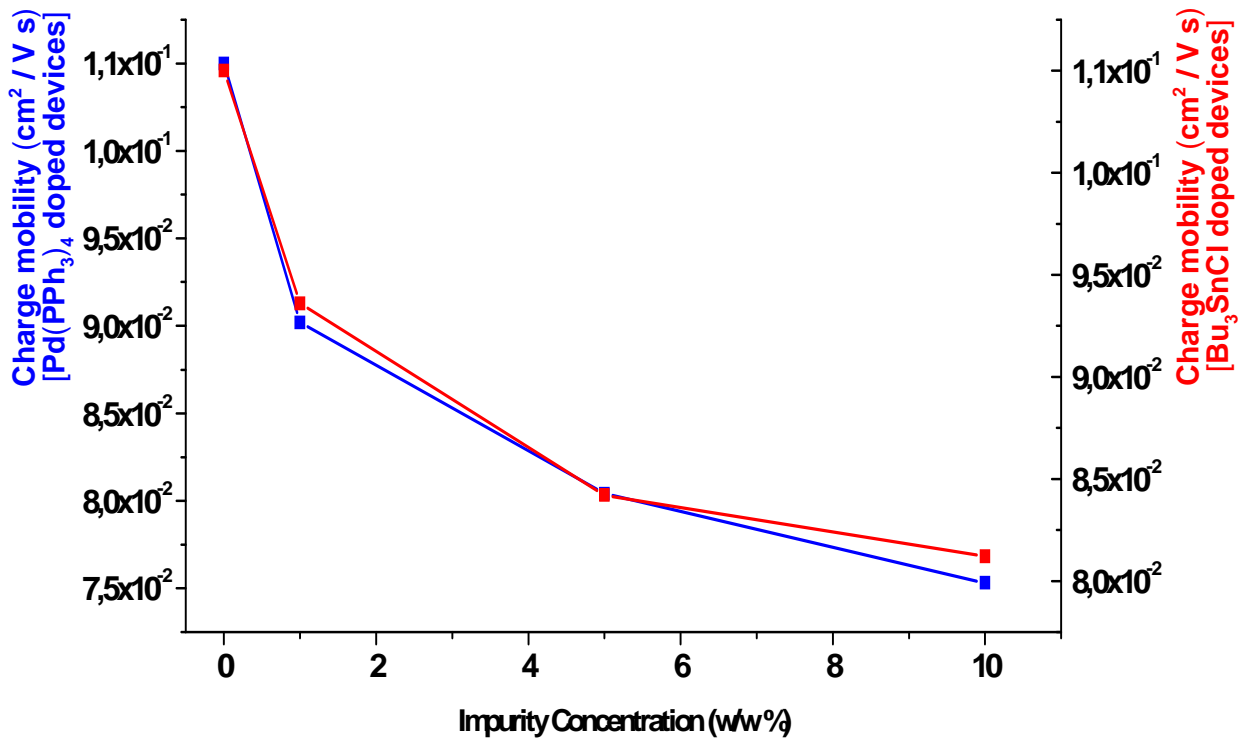


Figure 2.47: effects of the impurities concentrations on the DH4T charge mobility.

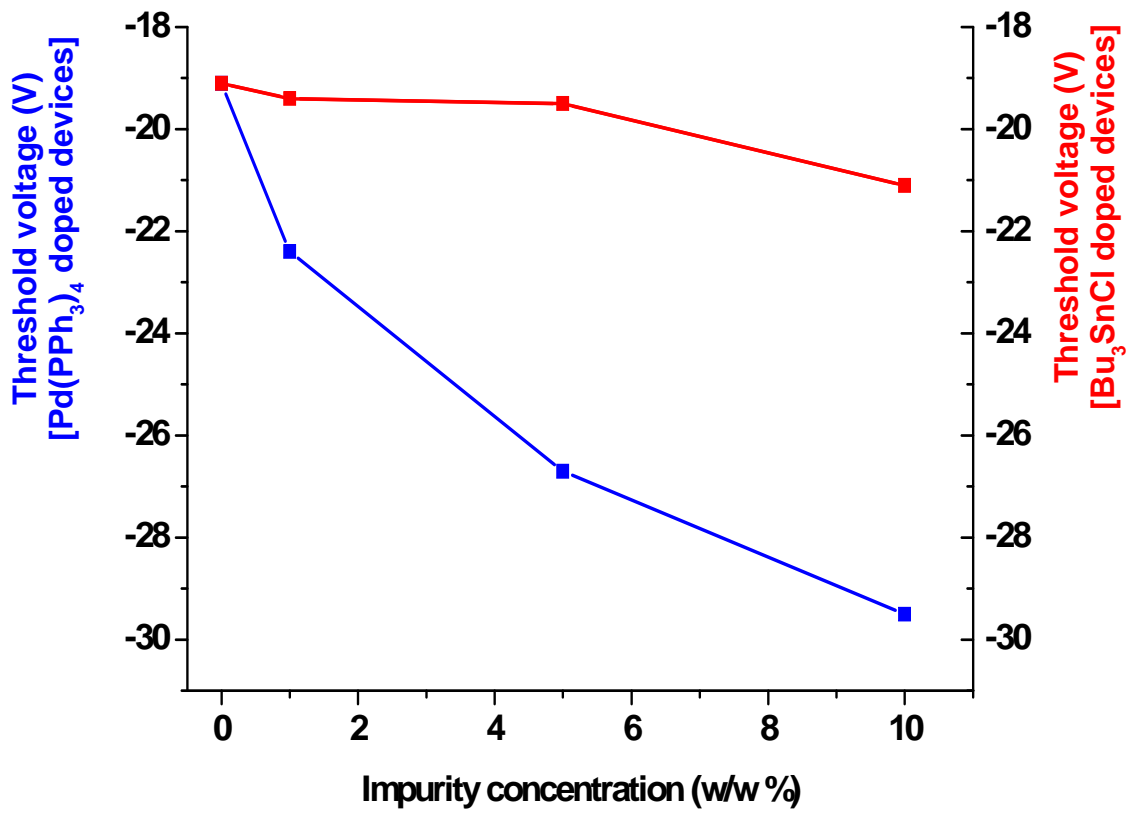


Figure 2.48: effects of the impurities concentrations on the DH4T threshold voltage.

2.6 Synthesis of the organic impurity and study of its effects on DH4T performances

From the classic catalytic approach to the oligothiophene semiconductors two kinds of polluting agent can contaminate the target molecules (see Paragraph 2.1): organometallic compounds, which are byproducts or sideproducts of the involved reactions, and organic small molecules generated from homo- and cross-coupling processes. To separate the last ones from the wanted semiconductor by laboratory techniques is a very challenging task.

DH4T commercial synthesis produces an unknown amount of 5-hexyl-2,2':5',2"-terthiophene (**HexT₃**), whose chemical characteristics make the semiconductor purification an hard job.

HexT₃ is not commercially available, thus to study the role its impurities play in **DH4T** OFET devices it was first necessary to find a way to synthesize it: microwave chemistry offered a quick and efficient way to achieve this goal.

All the kinetically hindered syntheses take a lot of time to proceed, even at high temperatures or in presence of a catalyst, often showing a poor yield. This happens because traditional heating methods do not guarantee temperature uniformity in the reaction bath: they are inefficient in transferring energy to the molecules involved in the reaction because their working is based on convection currents and on the thermal conductivity of the various materials that must be penetrated [15].

Microwave support offers a efficient internal heating by direct coupling of microwave energy with the molecules that are present in the reaction mixture [16]: every heteropolar chemical bond is an electric dipole which can interact with an electric field, aligning itself with this latter.

When microwaves irradiate chemical compounds, the bond dipoles are unrelentingly stimulated by the oscillating electric field and they attempt to realign themselves without stop: the ability of a specific material or solvent to convert microwave energy into heat at a given frequency and temperature is determined by the so-called loss

tangent, which is calculated for every substance at the standard frequency of 2.45 GHz [17].

Due to this specific functional groups heating, microwave support carries to reaction rate acceleration in milder conditions, to higher yields, to lower energy usage and to higher selectivity.

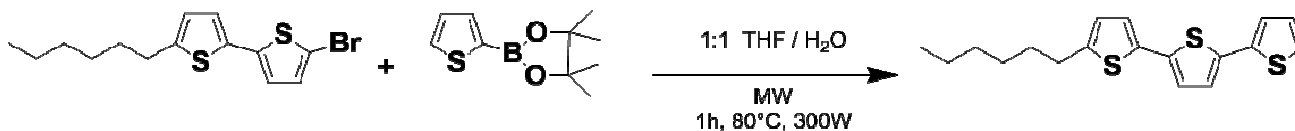


Figure 2.49: scheme of HexT₃ synthesis.

In a microwave reactor the HexT₂Br (synthesized as shown in Paragraph 2.3) was dissolved in a 1:1 blend of THF and H₂O along with 3 equivalents of Thiophene-2-boronic acid pinacol ester (Sigma Aldrich), 5 equivalents of KF (Sigma Aldrich) and a 5% w/w of Pd(dppf)Cl₂ catalyst

([(1,1'-Bis(diphenylphosphino)ferrocene]dichloropalladium(II), Sigma Aldrich).

After 1h at 80°C under 300 W of irradiating power, the Suzuki crude product was washed with DCM/H₂O (x 3); the organic fraction was dried with Na₂SO₄ and, after removing the solvent, the product purification was carried on with a chromatographic column (silica flash as solid phase and 95:5 blend of petroleum ether 30-40 and DCM as eluent).

Reaction yield is about 67%.

CHARACTERIZATION DATA OF HexT₃

<p>EI-MS (<i>m/z</i>): 332.</p> <p>¹H-NMR: (400 MHz, CDCl₃, 25°C TMS) δ 0.90 (t, 3H), 1.30-1.40 (m, 6H), 1.68 (quint. , 2H), 2.79 (t, 2H), 6.68 (d, 1H), 6.98-7.02 (m, 3H), 7.05 (d, 1H), 7.16 (dd, 1H), 7.20 (dd, 1H).</p> <p>¹³C-NMR: (100.6 MHz, CDCl₃, 25°C TMS) δ 14.4 (CH₃), 22.3 (CH₂), 28.9 (CH₂), 30.1 (CH₂), 31.8 (CH₂), 32.2 (CH₂), 122.6 (CH), 123.6 (CH), 123.9 (CH), 124.2 (CH), 124.5 (CH), 124.8 (CH), 126.8 (CH), 135.9 (C_q), 136.2 (C_q), 136.8 (C_q), 137.1 (C_q), 146.1 (C_q).</p>
--

The organic doping agent was tested apart in different concentration using for each one a 10 mg batch of virgin **DH4T**; in Table 2.7 the doping data are reported.

HexT ₃ dissolved in DCM* (mg/10 ml)	Impurity concentration in a 10 mg DH4T batch (w/w %)
1	1
5	5
10	10
* = 1 ml of solution is added to a 10 mg DH4T batch and the solvent is then removed.	

Table 2.7: controlled doping data for the organic impurity.

With every **DH4T** batch OFET devices were fabricated as explained in Paragraph 2.3 plus reference OFET devices made with virgin **DH4T**.

After completing the high vacuum sublimation process, the field-effect transistors were fully characterized: the collected plots are shown from Figure 2.50 to Figure 2.62 while the elaborated statistical data are reported in Table 2.8.

HexT ₃ concentration (w/w %)	Charge mobility ± standard deviation (cm ² /V·s)	Threshold voltage ± standard deviation (V)	ON / OFF ratio (only magnitude)
Reference virgin DH4T (0 %)	$(9.95 \pm 0.04) \cdot 10^{-2}$	-18.7 ± 1.1	10^4
HexT ₃ (1 %)	$(8.43 \pm 0.23) \cdot 10^{-2}$	-20.1 ± 1.9	10^3
HexT ₃ (5 %)	$(7.12 \pm 0.05) \cdot 10^{-2}$	-22.5 ± 1.3	10^3
HexT ₃ (10 %)	$(6.78 \pm 0.17) \cdot 10^{-2}$	-24.8 ± 2.4	10^3

Table 2.8: electric parameters measured for each HexT₃ concentration.

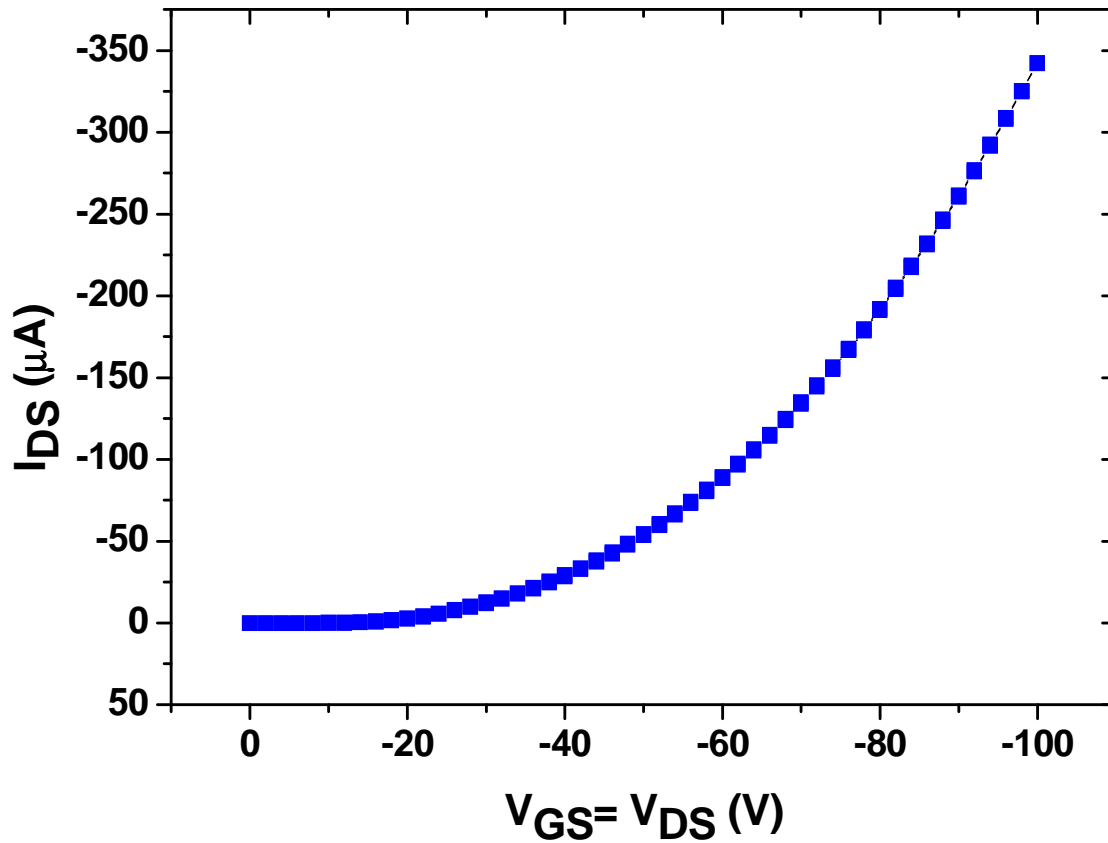


Figure 2.50: LOCUS curve of DH4T doped with 1 % w/w of HexT₃.

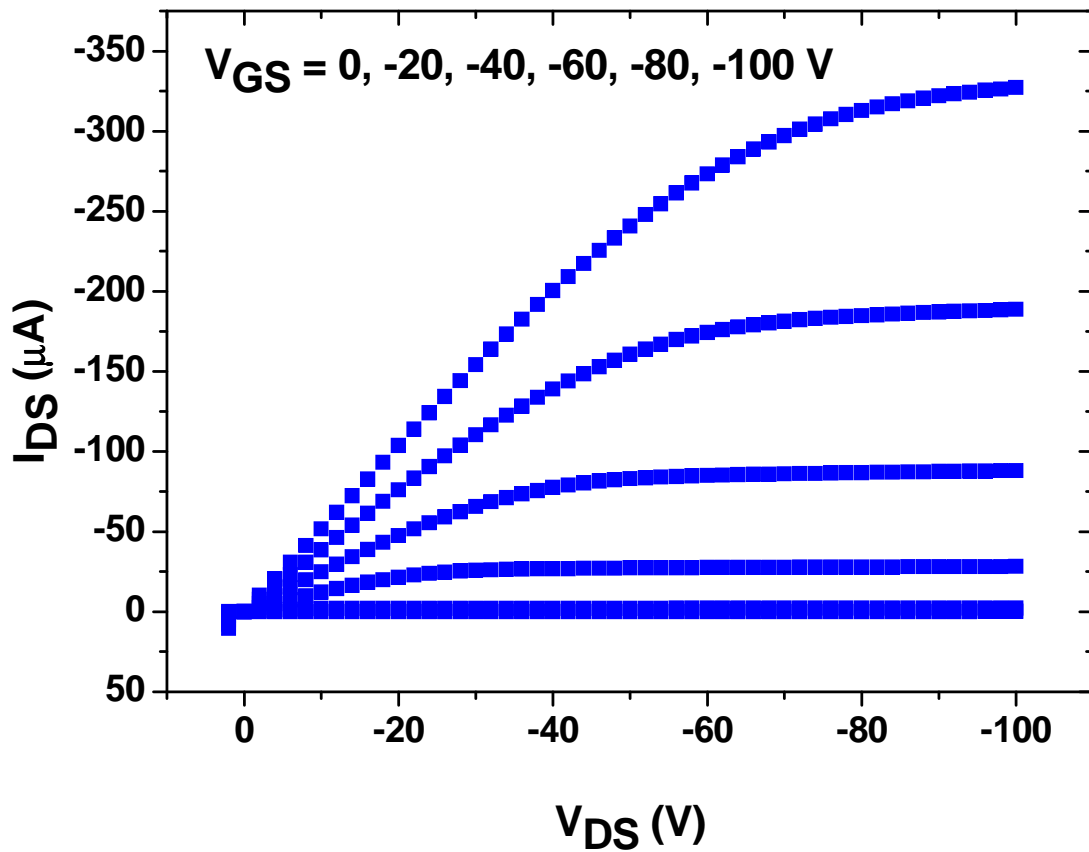


Figure 2.51: MULTIPLE OUTPUT curves of DH4T doped with 1 % w/w of HexT₃.

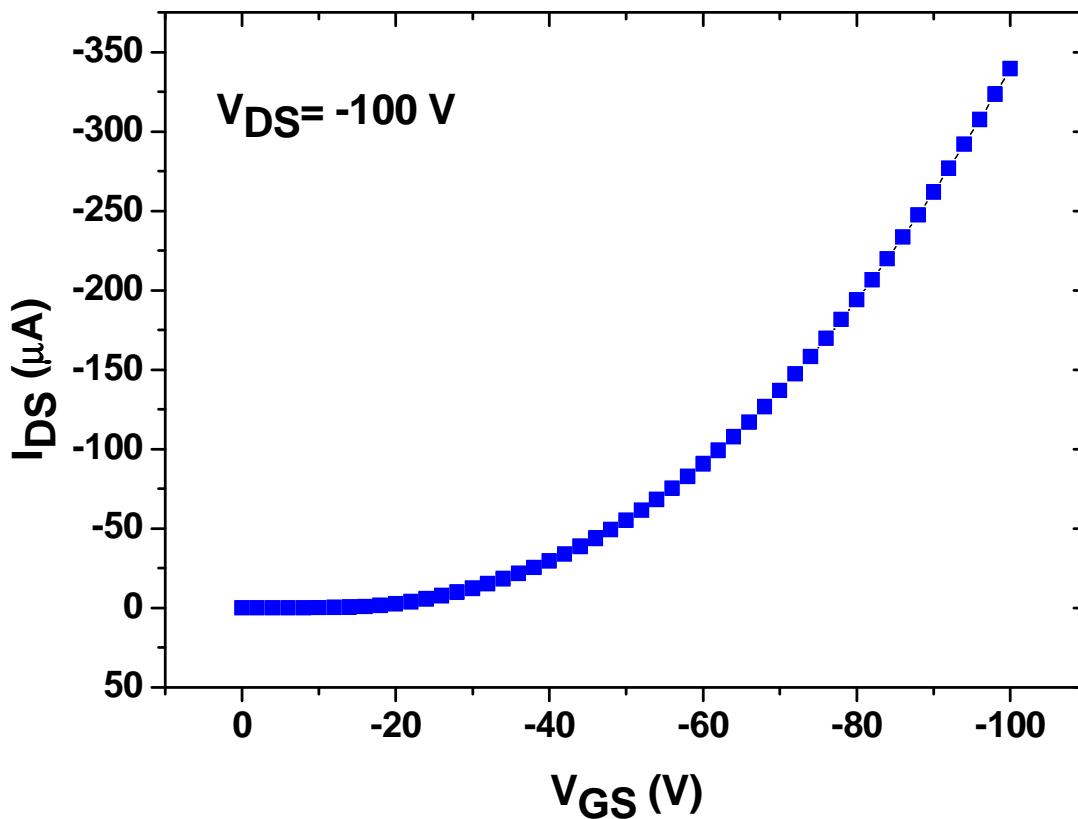


Figure 2.52: SATURATION TRANSFER curve of DH4T doped with 1 % w/w of HexT₃.

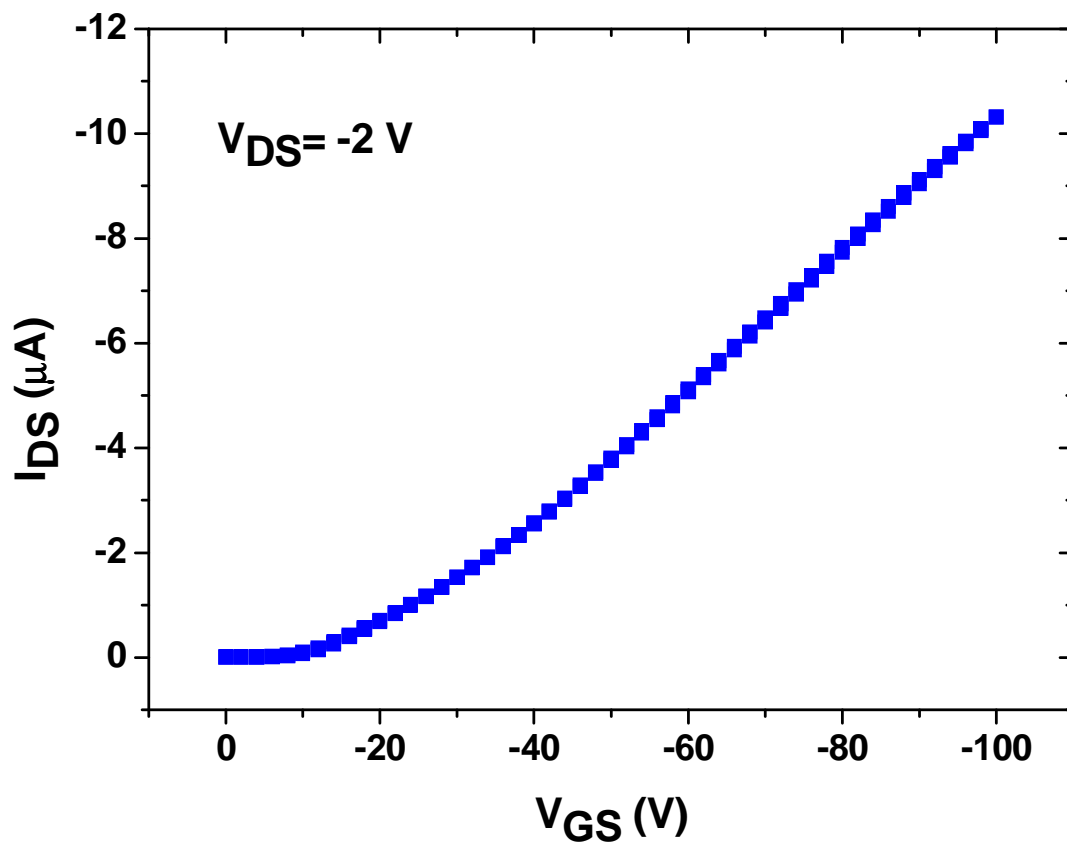


Figure 2.53: LINEAR TRANSFER curve of DH4T doped with 1 % w/w of HexT₃.

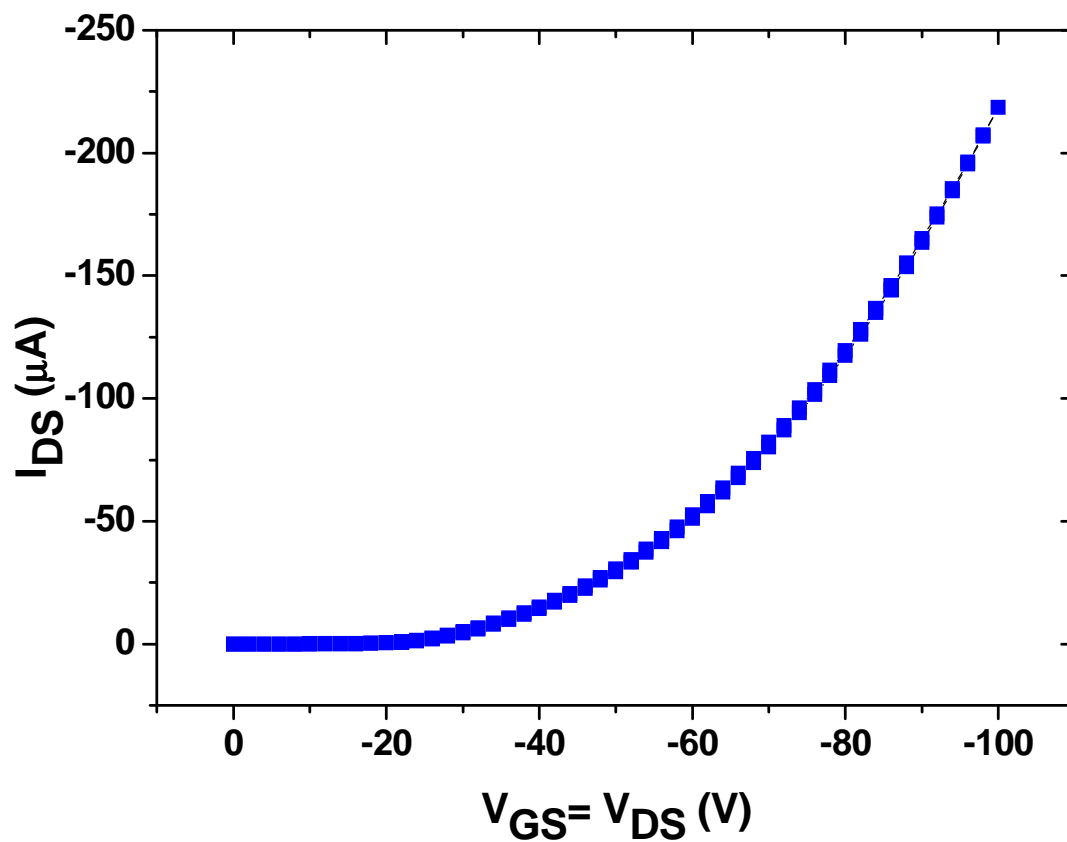


Figure 2.54: LOCUS curve of DH4T doped with 5 % w/w of HexT₃.

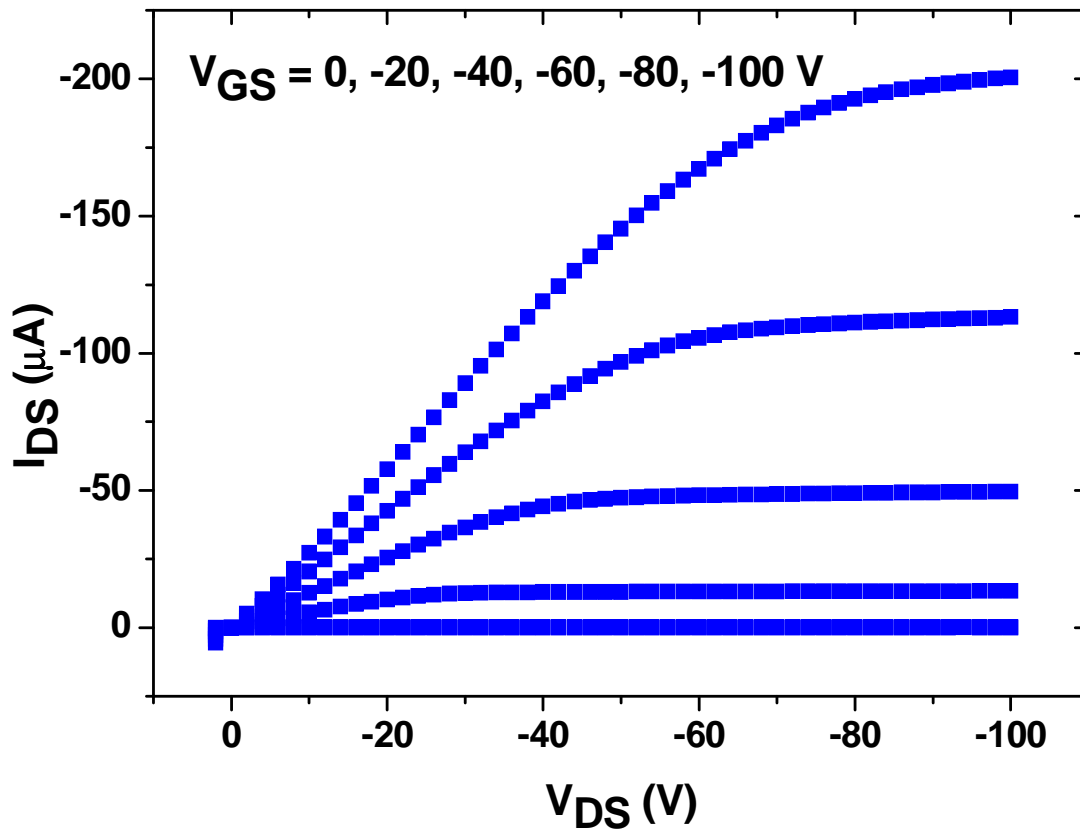


Figure 2.55: MULTIPLE OUTPUT curves of DH4T doped with 5 % w/w of HexT₃.

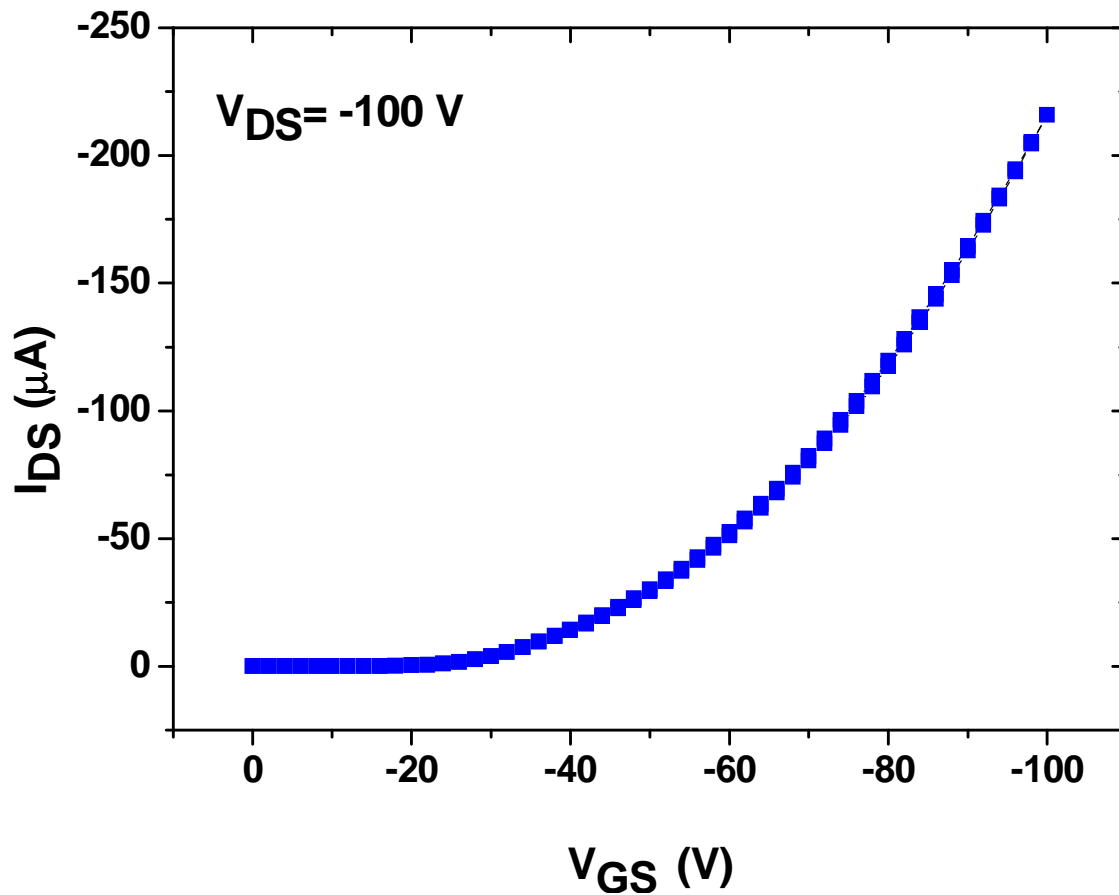


Figure 2.56: SATURATION TRANSFER curve of DH4T doped with 5 % w/w of HexT₃.

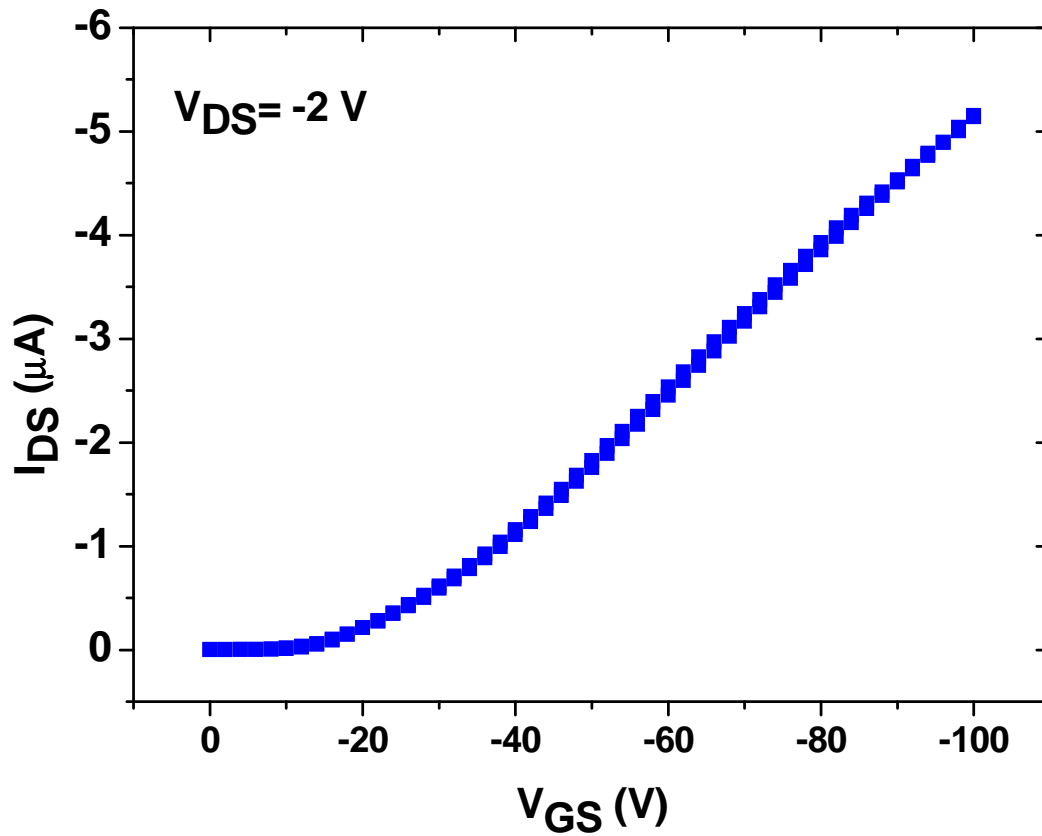


Figure 2.57: LINEAR TRANSFER curve of DH4T doped with 5 % w/w of HexT_3 .

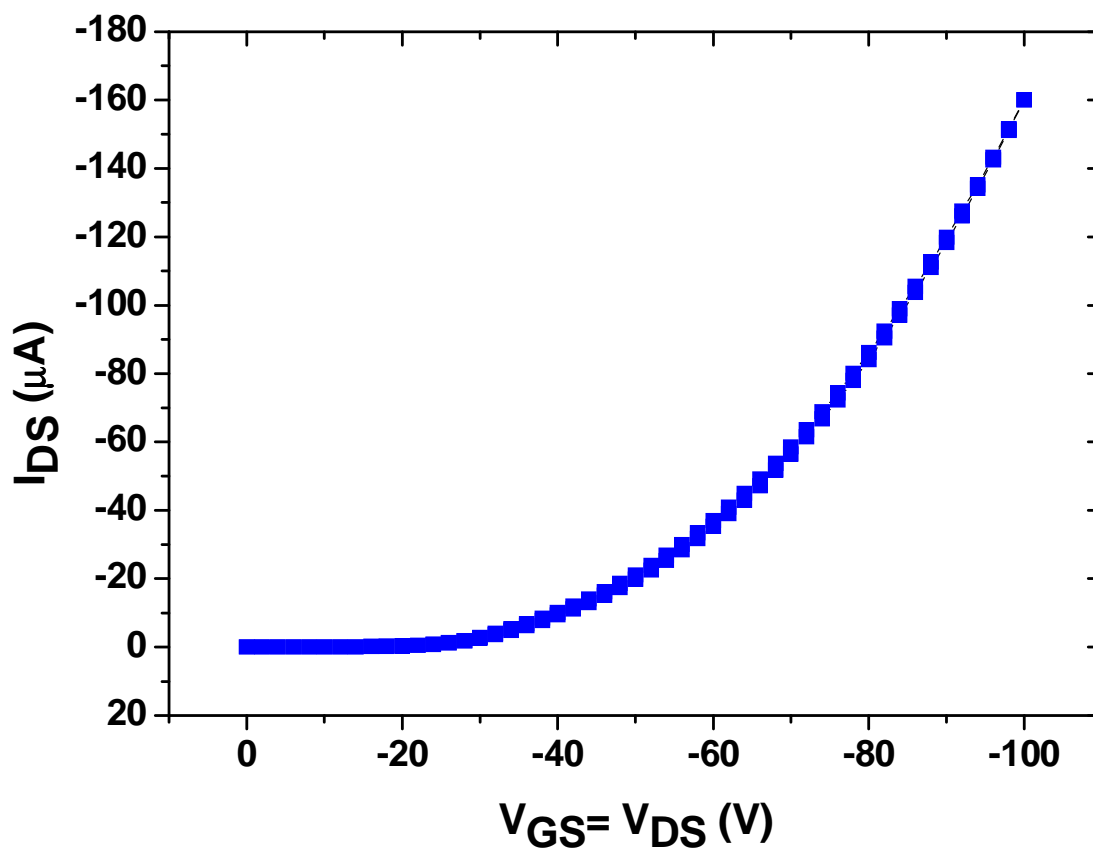


Figure 2.58: LOCUS curve of DH4T doped with 10 % w/w of HexT_3 .

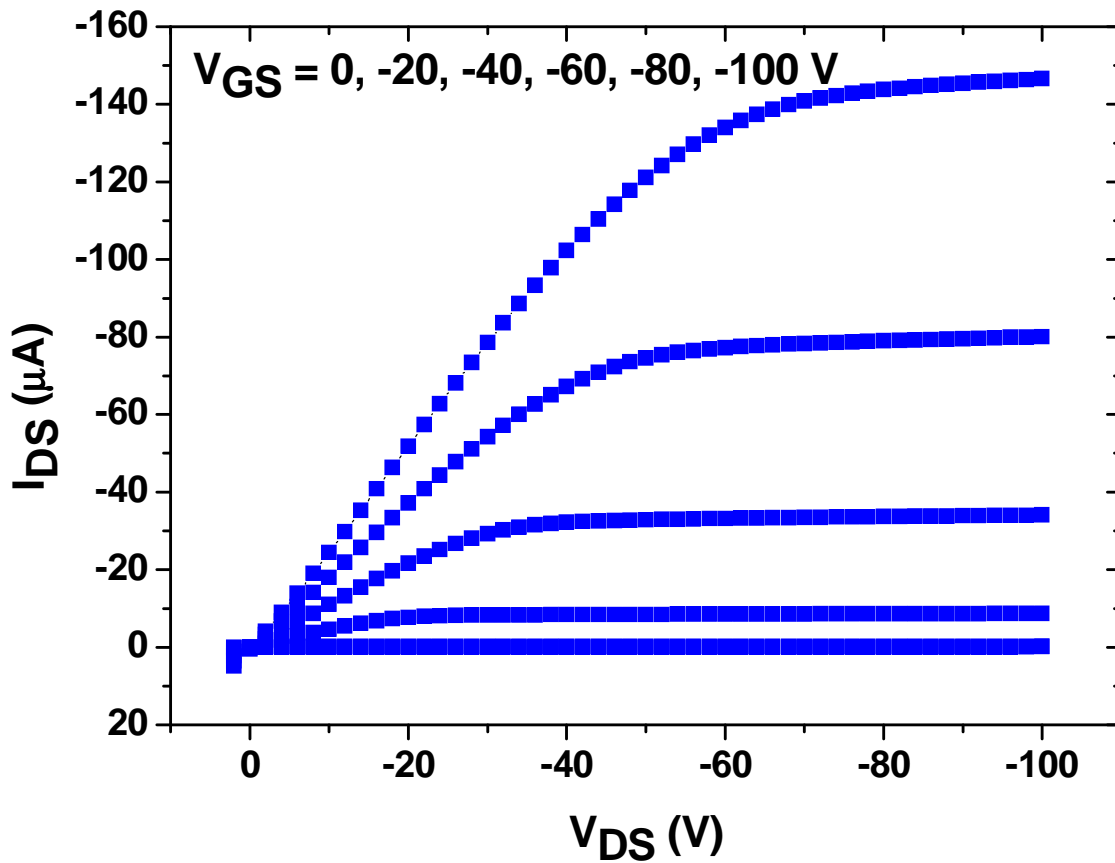


Figure 2.59: MULTIPLE OUTPUT curves of DH4T doped with 10 % w/w of HexT₃.

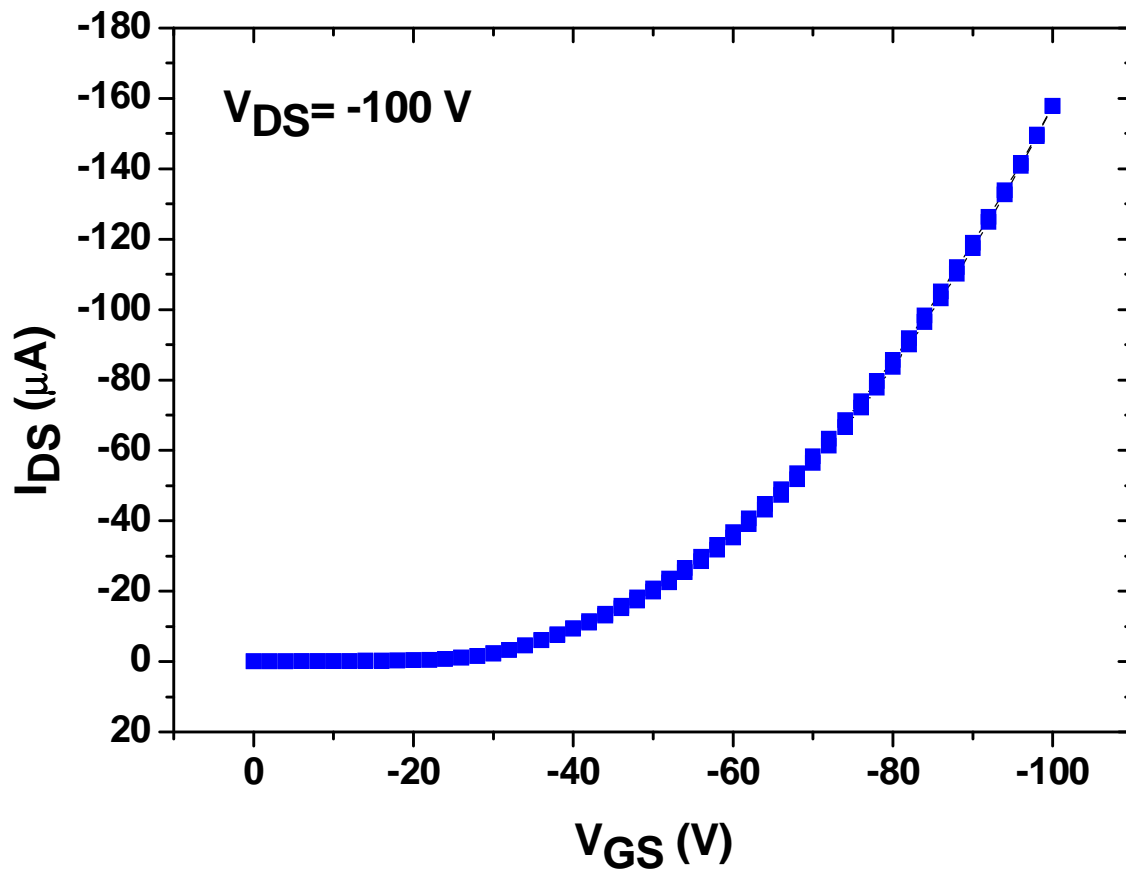


Figure 2.60: SATURATION TRANSFER curve of DH4T doped with 10 % w/w of HexT₃.

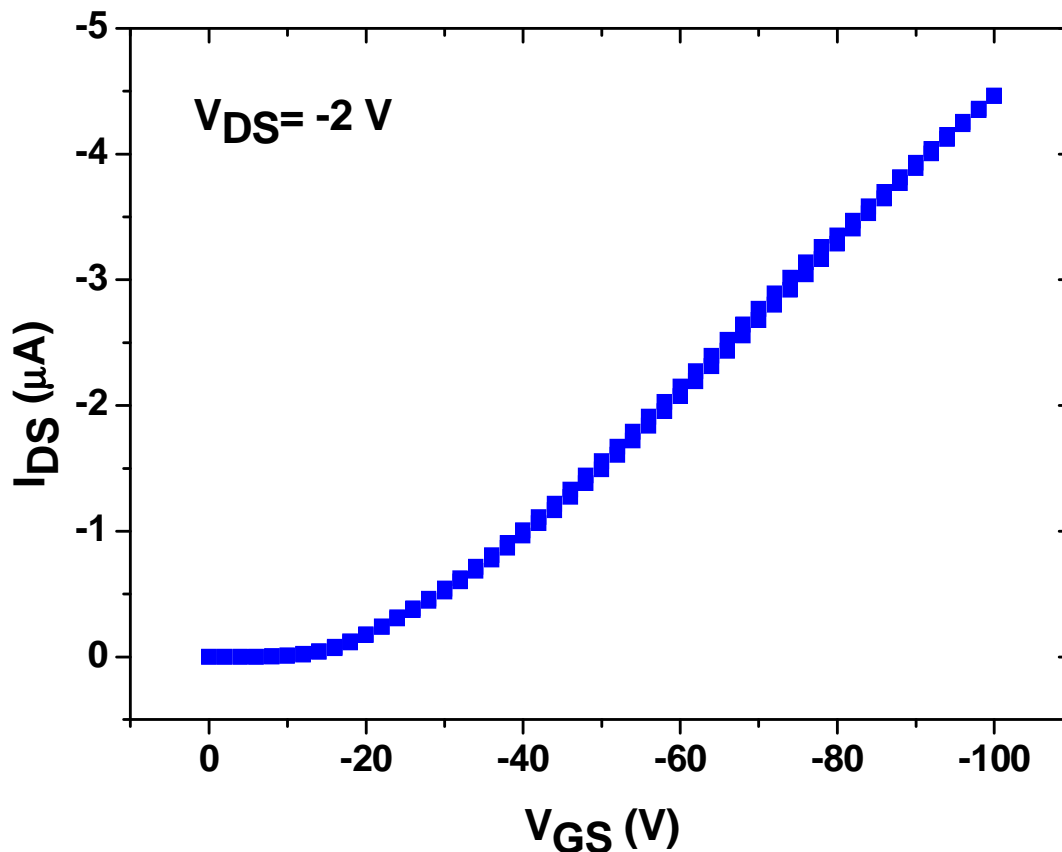


Figure 2.61: LINEAR TRANSFER curve of **DH4T** doped with 10 % w/w of **HexT₃**.

The LOCUS plots don't show hysteresis affection, while the linear ohmic part increases its length as the pollutant concentration becomes higher: this last behavior is the evidence of the interaction between the **HexT₃** orbitals and the **DH4T** ones, which have very similar HOMO and LUMO energy levels. The charge transport is thus made worse, so the Drain current reaches lower values as expected with an increasing impurity addition.

MULTIPLE OUTPUT curves show their linear parts crossing in one origin, revealing neither dielectric current leakage nor free charges in dielectric/active layers interface; the saturation zones are flat, thus the devices have no free charges localized in the boundary between the dielectric and the active layers.

Every SATURATION TRANSFER plot is quite similar to the corresponding LOCUS: this is a very good feature that follows the true ideal behavior, because both kinds of measurement are collected in OFET saturation regime.

LINEAR SATURATION curves don't show hysteresis loop and almost all of them have a pretty constant slope, highlighting the perfect charge injection from the metal

electrodes; the final part of metal-free **DH4T** one show to be affected by charge injection inefficiency between Gold contacts and active layer.

As highlighted at the end of Paragraph 2.4, despite the organic pollutant was tested in very high concentrations it produces a charge mobility decrease of about 31 % at most. **HexT₃** affects the semiconductor charge mobility depressing it dramatically; furthermore this organic pollutant leads to small grows of threshold voltage.

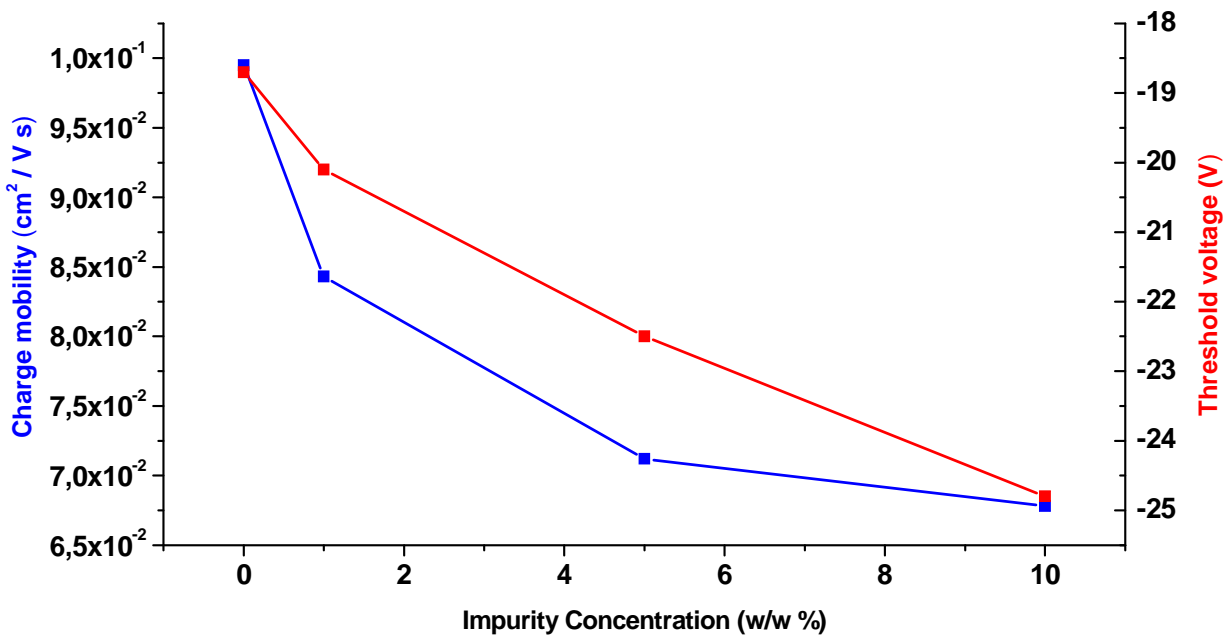


Figure 2.62: effects of the organic impurity concentrations on the **DH4T** charge mobility and threshold voltage.

2.7 Conclusions and remarks

The performances of 2,2'''-Dihexyl-2,2':5',2'':5'',2'''-quaterthiophene (**DH4T**), taken as model molecular organic semiconductor, are necessarily affected by organometallic and organic impurities. In order to control the presence of unwanted molecules, a new metal-free synthesis was developed to obtain **DH4T** batches without any contamination by the most common cross-coupling related products.

Virgin **DH4T** was then doped with organometallic pollutants, like Tetrakis(triphenylphosphine)palladium(0) (**Pd(PPh₃)₄**) and Tributyltin chloride (**Bu₃SnCl**), as well as with an organic impurity, like 5-hexyl-2,2':5',2''-terthiophene (**HexT₃**), in different concentrations (1, 5 and 10% w/w). Organic Field Effect Transistors (OFETs) were fabricated by vacuum sublimation using each of the doped batches; finally they were electrically characterized and their performances were compared to those built up with commercial **DH4T** as well as to the **DH4T** prepared by our Pd free methodology. Charge mobility, threshold voltage and ON/OFF ratio were measured and little affections were found between impurities concentrations and devices performances. The study demonstrated that **DH4T** metal-free synthesis provides a good way to exclude coupling byproducts and sideproducts, leading to easy removable waste and involving few steps without intermediate purifications.

Due to the radicalic mechanism the process efficiency has to be improved, but the results obtained until now are quite good especially considering the performances of the crude semiconductor compared with the commercial ones. Fabricating OFET with doped **DH4T** pointed out how good vacuum sublimation is as purification method even for crude semiconductors as well as a reliable way to fabricate high performing devices; this technique embodies the sublimation benefits with the smartness of the solvent-free fabrication, guarantying the removal of great part of impurities and the minimization of interferences from the environment. In few words, it is possible to build electronic devices while purifying the semiconductor itself in one step. Surely purification matters concerning organic semiconductors were not exhaustively

examined, but the goals achieved in this work make possible to imagine a new approach to organic electronics and to the problems related to it.

REFERENCES

- [1] T. Muck, V. Wagner, U. Bass, M. Leufgen, J. Geurts, L. W. Molenkamp, *Synt. Met.*, 146 (2004) 317–320;
- [2] G. Generali, R. Capelli, S. Toffanin, A. Facchetti, M. Muccini, *Microelectronics Reliability*, 50 (2010) 1861–1865;
- [3] R. Capelli, S. Toffanin, G. Generali, H. Usta, A. Facchetti, M. Muccini, *Nat. Mat.*, 9 (2010) 496-503;
- [4] D. A. Serban, V. Kilchytska, A. Vlad, A. Martin-Hoyas, B. Nysten, A. M. Jonas, Y. H. Geerts, R. Lazzaroni, V. Bayot, D. Flandre, S. Melinte, *App. Phys. Lett.*, 92, 143503 (2008);
- [5] P. A. Troshin, D. K. Susarova, Y. L. Moskvina, *Adv. Funct. Mater.*, 2010, 20, 4351–4357;
- [6] F. Garnier, R. Hajlaoui, A. El Kassmi, G. Horowitz, L. Laigre, W. Porzio, M. Armanini, F. Provasoli, *Chem. Mater.*, Vol. 10, No. 11, 1998, 3335;
- [7] *CRC Handbook of Chemistry and Physics*, 2008 version, p. 12–114;
- [8] A. Mishra, Chang-Qi Ma, P. Bäuerle, *Chem. Rev.*, 2009, 109, 1141–1276;
- [9] R. F. Heck, J. P. Nolley Jr., *J. Org. Chem.*, (1972), 37 (14), 2320–2322;
- [10] M. R. dos Santos et al., *New J. Chem.*, 2014, 38, 2958-2963;
- [11] F. C. Krebs, R. B. Nyberg, M. Jørgensen, *Chem. Mater.*, 2004, 16, 1313;
- [12] M. Leclerc, J. F. Morin, *Design and Synthesis of Conjugated Polymers*, pp. 45 – 98, Wiley, 2010;
- [13] P. A. Troshin, D. K. Susarova, Y. L. Moskvina, *Adv. Funct. Mater.*, 2010, 20, 4351–4357;
- [14] N. Camaioni, F. Tinti, L. Franco, M. Fabris, A. Toffoletti, M. Ruzzi, L. Montanari, L. Bonoldi, A. Pellegrino, A. Calabrese, R. Po, *Org. Elec.*, 13 (2012), 550-559;
- [15] C. O. Kappe, *Chem. Soc. Rev.*, 2008, 37, 1127–1139;
- [16] D. M. P. Mingos, D. R. Baghurst, *Chem. Soc. Rev.*, 1991, 20, 1;

[17] C. O. Kappe, A. Stadler, *Microwaves in Organic and Medicinal Chemistry*, Wiley-VCH, Weinheim, **2005**;

PART III

-

TECHNICAL DETAILS

CHAPTER 1

DESCRIPTION OF THE HIGH VACUUM SUBLIMATION CHAMBER FOR OFET FABRICATION

To fabricate the Organic Field-Effect Transistor devices discussed in Part 2, a dedicated machine was built up and optimized.

Thanks to Vincenzo Ragona, technician of Istituto per lo Studio Materiali Nanostrutturati (ISMN) of Centro Nazionale Ricerche in Bologna, a complete high vacuum sublimation working station was constructed in order to grow organic semiconductors and metals thin films.

It is necessary to remind that high vacuum sublimation system means a set of:

- a sealed chamber made of stainless steel with a glass dome, equipped with temperature and pressure measuring sensors, electric cables and mechanical manipulators;
- a rotary vane pump, called “primary” pump, whose duty is to evacuate the chamber from atmospheric pressure (1013 mbar) to about $1 \cdot 10^{-3}$ mbar;
- a turbomolecular pump, called “secondary” pump, whose duty is to evacuate the chamber from $1 \cdot 10^{-3}$ mbar pressure to about $1 \cdot 10^{-8}$ mbar;

Ragona’s work started from an Edwards AUTO306 (see Figure 1.1), which was modified to achieve the system then used to the thin film growth.



Figure 1.1: Edwards AUTO306 as it looked before the restyling.

After replacing the old oil primary pump with a multi-roots pump in order to avoid oil pollution in the chamber, a set of four Knudsen cells was assembled in order to sublime organic materials (see Figure 1.2); the cells were “effusion-type” patented by Mauro Murgia (pat. BO2000A-000272 del 15/05/2000; validation PCT-ET 01321252 del 08/01/2004).

The cells are put together in a aluminium / stainless steel cylinder and separated by stainless steel shields, in order to avoid reciprocal contamination and to limit the materials diffusion.



Figure 1.2: organic sublimation cells system.

In the centre of the cylinder there are two rotating rods, handled by two manual control knobs; on these rods it is possible to assemble two stainless steel shutters, that allow single material growth or co-sublimation growth.



Figure 1.3: organic sublimation cells system with shutters.

The heating cells control consists in two low-tension power supplies skippered by potentiometers and temperature controllers; each power supply refers to two cells.

The metals evaporation cell is made of two parts (see figure 1.4).

The first one is the continuous cooling circuit, made of two stainless steel glasses coaxially assembled and welded together on the top surface in order to make a little tank for water whose working temperature is about 8°C; the second part is the effusive core, where a tungsten wire wraps an high temperatures crucible. The wire has two terminals: one is connected to the cell body (which works as ground), the other is electrified copper plates.

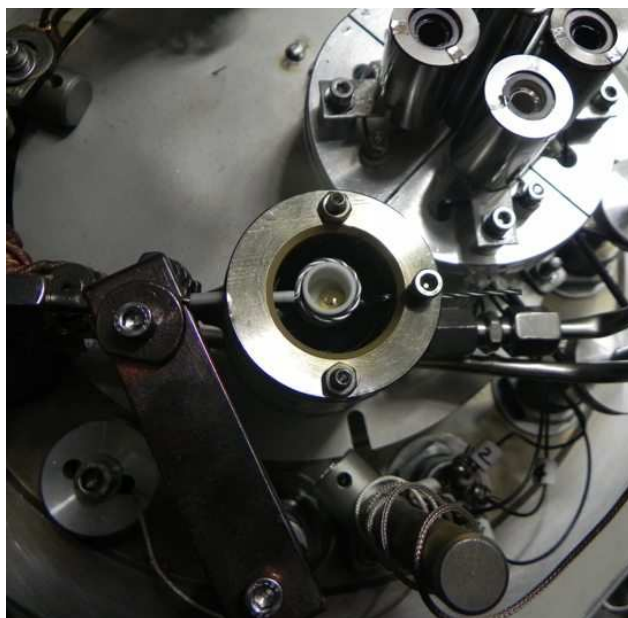


Figure 1.4: top view of the metals evaporation cell.

The heating cell control consists in a power supply skippered by a potentiometer, by which it is possible to change the current intensity and thus the thermal power given to the crucible.

Organic materials sublimation cells and metals evaporation cell are separated by a stainless steel shield, in order to avoid contamination.



Figure 1.5: panoramic view of the machine with the big shield half-assembled.

The aluminium lid, which closes the top of the glass cylinder, has incorporated in it the sample holder, the sample shutters and the masks rotator.



Figure 1.6: chamber lid with as it looks with all the mechanical devices assembled together.

The sample holder is a tray made of stainless steel, with two substrates notched shapes: it can be divided in two parts and substrates can be inserted in it by slight tracks (see Figure 1.7). Sample holder can be fixed to a magnetic support by a little sliding magnet (see Figure 1.8): it can rotate to put the substrates over the organic materials sublimation cells or over the metals evaporation.

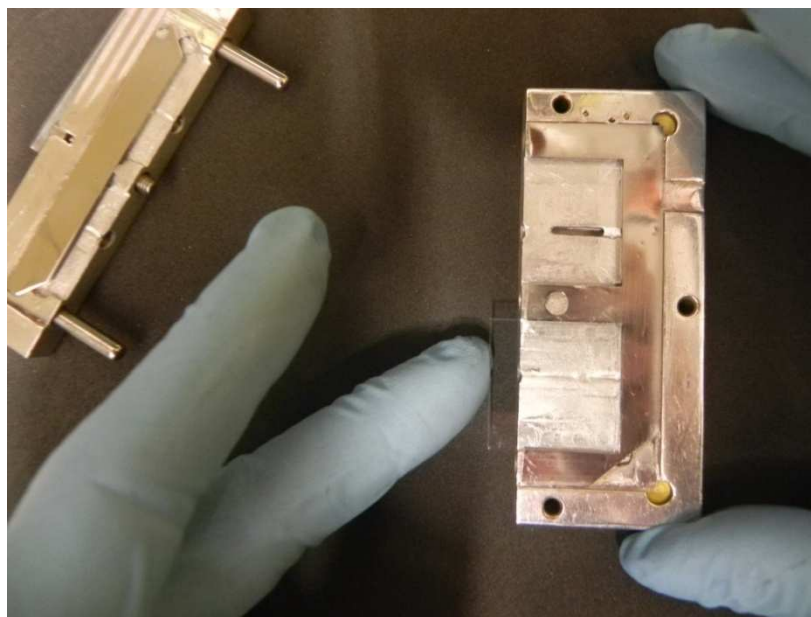


Figure 1.7: divided sample holder with a sampled inserted in the track.

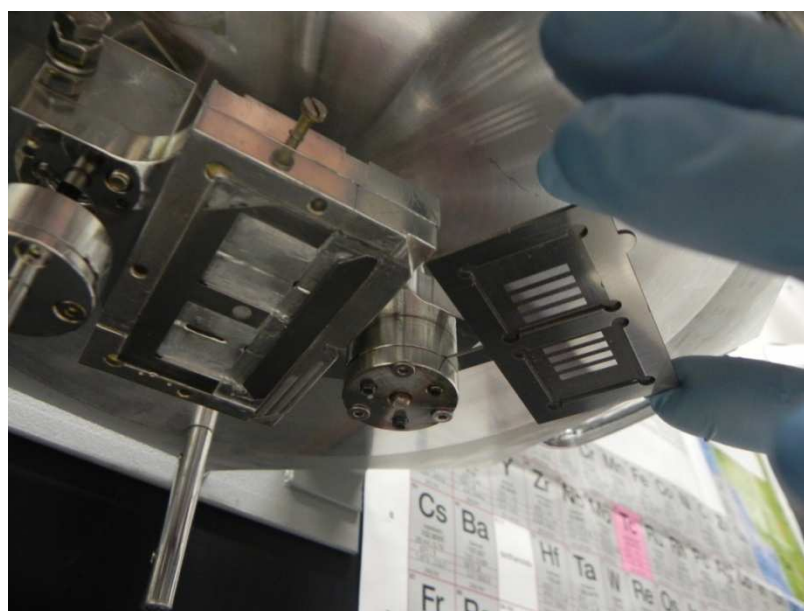


Figure 1.8: sample holder fixed to its support and a mask inserted in the mask swapper plate.

The sample holder support also carries the masks swapper welded on its front: a plate with three openings which the masks are inserted in (see Figure 1.9). The plate can swap masks by rotation, since it has a spring-pushed pivot whose function is to distance a mask from the substrates and to put the new selected mask close to them.

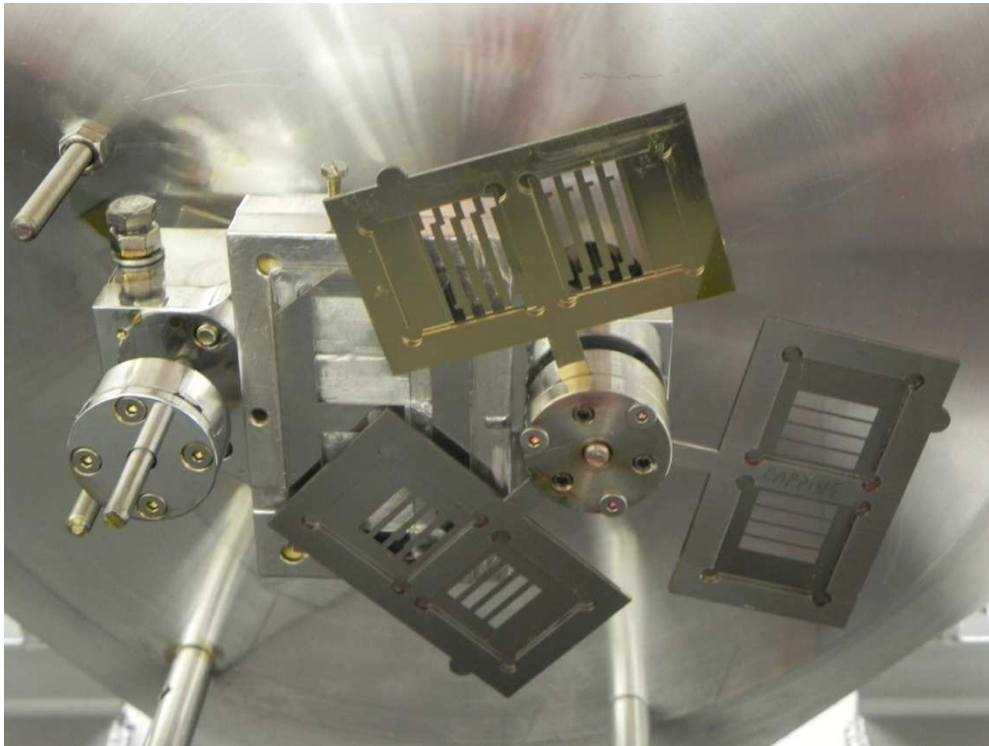


Figure 1.9: masks swapper with three mask for thin film growth; the golden mask is for Gold contacts evaporation.

The masks rotator is assembled just in front of the sample holder: it has an independent knob with a spherical screwdriver head as terminal to make the masks swapper plate rotate (see Figure 1.10).



Figure 1.10: masks rotator in action.

The sample shutter are handled by a knob which is coaxial with that of the sample holder. Shutter can be rotated to grow thin films on both samples or to cover selectively the samples one by one.

Additional shutters can be assembled to protect the unused masks during the process.

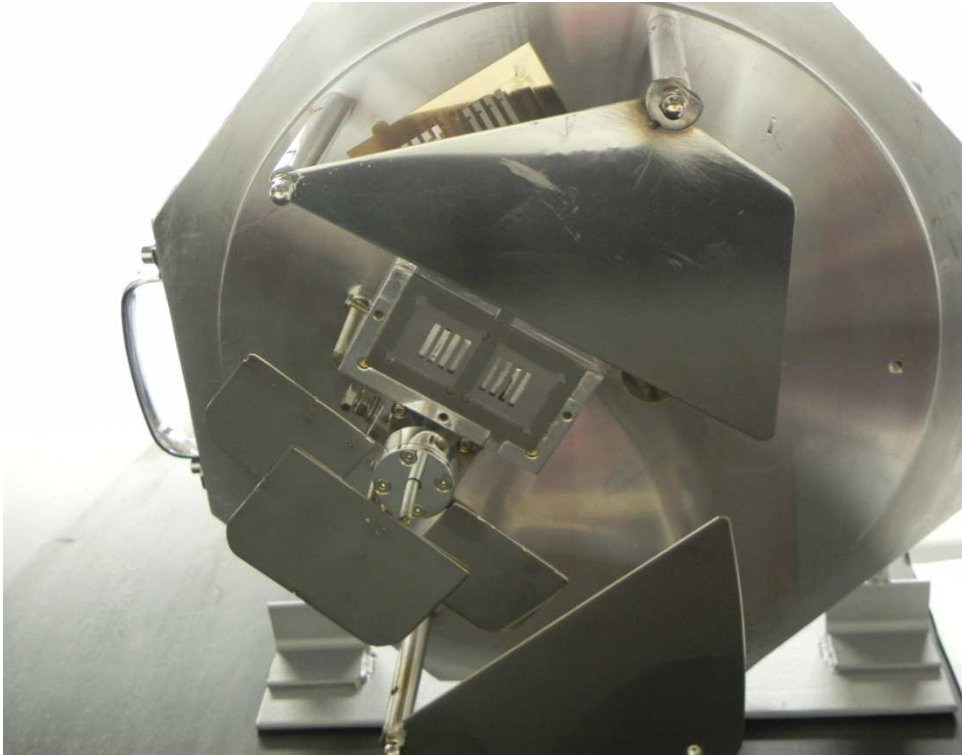


Figure 1.11: sample holder shutters and masks shutter.

CHAPTER 2

OFET DEVICE CHARACTERIZATION

The fully characterization of an Organic Field-Effect Transistors was carried out by an Agilent B1500A Semiconductor Device Analyzer, which is a modular instrument that supports both I-V and C-V measurements and also fast high-voltage pulsing. It presents extremely low-current, low-voltage, and integrated capacitance measurement capabilities with a measurement resolution of 0.1 fA / 0.5 μ V in I-V measurements. In order to prevent the environmental signal noise to be introduced in the collected low-current signals, we connect the Semiconductor Device Analyser with the probing system with triaxial cables in all the measurements.

Triaxial cables are very effective in protecting a voltage signal from unwanted influences. Typically, the outer shield is connected to the chassis or ground, the inner shield is connected to the guard and the signal is collected by the core wire. Since the guard surrounding the core wire and the core wire itself are at the same potential all the possible leakage currents are avoided and the current signal is completely screened from the outer environment. The guard technique reduces not only the leakage currents, but also the response time because cable charging is induced by low impedance source. So the polarization due to the signal current passing through is very little since the residual cable capacitance left.

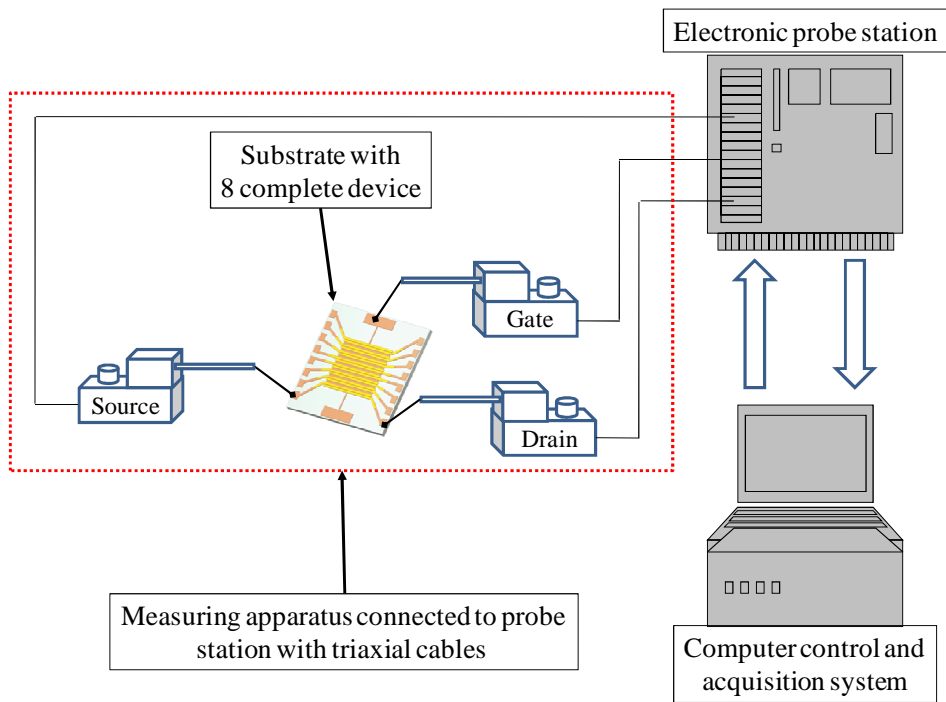


Figure 2.1: simplified scheme of OFET measuring setup.

Before discussing the operative OFET measurement, a fast reminding of Organic Field-Effect Transistor structure and biasing is worthy to be done. A simplified structure of a *common Source* biased OFET is reported in Figure 2.2 : the device architecture shown is very useful to easily understand the device physics and it will be.

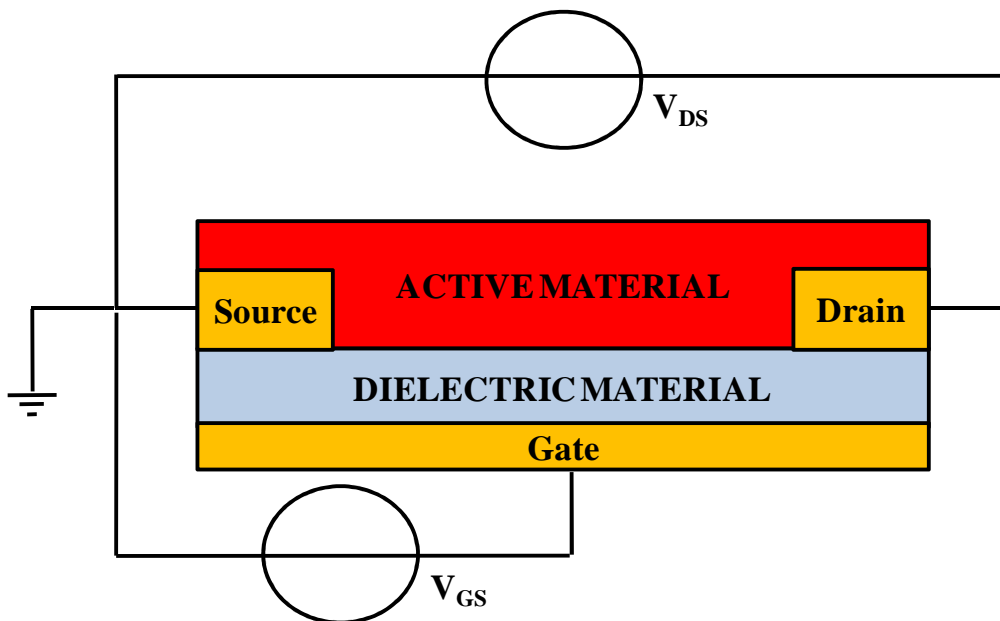


Figure 2.2: OFET architecture with *common Source* biasing.

All the devices, whose performances have been discussed in Part 2, were fabricated in *top contacts / bottom Gate* and they were measured in *common Source* configuration.

The first curve needed to be acquired is the LOCUS (see Figure 2.3): it is obtained sweeping V_{DS} and V_{GS} together from zero to the maximum value of 100 V simultaneously and then back. The device thus operates always in saturation regime and so LOCUS plot is essential to calculate electrical mobility (μ) and threshold voltage (V_{TH}).

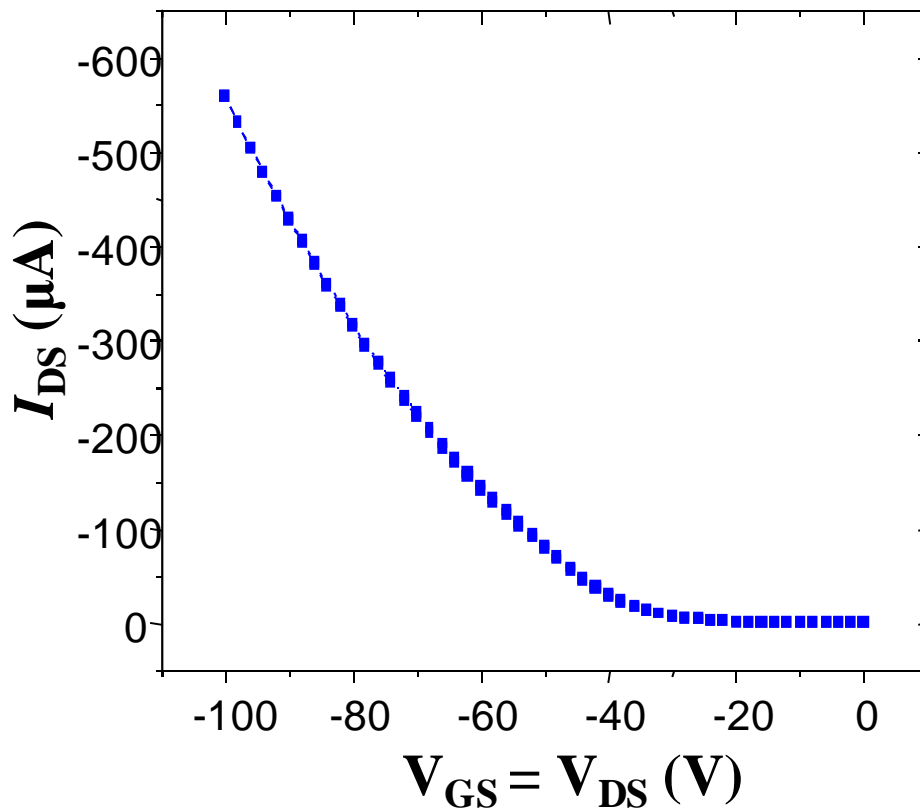


Figure 2.3: standard LOCUS curve for a *p*-type semiconductor.

Since LOCUS curve is acquired in saturation regime working conditions, it is useful to remind the proper relationship between I_{DS} and V_{GS} :

$$I_{DS} = \frac{W \mu C_i}{L} \frac{(V_{GS} - V_{TH})^2}{2}$$

Equation 2.1: mathematic relationship between Drain current and the voltages applied to OFET; W is the OFET channel width, L is the OFET channel length, C_i is the dielectric specific capacitance.

Equation 2.1 becomes a linear function if both equation terms are put under square root, thus giving Equation 2.2 :

$$\sqrt{I_{DS}} = \sqrt{\frac{W \mu C_i}{2 L}} (V_{GS} - V_{TH})$$

Equation 2.2: linear relationship between applied Gate voltage and the square root of Drain current.

Once obtained the LOCUS curve, it is then necessary to calculate the square root for every I_{DS} value and plot the new data series versus that of the applied voltage (no matter which voltage, since $V_{DS} = V_{GS}$).

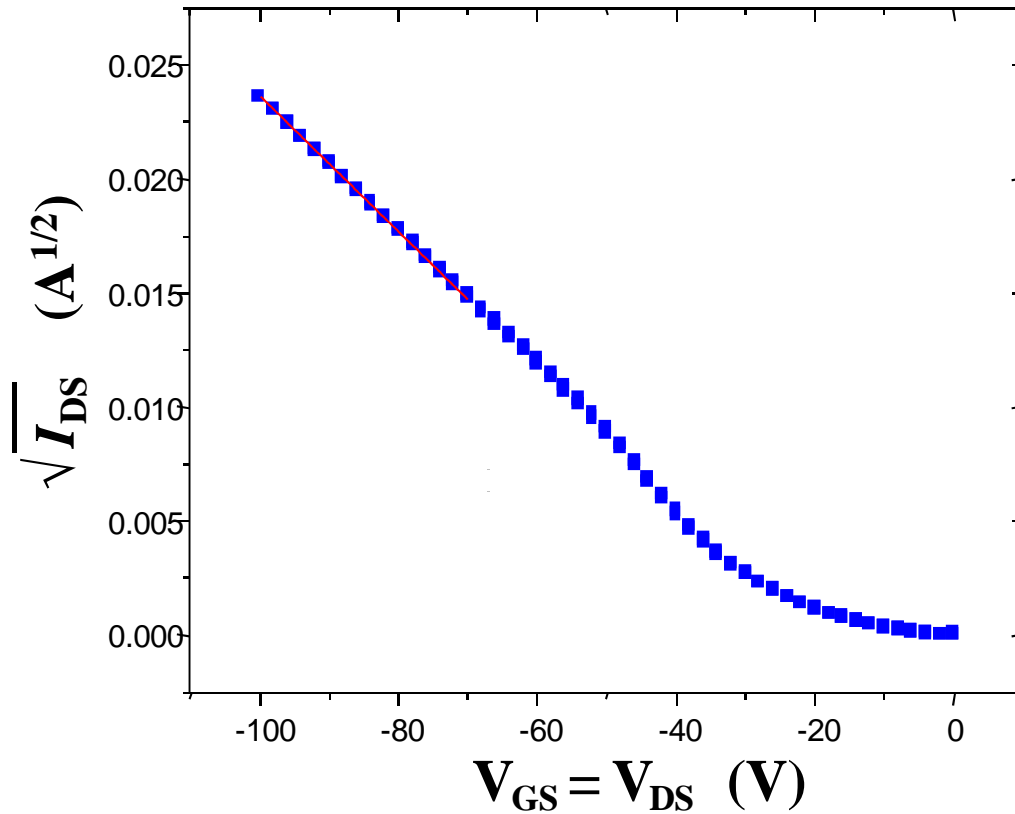


Figure 2.4: manipulated LOCUS curve for a *p*-type semiconductor.

The linear part of the plot shown in Figure 2.3 must be fitted with an interpolating function in order to obtain an linear equation like $y = a x + b$.

According with Equation 2.2, y is I_{DS} square root and x is V_{GS} .

Electrical mobility can be easily calculated from the slope of the fitting linear function:

$$\text{since } a = \sqrt{\frac{W \mu C_i}{2 L}} \text{ then } \mu = \frac{2 L a^2}{W C_i}$$

Threshold voltage is but the intersection between x axis and the fitting linear function:

$$\text{if } \sqrt{I_{DS}} = 0 \text{ then } V_{GS} = V_{TH}$$

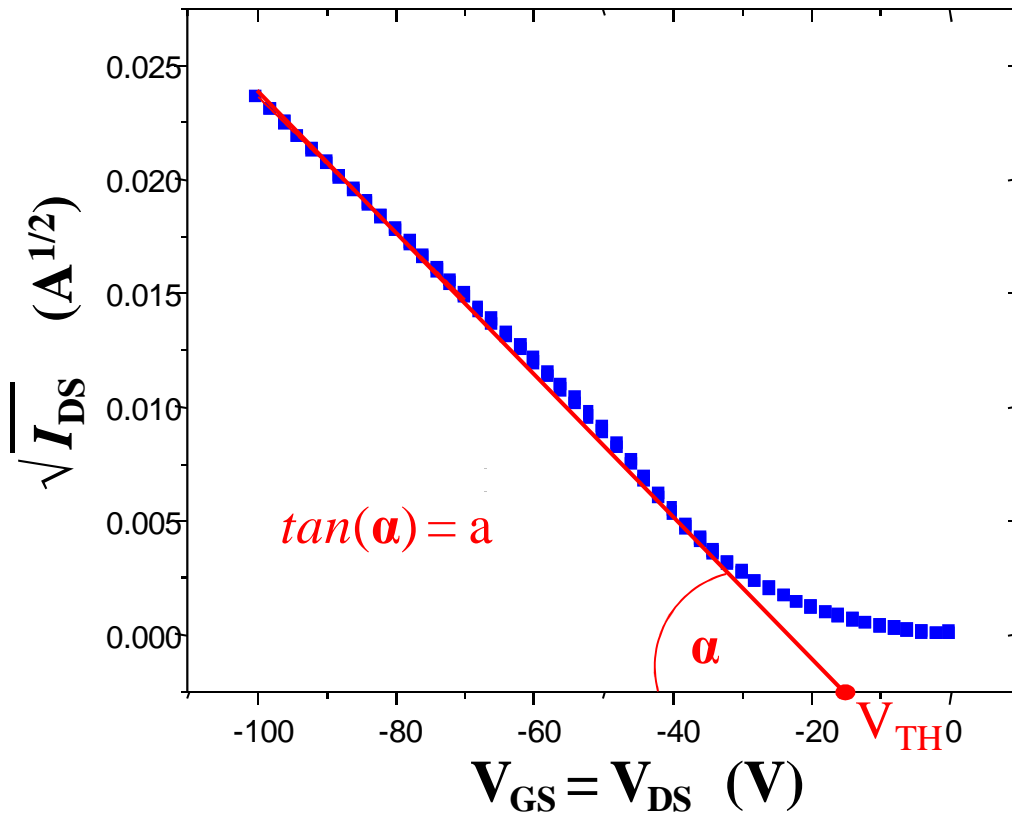


Figure 2.5: qualitative representation of the mathematical discussion.

The second kind of curve that must be acquired to characterize an OFET is the SATURATION TRANSFER (see Figure 2.6): it is obtained sweeping V_{GS} from zero to the maximum value of $|100|$ V and then back, while V_{DS} is constantly kept at the maximum value of $|100|$ V. The device thus operates in high stress saturation regime, especially for low V_{GS} values. For an ideal transistor SATURATION TRANSFER plot is identical to LOCUS one.

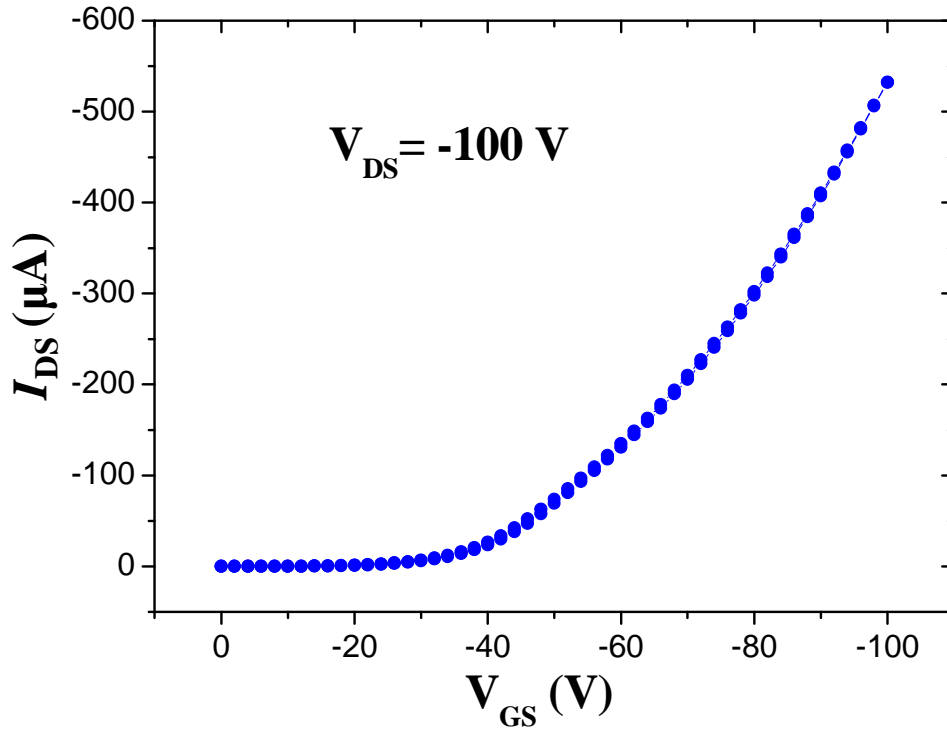


Figure 2.6: standard SATURATION TRANSFER curve for a *p*-type semiconductor.

This kind of plot is very useful in order to estimate the ON / OFF ratio: no calculus manipulation is needed, since it is enough to divide the maximum I_{DS} recorded at maximum applied V_{GS} by the I_{DS} value acquired for $V_{GS} = 0$, as shown in Figure 2.7 .

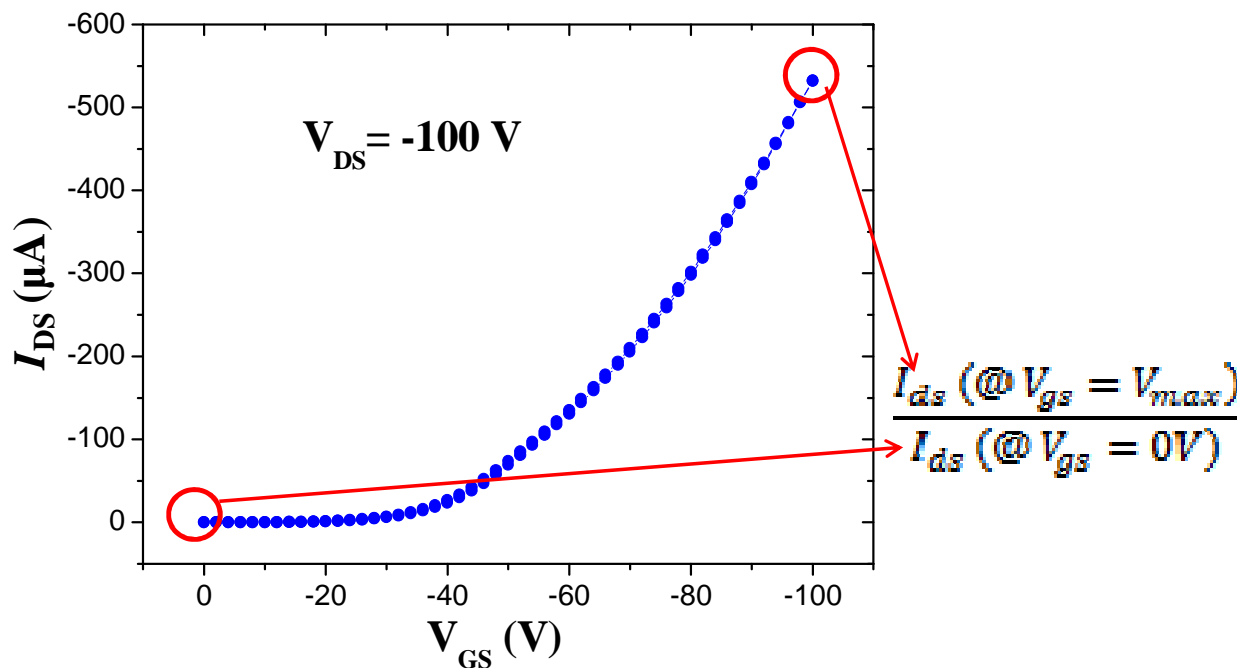


Figure 2.7: representation of ON / OFF ratio calculation.

The third kind of curve is called LINEAR TRANSFER (see Figure 2.8): it is obtained sweeping V_{GS} from zero to the maximum value of $|100|$ V and then back, while V_{DS} is constantly kept at the value of $|2|$ V. The device thus operates in linear ohmic regime, ideally showing a perfect constant slope. LINEAR TRANSFER is very useful to study the charge injection through the electrodes, which should be ohmic, and to evaluate the Gate leakage current.

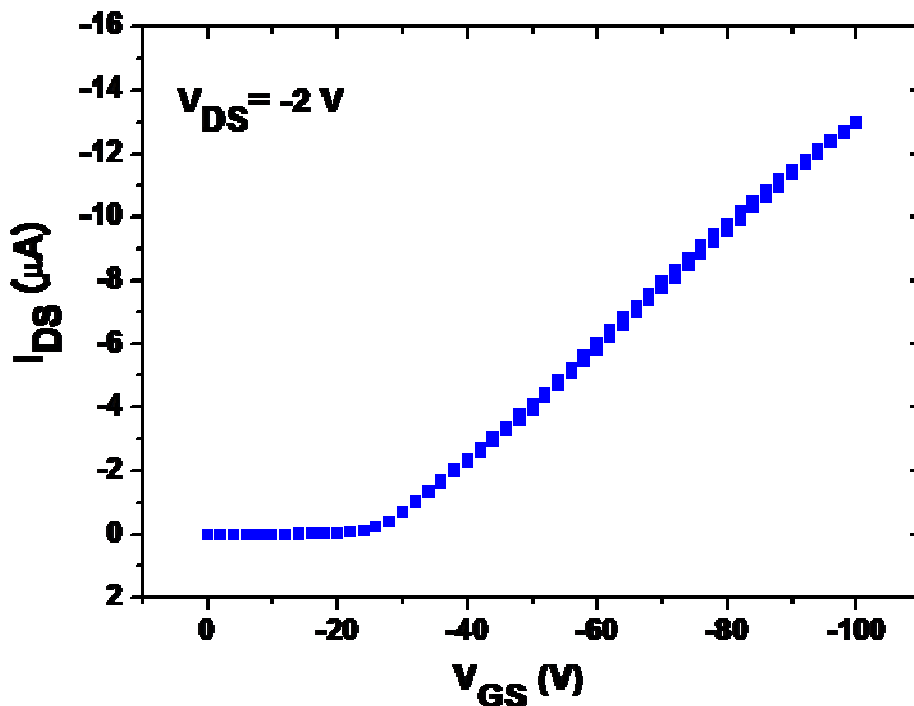


Figure 2.8: standard LINEAR TRANSFER curve for a p -type semiconductor.

Finally, the complete device characterization is made by acquiring the MULTIPLE OUTPUT curves (see Figure 2.9): they are the classical OFET response, obtained sweeping V_{DS} from zero to the maximum value of $|100|$ V several times, changing V_{GS} each time.

Each curve exhibits ohmic and saturation regimes. If the first part is not linear, then the device has problems at the interface between the active material and the metal electrodes; if the second part is not flat, then it is possible the presence of trapped charge within the interface between dielectric and active layers.

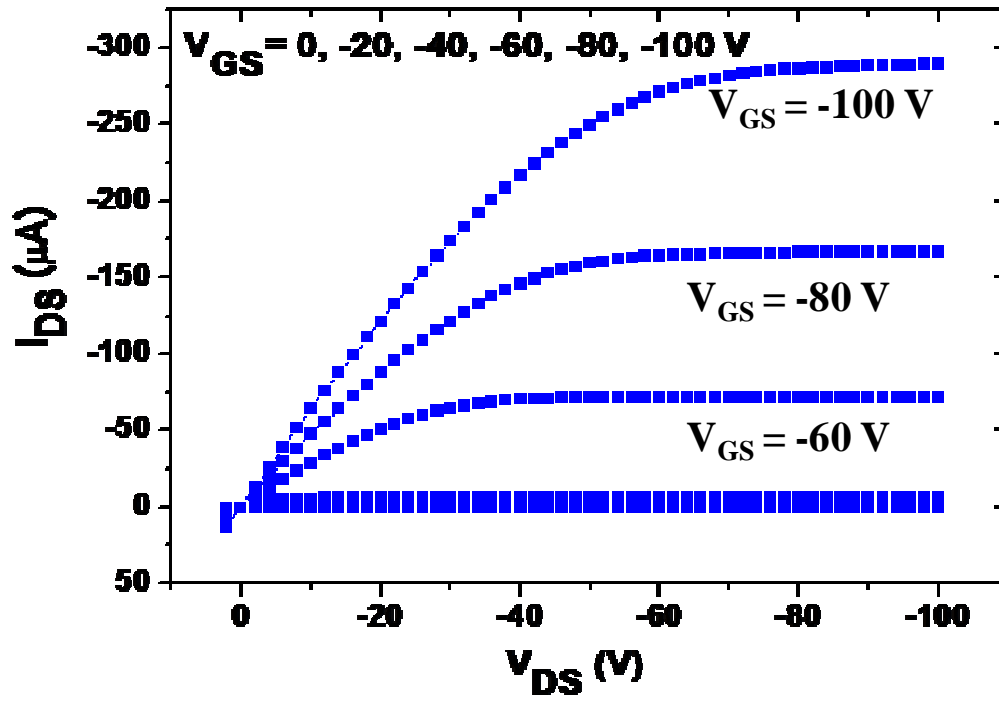


Figure 2.9: standard MULTIPLE OUTPUT curves for a p -type semiconductor.